UNIVERSITY OF LIVERPOOL

Department of Engineering

Centre for Engineering Sustainability

Mechanistic-Based Characterisation of Fatigue Resistance of Alternative Mix Designs

Thesis submitted in accordance with the requirements of

University of Liverpool for the degree of Doctor of Philosophy by

Husam Adnan S. Sadek

B.Sc., M.Sc.

October 2015

Abstract

The population and economy in the State of Qatar have been increasing significantly in the past 10 years. Accordingly, traffic loading has also increased rapidly, which merits consideration of the design and construction of long-lasting pavement structures that require minimal maintenance.

This study started with an investigation of the feasibility and performance of the current asphalt pavement materials and structures being used in the country. This investigation utilised the analysis approach implemented in the Mechanistic-Empirical Pavement Design Guide (M-E PDG) software. The results evidenced how effective it is to replace the conventional unmodified 60-70 Pen bitumen with polymer-modified PG76-10 bitumen for pavements in Qatar and other countries in the region with similar climatic conditions. In addition, the results showed that the use of perpetual pavement structures is a viable option economically and that they are much more accommodating of increase in traffic loading, without causing excessive damage, than conventional pavement structures.

The study also concentrated on the assessment of the long-term performance of different full-scale perpetual trial sections by conducting several field tests. The field performance evaluation results showed slightly low resistance to rutting, high IRI values, to some extent, and low stiffness during summertime when the temperature is high. These distresses and deteriorations are expected given the huge traffic loading and the big difference in temperature between seasons in Qatar.

Then several field cores, field mixtures, and laboratory mixtures were tested and evaluated in order to assess the performance of different asphalt concrete mixtures against rutting, fracture, temperature susceptibility and fatigue damage. The conducted tests were useful to characterise and assess the performance of the mixtures against several major distresses. The results indicated that resistance of asphalt concrete mixtures to rutting was

mainly affected by the bitumen grade, aggregate source and aggregate gradation. A well-designed mixture that uses polymer-modified bitumen (PMB) can achieve the high rut-resistance of asphalt mixtures either with Gabbro or limestone aggregates. The use of polymer-modified bitumen reduced the temperature and frequency susceptibility on the stiffness and rut-resistance.

According to these results, it is obvious that rutting and cracking would not be major distresses for asphalt mixtures in Qatar if the mixtures were designed following a Superpave mix design with the appropriate content of polymer-modified bitumen. However, given the current mixture design system in Qatar, which utilises very low bitumen content, fatigue damage or cracking in general is a main distress, and its characterisation should be investigated in depth. The traditional methods to interpret fatigue tests data are not sufficient to characterise and evaluate mixtures against fatigue damage. Therefore, two advanced fatigue characterisation approaches were performed on the raw data obtained from the fatigue test of specimens prepared from different mixtures. The analysis of the fatigue tests focused on calculating the dissipated energy (DE) and obtaining damage characteristics curves following a comprehensive viscoelastic continuum damage (VECD) approach. The test results showed that the use of the VECD approach has major advantages over obtaining DE results only. However, the predicted fatigue life (N_f) for each asphalt mixture was affected by the uncertainty associated with fatigue tests as well as with model parameters. Therefore, it was important to develop a probabilistic analysis approach that accounts for the uncertainty and the variability associated with fatigue tests and analysis, respectively.

To that end, a novel probabilistic analysis approach has been proposed in the last chapter of this study for predicting the performance of asphalt mixture against fatigue damage. The VECD characterisation approach was used in the development of this probabilistic analysis model. The random variables (RVs) of the fatigue life (VECD-N_f) model ($|E^*|_{LVE}$, a, b and α)

were generated following normal distribution functions. However, it is suggested that more specimens should be tested in the future to specify the true distribution functions for the RVs.

In conclusion, it is clear that the fatigue life results of the probabilistic analysis approach were much more consistent and reliable than those of the deterministic analysis approach. This probabilistic approach coupled with VECD results is very practical and useful for engineers and will be beneficial to predict fatigue cracking resistance of asphalt mixtures in the field.

Dedication

To my devoted parents and my sincere wife for their love, patience and encouragement

Acknowledgments

Before all and after all, I am ultimately grateful to Allah (God) for giving me the knowledge, intellect, and great blessings that I will never be able to count.

I am greatly thankful to my generous supervisors, **Dr Hussain Al-Khalid** and **Dr Eyad Masad**, for their continuous guidance and support. I consider myself fortunate to have had them as my advisors. I appreciate their boundless academic and social support all through the time that I studied at the University of Liverpool. It was my honour to work with them and learn the craft of research from their supervision and teaching.

Moreover, I would like to thank the University of Liverpool pavement group members and the Engineering Department Laboratory technical staff for their assistance and advice with the experimental work. Special thanks to **Dr Okan Sirin**, and my colleagues **Taher Ahmed** and **Dr Loujaine Mehrez** for their academic support all through my research work.

I greatly acknowledge the invaluable support from **my father Adnan** and **my mother Samia** all through my life. They have been always there for all types of social, educational, and academic support. I am proud of them, and I hope that they will be proud of me also. I would like to acknowledge my sincere wife, **Haneen Bsaisu**, for her patience, encouragement, and great help all through my research project. My great thanks to my brothers, **Mohammed** and **Haytham**, for their countless guidance in my studies. I also greatly appreciate the positive and pleasant support of my sister, **Lubna**.

List of Abbreviations

AADTT	Annual Average Daily Truck Traffic
AASHO	American Association of State Highway Officials
AASHTO	American Association of State Highway and Transportation Officials
AC	Asphalt Concrete
ALF	Accelerated Loading Facility
AMPT	Asphalt Mixture Performance Tester
ANOVA	Analysis of Variance
ASTM	American Society for Testing and Materials
ATB	Asphalt-Treated Base
AV	Air Voids
BS	British Standard
CBR	California Bearing Ratio
cdf	cumulative distribution function
CT	Computed Tomography
DBM	Dense Bitumen Macadam
DE	Dissipated Energy
DER	Dissipated Energy Ratio
DPSE	Dissipated Pseudo-Strain (or -Stress) Energy
DT	Direct Tensile
EICM	Enhanced Integrated Climatic Model
ELLPAG	European Long-Life Pavement Group
ESALs	Equivalent Single Axle Loads
FAM	Fine Aggregate Matrix
FAST	Fourier Amplitude Sensitivity Test
FD	Fatigue Damage
FN	Flow Number
FOS	Factor of Safety
FOSM	First-Order Second-Moment
FWD	Falling Weight Deflectometer
GI	Group Index
GPR	Ground-Penetration Radar
GSA	Global Sensitivity Analysis
GSAT	Global Sensitivity Analysis Toolbox
HiMB	Highly Modified Bitumen
HMA	Hot Mix Asphalt
IDT	Indirect Tensile
IRI	International Roughness Index
LCCA	Life-Cycle Cost Analysis
LHS	Left-hand Side
LL	Liquid Limit
LVDT	Linear Variable Differential Transducer
LVE	Linear Viscoelastic
MCS	Monte Carlo Simulation
MDD	Maximum Dry Density
M-E PDG	Mechanistic-Empirical Pavement Design Guide
mph	mile per hour

Mr	Resilient Modulus
MTS	Material Testing System
MVFOSM	Mean Value First-Order Second-Moment
NCAT	National Centre for Asphalt Technology
NCHRP	National Cooperative Highway Research Program
NLVE	Nonlinear Viscoelastic
NPV	Net Present Value
OMC	Optimum Moisture Content
pdf	probability density function
PEM	Point Estimate Method
PG	Performance Grade
PI	Plasticity Index
PL	Plastic Limit
PMB	Polymer-modified Bitumen
PRD	Percentage Refusal Density
PV	Plateau Value
PWA	Public Works Authority
QHDM	Qatar Highway Design Manual
RAP	Reclaimed Asphalt Pavement
RDEC	Ratio of Dissipated Energy Change
RHS	Right-hand Side
RILEM	International Union of Laboratories and Experts in Construction Materials
RV	Random Variable
SBS	Styrene-Butadiene-Styrene
SCB	Semi-Circular Bending
SDP	South Dakoda Profiler
SGC	Superpave Gyratory Compactor
SM	Safety Margin
SMA	Stone Matrix Asphalt Concrete
SMAC	Stone Mastic Asphalt Concrete
SPT	Simple Performance Test
ST	Starch
T/C	Tension and Compression
TRL	Transport Research Laboratory
t-TS	time-Temperature Superposition
UK	United Kingdom
US	United States
USA	United States of America
VECD	Viscoelastic Continuum Damage
VFB	Voids Filled with Bitumen
VIM	Voids In Mix
VMA	Voids in Mineral Aggregate

Table of Contents

List of Figures

List of Tables

1 Introduction

1.1 Motivation

The population in the State of Qatar has been increasing rapidly due to the tremendous economic growth over the past ten years. Accordingly, traffic loading has also increased significantly, which has adversely affected the performance of existing roads and highways. Based on records from the Qatar Statistics Authority (2013), the growth in residents in Qatar in the next five years is expected to be about 25%. In order to accommodate this increase, the government has decided to invest about $14 billion in improving the road network and infrastructure by the year 2019 (The Public Works Authority (Ashghal), 2012). This investment should be accompanied by the adoption of state-of-the-practice methods for the design and evaluation of asphalt pavement structures that can sustain the increase in traffic loading.

The Qatar Highway Design Manual (QHDM) is the current official reference that is used for pavement design in Qatar. It was issued in 1997 to replace an old version that was produced in 1989 by the Civil Engineering Department of the Ministry of Public Works. The QHDM provides the structures for various types of pavement construction in a series of tables. Based on the subgrade and traffic classes, the thicknesses of the layers are simply assigned for each pavement type. However, the current QHDM methods used in the design of asphalt pavement structures in Qatar are empirical and might not be suitable for the design of long-lasting/perpetual pavement structures. Many of the existing roads in Qatar suffer from many distresses and deteriorations, especially fatigue (top-down) cracking that is happening due to the rapid increase in the traffic loading, ageing of bitumen, in addition to the low bitumen content used in the asphalt concrete mixtures.

Given the significant increase in traffic volumes and loads, road authorities in the State of Qatar have been considering the use of mechanistic-empirical methods in the design and

analysis of asphalt pavement structures. Therefore, this research study was initiated to investigate the main factors causing poor performance of some current asphalt pavement structures and to suggest solutions. This implied the need for a suitable fatigue characterisation approach for field and laboratory asphalt mixtures in order to predict their service lives accurately.

1.2 Objectives

The main purpose of this study is the development of an approach for mechanistic-based characterisation and modelling of the performance of alternative asphalt concrete mixtures with a focus on fatigue characterisation in the State of Qatar. This research is conducted to achieve the following specific objectives:

- Evaluate the performance of the conventional asphalt pavement structures provided in the QHDM and currently used in Qatar against major distresses using the mechanistic-empirical pavement design approach.
- Assess the field performance of alternative full-scale trial asphalt pavement structures constructed as perpetual pavements in Qatar.
- Investigate the performance of alternative asphalt concrete mixtures against rutting, fracture cracking, temperature susceptibility and finally fatigue cracking using several laboratory tests.
- Evaluate and examine the limitations of conventional fatigue characterisation approaches.
- Enhance the ability of the viscoelastic continuum damage (VECD) approach to predict fatigue resistance for asphalt mixtures by incorporating probabilistic analysis into this approach.

1.3 Research contribution

The current methods for the design of asphalt mixtures and asphalt pavements in the State of Qatar are mostly based on empirical concepts and have not been examined for a long time. This study utilises mechanistic-based methods to characterise the performance of asphalt mixtures and analyse asphalt pavements. The result is a set of recommendations for improving the quality of asphalt pavements in the State of Qatar.

Fatigue cracking, especially top-down fatigue cracking, is a common pavement distress on roads with heavy traffic loading and mix designs that have low bitumen content, which is the case in the State of Qatar. Fatigue failure of asphalt concrete mixtures is a complicated phenomenon and the conventional fatigue characterisation approaches are not really adequate to predict the performance of asphalt concrete mixtures against it. There is a great deal of variation in the outputs and results of these approaches, which makes it difficult to predict the fatigue life of the tested asphalt mixtures accurately. The conventional fatigue characterisation approaches consider all input parameters as fixed and deterministic inputs. However, the models' parameters, such as traffic loading, climatic conditions, properties of materials, layers' structure and thicknesses, have uncertainty in design and construction which consequently cause uncertainty in the fatigue life prediction. Furthermore, the variability of the inputs of a fatigue life (N_f) model among specimens of a certain asphalt mixture makes it difficult to foresee its performance. Therefore, and as a main contribution, it was important for this study to develop a non-deterministic/probabilistic analysis approach using a fatigue life (N_f) model that considers all of these factors and accounts for the uncertainty associated with fatigue tests along with the models and the variability of their input parameters.

The fatigue characterisation approaches used in all previous probabilistic analysis studies were the classical ones that did not consider many factors. These factors are the effect of loading mode or level, the fatigue damage on the macro-scale level, the initial condition

(damage) of the asphalt mixture before fatigue testing and the viscoelastic effect on the estimation of fatigue damage. Consequently, the viscoelastic continuum damage (VECD) approach, which overcomes these shortcomings, was selected and implemented in this study.

Given the increasing cost of designing and constructing new asphalt pavements, the probabilistic analysis approach developed in this study will be helpful for engineers to design asphalt concrete mixtures that resist fatigue cracking based on an acceptable reliability level.

In addition, it is worth mentioning that this research work with all its components is the first for the State of Qatar and its outcomes are currently being considered to revise the asphalt concrete mixtures and designs in Qatar, and in promoting the use of mechanistic-empirical methods in the country.

1.4 Thesis structure and organisation

1.4.1 Chapter 1: Introduction

The thesis starts with an introductory chapter that discusses the motivation of this study, the main objectives and the research contribution. In addition, the thesis structure and organisation are presented in this chapter.

1.4.2 Chapter 2: Literature Review

The second chapter of this thesis provides a literature review pertinent to asphalt concrete pavement structures in the Middle East region, perpetual pavement structures and their fatigue characterisation approaches. Moreover, major probabilistic analysis studies on fatigue characterisation of pavement mixtures are presented and discussed.

1.4.3 Chapter 3: Performance Evaluation of Alternative Conventional and Perpetual Pavement Structures

In this chapter, the conventional asphalt concrete pavement structures currently used in Qatar are evaluated against major distresses and compared to a proposed perpetual pavement structure. This evaluation is performed using the Mechanistic-Empirical Pavement Design

Guide (M-E PDG) software. A life-cycle cost analysis (LCCA) is then performed to determine the pavement structure with the highest net present value (NPV) among the various options investigated.

In order to investigate the field performance of perpetual pavement structures in Qatar, a full-scale trial road with different pavement structures and subjected to heavy truck traffic was evaluated. The conditions, mechanical properties and performance of these trial sections were evaluated after a year and a half of service by conducting several measurements and field tests.

1.4.4 Chapter 4: Performance Evaluation of Alternative Asphalt Concrete Mixtures

Chapter 4 presents the evaluation of the performance of various asphalt concrete mixtures against rutting, fracture cracking, temperature susceptibility and finally fatigue cracking. The performance evaluation consists of different laboratory tests in order to characterise the tested mixtures against various common distresses.

1.4.5 Chapter 5: Fatigue Damage Characterisation of Asphalt Concrete Mixtures

In this chapter, the dissipated energy (DE) approach and the viscoelastic continuum damage (VECD) approach, in their latest form, are discussed in detail and then implemented to analyse the fatigue test data of different asphalt concrete mixtures to specify their fatigue lives.

1.4.6 Chapter 6: Probabilistic Analysis of Fatigue Life for Asphalt Concrete Mixtures Using the VECD Approach

In Chapter 6, the development of the probabilistic analysis approach using the VECD fatigue life model (VECD-N_f) model is introduced and discussed in detail. The objective of the developed probabilistic approach is to predict the performance of mixtures against fatigue damage to a highly reliable level. In addition, a sensitivity analysis is conducted in order to

specify the most significant input parameters affecting the prediction of fatigue life (N_f) for asphalt mixtures.

1.4.7 Chapter 7: Summary and Conclusions

The final chapter of this thesis summarises the major findings of this research work and suggests further areas to be investigated in the topic of fatigue characterisation of bituminous mixtures.

2 Literature Review

Prior to the 1920s, the thickness and design of asphalt roadway pavement structures were based purely on experience. The development of pavement design systems started in 1929 with empirical methods – California Bearing Ratio (CBR) and Group Index (GI) – that were based on the physical properties of the soil subgrade and implemented with and without a soil strength test, respectively. After that, Terzagi's classical bearing capacity formula in 1943 was applied to determine the thickness of pavement structures. Then, in 1961 the American Association of State Highway Officials (AASHO) published regression methods that were adopted based on some road tests and the performance of flexible asphalt pavements (AASHO, (1961) and Baus & Fogg, (1989)). Later, empirical-mechanistic design method was implemented in the 1970s based on the mechanics of materials which relate an input, such as wheel load, to an output or pavement response, such as stress, strain or deflection (Mathew & Krishna Rao, 2007). This method was later updated and revealed as the Shell method in 1977 and then as the Asphalt Institute method in 1981.

Typically, there are four different types of asphalt concrete pavement structures: flexible, rigid, and composite (flexible or rigid), as shown in Figure 1.

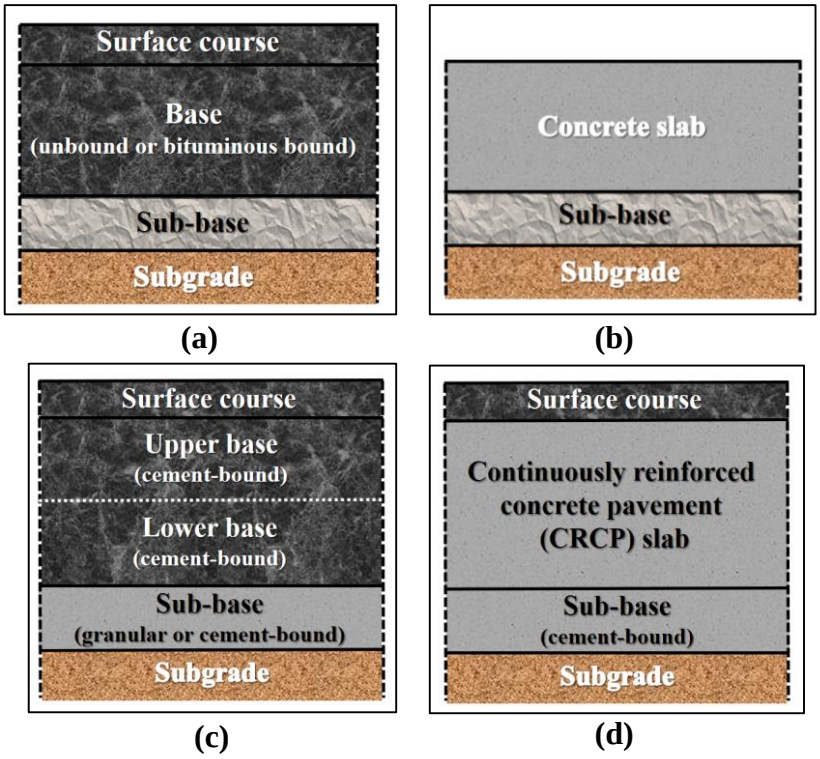

Figure 1. Typical cross section for: (a) flexible pavement structure, (b) rigid pavement structure, and (c) flexible-composite structure, (d) rigid-composite structure.

Flexible pavement structures, with a service life of 10-20 years, are used in traffic lanes with a wide range of traffic loading levels, ramps and parking areas. They are designed to bend, or flex, under loading and to spread the load from the top layer to the bottom layer. Thus, the applied compressive stresses, which are maximum at the top asphalt concrete (AC) layer and minimum on the top of the subgrade, are reduced. In addition, flexible pavement design structures are easily constructed and repaired, simply accepting additional thicknesses and adjusting themselves to limited differential settlement. Also, they are quieter than other pavement design structures.

The performance of flexible pavement structures has been investigated and characterised by several researchers in many previous studies. The main distresses of flexible pavement designs are fatigue cracking, permanent deformation (rutting) and thermal cracking. Fatigue cracking of flexible pavement could be a bottom-up (alligator) cracking phenomenon, which occurs due to horizontal tensile strain at the bottom of the asphaltic concrete layer.

However, a significant amount of fatigue cracking is also initiated at the pavement surface (top-down cracking) as a result of the complex contact stresses in the tyre-pavement interface. Permanent deformation (rutting) only happens along the wheel path on flexible pavements. Thermal cracking includes both low-temperature cracking and thermal fatigue cracking, which occur because of thermal stress exceeding the tensile strength of the asphalt concrete (AC).

In this chapter, a literature review pertinent to asphalt concrete pavement designs in the region and perpetual pavement designs and their fatigue characterisation approaches is presented. Moreover, major probabilistic analysis studies on fatigue characterisation of pavement mixtures are presented and discussed.

2.1 Asphalt concrete pavements studies in the Middle East region

The construction of highways and road networks in the Middle East region has experienced significant development in size and standards in the last 50 years. In Saudi Arabia, for instance, the total length of paved roadways in 1975 was 12,200 km, but, by 2000, the length had exceeded 40,000 km (Bubshait, 2001). Middle Eastern countries have invested hundreds of billions of dollars in the construction of new highways and paved roads to accommodate the rapid development rates that generated extremely large traffic volumes (Al-Abdul Wahhab, et al., 1999). However, the performance of these new highways against major distresses still needs a great deal of improvements and enhancement.

Only a few studies have been conducted in evaluating and improving the performance of the asphalt pavement mixtures and structures in Middle Eastern countries. Most of these regional studies considered the significant increase in the traffic loading, and the hot weather, which are the most important factors affecting the performance of the asphalt pavement designs (Al-Abdul Wahhab & Balghunaim (1994) and Al-Abdul Wahhab et al. (2001)). However, most of the studies focused on rutting as a major and prominent failure mode in the region; they did not give much attention to fatigue cracking, which is another major failure mode. In this

subsection, the main regional studies on performance evaluation and improvement are introduced and summarised. The main studied aspects and conclusions are highlighted, which will introduce the importance of the work of this thesis.

Bubshait (2001) discussed the main factors that contribute to the quality and the service life of asphalt concrete pavement structures in the Kingdom of Saudi Arabia. These factors are managerial-related factors (e.g. the contractor), design- and specifications-related factors, and construction-related factors. In order to identify the most affecting factors, a survey was prepared and forwarded to 61 highway contractors in Saudi Arabia. The results of the survey revealed that the asphalt pavement structures are not designed for regional conditions and the most important factors are the aggregate quality, aggregate characteristics and the mix design including bitumen characteristics. For example, unmodified 60-70 Pen bitumen is used widely in the Middle East; however, this bitumen is too soft given the high temperatures in the region. Therefore, it was suggested by Fatani, et al. (1992), Al-Abdul Wahhab and Balghunaim (1994) and Elseifi, et al. (2012) that either a harder bitumen or a polymer-modified bitumen (PMB) could be used to mitigate the poor performance that is associated with the use of unmodified 60-70 Pen bitumen. PMB has been found to enhance several properties of asphalt concrete (AC) mixtures such as temperature susceptibility, fatigue life, and resistance to permanent deformation (Al-Hadidy & Yi-qiu, 2010).

Al-Abdul Wahhab and Balghunaim (1994) stated that many parts of the highways in Saudi Arabia experienced severe levels of rutting just after being opened to traffic due to heavy traffic loading and high temperatures. The primary objective of this study was to demonstrate data on variations of temperatures of asphalt pavement structures in the arid coastal and inland Saudi environment. Asphalt concrete slabs of 150 mm, 200 mm and 300 mm thicknesses were constructed in Riyadh, the capital of Saudi Arabia, and a 250 mm asphalt-bound layer on top of a compacted aggregate sub-base was constructed in Dhahran, another city in Saudi Arabia.

The bitumen used was unmodified 60-70 Pen, which is locally produced and widely used in the region. Temperatures were measured for two years at the pavement surface, and at depths of 20, 40, 80 and 160 mm, as well as at the bottom of the pavement structure. In addition, the air temperature at a height of 1.5 m above the surface was measured as well. The data collected were statistically analysed and showed that the highest temperatures were at a depth of 20 mm and that, during the summer months, the temperature decreased as the pavement section depth increased. Moreover, it was concluded that rutting could be minimised and resisted by using modified bitumen that can withstand high temperatures.

Another regional study, by Al-Abdul Wahhab, et al. (1999), was conducted to specify possible factors for the premature rutting which occurred on many roads and highways in Saudi Arabia after a rapid increase in traffic volumes. Nineteen different test sections, each one kilometre in length, located on 12 major highways in Saudi Arabia were selected and subjected to field investigation and laboratory characterisations. Results depicted that rutting is affected directly by the percentage of air voids (AV), the percentage of voids in mineral aggregate (VMA), the percentage of voids filled with bitumen (VFB), resilient modulus (M_r) at 25 ºC, and bitumen viscosity. Furthermore, the rutting in the cores obtained from rutted test sections was localised only in the top 100 mm of the asphalt concrete layers, underneath the wheel path of the truck slow lane. Moreover, the study revealed that the pavement temperature approaches a high value of around 70 ºC during the months of May to September, which is one of the major external factors for rutting.

A comprehensive study by Al-Abdul Wahhab, et al. (2001) was carried out later based on his two previous studies, discussed earlier. This study was performed to discover trends of temperature variation and their consequences on the moduli of flexible pavement structures. A statistical model for the asphalt concrete resilient modulus (M_r), a second model to predict pavement temperature at different depths as a function of air temperature, and another model

for the resilient modulus-temperature correction factor correlation were all developed to be used in pavement analysis and design for Saudi Arabia. It was stated that no single study in Saudi Arabia had previously been conducted to develop mathematical models to simulate the temperatures to which local pavements are subjected and which are applicable to other parts of the Middle East region.

The advantages of utilising waste volcanic ash as a cheap local alternative to aggregate for pavement designs were investigated in a study conducted in Yemen by Naji and Asi (2008). This study contributed to waste management of this undesirable material. Four different mix designs of unmodified 60-70 Pen bitumen with replacement proportions for aggregate of 0, 10, 20, and 30% of the total weight of dry aggregate were used. The experimental results showed that the properties and characteristics of all mixes comprising volcanic ash aggregate, up to 20%, were within the specification limits of the Marshall mix design method. In addition, the resilient modulus (M_R) was increased, and the creep resistance properties improved. Mixtures with only 10% volcanic ash aggregate provided optimum results in terms of stripping resistance, creep resistance, fatigue and resilient modulus.

A study conducted in Jordan by Asi (2006) focused on a laboratory evaluation of the performance of stone matrix asphalt (SMA) mixtures compared to dense-graded mixtures in hot climates. SMA is a gap-graded mix with a high bitumen content, and is designed to provide better rutting resistance. The dense-graded mixture was designed according to the Marshall method and was used in this study with unmodified 60-70 Pen bitumen. Performance evaluation tests such as Marshall Stability, split tensile strength, resilient modulus, fatigue, and rutting testing were performed on both mixtures. Results concluded that the stability of Marshall mixtures is higher than SMA mixtures; however, the loss of stability of the Marshall mixtures is higher. In addition, SMA mixtures have better durability, lower fatigue life, and higher M_R values than Marshall mixtures. However, the test results indicated that the Marshall

mixtures resisted rutting better than the SMA mixtures. This result is counter-intuitive and might be affected by the limited number of specimens tested. The field performance of the SMA mixtures proved their superiority over conventional asphalt mixtures in terms of durability and resistance to rutting.

Al-Hadidy and Yi-qiu (2010) investigated the effect of Styrene-butadiene-styrene (SBS) and Starch (ST) used to modify bitumen on the performance of asphalt pavements. Marshall Stability, Marshall Quotient, tensile strength, tensile strength ratio, rutting resistance, flexural strength and resilient modulus tests were carried out on specimens of stone mastic asphalt concrete (SMAC) mixtures containing SBS and ST. The results of the tests depicted that the performance of SBS-modified SMAC is slightly better than ST-modified SMAC. In addition, the temperature susceptibility could be reduced by the addition of SBS and ST to the mixture.

Rutting has been the main failure mode considered in regional studies. However, fatigue cracking – especially top-down cracking – is also a prominent distress in the region because of the high traffic loading, low bitumen content used and over-compaction at relatively low temperatures. In addition, unmodified 60-70 Pen bitumen is extensively used in the region, despite evidence that this bitumen does not have the stiffness required to resist deformation at high temperatures. Therefore, the research study presented in this thesis was conducted to investigate all factors affecting the performance of the pavement structures and mixtures in the region, in particular against rutting and top-down cracking.

As mentioned earlier, Middle Eastern countries and specifically the State of Qatar are currently investing hundreds of billions of dollars in constructing their road networks and highways. The objective is to build a sustainable road network that is designed according to state-of-the-art standards and methods. Several field studies have shown that the current and projected traffic loads (axle weights and design traffic) are unprecedented in the State of Qatar.

Consequently, there is a need to evaluate whether the current mix designs and materials are suitable for these projected loads.

The only study available in the open literature about performance of pavement materials in Qatar was conducted by Masad, et al. (2011). The study aimed to make recommendations for materials and test methods that can be used to construct long-life roads that are necessary to support economic growth. Asphalt concrete materials that are used in road construction in Qatar were collected from different sources and field cores were extracted from in-service asphalt pavement structures. Many laboratory tests were performed to assess the physical, chemical, and mechanical properties of these materials. The study concluded that the conventional imported aggregates, Gabbro (igneous rock), can resist skid and degradation better than the local Limestone aggregates (sedimentary rock). However, Gabbro has less resistance to moisture damage than Limestone aggregate. In addition, the results of dynamic mechanical analysis tests performed on the asphalt mixtures demonstrated the benefits of using modified bitumen instead of the unmodified bitumen currently used in the country. Moreover, the results of the laboratory tests conducted on extracted field cores showed good resistance to permanent deformation (rutting); however, the field cores could be susceptible to fatigue cracking, given the low bitumen content used in these mixtures.

2.2 Perpetual pavement structures

The theory relating to perpetual, or long-life, flexible asphalt pavement structures is not new. The idea of full-depth asphalt pavements started in the 1960s and it has become a sustainable pavement alternative in the United States, United Kingdom, Europe and Far East for decades (Liu & Wang (2012) and Timm & Tran (2014)). Timm and Newcomb (2006) reported that the service life of long-life asphalt pavements could exceed 50 years. In addition, the cost of reconstruction at the end of the structural life is low and the amounts of non-renewable resources consumed, such as bitumen and aggregate, are significantly lower.

Ferne (2006) stated that a European study by the European Long-Life Pavement Group (ELLPAG) defined a long-life pavement as: “a well designed and constructed pavement that could last indefinitely without deterioration in the structural elements provided it is not overloaded and the appropriate surface maintenance is carried out”. The concept of perpetual flexible pavement structural design implies prevention of the onset of deterioration and distresses in the form of rutting and fatigue cracking (top-down or bottom-up) in the asphalt concrete (AC) layers, which is a result of increased traffic loading and high temperatures. This could be achieved by reducing the stress and the strain in the AC layers, either by increasing the thickness of the pavement layers or by using stiffer materials (Merrill, et al., 2006).

Many studies in the United States, Europe and Far East have shown the significantly improved performance of perpetual pavement structures in terms of resistance to surface distresses and deteriorations when compared to the conventional or “Determinate Life” pavement structures (Ferne (2006), Merrill, et al. (2006) and Timm & Newcomb (2006)).

Merrill, et al. (2006) reported some observations on the behaviour and performance of perpetual flexible pavement structures in a number of European countries. Results showed that all pavement sections with thin asphalt layers (< 80 mm) exhibited full-depth cracking in the asphalt layers. However, for the thicker pavements (> 290 mm of the asphalt layer), only 28% of the sections showed cracking, and that was confined to the top asphaltic layers (top-down cracking).

In another study, Timm and Priest (2006) reported the results from evaluating the performance of perpetual pavement sections with control sections that were constructed in China. These control sections were built with a thin AC layer on top of cement-stabilised granular layers, which is a commonly used highway design in China. The evaluation study was conducted by a team of pavement engineers and researchers representing transportation agencies and research centres in the United States. The results demonstrated that the perpetual

sections avoided the overstressing that causes early cracking, which happened in the control sections.

In another work by Timm, et al. (2014), two perpetual pavement structures were constructed in 2003 and were evaluated using the National Centre for Asphalt Technology (NCAT) Test Track. Figure 2 displays the as-built structural cross sections and instrumentation.

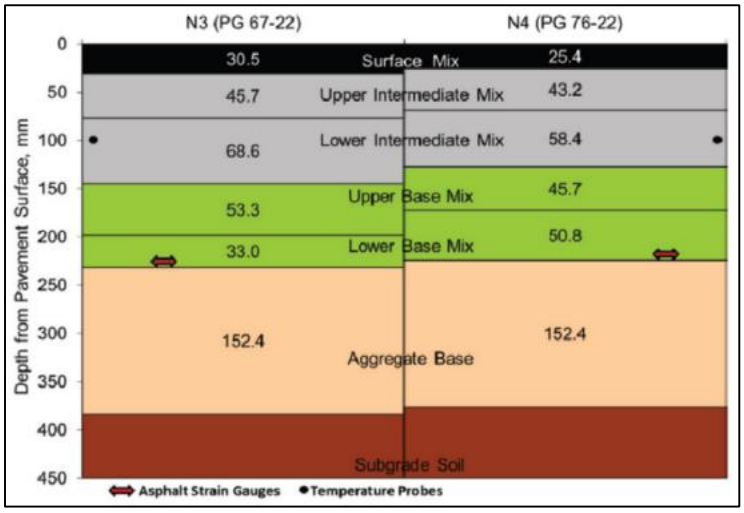

Figure 2. As-built structural cross sections and instrumentation (Timm, et al., 2014).

The asphalt concrete (AC) moduli of each structure were back-calculated from falling weight deflectometer (FWD) testing. The strain responses of AC layers relative to laboratory-determined endurance limits were measured to assess the pavement performance over time. The results showed increasing AC moduli of the test structures over time, which is indicative of an ageing pavement structure, without any crack propagation. In addition, the performance of both perpetual structures against rutting was excellent (< 8 mm). They had minor cracking and a very low International Roughness Index (IRI) value (< 1 m/km), which is expected for perpetual pavement structures.

Liu and Wang (2012) evaluated dense-skeleton asphalt-treated base (ATB) mixtures that were developed for perpetual pavement structures by conducting wheel tracking and indirect tensile (IDT) fatigue tests. The IDT fatigue test was performed using servo-hydraulic closed-loop testing equipment. The number of load cycles at which the stiffness decreases to

50% of the initial value was defined as the fatigue life of the specimen. The fatigue life was higher for the ATB mixtures than for the conventional mixtures.

In the State of Qatar, there have been significant efforts in the past eight years to improve specifications for pavement materials. The motivation of these efforts was the rapid increase of traffic loading and the realisation that current specifications do not accommodate the international developments in material testing and improvement of properties. This high traffic loading necessitates consideration of the design and construction of perpetual or "long-life" pavement structures. However, a comprehensive study with field and laboratory tests should be performed in order to examine their suitability for the conditions of the State of Qatar.

2.3 Fatigue characterisation of asphalt concrete mixtures

Fatigue cracking is one of the major and common load-related distresses for asphalt concrete pavement mixtures that causes loss of serviceability. It could be top-down or bottom-up cracking, and it occurs when an asphalt pavement structure is subjected to repeated heavy traffic loadings (Artamendi & Khalid (2005) and Bhasin, et al. (2009)). The bottom-up fatigue cracking happens in thin pavement structures ($\leq$ 50 mm) when the cracking initiates at the bottom of the hot mix asphalt (HMA) layers due to the high horizontal tensile stress, then propagates upward to the surface. The top-down fatigue cracking occurs in thick pavement structures ($\geq$ 150 mm) when the cracks start from the top in areas of high localised tensile stresses due to the tyre-pavement interaction and ageing of the bitumen, and then migrate downward (Molenaar, 1983). Fatigue cracking in general affects the ride quality significantly and can be a key factor for rehabilitation or replacement of an entire asphalt mixture (Kutay, et al. (2009) and Mbarki, et al. (2012)).

During the last five decades, many studies have been conducted to understand and characterise fatigue damage in asphalt concrete mixtures. Characterisation of fatigue cracking

is an important part of the development of a pavement design process. The fatigue failure of asphalt concrete mixtures is a complicated phenomenon because processes of crack initiation and propagation evolve under different physical laws (Gdoutos, 2005). It is difficult to characterise fatigue damage in hot mix asphalt (HMA) mixtures. This can be attributed to the composite nature of the material, the different constitutive laws that govern its constituents, the aggregate gradation, variation of bitumen film thickness within the mastic, air void size distribution and the dependency of bitumen behaviour on time and temperature (Masad, et al., 2008).

Several laboratory test methods are available for researchers in order to characterise fatigue cracking of asphalt bitumen, mastic and mixtures. These methods differ in the geometry of test specimen, loading mode and configuration, frequency of loading, rest periods, test temperature and form of cyclic load applied to the test specimen (Bhasin, et al., 2009). Furthermore, the fatigue test methods vary in their ability to simulate field conditions and in the applicability of test results for modelling and predicting asphalt pavement performance (Tangella, et al., 1990). Figure 3 illustrates the main configurations of fatigue tests; the arrows in each test set-up indicate the direction of the applied loading.

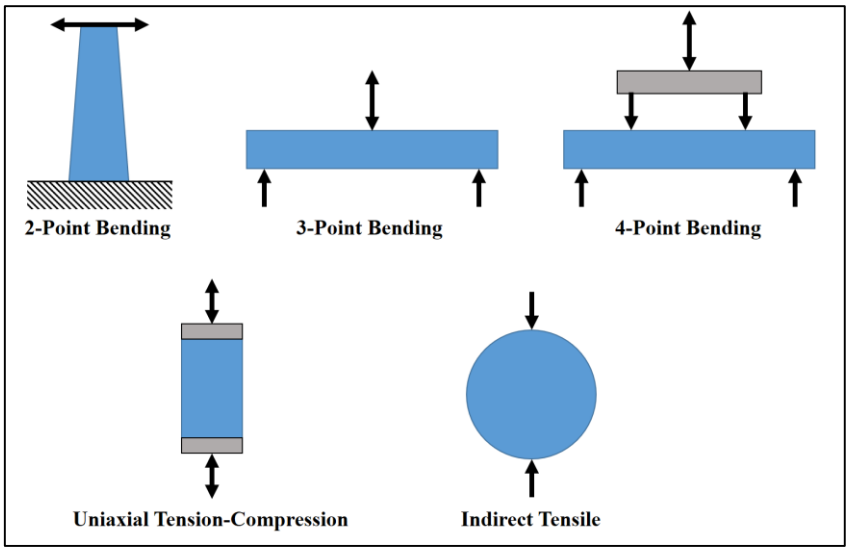

Figure 3. Schematic demonstrating the main fatigue test configurations.

Fatigue laboratory tests can be conducted under two loading modes: controlled-strain (or controlled-displacement) mode or controlled-stress (or controlled-load) mode. Controlled-stress mode has been recommended for mixtures that are used in thick pavement structures (or perpetual pavements) where high stiffness is the paramount parameter that reinforces fatigue life. Controlled-strain mode, in contrast, has been associated with thin flexible asphalt pavements where the elastic recovery properties of the material have a significant effect on its fatigue life (Artamendi & Khalid, 2005). In controlled-stress mode tests, the failure of the specimen is the criterion. In the controlled-strain mode tests, however, the loss of stiffness is the criterion for failure. In addition, fatigue test data are known to show more scatter in the controlled-strain mode, which makes it more difficult to interpret or analyse (Tayebali, et al. (1994) and Tangella, et al. (1990)).

Fatigue laboratory tests shown in Figure 3 are typically conducted in two different loading configurations or waveforms: repeated sinusoidal or cyclic haversine loading. In the sinusoidal loading, a repeated sine loading wave is applied to a specimen tested under 2-Point, 3-Point or 4-Point bending tests or the uniaxial tension or tension-compression (T/C) fatigue test. In the haversine loading, half the value of the versed sine loading wave (displaced sine wave with full amplitude on tension side of zero) is applied to a specimen tested under indirect tensile fatigue test.

Furthermore, the fatigue tests are also categorised into two types according to the stress-strain distribution throughout the tested specimen. If the stress-strain distribution is uniform, the test is called a homogeneous test, which is the case in the uniaxial T/C fatigue test. Otherwise, it is called a non-homogeneous fatigue test, as is the case in the bending tests and the indirect tensile test.

According to a study by Li, et al. (2013), the fatigue life results of a uniaxial T/C fatigue test are not affected by the specimen size, which is not the case for the results of other tests. In

addition, the uniaxial T/C fatigue test is a simple and efficient test in comparison to the traditional beam fatigue tests (Kutay, et al., 2008). For these reasons, this test was used later in this study to evaluate the fatigue cracking resistance of different asphalt mixtures.

The fatigue life of asphalt concrete mixtures is defined in a study by Si, et al. (2002) as "the number of loading cycles during which damage increases according to a crack propagation law from an initial undamaged state to a critical level". The fatigue process based on the fracture mechanics theory includes three distinctive stages: initiation, propagation, and finally failure.

Researchers have developed various experimental-based methods and analytical models to evaluate resistance to fatigue cracking of mixtures, and to develop a criterion for predicting fatigue life.

First, the classical fatigue empirical model by Monismith, et al. (1985) shown in equation 1 was proposed for the prediction of fatigue life (N_f) as a function of tensile strain/stress and initial stiffness of the mixture as follows:

$$\boldsymbol{N_f = a\left(\frac{1}{\varepsilon_0}\right)^b\left(\frac{1}{E_0^*}\right)^c} \quad \textbf{or} \quad \boldsymbol{N_f = a\left(\frac{1}{\sigma_0}\right)^b\left(\frac{1}{E_0^*}\right)^c} \qquad \textbf{Equation 1}$$

where, ε_0 is the strain amplitude; E_0^* is the initial dynamic modulus of the asphalt mixture; σ_0 is the stress amplitude; and *a*, *b* and *c* are the model parameters. This model was used in the Shell method in 1977 and then as the Asphalt Institute method in 1981 (Tsai, et al., 2005). However, this empirical method has several limitations and does not take into consideration the effect of viscoelasticity.

The dissipated energy (DE) approach hypothesised by Van Dijk and Visser (1977) is another fatigue characterisation approach proposed to predict fatigue life when the mixture is sinusoidally loaded. The total dissipated energy required for a complete failure due to fatigue damage is calculated from the total area enclosed by a stress-strain hysteresis loop multiplied

by the number of cycles (N). The development of this approach, its advantages and its limitations are presented in detail later in this thesis.

In addition, the viscoelastic continuum damage (VECD) approach was developed based on Schapery's viscoelastic constitutive theory (Schapery, 1987) to predict the fatigue life of asphalt mixtures. VECD theory ignores the micro-scale behaviour and attempts to describe the fatigue damage in a material on the macro-scale as a reduction in the effective stiffness (Lee, et al. (2000) and Underwood, et al. (2012)). Moreover, in the VECD approach, one uniaxial tension-compression (T/C) fatigue test is required to identify the fitting parameters of the mixture's damage characteristics curve (pseudo-stiffness-versus-internal damage curve) and then the fatigue life (N_f) can be predicted for any temperature, frequency or loading modes/levels. More details on this approach and its procedure are presented later in this thesis.

There are many different fatigue failure criteria discussed in the literature. First, fatigue life (N_f) is determined in many studies as the number of loading cycles corresponding to a 50% reduction of the initial stiffness or dynamic modules ($|E^*|$) of the test specimen. This failure criterion is commonly used in controlled-strain tests (AASHTO TP 8-64, 2002).

In some other studies, when a fatigue test is conducted with a constant frequency, the 50% reduction in pseudo-stiffness can be used as a failure criterion (AASHTO TP8-64 (2002) and Kutay, et al. (2008)). The pseudo-stiffness is the ratio between the dynamic modulus ($|E^*|$) at a test cycle and the initial linear viscoelastic dynamic modulus ($|E^*|_{LVE}$) value of an asphalt mixture.

Additionally, for analysing and interpreting fatigue test data, some researchers use a 90% reduction in the initial complex modulus of an asphalt mixture as a fatigue failure criterion, while fatigue life (N_f) in some studies is determined as the number of cycles corresponding to a 100% increase in the initial strain value (Bhasin, et al. (2009) and Al-

Khateeb (2011)). Furthermore, one of the failure criteria is defined as reaching a specific value or upper limit for phase angle (φ) during the fatigue test (Bhasin, et al., 2009).

In some research studies, the number of loading cycles corresponding to a rapid increase in the dissipated energy (DE) between consecutive cycles indicating growth of a macro-crack is also considered as a failure criterion.

Finally, the peak of the change in dynamic modulus is also a fatigue failure criterion, which is defined as the number of loading cycles at which the value of the function $\frac{N|E_N^*|}{|E_1^*|}$ becomes maximum (Castelo Branco, et al., 2008). However, this failure criterion has a very high coefficient of variation.

Referring to the literature, many studies have been conducted to evaluate the performance of asphalt concrete mixtures against fatigue cracking and to predict their fatigue life (N_f). Several studies implemented the DE approach with its different means (e.g. RDEC, DPSE, etc.) to evaluate the resistance of asphalt mixtures against fatigue cracking.

The raw data of the 4-Point bending tests conducted in a study by Artamendi and Khalid (2005) in order to investigate the fatigue characteristics of two asphalt concrete mixtures were analysed using the DE approach. Dense bitumen macadam (DBM) and stone mastic asphalt (SMA), typical mixtures used in road applications in the UK, were tested sinusoidally using the 4-Point bending fatigue test at a temperature of 10 °C and 10 Hz frequency with no rest periods. The test was conducted under controlled-stress (1.25 and 2 MPa peak-to-peak amplitudes) and controlled strain (125 and 200 peak-to-peak amplitudes) modes on beam specimens of 300 mm × 50 mm × 50 mm. The tested mixtures were evaluated using the dissipated energy ratio (DER) method which helped in ranking the mixtures in the same order as the classical approach.

In addition, Pasetto and Baldo (2015) investigated the performance of asphalt concrete mixtures for base courses, produced with conventional and polymer-modified bitumen against

fatigue damage by conducting the 4-Point bending test as well. The fatigue test was conducted in controlled-stress and -strain modes at a temperature of 20 °C and 10 Hz frequency without rest periods. The stress amplitudes used in the tests were 0.75, 1.00 and 1.25 MPa, while the strain amplitudes used in the controlled-strain tests were 250, 275 and 300 με (peak-to-peak). The fatigue test data of beam specimens (300 mm × 50 mm × 50 mm) were analysed using the DE approach and the classical method based on a 50% reduction in the initial stiffness of the mixture. The results revealed the advantage of implementing the DE approach over the classical approach and indicated the superiority of mixtures with PMB in resisting fatigue cracking.

In a study by Daniel et al. (2004), a comparison between the viscoelastic continuum damage (VECD) and dissipated energy (DE) approaches as fatigue characterisation approaches was performed under sinusoidal loading using uniaxial direct tension (DT) fatigue tests on eight different asphalt mixtures. The cylindrical specimens were cored to be 75 mm in diameter and 150 mm high. The cyclic fatigue test was controlled-strain at different strain amplitudes and conducted at a frequency of 10 Hz and temperatures of 5 and 20 °C. The failure criterion was defined as a 50% reduction in initial stiffness of the tested specimen. The study concluded that the fatigue lives (N_f) obtained using the VECD and DE approaches were highly correlated. In addition, the VECD approach successfully ranked the mixtures' performance against fatigue even with various air voids and bitumen contents for a particular gradation.

Haggag, et al. (2011) performed uniaxial tension-compression (T/C) fatigue tests on warm-mix asphalt (WMA) mixtures produced using PG64-22 virgin bitumen with different WMA technologies (Advera, Evotherm 3G and Sasobit). The tests were conducted at temperatures of 4 and 20 °C at a frequency of 10 Hz by using a low strain level of 150 με and a high strain level of 260 με (peak-to-peak) in order to evaluate the impact of the three WMA additives on the fatigue cracking resistance using the VECD approach. The results concluded

that the use of Advera enhanced the WMA's fatigue performance and increased its fatigue life (N_f) slightly, but further investigation is needed.

In an experimental study by Kutay, et al. (2008), a uniaxial T/C fatigue test was performed on laboratory specimens prepared from 12 different polymer-modified asphalt mixtures. These mixtures were used in the field lane tests at the Accelerated Loading Facility (ALF) of the Turner-Fairbank Highway Research Center in the US. The uniaxial T/C fatigue test was conducted using a servo-hydraulic Material Testing System (MTS) machine to predict the fatigue life of the mixtures under both loading modes: controlled-stress and controlled-strain. The applied peak-to-peak stress in the controlled-stress test was 1220 kPa, while, in the controlled-strain test, the peak-to-peak strain level was 300 με. The tests were performed at a temperature of 19 °C and a frequency of 10 Hz. The failure criterion was selected to be 50% reduction in pseudo-stiffness (C) of the tested mixtures. The results revealed that the predicted fatigue life (N_f) using the controlled-strain fatigue test matched the trend of the field performance. In addition, it was stated that the use of the VECD approach was useful to characterise the performance and predict the service life of the asphalt mixtures.

A study by Mbarki, et al. (2012) inspected the fatigue resistance of field specimens obtained from different field lanes located in Virginia in the US, as well as laboratory-produced specimens prepared using the same materials and mix designs as the field specimens. Fatigue testing was conducted using the uniaxial (T/C) fatigue test on the AMPT in controlled-strain mode (300 με peak-to-peak) at a temperature of 19 °C and a frequency of 10 Hz. The test results for each mixture were analysed using the VECD approach. Comparisons were made between the laboratory and field specimens and the analysis findings revealed that the specimens exhibited different damage characteristic curves and different fatigue lives (N_f). In addition, it was noticed that ageing of the field specimens had affected the performance of PMB mixtures.

Many studies have clearly shown the advantages of using the viscoelastic continuum damage (VECD) approach in assessing the performance of AC mixtures against fatigue damage. However, the VECD analysis performed in these studies was based on the average values of the fatigue test data and neglected any variations or uncertainty in the fatigue life (N_f) inputs of the specimens for the same mixture. Therefore, it is necessary to transform the deterministic fatigue characterisation approach to a probabilistic approach to account for variability in the inputs. The following subsection concentrates on previously performed probabilistic analysis studies of fatigue damage characterisation.

2.4 Probabilistic analysis of fatigue characterisation

Uncertainty is inevitable in real-world applications and one of these is the performance evaluation of asphalt concrete (AC) mixtures against fatigue cracking. Essentially, performance evaluation of AC mixtures is complicated due to uncertainty in the mixtures themselves. In a study by Mehrez, et al. (2015), the primary sources of uncertainty in AC mixtures were categorised and summarised as follows:

1. Aggregate phase: material and geometric properties in addition to the spatial distribution.
2. Fine aggregate matrix (FAM) phase: material properties, temporal dependency, spatial distribution, adhesive and cohesive properties besides damage initiation and development.
3. Air void phase: spatial distribution, connectivity and tortuosity in addition to temporal variation with damage.

It is well known that fatigue characterisation is complicated, regularly showing extensive scatter because fatigue resistance of asphalt mixtures is affected by an assortment of factors. These factors can be summarised as temperature, surface finish, loading conditions, microstructure heterogeneity and ageing effects (Darter, et al. (1972), Tigdemir, et al. (2002),

Masad, et al. (2008) and Xiao, et al. (2009)). Accordingly, the uncertainty associated with fatigue tests and specimen sizes, along with the fatigue models and the variability of their input parameters, has a major influence on the predicted fatigue life (Luo, et al., 2013).

The conventional fatigue characterisation approaches of asphalt pavement mixtures presented in the previous sections (e.g. DE, DPSE, VECD, etc.) are deterministic, in which all input parameters are considered as fixed and deterministic values. However, the input parameters of the models have uncertainty, especially for specimens prepared from field mixtures (Liu (2014) and Luo (2014)).

Based on the results of several fatigue characterisation studies, the deterministic prediction of fatigue life (N_f) of asphalt mixtures may not be sufficient or meaningful due to the significant scatter in the input data and the results (Jie, et al. (2011) and Luo, et al. (2013)).

To investigate the effect of uncertainty and variability in asphalt concrete mixtures on fatigue life prediction, a probabilistic or a reliability-based analysis approach is appropriate and needed. However, only a limited number of studies on the probabilistic analysis approach of asphalt mixtures, especially for fatigue resistance evaluation, are available in the literature. In the following subsections, different probabilistic approaches used in fatigue analyses are presented and discussed.

2.4.1 Reliability index approaches

The concept of reliability in pavement design was addressed as early as the 1970s. From an engineering point of view, reliability can be defined as the ability of a system or component to perform its required functions under stated conditions for a desired service life. In other words, it is complementary to the probability of failure (p_f):

$$\boldsymbol{Reliability}\ (\boldsymbol{R}) = \mathbf{1} - \boldsymbol{p_f} \qquad \textbf{Equation 2}$$

For asphalt concrete mixtures, reliability is defined as the probability that the allowable number of loading cycles (N_{all}) would be greater than the number of applied loading cycles (N_{app}). The N_{all} and N_{app} values are independently affected by many uncertain inputs and are treated as random variables (RV). The classical approach to estimate the failure risk is made using factor of safety (FOS), as discussed by Maji and Das (2008):

$$FOS = \frac{N_{all}}{N_{app}} \qquad \textbf{Equation 3}$$

The pavement structure is considered safe if the FOS is greater than one or if the safety margin (SM = N_{all} – N_{app}) is more than zero (Harr, 1987). The probability of failure (p_f) is dominated by the amount of overlap of the probability density functions (pdf) of N_{app} and N_{all} [$p_f = p(SM \leq 0)$], as shown in the shaded area of Figure 4.

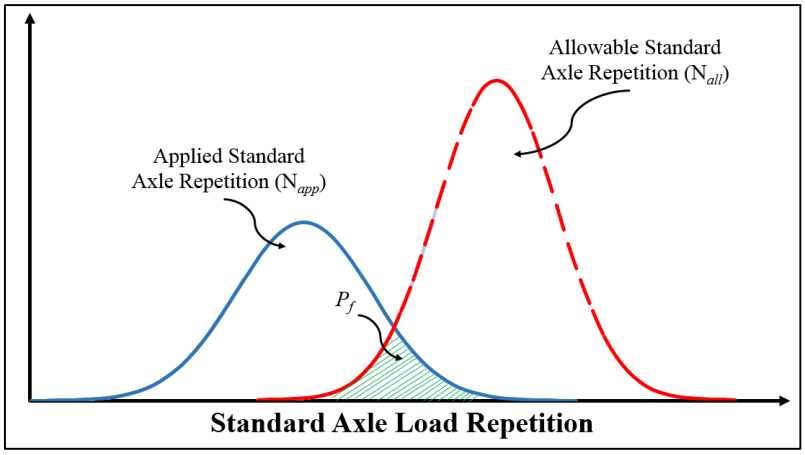

Figure 4. Schematic plot of probability distributions of allowable and applied standard axle repetitions.

The mean of the safety margin (μ_{SM}) follows a distribution function depending on those of N_{all} and N_{app}. Then, by assuming that N_{all} and N_{app} are independent, uncorrelated and normally distributed RVs, the mean values of N_{all} and N_{app} are used to determine the mean value of the safety margin (μ_{SM}) as follows:

$$\mu_{SM} = \mu_{all} - \mu_{app} \qquad \textbf{Equation 4}$$

Then, the standard deviation of the safety margin (σ_{SM}) can be calculated using the standard deviations of the allowable and the applied number of loading cycles (N_{all} and N_{app}):

$$\boldsymbol{\sigma_{SM} = \sqrt{\sigma_{all}^2 + \sigma_{app}^2}} \qquad \textbf{Equation 5}$$

In order to evaluate the reliability of a pavement mixture/structure against a distress type, the reliability index (β) is calculated as a ratio between the mean value of the safety margin (μ_{SM}) and its standard deviation (σ_{SM}) as per Maji and Das (2008):

$$\boldsymbol{\beta = \frac{\mu_{SM} - SM}{\sigma_{SM}}} \qquad \textbf{Equation 6}$$

where, the asphalt concrete mixture/structure is considered safer with a bigger reliability index value (smaller variation "σ").

Referring to the literature, there are a number of methods by which the reliability index (β) can be developed and calculated. The following subsections briefly discuss these methods and present some related studies from the literature.

2.4.1.1 Point estimate method (PEM)

The point estimate method (PEM) is a simple and efficient reliability index (β) method originally developed by Emilio Rosenblueth (1975). In the PEM method, the moments of an output function of independent and uncorrelated random variables are numerically approximated. Starting from the low-order moments of the independent input variable (x), the PEM method provides approximations for the low-order moments for the dependent output variable (y) (Christian & Baecher, 1999). If the distribution function of the input variable (x) is assumed to follow a normal distribution function for simplicity, the mean value (μ_x) plus and minus one standard deviation (σ_x) are estimated (Luo, et al., 2013). Then, the output function [$y_{\pm} = f(x_{\pm})$] can be used to determine the distribution function and the moments of the output y, as shown in Figure 5.

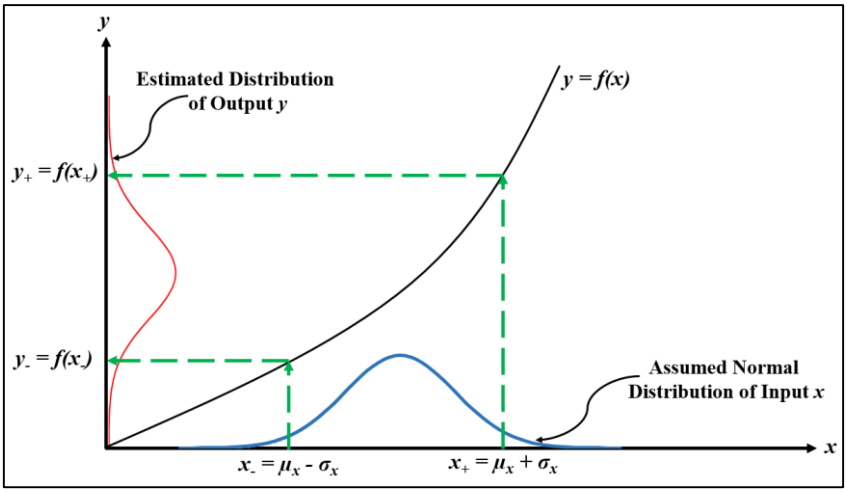

Figure 5. Illustrative diagram for the point estimate method with one normal distributed input.

Subsequently, the mean (or expected value) and the standard deviation of the estimated normally distributed output, μ_y and σ_y, are determined as follows:

$$\boldsymbol{\mu_y = E[y] = p_+ y_+ + p_- y_-} \qquad \textbf{Equation 7}$$

$$\boldsymbol{\sigma_y = \sqrt{E[y^2] - (E[y])^2}} \qquad \textbf{Equation 8}$$

where, p_+ and p_- are the weighting factors equal to 0.5 for the non-skewed distributions such as normal distribution. If the output function involves more than one input variable, the PEM method can be easily adapted for the probabilistic analysis [e.g. $y = f(x_1, x_2, x_3)$].

Consequently, the reliability index (β) under the normal distribution assumption for the random variables can be calculated similar to equation 6, as per Luo, et al. (2013).

This method is straightforward and easy to implement compared to other probabilistic methods (Christian & Baecher, 1999). However, it has some limitations and disadvantages, which will be discussed in the subsection on the next reliability index method.

2.4.1.2 First-order second-moment (FOSM) method

The first-order second-moment (FOSM) method is another well-known reliability index (β) method, which is used to determine the stochastic moments of a function with random variables (x_i). This method is also referred to as a mean value first-order second-moment

(MVFOSM) method. FOSM takes the first-order (moment) of Taylor series approximation of the limit state function of independent, uncorrelated and normally distributed RVs with the mean values as:

$$\boldsymbol{E[g(x_1, x_2, \dots, x_i)] = g(\mu_1, \mu_2, \dots, \mu_i)} \quad \textbf{Equation 9}$$

Then, by taking the second moment of the random variables and the first order terms of the Taylor series approximation, the variance can be determined as (Maji & Das, 2008):

$$\boldsymbol{V[g(x_1, x_2, \dots, x_i)] = \sum_1^i \sum_1^j \left(\frac{\partial g}{\partial x_i}\right)\left(\frac{\partial g}{\partial x_j}\right) \times COV[x_i, x_j]} \quad \textbf{Equation 10}$$

The mean and variance equations can be used to calculate the reliability index (β) of a system, as discussed earlier in equation 6.

However, reliability index (β) methods (PEM and FOSM) have some limitations and deficiencies. They do not use the actual distribution of the random variable but transform it to the standard normal or log-normal distribution for simplicity. In addition, if the output function is non-linear, neglecting the higher-order term in the Taylor series expansion introduces significant error in the calculation of reliability index (β). The more important observation is that the PEM and FOSM methods do not lead to the same value of probability of failure (or β) for mechanically equivalent formulations (FOS and SM) of the same performance output function (Maji & Das (2008) and Retherford & McDonald (2010)).

2.4.2 Graphical and mathematical methods

Graphical and mathematical probabilistic methods were proposed for fatigue failure of concrete by McCall (1958) and then modified slightly by Singh, et al. (2006). In a study by Graeff, et al. (2012), both methods were explained, implemented and then their results were compared. The study aimed to develop an understanding of fatigue behaviour of asphalt concrete (AC) mixtures reinforced with recycled steel fibres recovered from old tyres. Seven different AC mixtures were used to prepare 118 prisms (150 × 150 × 550 mm) for a controlled-

stress cyclic third-point flexural fatigue test, and the crack mouth opening was measured. The tests were conducted in a three-specimen set-up (Figure 6) with the cyclic loads applied at three different flexural stress levels (0.5, 0.7 and 0.9), which is the ratio between the dynamic flexural strength and the static peak flexural strength.

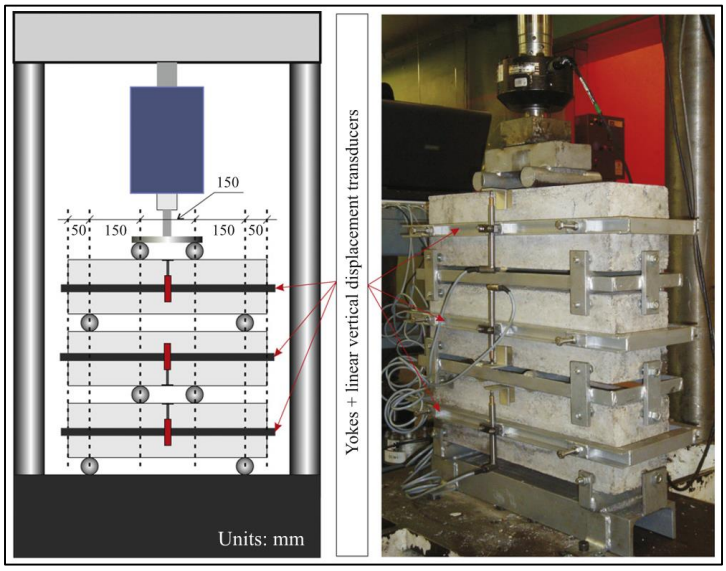

Figure 6. Set-up of fatigue test (Graeff, et al., 2012).

In addition, the test was conducted at a frequency of 15 Hz, with rollers between the specimens to transfer the load, and the preselected failure criterion was to reach 2 million cycles (a criterion commonly used for concrete fatigue tests) unless one of the specimens failed earlier. The probability of fatigue failure (p_f) for these specimens was estimated based on the applied stress levels and the number of cycles using the graphical and mathematical methods.

In the probabilistic graphical method, the mean (μ) and the standard deviation (σ) values of the fatigue test output (number of cycles to failure ($\log(N_i)$)) for each stress level and each specimen of the mixture were initially calculated. Then, the specimens were ranked according to the increasing number of cycles for each stress level. The p_f was obtained by dividing the rank of the specimen *i* by (n+1), where "n" is the total number of tested specimens per stress level. After that, the stress-log(N) linear regression curves for each p_f were obtained,

as shown in Figure 7a. Then, the p_f-log(N) plot shown in Figure 7b was used with the stress-log(N) plot to graphically interpolate the stress-p_f plot.

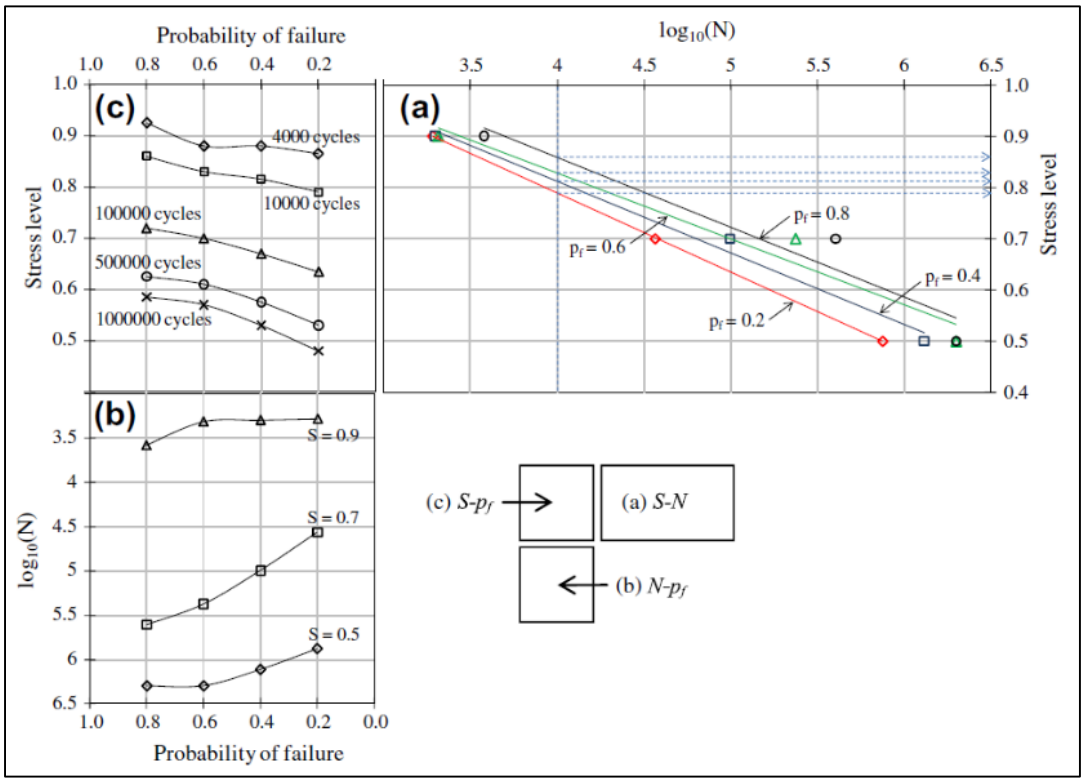

Figure 7. Family of stress-log(N)-p_f curves of one of the tested mixtures (Graeff, et al., 2012).

In contrast, the probabilistic mathematical method was implemented in the study by Graeff, et al. (2012) by deriving a general equation for the p_f by utilising the experimental fatigue raw data and stress-log(N)-p_f curves for each probability of failure (p_f) and stress level as follows (Graeff, et al., 2012):

$$p_f = 1 - 10^{-aS^b logN^c} \qquad \textbf{Equation 11}$$

where, S is the stress level; N is the number of cycles; and a, b and c are experimental constants that can be determined for each mixture by procedures explained in McCall (1958), and Singh, et al. (2005) and (2008).

A comparison between the results of the graphical and mathematical methods for one of the tested mixtures in this study is shown in Figure 8.

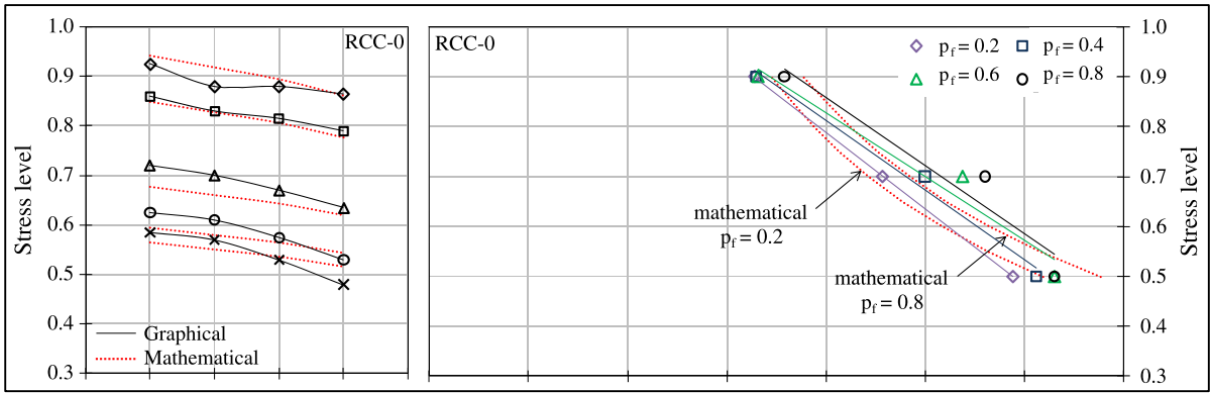

Figure 8. Family of S–p_f and S–N curves of one of the tested mixtures (graphical and mathematical methods) (Graeff, et al., 2012).

The results for both methods in most mixtures tested in this study were not identical due to the low number of results for each stress level. However, it was stated that the mathematical method was simpler and more accurate in its results than the graphical method (Graeff, et al., 2012).

2.4.3 Monte Carlo simulation (MCS) method

Monte Carlo Simulation (MCS), which was invented in the late 1940s, is the most accurate probabilistic analysis method. MCS is always being used in different fields to realise the effect of uncertainty in any estimating model. MCS approximates the probability of a certain deterministic model by running a large number of simulations using the entire distributions of the random variables (Maji & Das (2008) and Retherford & McDonald (2010)). Monte Carlo Simulation has been applied to an extremely varied range of problems involving random behaviour in science, engineering, finance and applications in almost every industry. However, the trade-off is that extensive computational time is required (Luo (2014) and Retherford & McDonald (2010)).

The MCS process starts by identifying the distribution function for each random variable and also any joint distribution between the random variables of the output model. Then, a large number of simulations (e.g. one million) are generated for each distribution and they are used to estimate the models' output in the shape of a cumulative distribution function

(cdf) describing the area under a probability density function (pdf) from minus infinity to a specific value of the output.

In a study by Luo, et al. (2013), two probabilistic approaches, Point Estimate Method (PEM) and Monte Carlo Simulation (MCS), were employed in order to investigate the effect of parameter uncertainty on the predicted fatigue life (N_f) of rubberised asphalt mixtures containing crumb rubber and/or reclaimed asphalt pavement. A total of 248 specimens of rubberised asphalt concrete beams were tested under controlled-strain repeated sinusoidal loadings at a frequency of 5 Hz, and temperatures of 5 °C and 20 °C, according to the AASHTO fatigue test procedure (AASHTO TP T 321-03, 2007). The classical fatigue empirical model defined by Monismith, et al. (1985) and shown earlier in equation 1 was used in a simplified view of variables by transforming it logarithmically as:

$$\boldsymbol{log\ N_f = log\ a - b\ log\varepsilon_0 - c\ logE_0^*} \qquad \textbf{Equation 12}$$

This logarithmic empirical fatigue model, in addition to two conventional statistical models based on voids filled with bitumen (VFB) and initial air voids (V_0), was used in this study as follows:

$$\boldsymbol{\ln(N_f) = a - b\ln(\varepsilon_0)\ - c\ \ln(E_0^*) + E} \qquad \textbf{Equation 13}$$

$$\boldsymbol{\ln(N_f) = d + e\ln(\varepsilon_0) + f\ VFB + g\ \ln(E_0^*) + E} \qquad \textbf{Equation 14}$$

$$\boldsymbol{\ln(N_f) = h + i\ln(\varepsilon_0) + j\,V_0 + k\ln(E_0^*) + E} \qquad \textbf{Equation 15}$$

where, *a* through *k* are regression coefficients obtained using the least square analysis, and *E* represents the model error.

The PEM method was adopted first under the normal distribution assumption of inputs and output (*y*) to calculate the reliability index (β), as discussed previously. The fatigue failure criterion was chosen as the point of failure to satisfy the minimum life of 10,000 cycles, as

displayed in Figure 9. Therefore, the probability that fatigue life is less than the limiting life ($N_{f\,lim}$) can be computed as follows:

$$\boldsymbol{p_f = P\left[y < N_{f\,lim}\right] = 1 - \Phi(\beta)} \qquad \textbf{Equation 16}$$

where, Φ is the cumulative standard normal distribution of the reliability index (β).

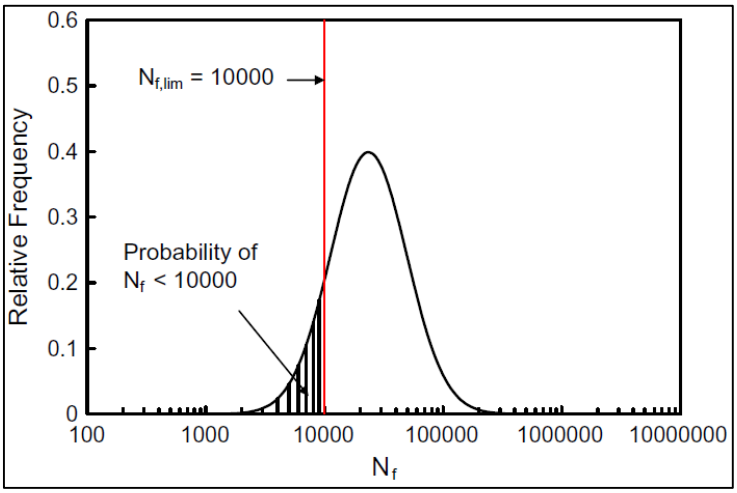

Figure 9. Example of the probability of fatigue life (p_f < 10,000) under normal distribution of ln(N_f) (Luo, et al., 2013).

Furthermore, the accuracy and effectiveness of the PEM approach were compared to those of the MCS method in the same study. The input parameters of the three fatigue models presented above were randomly generated from their assumed normal distributions and, after a number of simulations (n), the probability of fatigue failure (p_f) was computed as:

$$\boldsymbol{p_f = \frac{n_f}{n}} \qquad \textbf{Equation 17}$$

where, n_f is the number of simulations counted when the predicted fatigue life is smaller than the limiting fatigue life (i.e. $N_{f\,lim}$ = 10,000). As shown in Figure 10, both approaches, PEM and MCS, were surprisingly identical and generated a similar probability of fatigue failure in different cases (Luo, et al., 2013). In this study, the variation of input parameters such as ln(ε_0), VFB, V_0 and ln(E_0^*) was very small and their coefficient of variation (COV) was assumed to be the same for simplicity (Luo, et al., 2013). This explains how the PEM and MCS methods provided the exact same results.

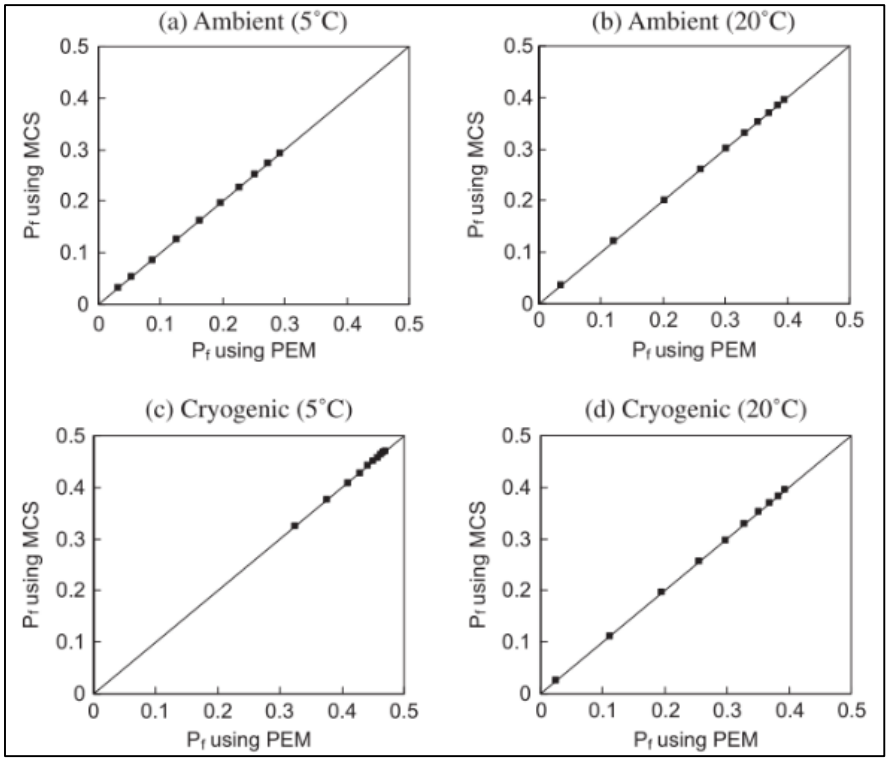

Figure 10. Comparison of the estimated probability of fatigue failure (p_f) between PEM and MCS methods using the conventional fatigue failure empirical model (Luo, et al., 2013).

In a study by Luo et al. (2014), an efficient approach for reliability-based mechanistic-empirical pavement design considering fatigue cracking and rutting was developed. The reliability-based (β) approach was implemented in a spreadsheet, which necessitates much less computational effort, and was compared to the use of the MCS method. The classical fatigue empirical model described earlier in equation 1 was used for fatigue cracking analysis and the following empirical model suggested by the Asphalt Institute was used for the number of loading cycles to rutting (permanent deformation) failure:

$$N_f = a\left(\frac{1}{\varepsilon_v}\right)^b \qquad \textbf{Equation 18}$$

where, ε_v is the vertical compressive strain developed at the top of the subgrade layer of the asphalt concrete pavement structure, and a and b are the model parameters.

In the developed reliability-based (β) approach of this study by Luo et al. (2014), several input parameters (wheel loads, asphalt layers in addition to granular layer and subgrade properties) were treated as random variables and assumed to follow normal distributions. The

results of the reliability-based (β) approach were compared to those obtained using MCS and both approaches yielded comparable results (Luo, et al., 2014).

2.5 Conclusions

This chapter has provided an overview of and discussed the main regional studies on asphalt concrete mixtures in addition to the studies in the literature on the use of perpetual pavement structures. Then, the major fatigue characterisation approaches have been summarised, and the available studies on the probabilistic analysis of fatigue characterisation described and discussed.

The literature review in this chapter shows that rutting (permanent deformation) has been the main failure mode considered in regional studies. However, observations in the region and specifically in Qatar indicated that longitudinal (top-down) cracking is also a prominent distress. No data are available for the performance of in-service pavement structures, but top-down cracking is shown on the existing roads in Qatar. This can be attributed to the uncontrolled huge traffic loading, ageing of the bitumen reflected in a sharp increase in stiffness, low bitumen content used and over-compaction performed at a relatively low temperature, as will be shown later in this study. In addition, unmodified 60-70 Pen bitumen is extensively used in the region despite the fact that this bitumen does not perform well under the range of temperatures in Qatar. The previous regional studies show the poor performance of the existing mix designs and materials including the unmodified 60-70 Pen bitumen against different distresses. The majority of the test methods currently specified in the Qatar Construction Specifications (QCS (2010)) predate the Superpave method. However, around 2009, some new projects started to use polymer-modified bitumen (PMB), replacing unmodified 60-70 Pen bitumen.

Several international studies have shown the significantly improved performance of perpetual pavement structures in terms of resistance to surface distresses and deteriorations

when compared to the conventional or “Determinate Life” pavement structures. The high traffic loading in the State of Qatar necessitates considering the design and construction of perpetual or long-lasting pavement structures.

In addition, the presented fatigue characterisation approaches revealed that the dissipated energy (DE) approach in its latest form comprises all factors affecting fatigue cracking, while the viscoelastic continuum damage (VECD) approach describes the fatigue damage on a macro-scale as a reduction in stiffness. Moreover, in the VECD approach, only one uniaxial (T/C) fatigue test is needed to identify the fitting parameters (*a* and *b*) and then the fatigue life can be predicted for any temperature, frequency or loading modes/levels. However, the deterministic prediction of fatigue life (N_f) of asphalt mixtures may not be sufficient or meaningful due to the variability in the input parameters which is affecting the reliability of the output results. In the literature, a few probabilistic analysis studies could be found that account for the high variability in estimating and predicting fatigue life (N_f). However, the empirical fatigue models (e.g. Equation 1) used and the probabilistic analysis methods implemented were not suitable enough to help engineers in predicting fatigue life of asphalt mixtures accurately.

Accordingly, in-depth research is needed to better characterise the resistance of flexible pavement structures and asphalt mixtures to different common distresses for the State of Qatar. The following chapters discuss the performance evaluation of altered asphalt concrete mixtures and structures using different field and laboratory tests, and different analysis approaches in addition to the performance prediction using the Mechanistic-Empirical Pavement Design Guide (M-E PDG) software. In addition, a probabilistic analysis is also needed to provide a more rational fatigue characterisation, fatigue life prediction, and decision-making for the design of asphalt concrete mixtures.

3 Performance Evaluation of Alternative Conventional and Perpetual Pavement Structures

The State of Qatar is experiencing tremendous growth in infrastructure including the road network and highways. The current methods used in the design of asphalt concrete structures in the country are empirical and might not be suitable for the design of long-lasting or perpetual pavement structures. Given the significant increase in traffic, the Public Works Authority (PWA) in the State of Qatar has developed several programmes and initiated projects to enhance the specifications and design of pavement structures in Qatar. One of these initiatives is the "Road Pavement Technology" project with the Transport Research Laboratory (TRL). This project involves reviewing conventional asphalt concrete pavement structures and assessing their performance besides developing new pavement structures for Qatar. Road authorities (i.e. PWA and TRL) in the State of Qatar have been considering the use of mechanistic-empirical methods in the design and analysis of asphalt concrete pavement structures. Therefore, a comprehensive study was needed in the country in order to identify the major distresses from which pavement structures are suffering and propose solutions to improve their performance. Thus, as a starting point for this study, the asphalt pavement structures used currently in the State of Qatar need to be evaluated thoroughly against different distresses and deteriorations.

In this chapter, the conventional asphalt concrete pavement structures available in the Qatar Highway Design Manual (QHDM, (1997)) are evaluated against major distresses and compared to a proposed perpetual (long-lasting) pavement structure. This evaluation is performed using the Mechanistic-Empirical Pavement Design Guide (M-E PDG) software that is going to be part of the new design manual in Qatar. A life-cycle cost analysis (LCCA) is then performed to determine the pavement structure with the highest net present value (NPV) among the various options investigated.

In order to investigate the field performance of perpetual pavement structures in Qatar, a full-scale trial road with six different pavement sections was constructed by TRL in 2010 on a route used by heavy truck traffic. The conditions, performance and mechanical properties of these trial sections were evaluated after a year and a half of service by conducting several measurements and field tests.

The main objective of this chapter is to specify firmly the main distresses affecting the performance of asphalt concrete pavement structures in Qatar and propose solutions to these issues.

3.1 Performance evaluation of conventional and perpetual pavement structures using M-E PDG software

In the first part of this assessment analysis, the conventional asphalt pavement structures in the State of Qatar and a proposed perpetual pavement structure are assessed against cracking, deformation and smoothness using the M-E PDG software. The following subsections describe the methodology, assumptions and limitations of the software as well as the performance evaluation results for the assessed pavement structures.

3.1.1 M-E PDG methodology

The Mechanistic-Empirical Pavement Design Guide (M-E PDG) software, version 1.1 (Applied Research Associates, Inc., Arizona State University, USA (2009)), has been developed under the National Cooperative Highway Research Program (NCHRP) Project 1-37A by the AASHTO Joint Task Force and a research team consisting of several internationally recognised asphalt pavement design experts. This software includes procedures for the evaluation, analysis and design of existing, new, reconstructed, and rehabilitated asphalt concrete pavement structures.

The software is based on an iterative process of a mechanistic-empirical design procedure and is briefly illustrated in the flowchart in Figure 11.

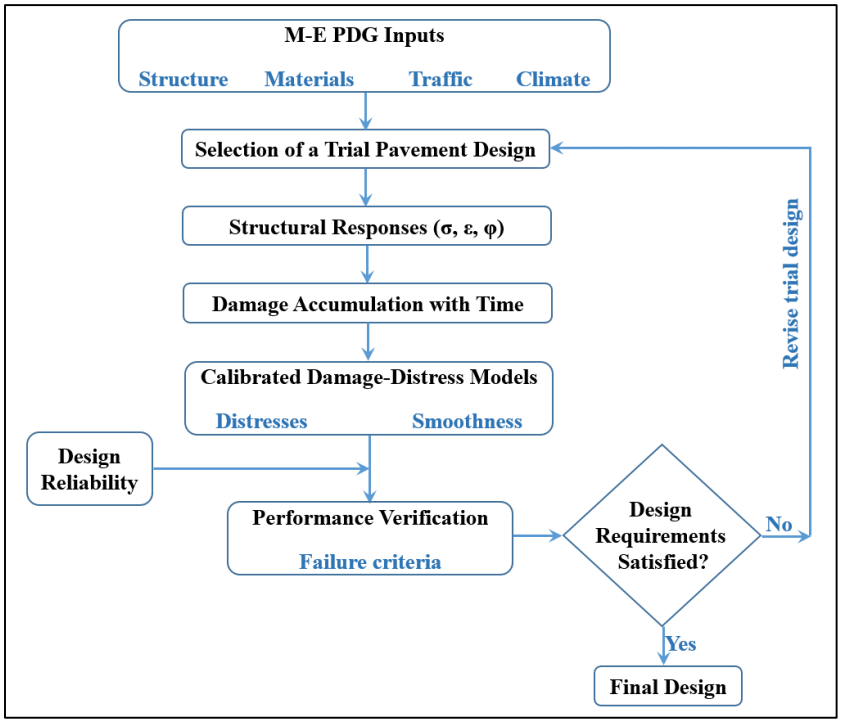

Figure 11. M-E PDG design iterative process flowchart.

Referring to the flowchart in Figure 11, the designer starts with the inputs of a trial pavement design, which includes the structure, materials, traffic loading and climatic conditions. Then, the M-E PDG software estimates the damage and main distresses over the design life (i.e. 20 years) of this trial pavement structure. Finally, the design is verified against the performance criteria and may be modified as needed to meet performance and reliability requirements.

The M-E PDG is used at input level 3 in all analyses documented in this study because levels 1 and 2 require detailed inputs that are not available yet in Qatar. Input level 3 provides some default and typical average values for the traffic volume adjustment factors, axle load distribution factors and axle configuration for the selected region/city. The M-E PDG software implements a combined group of mechanistic-empirical models for climate, traffic and materials to predict future performance in terms of cracking, rutting, faulting, etc. Thus, this will provide more appropriate designs and better performance for asphalt concrete pavement structures (Ceylan & Coree (2008) and Ceylan, et al. (2009)).

In order to consider the effect of climatic conditions on performance, temperatures and moisture profiles in the pavement structure and subgrade and the temperature gradient over the asphalt concrete thickness are all modelled using the Enhanced Integrated Climatic Model (EICM) software, which is incorporated into the M-E PDG software. The EICM is a one-dimensional coupled heat and moisture flow program that simulates changes in the behaviour of asphalt pavements and subgrade materials in conjunction with climatic conditions over 20 years of service. The M-E PDG user recalls climatic inputs by simply selecting a climate file for a particular weather station in the existing database.

Traffic loading data are another main input for performance evaluation in the M-E PDG software. Unfortunately, detailed traffic data in Qatar are not available for the M-E PDG analysis. Therefore, the default loadings from the QHDM were employed in this study. The traffic module of the software asks for the 2-way Annual Average Daily Truck Traffic (AADTT) as input. Then, the axle load distribution for single, tandem, tridem and quad axles is created over the design life to accurately determine the 80 kN (18 kips) Equivalent Single Axle Loads (ESALs) that will be applied to the AC pavement structure in each time increment of the damage accumulation process. To create this axle load distribution, the software assumes the following values:

- Design life (years): 20
- Number of lanes in design direction: 2
- Percentage of trucks in design direction: 50%
- Percentage of trucks in design lane: 95%
- Operational speed (mph): 60
- Traffic growth: 4%

At input level 3, the volume of traffic is distributed automatically across the various truck classes and further, over different hours of the day, months of the year, and years of the design life of the assessed pavement structure.

According to the Guide for Mechanistic-Empirical Design of New and Rehabilitated Pavement Structures (NCHRP 1-37A Final Document: Appendices GG-1 and II-1 (2004)), responses of pavement structures to the top-down (longitudinal) cracking, bottom-up (alligator) cracking and permanent deformation (rutting depth) are calculated in the M-E PDG software using the following mechanistic-empirical models:

For top-down (longitudinal) cracking:

$$\textbf{Top-down Cracking (ft/mile)} = \frac{10{,}560}{1 + e^{(7.0 - 3.5\ logFD)}} \qquad \textbf{Equation 19}$$

For bottom-up (alligator) cracking:

$$\textbf{Bottom-up Cracking (\%)} = \frac{100}{1 + e^{c_2'(-2 + \log FD)}} \qquad \textbf{Equation 20}$$

where, FD is the cumulative fatigue damage concept given by Miner's law and is calculated from the actual number of traffic loads within a specific time (n_i) divided by the number of allowable repetitions to failure for top-down or bottom-up cracking (N_f). The N_f equation for both cracking types is the classical fatigue empirical model defined by Monismith, et al. (1985) as follows:

$$N_f \textbf{ (cycles)} = 0.00432\ k_1' c \left(\frac{1}{\varepsilon_t}\right)^{3.9492} \times \left(\frac{1}{E^*}\right)^{1.281} \qquad \textbf{Equation 21}$$

where, N_f of the top-down cracking and the bottom-up cracking is determined using the tensile strain (ε_t) near the surface and at the bottom of the asphalt concrete layer, respectively. It is worth mentioning that the top-down cracking is a surface-related phenomenon and is highly affected by the contact pressure distribution and the stiffness of the surface course. Therefore, further development and calibration are needed for the top-down cracking model.

The mixture dynamic modulus ($|E^*|$) value (in psi) of each AC layer in the N_f model can be used directly if known from field tests (e.g. Falling Weight Deflectometer test); otherwise, it can be obtained using the Hirsch model (Al-Khateeb, et al. (2006) and Dongre, et al., (2005)) incorporated in the software, as follows:

$$|E^*| = P_c\left\{4,200,000\left(1-\frac{VMA}{100}\right)+3|G^*|_b\left[\frac{VFB\times VMA)}{10,000}\right]\right\}+\frac{1-P_c}{\left(\frac{1-\frac{VMA}{100}}{4,200,000}+\frac{VMA}{3\,VFB\,|G^*|_b}\right)} \quad \textbf{Equation 22}$$

where, values of bitumen shear complex modulus ($|G^*|_b$) in psi, percentage of voids filled with bitumen (VFB) and voids in mineral aggregate (VMA) can be determined from some laboratory tests. The value of P_c can be calculated as:

$$P_c = \frac{\{20+[VFB(3\,|G^*|_b)/VMA]\}^{0.58}}{650+[VFB(3\,|G^*|_b)/VMA]^{0.58}} \quad \textbf{Equation 23}$$

Going back to the N_f equation above, the value of parameters "c" and "k_1'" can be calculated as follows:

$$c = 10^{4.84\left(\frac{V_b}{V_a+V_b}-0.69\right)} \quad \textbf{Equation 24}$$

$$k_1' \textbf{ (top-down cracking)} = \frac{1}{0.01+\frac{12}{1+e^{15.676-2.8186\,h_{AC}}}} \quad \textbf{Equation 25}$$

$$k_1' \textbf{ (bottom-up cracking)} = \frac{1}{0.000398+\frac{0.003602}{1+e^{11.02-3.49\,h_{AC}}}} \quad \textbf{Equation 26}$$

where, V_a and V_b are the air voids and bitumen content in the total AC layer, respectively. The h_{AC} is the thickness of the AC layer in inches.

The parameter "c_2'" in the bottom-up fatigue cracking model is a calibration factor that depends on the thickness of the AC layer, in inches, and can be computed as follows:

$$c_2' = -2.40874-39.748\,(1+h_{AC})^{-2.856} \quad \textbf{Equation 27}$$

After that, the permanent deformation (rutting depth) for AC layers is calculated in the M-E PDG software using the following model:

Permanent Deformation for AC layers (Rutting) $= \delta_{AC} = \sum_1^m h_i \varepsilon_{p(AC)_i}$ **Equation 28**

where, h_i is the thickness of each AC layer in inches and $\varepsilon_{p(AC)i}$ is the vertical permanent strain of each AC layer, which is calculated by:

$$\varepsilon_{p(AC)_i} = \varepsilon_{v(AC)_i} \times \left(\beta_1 k_1 10^{-\beta_2 \times 3.35412}\, T^{\beta_3 \times 1.5606}\, N^{\beta_4 \times 0.4491}\right) \quad \textbf{Equation 29}$$

where, $\varepsilon_{v(AC)i}$ is vertical compressive strain at mid-depth of each AC layer; $\beta_{1,2,3,4}$ are regional calibration factors that are assumed to be 0.7 based on preliminary work conducted by researchers at Texas A&M University at Qatar; and k_1 is a coefficient calculated from the thickness (in inches) of the AC layer as follows:

$$k_1 = (C_1 + C_2 \times h_{AC}) \times 0.328196^{h_{AC}} \quad \textbf{Equation 30}$$

where, $C_1$and C_2 are calibration factors that also depend on the thickness of the AC layer (in inches) and can be found as follows:

$$C_1 = -0.1039\, h_{AC}^2 + 2.4868\, h_{AC} - 17.342 \quad \textbf{Equation 31}$$

$$C_2 = 0.0172\, h_{AC}^2 - 1.7331\, h_{AC} + 27.428 \quad \textbf{Equation 32}$$

Going back to the vertical permanent strain in equation 29, N is the actual traffic load number (ESALs); T is the pavement temperature at the middle of each AC layer (in inches) acquired from the SHRP model:

$$T(°F) = T_{air}\left(1 + \frac{1}{depth+4}\right) + \frac{34}{depth+4} + 6 \quad \textbf{Equation 33}$$

Then, permanent deformation (rutting depth) for base, sub-base and subgrade layers is computed in the M-E PDG software as follows:

Permanent Deformation for Sub-layers (Rutting) $= \delta = \sum_1^m h_i \varepsilon_{pi}$ **Equation 34**

where, ε_{pi} is vertical plastic strain of each sub-layer that is calculated by:

$$\boldsymbol{\varepsilon_{pi} = \varepsilon_{vi} \times 1.35 \times \left[0.5\left(0.15 \times e^{(\rho)^{\beta}} + 20 \times e^{(\frac{\rho}{10^9})^{\beta}}\right)\right] e^{-(\frac{\rho}{N})}} \quad \textbf{Equation 35}$$

where, ε_{vi} is the vertical compressive strain at mid-depth of each sub-layer; β is 1.673 and 1.35 for base or sub-base layers and subgrade layer, respectively; and ρ is a parameter that can be calculated as follows:

$$\boldsymbol{\rho = 10^9 \left(\frac{-4.89285}{1-(10^9)^{\beta}}\right)^{\frac{1}{\beta}}} \quad \textbf{Equation 36}$$

Using equations 28 and 34, the M-E PDG software calculates the total rutting depth of the asphalt concrete pavement structure.

The International Roughness Index (IRI) of the AC pavement structure evaluated over the design life depends upon the initial as-built profile of the pavement structure from which the initial IRI is computed and upon the subsequent evolution of distresses (e.g. rutting, fatigue cracking and thermal cracking) over time. The IRI model uses the distresses predicted using the models described above, initial IRI, and field factors to predict smoothness over time. The field factors include subgrade and climatic factors to account for the roughness caused by shrinking or swelling soils and frost heave conditions. IRI is also estimated incrementally over the entire pavement design period.

In addition to all previous distresses models used in the M-E PDG software, an incremental damage approach is used to calculate the accumulated damage in the pavement structure over the design life (e.g. 20 years). The design life is divided into time periods of two weeks for flexible AC pavements and one month for rigid AC pavements. In each time period, the daily, seasonal, and long-term changes in material properties, traffic loading and environmental conditions are considered. The total distress damage (i.e. cracking, rutting and IRI) over the design life of the AC structure is the sum of the damage accumulated in each time period. In the M-E PDG, each performance criterion has a design limit, as given in Table 1.

The design reliability is defined as the probability that each of the investigated distress types and smoothness will be less than a preselected critical level over the design period.

Table 1. M-E PDG design limits for the performance criteria of pavement structures.

Performance criteria	Design limit
Top-down (longitudinal) cracking	378 m/km (2000 ft/ml)
Bottom-up (alligator) cracking	25%
Total rutting depth	19 mm (0.75 in)
International roughness index (IRI)	2.717 m/km (172 in/ml)

The designer selects the design based on the pavement structure that meets certain performance criteria. Otherwise, the pavement designer can modify the trial design as needed until the criteria are met.

3.1.2 M-E PDG analysis of conventional and perpetual pavement structures

A total of three asphalt concrete structures using 32 different cases were analysed using the M-E PDG. The first type is a flexible pavement structure that is referred to as “asphalt concrete design” in the Qatar Highway Design Manual (QHDM, (1997)). This structure is the most common in Qatar and consists of a surface course, asphalt concrete base course and granular sub-base over the subgrade. The second type is referred to as “flexible-composite design” in the QHDM. This structure consists of a surface course, upper asphalt concrete base, cement-stabilised lower base and granular sub-base over the subgrade. The third type is the “perpetual pavement”, which is not part of the QHDM, and consists of a surface course, asphalt concrete upper base, asphalt concrete lower base and cement-stabilised sub-base over the subgrade. The cross sections of these pavement structures are shown in Figure 12.

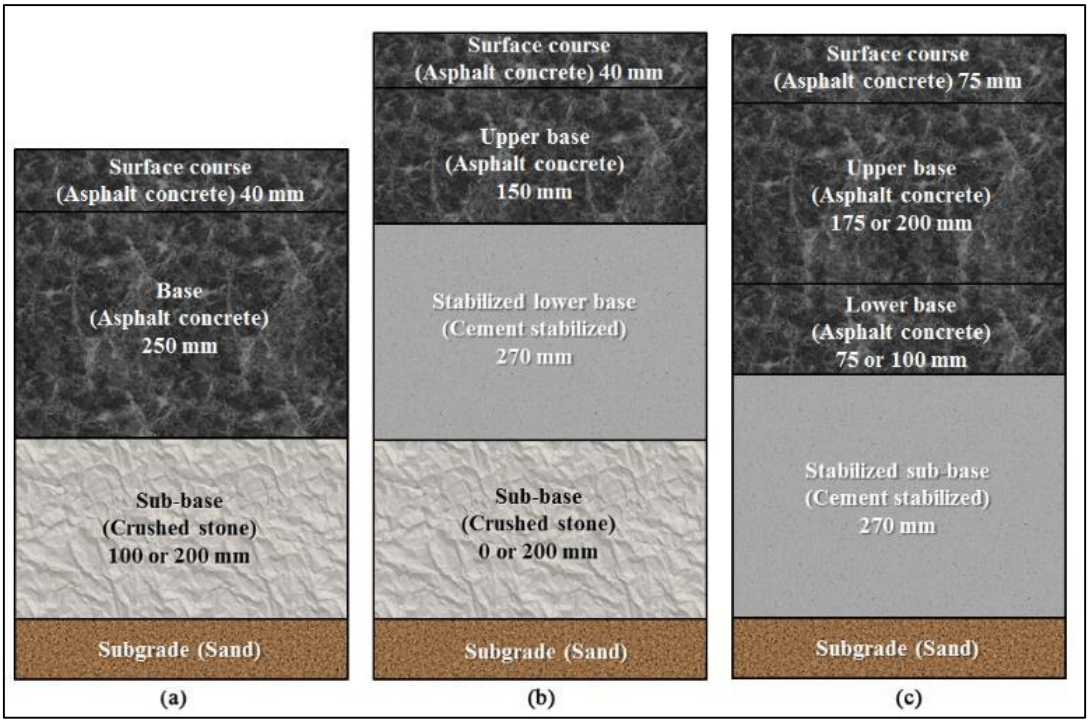

Figure 12. Cross sections for the assessed asphalt pavement structures: (a) asphalt concrete (flexible) design; (b) flexible-composite design; (c) perpetual pavement.

The two conventional pavement structures used in Qatar in addition to the proposed perpetual pavement structure were analysed and evaluated under the default traffic loading classes T4, T5 and T6 provided in QHDM as 2-way AADTT inputs in the M-E PDG, as shown in Table 2.

Table 2. AADTT input for the required ESALs and traffic classes.

Traffic class*	ESALs (million)	2-way AADTT (M-E PDG input)
T4	10	1594
T5	20	3188
T6	50	7970

* The traffic classes follow the designations used in the Qatar Highway Design Manual (QHDM).

The highest traffic loading class (i.e. T6) in QHDM is 50 million ESALs, and by back-calculating the 80 kN (18 kips) standard single axle load for trucks by assuming 312 working days every year during the 20 years of service (six days/week), the truck loading factor will be only 1.01 ESAL. This is considered very low for Qatar, as will be shown later in this study.

In order to perform the analysis in the M-E PDG software, the State of Qatar's climatic conditions were required, but they were not available. Therefore, a careful examination of

numerous climatic files was performed to find out climatic data in the software with a temperature profile as similar as possible to that in Qatar. The weather in Qatar is, in general, hot with very little precipitation. The temperature profile at Needles Airport in California, USA, was found to reasonably resemble the temperature profile in Qatar. The latitude of this station is 34.46°N and the longitude is 114.37°W. Table 3 shows the mean high air temperature for Qatar and Needles Airport. Figure 13 shows a comparison of the yearly mean high air temperature profiles between the two locations.

Table 3. Mean high air temperature every month for Needles Airport in the United States and Qatar.

Month	Location	Jan	Feb	Mar	Apr	May	Jun	Jul	Aug	Sep	Oct	Nov	Dec
Mean high air temp. (°C)	Needles	16.0	17.9	23.6	28.5	35.2	40.4	43.5	41.4	37.2	29.1	19.7	14.3
	Qatar	18.2	22.8	22.8	29.1	35.4	40.0	41.7	40.0	35.4	29.1	22.8	18.2

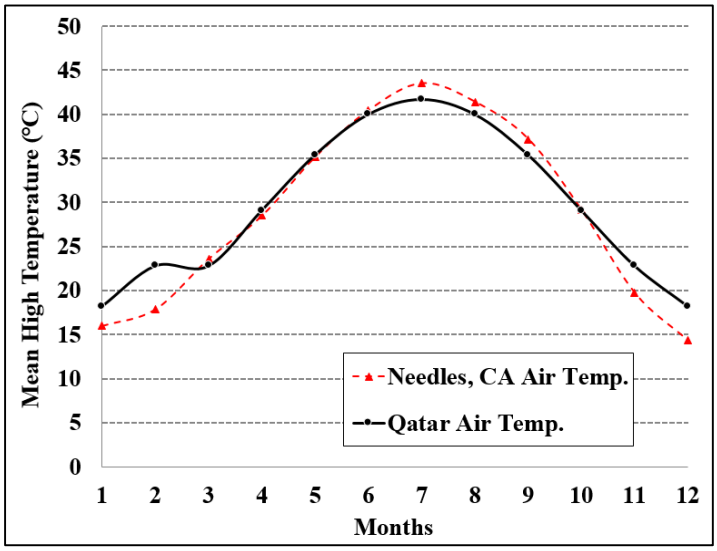

Figure 13. Yearly mean high air temperature for Qatar and Needles Airport Station in the USA.

It can be seen from the table and the figure that the yearly mean high air temperatures for both locations are very close to each other especially in the summertime (June to September), which is the hottest and the most critical period in Qatar. Therefore, it is deemed acceptable to use the air temperature data from Needles Airport California State to represent the weather condition in Qatar.

The properties of the materials used in the pavement structures shown in Figure 12 and evaluated using the M-E PDG software were carefully selected based on the data available in the QHDM, QCS (2010) and the experimental measurements of local materials (Masad, et al., 2011). These properties are discussed in the following subsections.

3.1.2.1 Asphalt concrete surface course

For the surface course, the M-E PDG analysis was carried out using unmodified 60-70 Pen and modified PG76-10 bitumen for conventional pavement structures in order to examine the effect of modified bitumen on performance. Modified PG76-10 bitumen was used for the asphalt concrete surface course in the perpetual pavement structure case. Unmodified 60-70 Pen bitumen has been in use for many years to produce hot mix asphalt (HMA) mixtures in Qatar, as well as in other countries in the region such as Saudi Arabia, the United Arab Emirates, Oman, Yemen, and Jordan. However, as discussed in section 2.1, several studies have shown that this bitumen grade is not suitable for the prevailing climatic conditions. In addition, the PG grade was selected based on analysis of climatic conditions in the State of Qatar and on evidence reported in regional studies indicating the advantages of harder or modified bitumen to withstand high temperatures and resist cracking and rutting. In the M-E PDG analysis of conventional and perpetual structures, the effective bitumen content – by weight of the mixture – was 5% and the air voids percentage – by volume – was 6%. These volumetric/compositional properties were selected based on the QHDM and the typical AC mixtures used in the State of Qatar.

3.1.2.2 Asphalt concrete base course

Timm and Priest (2006) stated that using extra-flexible asphalt mixtures could enable a pavement to resist fatigue cracking in the lower asphalt base course. The upper asphalt base course is designed to resist traffic load and rutting, which can be achieved by using bitumen with the appropriate high-temperature grading. Consequently, the analysis was carried out

using unmodified 60-70 Pen and modified PG76-10 bitumen for conventional pavement structures to evaluate the impact of modified bitumen in a base course on the performance while, for perpetual pavement structures, modified PG76-10 bitumen was used for the AC layers with a bitumen content of 6% (more than the surface course) and 5% air voids. Figure 14 illustrates an example of the input properties of asphalt concrete layers (surface and base courses) in the M-E PDG software.

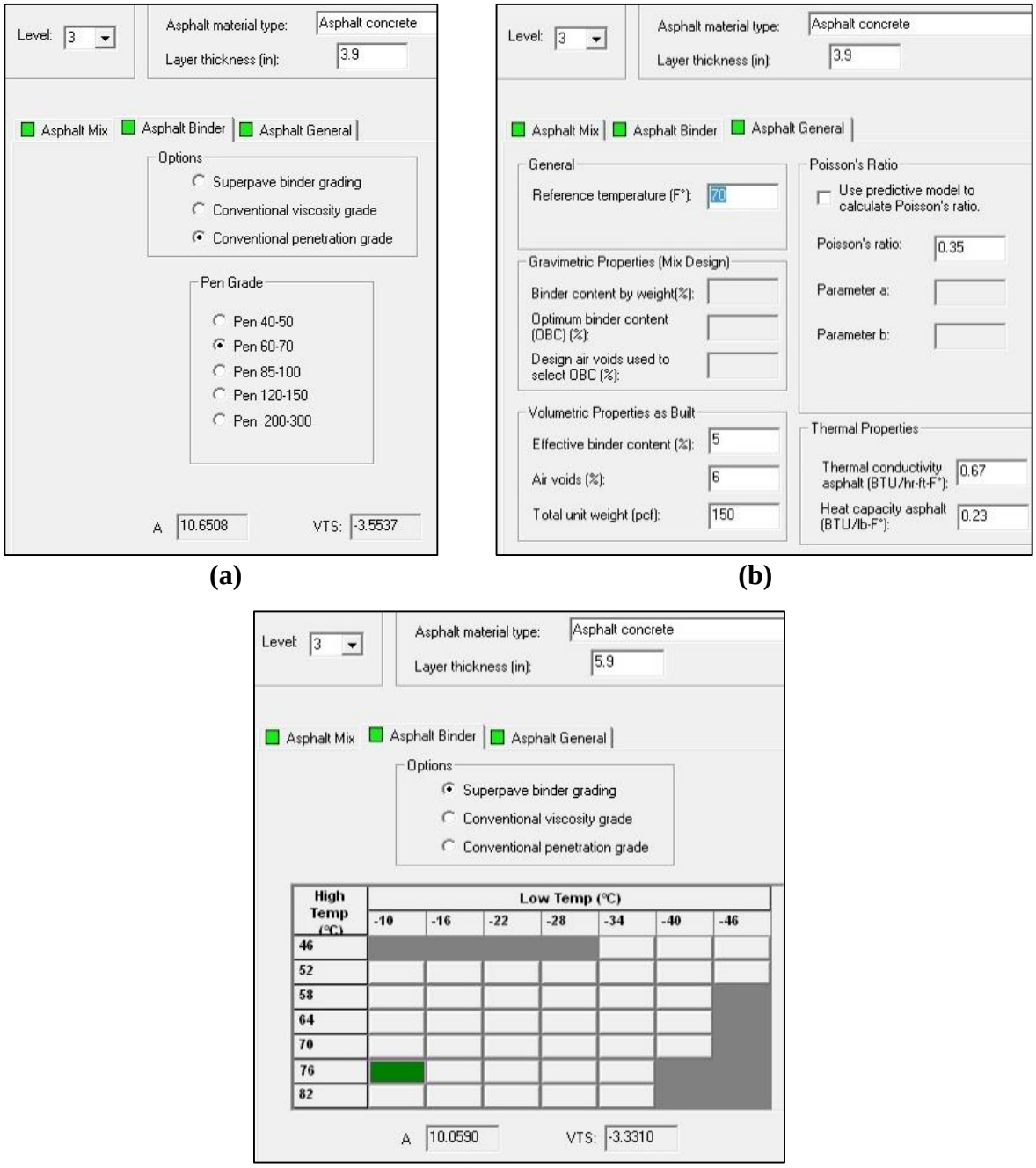

Figure 14. Asphalt concrete layers' inputs in M-E PDG.

3.1.2.3 Cement-stabilised base and sub-base course

The cement-stabilised base (or sub-base) layer was used only in the cases of flexible-composite and perpetual pavement structures as shown in Figure 12. This material comprises sand, gravel or crushed rock that is mixed with cement either in situ or in an off-road mixer. As shown in Figure 15, the resilient modulus value for this material was determined to be 2413 MPa (350,000 psi) using the empirical relationship M_r (MPa) ≈ Compressive Strength (MPa) × 750 (Thompson, 1966). The compressive strength was assumed to be 3.2 MPa based on the typical values in Qatar. The modulus of rupture was 1.0 MPa (150 psi) and Poisson's ratio was 0.2, based on data provided by the QHDM and available field-testing reports.

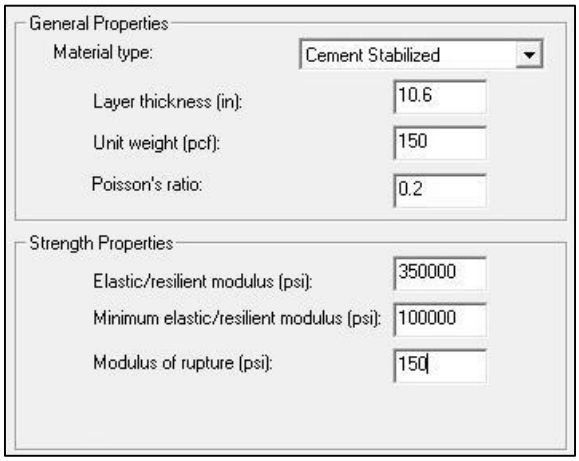

Figure 15. Cement-stabilised material inputs in M-E PDG.

3.1.2.4 Granular sub-base course

Granular materials are used for the sub-base course in conventional pavement structures of the QHDM. The granular materials may consist of crushed stone or gravel. The QHDM specifies a minimum of 60% CBR value for the sub-base layer. The modulus was calculated based on AASHTO T193 (2010) to be 242 MPa (35,100 psi) using the following empirical relationship:

$$\boldsymbol{M_r(psi) = 2555\ (CBR)^{0.64}} \qquad \textbf{Equation 37}$$

where, CBR is in percentage. The Poisson's ratio of 0.35 for the crushed stone was assumed, as shown in Figure 16.

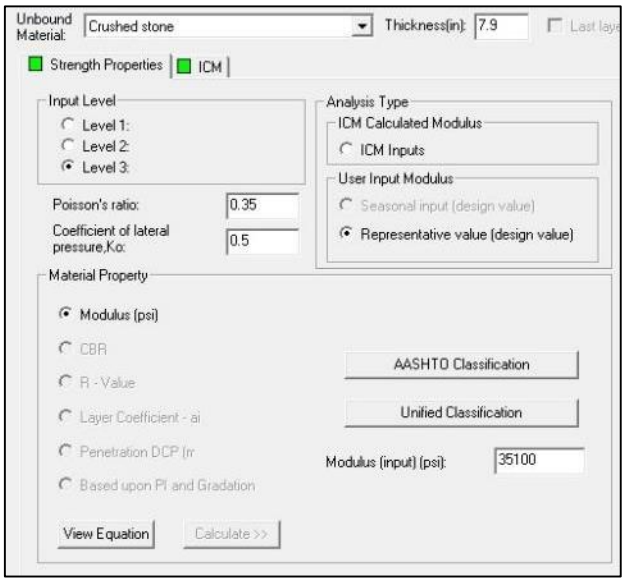

Figure 16. Granular sub-base inputs in M-E PDG.

3.1.2.5 Subgrade

The State of Qatar has high-strength natural soils (high CBR value) consisting of weathered Limestone or sand. Therefore, silty or clayey gravel and sand "A-2-4" in addition to stone fragments, gravel and sand "A-1-b", based on the AASHTO Soil Classification System, were used in this study in order to inspect the effect of subgrade strength on performance. The conventional pavement structures in the QHDM include three classes of subgrade defined by California Bearing Ratio (CBR) as follows:

S1: $\geq 15\%$ and $< 25\%$

S2: $\geq 25\%$ and $< 50\%$

S3: $\geq 50\%$

The A-2-4 and A-1-b soils are referred to as S1 and S3, respectively, in the QHDM. However, in the M-E PDG software, the modulus of the subgrade is required for input level 3 not the CBR value. Therefore, CBR values were again used in equation 37 to calculate the

subgrade modulus, as shown in Table 4. In addition, a Poisson's ratio of 0.35 was assumed for the subgrade soils in the analysis, as presented in Figure 17.

Table 4. Subgrade modulus required for subgrade classes used in the M-E PDG.

Subgrade class	AASHTO classification	CBR selected value	Modulus (M-E PDG input)
S1	A-2-4	20%	120 MPa (17,500 psi)
S3	A-1-b	60%	242 MPa (35,100 psi)

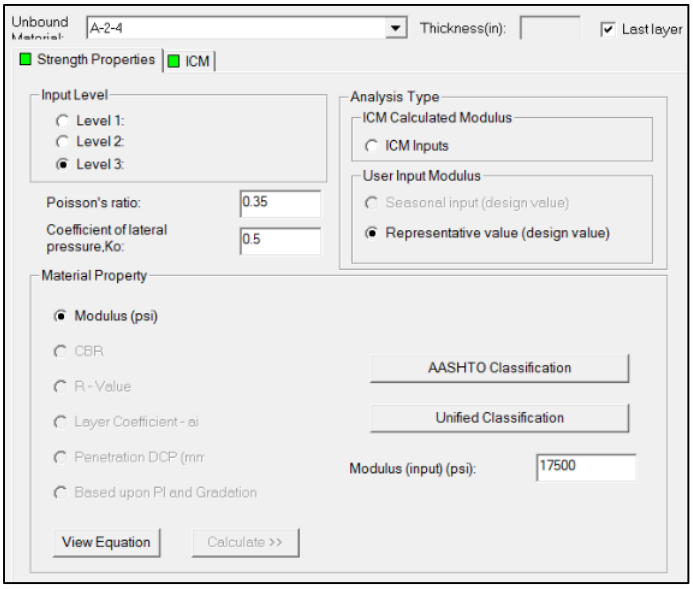

Figure 17. Subgrade A-2-4 inputs in the M-E PDG.

In order to inspect the effect of the AC layer's thickness on performance, the perpetual pavement structure was analysed and evaluated using minimum thicknesses of 75 and 175 mm for the upper and lower asphalt base courses, respectively. The analysis was also conducted using maximum thicknesses of 100 and 200 mm, as shown earlier in Figure 12. Details of traffic, layer thicknesses, bitumen grade and all other material properties used in the 32 different pavement structure cases are summarised in Table 5.

Table 5. Layers, materials and properties of the evaluated conventional and perpetual pavement structures.

Pavement Structure type	Analysis case	Soil subgrade		AADTT	Crushed stone sub-base		AC surface course	AC base course	Bitumen	Cement-stabilised base & sub-base	
		Material	M_r, MPa		Thickness, mm	M_r, MPa	Thickness, mm	Thickness, mm		Thickness, mm	M_r, MPa
Asphalt concrete (Flexible)	1	A-2-4	120	1594	200	242	40	250	60-70 Pen	-	-
	2	A-2-4	120	1594	200	242	40	250	PG76-10	-	-
	3	A-2-4	120	3188	200	242	40	250	60-70 Pen	-	-
	4	A-2-4	120	3188	200	242	40	250	PG76-10	-	-
	5	A-2-4	120	7970	200	242	40	250	60-70 Pen	-	-
	6	A-2-4	120	7970	200	242	40	250	PG76-10	-	-
	7	A-1-b	242	1594	100	242	40	250	60-70 Pen	-	-
	8	A-1-b	242	1594	100	242	40	250	PG76-10	-	-
	9	A-1-b	242	3188	100	242	40	250	60-70 Pen	-	-
	10	A-1-b	242	3188	100	242	40	250	PG76-10	-	-
	11	A-1-b	242	7970	100	242	40	250	60-70 Pen	-	-
	12	A-1-b	242	7970	100	242	40	250	PG76-10	-	-
Flexible-composite	13	A-2-4	120	3188	200	242	40	150	60-70 Pen	270	2413
	14	A-2-4	120	3188	200	242	40	150	PG76-10	270	2413
	15	A-2-4	120	7970	200	242	40	150	60-70 Pen	270	2413
	16	A-2-4	120	7970	200	242	40	150	PG76-10	270	2413
	17	A-1-b	242	3188	-	-	40	150	60-70 Pen	270	2413
	18	A-1-b	242	3188	-	-	40	150	PG76-10	270	2413
	19	A-1-b	242	7970	-	-	40	150	60-70 Pen	270	2413
	20	A-1-b	242	7970	-	-	40	150	PG76-10	270	2413
Perpetual (Long-life)	21	A-2-4	120	7970	-	-	75	250	PG76-10	270	2413
	22	A-2-4	120	23910	-	-	75	250	PG76-10	270	2413
	23	A-2-4	120	47820	-	-	75	250	PG76-10	270	2413
	24	A-2-4	120	7970	-	-	75	300	PG76-10	270	2413
	25	A-2-4	120	23910	-	-	75	300	PG76-10	270	2413
	26	A-2-4	120	47820	-	-	75	300	PG76-10	270	2413
	27	A-1-b	242	7970	-	-	75	250	PG76-10	270	2413
	28	A-1-b	242	23910	-	-	75	250	PG76-10	270	2413
	29	A-1-b	242	47820	-	-	75	250	PG76-10	270	2413
	30	A-1-b	242	7970	-	-	75	300	PG76-10	270	2413
	31	A-1-b	242	23910	-	-	75	300	PG76-10	270	2413
	32	A-1-b	242	47820	-	-	75	300	PG76-10	270	2413

3.1.3 Performance evaluation results using the M-E PDG software

The performance of conventional and perpetual pavement structures after 20 years of service in terms of surface distresses – longitudinal cracking, alligator cracking, total rutting

depth and IRI – using the M-E PDG software was observed and evaluated. In this section, the M-E PDG analysis results for the 32 cases of pavement structures are presented and discussed.

3.1.3.1 Effect of bitumen type

Asphalt concrete (flexible) pavement structures and flexible-composite pavement structures were evaluated using M-E PDG by comparing the performance using unmodified 60-70 Pen bitumen and polymer-modified bitumen (PG76-10). The comparison also focused on the usage of soil subgrade classes S1 and S3 to evaluate the effect on performance of having a high subgrade modulus.

The M-E PDG results for cases 1 to 6 are shown in Table 6, while Figure 18 shows examples of graphs for the investigated distresses comparing the use of 60-70 Pen and PG76-10 for asphalt concrete (flexible) structures. It can be seen that the use of modified PG76-10 bitumen generally improved the performance and increased the service life of this conventional pavement structure for subgrade class S1. The graphs also confirm that the top-down (longitudinal) cracking is the most critical distress for the conventional pavement structures, as discussed earlier in the previous chapter. However, the use of modified bitumen improved the performance significantly and at least doubled the service life for traffic classes T4, T5 and T6.

In addition, the total rutting depth and IRI were reduced slightly by the use of modified bitumen (PG76-10) but total rutting is still high enough for the pavement to require maintenance and rehabilitation at the end of its service life. In addition, the rutting and IRI results are increasing with the increase in the traffic loading (T4 to T6), which confirms the incapacity of the conventional pavements to resist major distresses if the traffic loading is very high.

On the other hand and as expected, bottom-up (alligator) cracking was not an issue in the evaluated conventional pavement structures, as shown in Table 6. This can be attributed to

the high thickness of the AC base layer (250 mm) in the conventional flexible structures where no cracks can be initiated at the bottom of the AC base layer.

Table 6. M-E PDG results for asphalt concrete structures using 60-70 Pen or PG76-10 for subgrade class S1.

Traffic classes	T4			T5			T6		
Analysis cases	1	2	% Improved	3	4	% Improved	5	6	% Improved
	Pen	PG		Pen	PG		Pen	PG	
Longitudinal cracking (m/km)	172.0	46.0	73%	641.0	292.6	54%	764.2	417.7	45%
Alligator cracking (%)	4.43	3.38	24%	5.34	4.12	23%	5.52	4.28	22%
Total rutting (mm)	16.2	13.8	15%	20.4	17.2	16%	23.3	19.6	16%
IRI (m/km)	1.75	1.68	4%	1.86	1.78	4%	1.94	1.84	5%

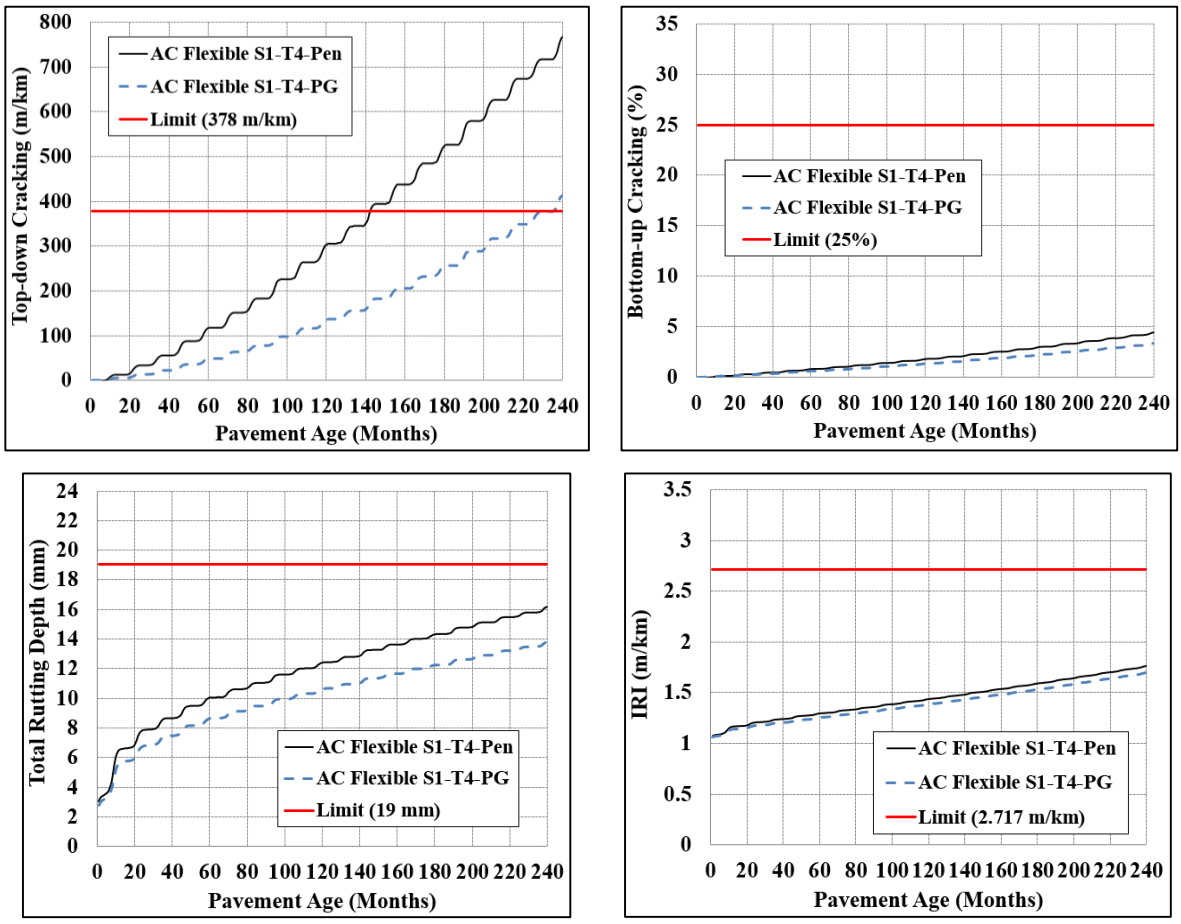

Figure 18. Performance graphs of conventional flexible pavement structures comparing the effect of bitumen type for traffic T4 and subgrade S1 against major distresses.

The M-E PDG results for the analysis of conventional flexible pavement cases 7 to 12 are presented in Table 7. In general, the results indicate that the use of modified PG76-10

bitumen instead of unmodified 60-70 Pen bitumen enhanced the performance of these conventional pavement cases with subgrade S3 against the major distresses and increased their service life for traffic classes T4, T5 and T6. However, the results show again that the top-down (longitudinal) cracking is still a critical distress type for the conventional flexible pavement structures. Surprisingly, a higher amount of longitudinal (top-down) cracking was obtained for the high-modulus subgrade S3 compared to S1, which emphasises that the top-down model shown earlier in equation 19 needs more development and calibration.

In addition, the total rutting depth was reduced slightly by the use of modified bitumen (PG76-10) but it is still high enough for the pavement to require maintenance and rehabilitation at the end of its service life (i.e. 20 years). Moreover, the total rutting and IRI are again becoming higher with the increase of the traffic class (T4 to T6). This confirms the effect of the increase of the traffic loading on these conventional structures.

As expected from pavement structures with thick asphalt concrete layers and high-modulus subgrade, bottom-up (alligator) cracking was not an issue in the evaluated conventional flexible pavement structures, as shown in Table 7.

Table 7. M-E PDG results for asphalt concrete designs using 60-70 Pen or PG76-10 for subgrade class S3.

Traffic classes	T4			T5			T6		
Analysis cases	7	8	%	9	10	%	11	12	%
	Pen	PG	Improved	Pen	PG	Improved	Pen	PG	Improved
Longitudinal cracking (m/km)	608	273	55%	1059	693	35%	1169	849	27%
Alligator cracking (%)	3.18	2.37	25%	3.63	2.73	25%	3.50	2.70	25%
Rutting (mm)	14.7	12.4	16%	18.8	15.7	16%	22.0	18.0	17%
IRI (m/km)	1.68	1.62	4%	1.79	1.71	4%	1.90	1.80	5%

In conclusion, the results in both subgrade classes (S1 and S3) show clearly that longitudinal (top-down) cracking and rutting are the major problems in the conventional flexible pavement structures, even if polymer-modified bitumen (PMB) is used. This means that the mix design and the structure of the pavement should be amended. In addition, the M-

E PDG analysis results showed that increasing the subgrade strength (S1 to S3) improved pavement structure performance, where the magnitudes of alligator cracking, total rut depth and IRI all decreased. In contrast, longitudinal (top-down) cracking increased significantly. This is counter-intuitive because it is not clear why a better support could result in more cracking. A reason for this counter-intuitive result could not be found; however, this finding may suggest that the top-down cracking model needs to be carefully examined and calibrated using field data.

Flexible-composite pavement structures in cases 13 to 16 were also analysed and evaluated using M-E PDG to examine the effect of PMB and subgrade class on performance. As shown in Table 8 and Figure 19, the flexible-composite pavements did not suffer from top-down or bottom-up cracking. The use of PG76-10 bitumen as a replacement for 60-70 Pen bitumen improved the performance, especially for longitudinal (top-down) cracking, which decreased by 83% and 92% for traffic classes T5 and T6, respectively. However, the major problem with the flexible-composite pavement structures is still the rutting depth, even with the use of PMB. On the other hand, there was no alligator (bottom-up) cracking for either bitumen type. This could be due to the existence of the stabilised lower base layer just beneath the asphalt concrete layer, which prevents any cracks starting from the bottom of the AC layer to the top of the pavement structure. In addition, it was noticed that an increase in traffic loadings (T5 to T6) increased the cracking, rutting depth and IRI.

Table 8. M-E PDG results for flexible-composite structures using 60-70 Pen or PG76-10 for subgrade class S1.

Traffic classes	**T5**			**T6**		
Analysis cases	**13**	**14**	**% Improved**	**15**	**16**	**% Improved**
	Pen	**PG**		**Pen**	**PG**	
Longitudinal cracking (m/km)	1.17	0.20	83%	51.0	4.1	92%
Alligator cracking (%)	0.0	0.0	-	0.0	0.0	-
Rutting (mm)	23.9	19.9	17%	32.5	26.8	18%
IRI (m/km)	1.91	1.81	5%	2.12	1.98	7%

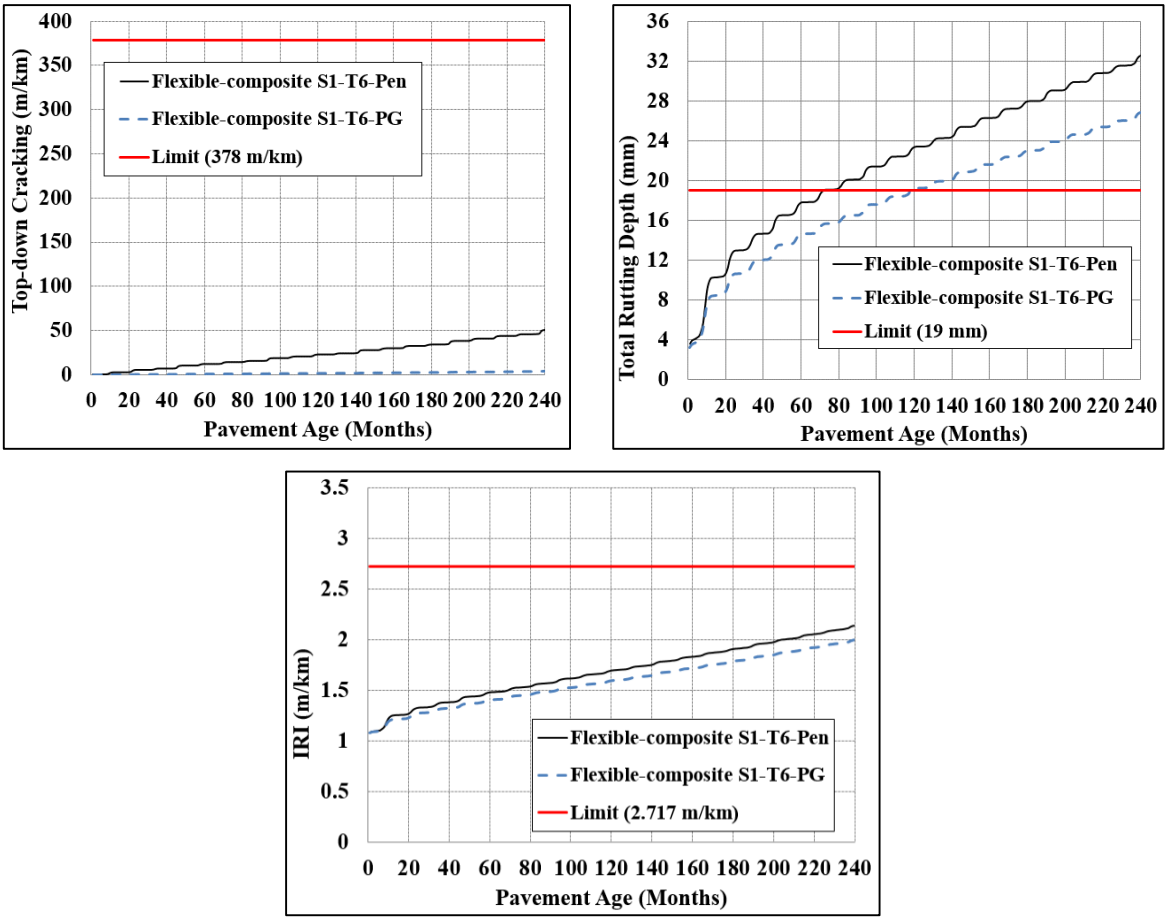

Figure 19. Performance graphs of conventional flexible-composite pavement structures comparing the effect of bitumen type for traffic T6 and subgrade S1 against major distresses.

The analysis results for cases 17 to 20 of conventional flexible-composite pavement structures with subgrade class S3 are given in Table 9. Similar to the cases of subgrade class S1, the results indicated that using PG76-10 enhanced the performance of this conventional pavement structure for subgrade class S3, especially for longitudinal (top-down) cracking, which decreased by 62% and 82% for traffic classes T5 and T6, respectively.

However, the main issue with the flexible-composite pavement structures is again the rutting depth, even with the use of PMB. There was no bottom-up cracking for either bitumen type, which could be due to the existence of the stabilised layer that prevents any cracks starting from the bottom of the AC layer to the top of the pavement structure.

The subgrade class S3 in these cases decreases the rutting and IRI results but surprisingly increased the top-down cracking compared to the results for subgrade S1. Similar

to the previous cases, the increase in traffic loading (T5 to T6) increased the top-down cracking, total rutting depth and IRI.

Table 9. M-E PDG results for flexible-composite designs using 60-70 Pen or PG76-10 for subgrade class S3.

Traffic classes	T5			T6		
Analysis cases	17	18	% Improved	19	20	% Improved
	Pen	PG		Pen	PG	
Longitudinal cracking (m/km)	18.1	6.8	62%	224.5	39.3	82%
Alligator cracking (%)	0.0	0.0	-	0.0	0.0	-
Rutting (mm)	22.4	18.6	17%	30.9	25.3	18%
IRI (mm/km)	1.85	1.75	5%	2.06	1.92	7%

The M-E PDG analysis results for both subgrade classes using different bitumen types revealed clearly that only rutting is a critical problem in the conventional flexible-composite structures, even if polymer-modified bitumen is used. The longitudinal (top-down) cracking is resisted better in the flexible-composite pavements compared to the flexible pavements due to the existence of a cement-stabilised base. Similar to the cases of flexible structures, the use of high-modulus subgrade S3 in conventional flexible-composite structures improved the performance against all distresses except top-down cracking – which was increased significantly, but still below the design limit – compared to the use of subgrade class S1. This is again counter-intuitive and it is suggested that the top-down cracking model needs to be carefully examined and calibrated using field data.

Based on the first stage of the M-E PDG analysis in this study, it can be stated that the conventional pavement structures provided in the QHDM are not suitable for the high temperature and uncontrolled high traffic loading in the State of Qatar. The use of PMB instead of the conventional unmodified bitumen is very useful but not enough to resist the major road distresses (i.e. rutting and top-down cracking) in the flexible pavement structures that are used widely in the country. In addition, increasing the subgrade strength (S1 to S3) improved the

performance of the conventional pavement structures against all distressed except top-down cracking.

Consequently, it was important to investigate the performance of pavement structures if the perpetual pavement concept is implemented with polymer-modified bitumen and different subgrade classes (S1 and S3) under extremely high traffic loading.

3.1.3.2 Effect of implementing perpetual pavement structures

In this part of the M-E PDG analysis, three high traffic loadings, T6 (50 million ESALs), three times T6 (150 million ESALs) and six times T6 (300 million ESALs), were used to analyse and compare the performance of conventional and perpetual pavement structures using the M-E PDG software. These huge traffic loading scenarios were assumed based on the fact that the maximum traffic class provided by the QHDM (i.e. T6) and the standard axle load of 1.01 ESAL do not represent the real situation in the State of Qatar, as will be shown later in this study. Unmodified 60-70 Pen bitumen and polymer-modified PG76-10 bitumen were used for conventional and perpetual pavement structures, respectively. The objective is to check if the perpetual pavement structures can perform better than the conventional structures given the traffic and temperature conditions in Qatar.

The M-E PDG analysis results for cases 21, 24, 27 and 30, being the perpetual pavement structures, compared to conventional structures under T6 traffic load are presented in Table 10 and Figure 20. The perpetual pavement concept significantly improved the performance of the pavement structures against all distresses, particularly in the case of the 300 mm-thick asphalt base course. The analysis results indicated that the proposed perpetual pavement structure with a thick base course, PMB and any subgrade class (S1 or S3) can prevent any major distress, enhance the performance and increase the service life significantly. This conclusion was expected due to the significant role of modified bitumen used in a perpetual pavement on performance.

Table 10. M-E PDG results for conventional and perpetual pavement structures for traffic T6.

Pavement structure type	Asphalt concrete (flexible) [60-70 Pen]		Flexible-composite [60-70 Pen]		Perpetual pavement [PG76-10]			
Performance after 20 years	S1	S3	S1	S3	250 mm		300 mm	
					S1	S3	S1	S3
Longitudinal cracking (m/km)	172.0	608.0	51.0	224.5	32.0	122.0	0.0	0.0
Alligator cracking (%)	5.52	3.50	0.0	0.0	0.0	0.0	0.0	0.0
Rutting (mm)	23.3	22.0	32.5	30.9	14.9	13.6	11.8	10.5
IRI (m/km)	1.94	1.90	2.12	2.06	1.69	1.63	1.61	1.56

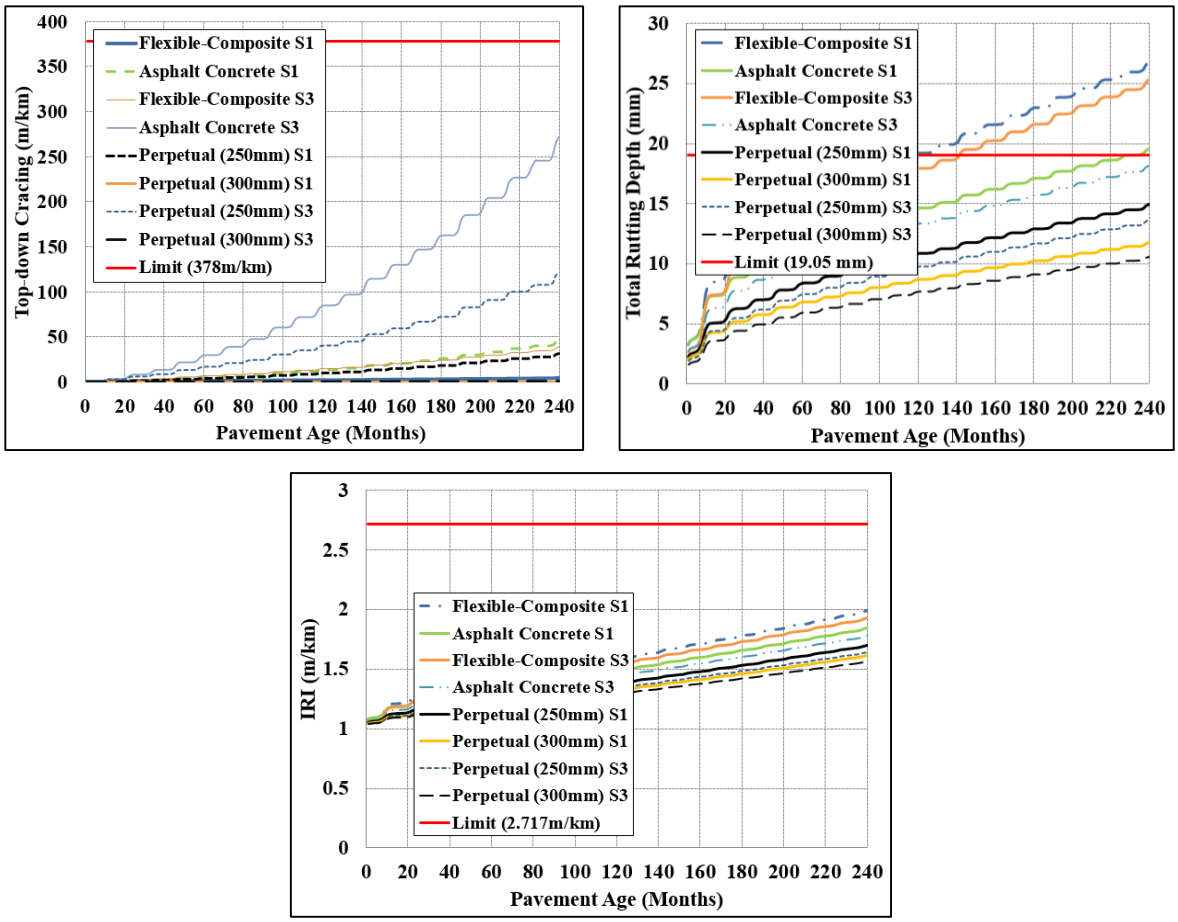

Figure 20. Performance graphs of conventional and perpetual pavement structures for traffic T6 against major distresses.

In order to investigate the effect of the unexpected increase in traffic loading, M-E PDG analysis was also performed under 3×T6 (150 million ESALs). Table 11 summarises the M-E PDG analysis results for cases 22, 25, 28 and 31, perpetual pavement structures, compared to the conventional structures currently used in Qatar.

It can be seen from Table 11 that the use of perpetual pavement structures significantly enhanced the performance against major distresses. The analysis results indicated that the proposed perpetual pavement structure with a thick base course (300 mm), PMB and any subgrade class (S1 or S3), can resist all major distresses, enhance the performance and increase the service life significantly. However, the rutting depth was a little high and it might reach the design limit a few years after the design life (i.e. 20 years), which is expected due to the very high traffic loading (3×T6) applied in the analysis. In addition, the top-down fatigue cracking is still an issue when the AC layer in the perpetual pavement structure is 250 mm and the subgrade is S3. This is similar to the case of flexible pavement structure analysed in the previous section with the S3 subgrade. This shows clearly the effect of the proper thickness of the AC layer on the performance against longitudinal cracking. Although the M-E PDG results show that the thickness of the AC layer clearly affects the amount of top-down cracking, many other studies have shown that this is a surface-related phenomenon and is highly affected by the contact pressure distribution and the stiffness of the surface course. As mentioned earlier, this emphasised the need to examine the suitability of the top-down cracking model used in the M-E PDG.

Table 11. M-E PDG results for conventional and perpetual pavement structures for traffic 3×T6.

Pavement structure type	**Asphalt concrete (flexible) [60-70 Pen]**		**Flexible-composite [60-70 Pen]**		**Perpetual pavement [PG76-10]**			
Performance after 20 years	**S1**	**S3**	**S1**	**S3**	**250 mm**		**300 mm**	
					S1	**S3**	**S1**	**S3**
Longitudinal cracking (m/km)	670.0	1409.1	244.5	854.7	158.0	514.0	1.2	0.0
Alligator cracking (%)	15.8	10.5	0.40	0.46	0.0	0.0	0.0	0.0
Rutting (mm)	35.8	34.2	52.2	50.4	23.0	21.5	17.8	16.3
IRI (m/km)	2.33	2.22	2.61	2.54	1.89	1.83	1.76	1.70

Finally, M-E PDG analysis results in the case of using 6×T6 traffic loading are provided in Table 12. Similar to the previous case (3×T6), it can be concluded that the use of perpetual

pavement structure, cases 23, 26, 29 and 32, improved the performance against surface distresses mainly in the case of the 300 mm-thick asphalt base course. Rutting is still the main problem when the load is extremely high, but it can be solved by using the suitable polymer-modified bitumen grade. In addition, the results presented that the use of a 250 mm AC layer for a perpetual pavement structure is not enough to resist top-down cracking during its service life. A thick perpetual pavement structure is needed when the traffic is extremely high.

Table 12. M-E PDG results for conventional and perpetual pavement structures for traffic 6×T6.

Pavement structure type	Asphalt concrete (flexible) [60-70 Pen]		Flexible-composite [60-70 Pen]		Perpetual pavement [PG76-10]			
Performance after 20 years	S1	S3	S1	S3	250 mm		300 mm	
					S1	S3	S1	S3
Longitudinal cracking (m/km)	1174.3	1755.6	573.7	1372.5	397.0	1001.0	3.4	10.2
Alligator cracking (%)	28.1	19.7	0.84	0.97	0.0	0.0	0.0	0.0
Rutting (mm)	47.5	46.0	69.3	67.5	30.7	29.0	23.5	21.8
IRI (m/km)	2.75	2.60	3.04	2.97	2.08	2.00	1.90	1.84

From the analysis performed in this section, one can conclude that the conventional pavement structures (flexible and flexible-composite) currently used in Qatar might not be suitable for the traffic and temperature profile prevailing in Qatar, even if polymer-modified bitumen is used. The results of the M-E PDG analysis clearly showed that the use of thick perpetual pavement structures (300 mm base course) with polymer-modified bitumen (PG76-10) improved the resistance to top-down cracking, prevented bottom-up cracking and reduced the total rutting depth and IRI values. However, if the traffic loading is extremely high (3×T6 or 6×T6), permanent deformation (rutting) distress stays as a main distress but can be improved by implementing improved mix designs (e.g. the Superpave procedure) with suitable bitumen content and air voids percentages. The effect of using the Superpave mix design procedure is investigated and discussed in the following chapter.

Finally, it is worth mentioning that the analysis performed using the M-E PDG software was based on level 3 inputs, and some assumptions were made because levels 1 and 2 require detailed inputs that are not available yet in Qatar. Consequently, in order to deeply investigate the major distresses affecting the performance of perpetual pavement structures in Qatar, full-scale perpetual pavement structures were constructed in Qatar with different mix designs, aggregate gradations and types in addition to altered bitumen grades and types.

3.2 Performance evaluation of perpetual pavement structures used in a full-scale trial road

For the purpose of investigating the field performance of perpetual pavement structures in Qatar and comparing them with the results of the M-E PDG analysis, in 2010, a full-scale trial road was constructed by the Transport Research Laboratory (TRL) on a route used by heavy truck traffic. This trial road consists of one lane per direction and involves six different perpetual pavement trial sections in order to clearly identify their major problems and to investigate the influence of materials and mixture design on performance.

In this part of the study, the conditions, performance and mechanical properties of these trial sections were evaluated after about a year and a half of service by conducting the following measurements and field tests:

- Measurements by means of the Automatic Road Analyser vehicle to profile the trial road, measure pavement permanent deformation (rutting) and evaluate the ride quality or smoothness of the roadway (longitudinal profile/roughness (IRI)),
- Falling Weight Deflectometer (FWD) field tests during the spring and summer seasons in order to evaluate the stiffness of pavement layers at different climatic conditions.

The following subsections describe the field-testing methodologies, and provide a detailed description of the tested field-trial sections and traffic loading data. In addition, the performance evaluation results for the assessed pavement trial sections are presented.

3.2.1 Field testing methodology

In January 2012, 18 months after the opening of the trial road, the field-testing started by collecting pavement condition data using the automatic road analyser vehicle (Roadware GRP Company) shown in Figure 21. This vehicle is a high-speed inertial profiler, which was used to make profile-based roughness measurements in each wheel path on the surface of the test trial sections. In addition, it was used to measure the total rut depth and to collect layer thickness information from the ground-penetration radar (GPR) data of left and right wheel paths of each trial section for both directions. These data were collected continuously with very high accuracy at a speed of 15 mph (24.1 km/h).

Figure 21. Automatic road analyser vehicle collecting data from the trial road.

As a part of the automatic road analyser vehicle, the Laser South Dakoda Profiler (SDP) is an advanced longitudinal profile measurement system that has been accepted as a Class A device under ASTM950 and proven over a large range of agencies in the world. The 64 kHz Laser SDP provides road profile data and international roughness index (IRI) data using a combination of high-speed lasers and accelerometers. The Laser SDP samples at 12.5 mm

intervals and measures bumps as short as 100 mm at variable speeds up to 62.0 mph (100 km/h) without loss of accuracy.

The wire model algorithm was employed for measuring rut depth using the automatic road analyser vehicle. The wire model algorithm within the automatic road analyser system connects the high points on the pavement's transverse profile and establishes the rut depth under these points, as illustrated in Figure 22. The automatic road analyser vehicle has 1028 data points across the 4-metre transverse profile; the data were filtered down to 40 data points across that profile. From that, the wire model will connect the high points across a 3-metre stretch centred along the profile; the model will then take the highest distance from the wire to the pavement structure for either 1.5-metre side and records that as the left/right wheel path rut depth.

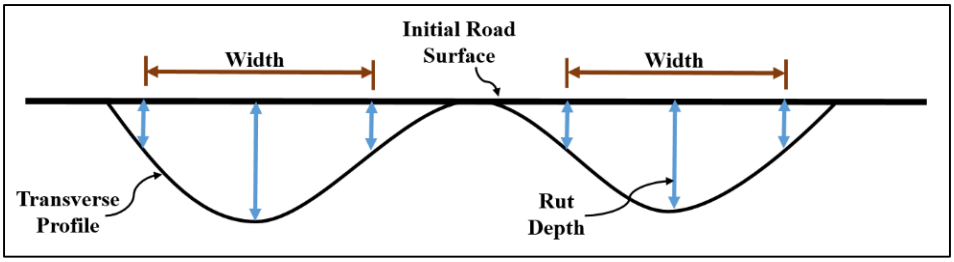

Figure 22. A schematic diagram for the measurement of rutted widths and rut depths from pavement transverse profile data using the wire model algorithm.

The GPR technique in the automatic road analyser vehicle is useful to monitor the construction quality. The GPR transmits pulsed radio waves through the pavement structure materials and these waves reflect at material boundaries. Arrival time and strength of reflections determine material depth, thickness and properties.

The falling weight deflectometer (FWD) test, shown in Figure 23, was also conducted in the field to evaluate pavement structural condition by acquiring the deflections of each layer.

Figure 23. FWD test carried out on the trial road.

These deflections are measured by geophones after applying dynamic loads at the surface of the road simulating a single heavy-moving wheel load. In addition, the pavement temperature is also measured by the FWD using two types of temperature sensors, an air temperature sensor and an infrared (IR) surface-temperature sensor. The temperature data from these two sensors, combined with data from a nearby weather station, are used for estimating the temperature of the various materials in the pavement structure. The measured deflections, temperatures and thicknesses of the layers were then used to back-calculate the moduli (stiffnesses) of the various layers – asphalt concrete, granular sub-base and subgrade – using the Deflection Basin Fit tool in the Elmod6 software (Dynatest Elmod6 Version 6.1.44.), as shown in Figure 24.

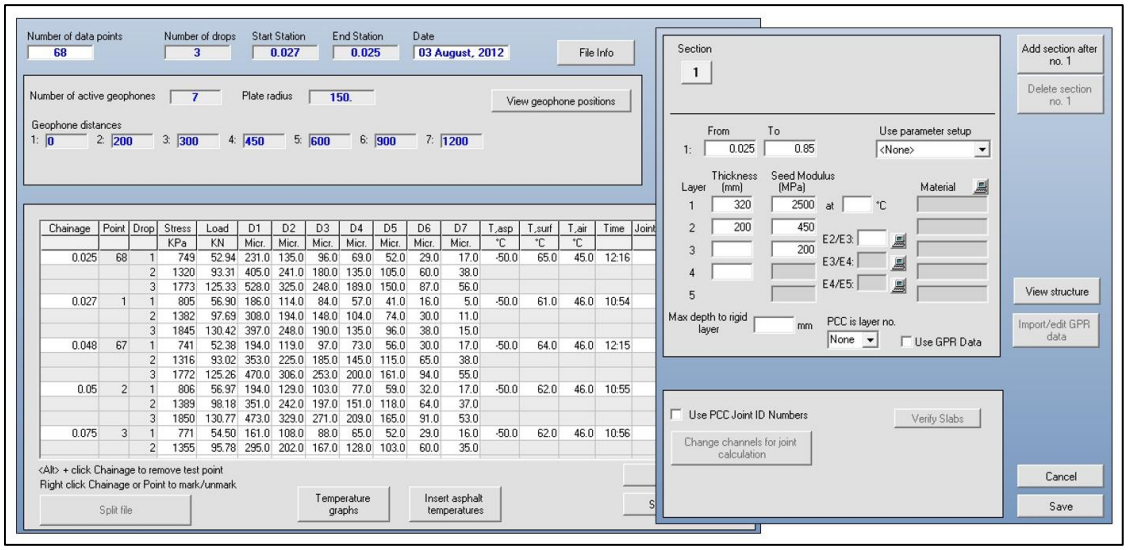

Figure 24. FWD data and thicknesses of layers used to back-calculate the moduli in Elmod6.

The FWD tests were conducted in February (spring season) and August (summer season) in 2012 to monitor the temperature susceptibility of the trial sections at low and high temperatures.

3.2.2 Location, materials, structures and construction of the trial road

Six different AC pavement structures, each about 150 m long, were constructed in 2010 as a part of an access road to a sand-washing plant in the south of Qatar. The location, shown in Figure 25, is 60 km away from the capital, Doha and was selected for construction of the trial road due to its high traffic loading.

Figure 25. Location of the trial road in Qatar (image © 2014 Google; map data © 2014 Google).

The asphalt pavement structures of the full-scale trial road were designed as perpetual pavements to examine the effect of bitumen grade/type, aggregate gradation/type and mix design against different surface distresses and deteriorations under the same traffic condition. The aim was to examine the performance of perpetual pavement structures in Qatar and identify their main advantages and problems. The transverse profile of the trial road is not available, unfortunately, but the layers and materials used in each trial section are shown in Figure 26. The aggregate gradation for the surface and base courses of the full-scale trial sections is shown in Table 13 and Table 14, respectively.

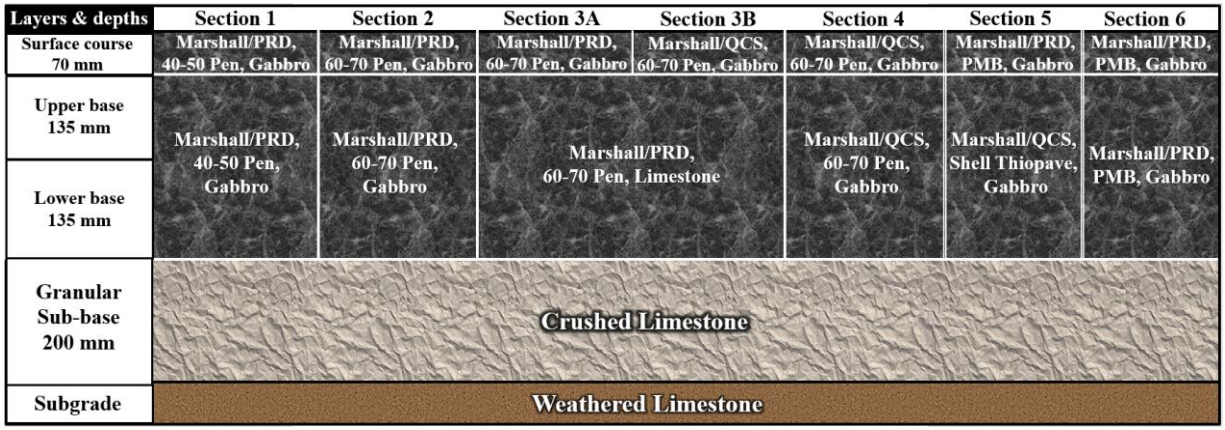

Figure 26. Layers and materials' properties for all trial sections (TRL Client Project Report 282, Phase D, 2010).

Table 13. Aggregate gradation for surface course of the trial sections.

BS sieve size (mm)	Cumulative passing (%)			
	Section 1	Section 2 & 3A	Section 3B & 4	Section 5 & 6
20.0	100.0	100.0	100.0	100.0
14.0	84.0	82.1	90.7	82.0
10.0	72.4	68.9	70.4	68.6
5.00	48.9	51.8	54.9	51.7
2.36	36.1	34.4	33.1	32.9
0.30	13.0	11.4	12.1	11.0
0.150	9.1	8.4	8.2	7.0
0.075	5.7	5.0	4.2	5.1

Table 14. Aggregate gradation for base course of the trial sections.

BS sieve size (mm)	Cumulative passing (%)					
	Section 1	**Section 2**	**Section 3**	**Section 4**	**Section 5**	**Section 6**
37.5	100.0	100.0	100.0	100.0	100.0	100.0
28.0	99.0	98.0	96.0	98.0	97.9	97.0
20.0	90.0	88.9	93.2	86.1	84.2	90.1
10.0	47.1	51.2	49.3	60.2	60.1	49.8
5.00	34.5	34.8	40.3	42.8	41.8	31.6
2.36	27.9	30.0	28.3	29.0	26.9	26.8
0.30	12.1	13.1	13.0	10.0	11.1	13.9
0.150	8.4	9.2	9.8	7.6	7.9	8.1
0.075	6.3	5.6	6.7	4.6	4.1	5.2

As shown in Figure 26, the Percentage Refusal Density (PRD) design method (BS EN 12697-32:2003) was used in most of the mixtures of the trial pavement sections. The PRD design method is a Marshall method but with more blows to simulate the field compaction and loading until the density becomes refusal. The PRD value is defined as the ratio of the initial dried bulk density of the sample to the final density (refusal density) expressed as a percentage. In the PRD design method, a test is performed to obtain the design's optimum bitumen content at which the voids in the mix (VIM) at refusal density are only 3%. This requirement is supposed to reduce the chance of plastic deformation, which is associated with VIM in the field lower than 3%, occurring.

Unmodified 40-50 Pen bitumen was used in trial section 1 (surface and base courses), while unmodified 60-70 Pen bitumen was used in all other trial sections except sections 5 and 6. Trial section 4 is the control pavement structure that was designed and constructed following the standards of Qatar Construction Specifications (QCS-2010), which essentially follow the Marshall method. Trial section 5 involved the use of a sulphur-extended bitumen, Shell Thiopave, while trial section 6 comprised polymer-modified bitumen (PMB) with a Styrene-Butadiene-Styrene (SBS) modifier that was graded as PG76-22. Unmodified 60-70 Pen base bitumen was used to produce the PMB and its fresh characteristics can be found in Appendix A. Unfortunately, no attempts were made in recovery and testing the bitumen (DSR, Pen,

TR&B) of the mixtures as laid. Such an effort, however, is highly recommended for future projects since it will allow a much better analysis of pavement performance.

The aggregate used in the surface course for all trial sections was Gabbro, which was imported from the United Arab Emirates. This aggregate is an igneous rock that has been used in road construction for a long time in the Arabian Gulf region. A local aggregate in Qatar, Limestone, was used only in the base course of trial section 3 to compare it with the performance of trial sections in which Gabbro was used. The aggregate gradations shown in Table 13 and Table 14 are all within the QCS limits; no big differences between them were observed.

The same granular sub-base with Limestone aggregate was used for all trial sections with an estimated design modulus of 450 MPa, and the subgrade was weathered Limestone with a design modulus of 200 MPa (TRL Client Project Report 282, Phase C (2010) and TRL Client Project Report 282, Phase D (2010)).

For the construction of the trial road, the weathered Limestone subgrade was excavated to a depth of 540 mm to allow the top of the trial road to be at the same level as that of the old carriageway. The 200 mm sub-base material was laid over the entire area and then sprayed with a bituminous prime coat of cut-back 60-70 Pen bitumen, ready for the first AC layer to be constructed (TRL Client Project Report 282, Phase D, 2010). The compaction was undertaken by two vibrating rollers of 10-tonnes deadweight, two 18-tonne deadweight pneumatic-tyred and two 20-tonne deadweight pneumatic-tyred rollers together with a 3-tonne vibrating roller for the transverse joints. A K1-40 emulsion bitumen tack coat was applied to each AC layer using a tanker before it was overlaid with the next layer. The asphalt concrete (AC) base layers were constructed in two layers, about 135 mm each, which is not the typical compaction thickness in Qatar (usually 70-90 mm each). The 135 mm thickness was used for the purpose of obtaining field cores later from these base courses. In order to resist rutting, the current

practice in Qatar is to over-compact the AC layers at a relatively low temperature for up to 4 or 5 hours to achieve the required low air void content (≈ 3.0%) in spite of the low bitumen content. This might cause grinding of the hard aggregate (Gabbro) used in the constructed roads and might even cause micro-cracking.

A day after paving the trial sections, three pairs of field cores were extracted from each trial section and tested for compositional analysis, and the results are summarised in Table 15.

Table 15. Compositional analysis summary for all trial sections (TRL Client Project Report 282, Phase D, 2010).

Layer	Section # (mix)	Bitumen content (%)		VIM (%)	VMA (%)	VFB (%)	Stability (kN)	Flow (mm)	Stiffness (kN/mm^2)
		By weight	By volume						
Surface course	1 (PRD)	3.9	10.2	4.0	14.2	71.7	14.8	2.6	6.2
	2 & 3A (PRD)	3.8	9.4	4.9	14.3	69.1	14.7	2.6	5.7
	3B & 4 (QCS)	3.8	9.5	5.3	14.8	64.4	13.4	2.7	5.2
	5 & 6 (PRD)	3.8	9.4	4.7	14.1	68.5	14.4	2.5	5.8
Base course	1 (PRD)	3.6	9.2	4.1	13.3	69.0	15.2	3.1	4.9
	2 (PRD)	3.4	8.7	4.5	13.2	65.8	14.1	2.6	5.5
	3 (PRD)	4.4	10.0	4.2	14.2	71.2	11.5	2.9	4.0
	4 (QCS)	3.5	8.9	4.8	13.7	64.9	14.1	2.6	5.4
	5 (QCS)	3.9	9.5	4.2	13.7	69.4	18.1	2.6	7.1
	6 (PRD)	3.5	9.5	4.2	13.2	67.9	15.2	2.6	5.9

According to the compositional analysis summary table, the average bitumen content by weight for the surface course and the base course is 3.8% and 3.7%, respectively. These bitumen content values are low enough to make the mixtures too stiff, as shown in the stiffness results in the table, which raises a concern about the durability and fatigue resistance of these mixtures.

3.2.3 Traffic loading data

The trial road was constructed as a part of an access road to a sand-washing plant in the south of Qatar. This trial road consists of one lane only in each direction, and heavily loaded trucks are arriving at and leaving the sand-washing plant fully loaded (45 tons) with washed or unwashed sand. After the opening of the trial road in August 2010, the traffic was more

controlled, and during the peak hour around 90 heavily-loaded trucks pass along the trial road in each direction. This traffic loading was assumed to be consistent during the day (16 working hours) in order to simulate the maximum loading scenario. So, 1440 heavily loaded trucks were assumed to pass in each direction of the trial road daily with washed or unwashed sand.

The collected traffic data showed that three axle configurations were used on the trucks that were passing the trial road six days a week: five-axle, four-axle and three-axle trucks. The total axle-load equivalent factors for these trucks were calculated based on the 80 kN (18 kips) standard axle load to be 11.3, 10.5 and 4.5, respectively. Table 16 summarises the traffic loading volumes on the trial road.

Table 16. Traffic loading configurations and volumes on the trial road.

Axle configuration	Fully loaded truck factor	Trucks/day (each direction)	Trucks/year (each direction)	20-years ESALs (million) [truck factor × trucks/year × 20]
Five-axle	11.3	480	1.5×10^5	34.0
Four-axle	10.5	800	2.5×10^5	52.5
Three-axle	4.5	160	0.5×10^5	4.5
Total	**-**	**1440**	**4.5×10^5**	**91.0**

According to Table 16, the design 20-years ESALs load was calculated to be 91 million. Up to the moment when field measurements were performed on the trial road in summer 2013, traffic loading had reached approximately 13.5 million ESALs. The traffic loading on the trial road is considered to be very high, and almost 1.8 times the maximum traffic class T6 (50 million ESALs) provided in the QHDM. This huge loading was kept in mind during the performance evaluation of the trial sections in this study.

3.2.4 Performance evaluation results for the full-scale trial sections

As mentioned at the beginning of this section, the objective of the conducted field tests is to evaluate the performance of perpetual pavements in Qatar under high traffic loading and different temperature conditions. Therefore, it is important to specify the main distresses that

might be affecting the performance of the perpetual pavement structures. In this subsection, the results of each field test performed on the six trial sections are presented and discussed.

3.2.4.1 Automatic road analyser vehicle results

Ground-penetration radar (GPR) data of left- and right-hand sides (LHS and RHS) of wheel paths of each trial section were collected by the automatic road analyser vehicle. Table 17 presents thicknesses of surface and base courses calculated from the GPR data. These thicknesses were compared with the design thicknesses of the trial sections shown in Figure 26. The thickness of the surface course and top base course is, according to Figure 26, 205 mm, while the thickness of the lower base layer is 135 mm.

Table 17. Layer thicknesses calculated from GPR data of trial sections.

Section #	Location	Average thicknesses from GPR (mm)			
		Surface + top base course		Bottom base course	
		LHS	RHS	LHS	RHS
1	Wheel path	228	211	121	121
	Centre lane	226	212	125	123
2	Wheel path	223	205	143	127
	Centre lane	231	208	126	122
3	Wheel path	225	207	134	126
	Centre lane	223	202	135	124
4	Wheel path	202	202	156	134
	Centre lane	198	204	161	126
5	Wheel path	206	195	155	137
	Centre lane	214	199	148	139
6	Wheel path	203	191	154	140
	Centre lane	211	190	149	137
AVG	Wheel path	214.5	201.8	143.8	130.8
	Centre lane	217.2	202.5	140.7	128.5
Standard deviation	Wheel path	12.0	7.5	14.1	7.3
	Centre lane	12.0	7.6	14.3	7.5

The average GPR thicknesses are close to the layer thicknesses shown in Figure 26. Table 17, however, also shows a considerable variation in layer thickness. GPR thickness results will be used in Elmod6 software for back-calculating the FWD data to find the modulus of each layer in every trial section.

The rut depth and IRI of each trial section as measured by the automatic road analyser vehicle were reported as an average of 10 measurements (1 value/m). These rut depth and IRI values were measured for LHS and RHS for both directions and are shown in Table 18.

Table 18. Rut depth and IRI average values for LHS and RHS of both directions of the trial road.

Section #	Location	Rut depth (mm)		IRI value (m/km)	
		Average	Standard deviation	Average	Standard deviation
1	LHS	1.97	1.00	1.96	0.75
	RHS	1.84	1.05	2.39	0.74
	Both	**1.91**	**0.97**	**2.22**	**0.70**
2	LHS	2.38	0.44	2.03	0.53
	RHS	1.28	0.20	2.59	0.60
	Both	**1.84**	**0.25**	**2.31**	**0.54**
3A	LHS	2.36	0.24	1.97	0.50
	RHS	1.29	0.22	2.26	0.39
	Both	**1.83**	**0.18**	**2.11**	**0.43**
3B	LHS	2.30	0.43	2.07	0.40
	RHS	1.83	0.32	2.20	0.37
	Both	**2.07**	**0.23**	**2.14**	**0.31**
4	LHS	2.41	0.48	1.97	0.48
	RHS	1.56	0.43	2.18	0.55
	Both	**1.99**	**0.23**	**2.08**	**0.49**
5	LHS	1.65	0.26	2.59	0.65
	RHS	2.42	0.39	3.09	0.74
	Both	**2.04**	**0.26**	**2.84**	**0.68**
6	LHS	1.83	0.29	1.88	0.35
	RHS	1.79	0.45	2.55	0.51
	Both	**1.80**	**0.18**	**2.21**	**0.37**

It is interesting to see that after a year and a half of service (~13.5 million ESALs) almost all trial sections showed a high IRI and a relatively high rut depth. This was expected given the very large amount of heavy traffic loading passing the trial sections every day in addition to the climatic conditions. It is noticeable that the rutting results for the LHS of each direction are quite often more than those for the RHS, and this might be caused by the fact there is more overlapping of the wheel loads in the left-hand wheel path of each lane.

Assessing the effect of using different bitumen types but the same aggregate type and mix design was one of the major objectives of this part of the study. Thus, trial sections 1, 2

and 6 were compared against total rutting depth and IRI. Table 18 shows that trial section 6 has the lowest rutting depth and IRI value. This trial section consists of a surface course, and a base of Percentage Refusal Density design (PRD) with PMB bitumen (PG76-22) and Gabbro aggregate which shows the role of modified bitumen in enhancing the mixtures' resistance to rutting and smoothness.

Then, a comparison between trial sections 2 and 3A was conducted to assess the influence of using the local aggregate, Limestone, against rutting and IRI. Both trial sections consist of a surface course and a base of Percentage Refusal Density design (PRD) with 60-70 Pen bitumen but with different aggregate types for the base. As shown in Table 18, trial section 2 has higher IRI value than trial section 3A but almost similar rutting depth. The difference between both trial sections in IRI is not significant. This was expected because the rutting and IRI resistance is mainly affected by the mix design of the surface course, which is identical in this case.

A comparison between trial sections 2 and 4 with Gabbro aggregate and between 3A and 3B with Limestone was conducted to assess the effect of mix design method on performance. The comparison according to mix design method reflects the compaction level/quality, the bitumen content and air voids content which will certainly affect the performance against rutting and IRI. As presented in Table 18, trial section 4 has slightly higher rut depth but lower IRI values than those of trial section 2. On the other hand, the rut depth and the IRI values are slightly higher for trial section 3B than 3A. The results showed that the design method (the aggregate gradation and bitumen content) has slightly affected the IRI and the rut depth results. One might conclude that the QCS design method is generally better for Qatar than the PRD method.

Finally, rut depth and IRI average values for trial sections 5 and 6 were compared to evaluate the effect of having a different base layer. Both sections consist of a surface course of

PRD with PG76-22 bitumen but different base layer, as shown in Table 18. The results revealed that section 5 has higher IRI values and rut depth compared to section 6. Although the differences are small and the trial sections were only in service for one and a half years, the results tend to indicate that using Shell Thiopave bitumen in the base may not significantly improve the performance of the pavement structure.

Based on the automatic road analyser vehicle field results, it can be concluded that rutting and IRI are the governing problems for these perpetual pavement structures. With respect to the IRI values, it should be noted that these seem to be a bit high 18-month-old pavements. Unfortunately, IRI data immediately after construction were not available so it is hard to say to what extent traffic is the cause of these IRI values.

3.2.4.2 Falling weight deflectometer (FWD) results

Observing the effect of high temperature in Qatar on the stiffness of the trial sections was another objective of these field tests and evaluations. Therefore, the FWD test was conducted twice on the full-scale trial road. The first FWD test was conducted in the spring season (February 2012) when the average air temperature was about 23 °C while the average surface temperature of the trial road was about 25 °C as measured by the IR sensors of the FWD. The second test was conducted in the summer season (August 2012) when the average air temperature was 46 °C while the average surface temperature was about 63 °C. There is obviously a big difference in temperature between the two seasons, and this surely affects the performance of asphalt pavement structures and must therefore be taken into consideration.

In the FWD test, the measured deflections, air and surface temperatures, and thicknesses of layers were used to back-calculate the moduli (stiffnesses) of the different layers – asphalt concrete, granular sub-base and subgrade – using the Deflection Basin Fit tool in the Elmod6 software. The modulus of the AC layer was measured by the FWD as one layer (surface, upper and lower base courses).

According to TRL reports about the trial road, the seed modulus value used for the AC layers of the trial pavement sections was 2500 MPa and 6500 MPa in the summer and spring FWD tests, respectively. Also, the seed modulus value used for the sub-base and subgrade layers was 450 MPa and 200 MPa in summer and spring, respectively.

Figure 27 shows the dynamic moduli results for the various layers back-calculated from the FWD test in both seasons using Elmod6 software.

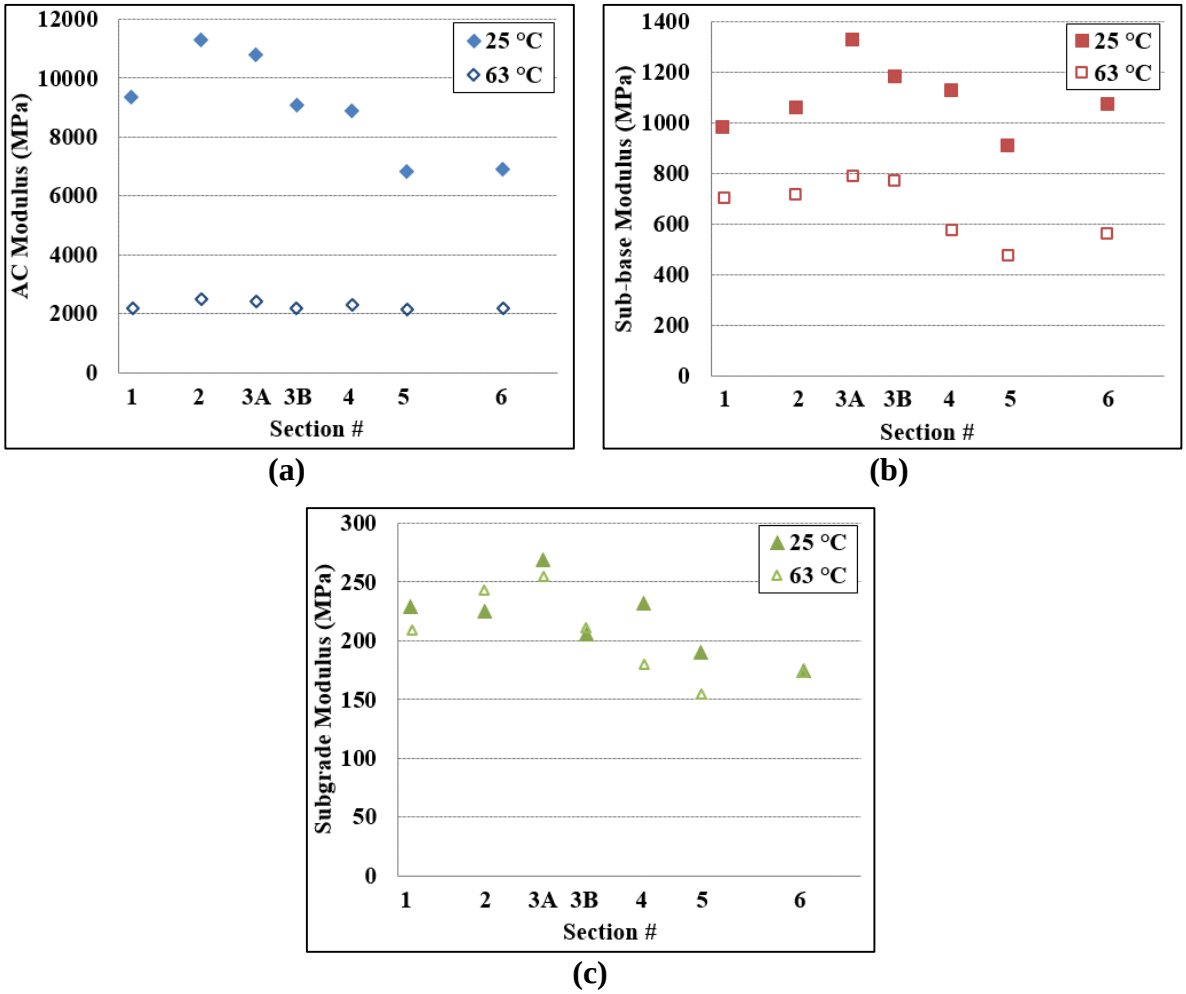

Figure 27. Comparison between moduli of each layer of the trial sections in low and high air temperatures.

As would be expected, the results illustrate that the moduli of the asphalt concrete layer and sub-base layer are higher at the lower air temperature (i.e. 23 °C). The difference in moduli results between the two seasons was highest for the AC layer (surface, upper and lower base

courses) because of the temperature dependency of the asphalt mixture stiffness. The difference between the moduli of the two seasons for the subgrade results was relatively small.

In general, the asphalt concrete layer with Thiopave in trial section 5 and PG76-22 in section 6 had the lowest temperature susceptibility, while section 2, with 60-70 Pen bitumen, had the highest temperature susceptibility. This result shows the role of polymer-modified bitumen in reducing the temperature's impact on the stiffness of the layers of the asphalt pavement structures.

The moduli for the asphalt concrete layers of the various trial sections in the summertime were very close to each other (≈ 2000 MPa), in contrast to the spring season. The stiffness of the asphalt concrete mixtures in the surface and sub-base layers decreased by around 80% between the spring and summer seasons, as shown in Figure 27. This will surely affect the performance of these trial sections against rutting and cracking.

In order to check the statistical difference of the dynamic moduli of each layer between the trial sections, one-way (or single-factor) analysis of variance (ANOVA) was conducted in this part of the study. The analysis was performed using a statistical significance level of 5% ($\alpha = 5\%$). In this analysis and assuming that the null hypothesis is true, the *p*-value is the probability of finding a test statistic at least as extreme as the one that was actually observed. One often "rejects the null hypothesis" when the *p*-value is less than the predetermined significance level α, indicating that the observed result would be highly unlikely under the null hypothesis. The hypotheses for one-way ANOVA are:

$H_0 : \mu_1 = \mu_2 = \ldots = \mu_k$

H_a : Not all population means are equal

Table 19 and Table 20 show the summary and results of ANOVA for FWD tests on the trial sections in both seasons.

Table 19. ANOVA results for dynamic modulus values of each layer of the trial sections in February 2012.

Section #	Count	Sum	Average	Variance	*p*-value
		Asphalt concrete layer			
1	10	93686	9368	5672269	6.71E-08
2	8	90309	11288	6263932	
3A	6	64705	10784	5821235	
3B	8	72691	9086	3529195	
4	8	71147	8893	4488666	
5	25	170850	6834	2210381	
6	13	90004	6923	1103870	
Section #	**Count**	**Sub-base layer**			
1	10	9795	979	102693	0.079
2	8	8458	1057	147928	
3A	6	7954	1325	295126	
3B	8	9461	1182	64248	
4	8	9032	1129	111667	
5	25	22736	909	68243	
6	13	13945	1072	67584	
Section #	**Count**	**Subgrade layer**			
1	10	2289	228	5234	0.082
2	8	1803	225	9335	
3A	6	1611	268	12541	
3B	8	1642	205	529	
4	8	1856	232	7132	
5	25	4762	190	3380	
6	13	2266	174	2186	

Based on the ANOVA results of dynamic modulus values for each layer in February 2012 shown in Table 19, only the *p*-value of the AC layer is less than 5%. Therefore, the null hypothesis is rejected, and there is a 95% confidence level that the mean dynamic modulus of this layer is statistically different among the trial sections. For the sub-base and subgrade layers, the *p*-value is more than 5%, and this means that the average dynamic modulus of each of these layers is not statistically different among the trial sections with 95% confidence.

Table 20. ANOVA results for dynamic modulus values of each layer of the trial sections in August 2012.

Section #	Count	Sum	Average	Variance	*p*-value
		Asphalt concrete layer			
1	10	21981	2198	190818	0.358
2	8	19903	2487	124348	
3A	6	14361	2393	99268	
3B	8	17459	2182	157912	
4	8	18256	2282	76579	
5	14	30042	2145	73285	
6	14	30393	2170	176022	
Section #	**Count**	**Sub-base layer**			
1	10	7023	702	22072	0.00027
2	8	5734	716	14439	
3A	6	4736	789	57722	
3B	8	6170	771	24418	
4	8	4605	575	12276	
5	14	6613	472	35806	
6	14	7881	562	31296	
Section #	**Count**	**Subgrade layer**			
1	10	2091	209	2188	1.92E-06
2	8	1942	242	1782	
3A	6	1527	254	85	
3B	8	1687	210	672	
4	8	1436	179	697	
5	14	2170	155	2258	
6	14	2428	173	1681	

On the other hand, ANOVA results for the dynamic modulus values of each layer in August 2012 shown in Table 20 revealed the opposite of results in Table 19 and only the *p*-value of the AC layer is more than 5%. This means that the difference in the average dynamic modulus of the AC layer is not statistically significant among the trial sections with 95% confidence.

In conclusion, the results of field performance evaluation of the perpetual trial pavement sections showed slightly low resistance to rutting, high IRI values, to some extent and low stiffness during summertime when the temperature is high. These distresses and deteriorations are expected consequences of the huge traffic loading and the big difference in temperature between spring and summer seasons. Accordingly, a more in-depth investigation

of the performance evaluation of AC mixtures – not structures – is recommended in order to precisely identify the major distresses and how to resist them.

It is worth mentioning that two trial pits, 150 kg each, were extracted from the trial road site; one of them is from section 2 (station 0+215) and the other one is from section 5 (station 0+625). The trial pits were taken to the laboratory in order to investigate the properties and the characteristics of the sub-base and subgrade materials. Particle size distribution, maximum dry density, optimum moisture content, California Bearing Ratio (CBR), liquid limit, plastic limit and plasticity index were all evaluated for both sub-base and subgrade layers, as can be seen in Appendix B. However, these laboratory tests were conducted on disturbed samples and unfortunately no in situ properties (e.g. density and moisture content) were collected, which are essential and which would provide a lot of information about the trial road.

3.3 Life-cycle cost analysis (LCCA)

In subsection 3.1.3.2, eight different asphalt concrete pavement structures (conventional and perpetual) were evaluated using the M-E PDG software based on performance and damage criteria for three levels of traffic loading (T6, 3×T6 and 6×T6). The objective was to assess the effect of implementing the perpetual pavement concept on performance of pavement structures in the State of Qatar. Curves were produced to show the evolution of damage with pavement age and when it reached the design limits (Figure 20). Results indicated that the most effective pavement structure is the perpetual pavement with a 300 mm-thick base course and S3 (A-1-b) as subgrade soil class.

Here, the cost of constructing and maintaining each of the eight asphalt pavement structures is evaluated. The cost of construction and rehabilitation of these structures has been used in a Life-Cycle Cost Analysis (LCCA) to obtain the Net Present Value (NPV). NPV is used in capital budgeting to analyse the profitability of a project or investment. A comparison

was made to evaluate the optimised net present value to enable selection of the most viable design for a traffic level of 300 million ESALs of 6×T6.

3.3.1 LCCA methodology and assumptions

The Life-Cycle Cost Analysis (LCCA) is an important tool that has been used in transportation engineering for a long time, but only in the last two decades has its use become more extensive. Investment alternatives are compared when using LCCA but, in the pavement engineering field, it is a systematic approach for considering most of the factors that go into making a pavement investment decision. Such factors include the initial construction cost or repairing a pavement structure, all significant maintenance costs expected over the pavement's service life, and the salvage value of the pavement structure at the end of its life (ARA, Inc., ERES Consultants Division, 2004).

As demonstrated in Figure 28, upon identifying altered investment strategy options, the maintenance/rehabilitation costs associated with each strategy option are determined and converted into Net Present Value (NPV) where the costs are adjusted to properly reflect the time value of money. The individual net present values are then summed with the initial cost and the total cost is compared with the total costs of the other strategy options, in order to identify the most economical investment option (ARA, Inc., ERES Consultants Division, 2004).

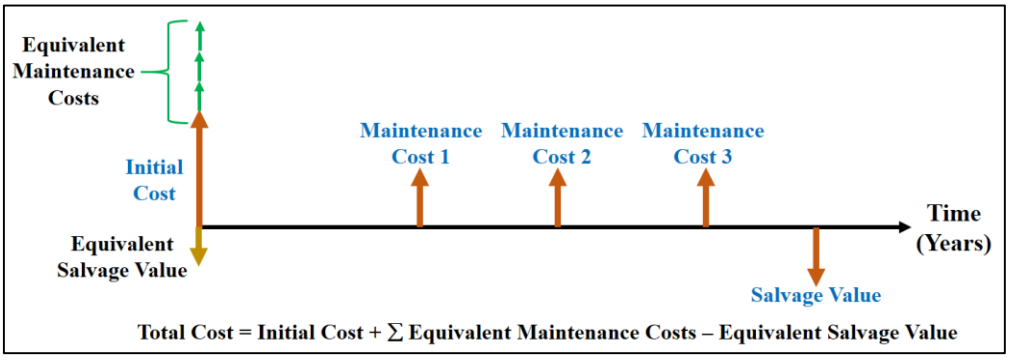

Figure 28. Determining life-cycle costs for alternative investment strategy.

LCCAExpress software, version 2.0, developed by Timm (2011), was used for conducting the life-cycle cost analysis in this study. The accuracy of LCCA results depends on the accuracy of each of the inputs. The software inputs include unit prices of the materials in the pavement structure, construction and rehabilitation activities/costs during its service life and recurring maintenance activities/costs in order to compute the Net Present Value (NPV) as shown in Figure 29.

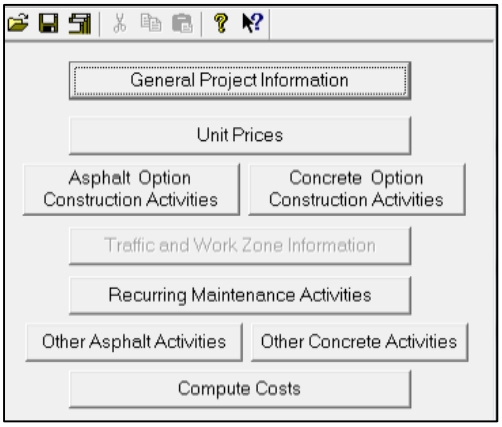

Figure 29. Inputs of life-cycle cost analysis using LCCAExpress software.

To simplify the analysis, some indirect costs such as work-zone user costs were deactivated from the software. In addition, some assumptions were made to limit the comparison to the construction and rehabilitation costs only. The assumptions were as follows:

- Road geometry is assumed to be one mile (1609 m) long and 24 ft (7.32 m) wide.
- Road has two lanes in each direction.
- Lane width is 12 ft (3.66 m).
- Speed limit is 60 mph (96.56 km/h).
- Overlay thickness is considered to be the same as the milling thickness.
- Same asphalt mix design is used for all cases.
- Discount rate used in the software is 4%.

It is worth mentioning that the discount rate represents the investor's minimum acceptable rate of return. Demos (2006) stated that the discount rate "reflects only the opportunity value of time because public sector project benefits should be dependent only upon real gains (cost savings or expanded output), rather than purely price effects".

3.3.2 Cases used for LCCA analysis

The eight pavement structure cases analysed earlier using M-E PDG in this chapter and included in the LCCA analysis are summarised in Table 21.

Table 21. Layers and thicknesses for pavement structure cases used in the LCCA analysis.

Pavement structure type	Case #	Thickness of layer (mm)						Code
		Surface course (AC1)	Upper base (AC2)	Lower base (AC3)	Stabilised base	Sub-base (Crushed stone)	Soil subgrade	
Perpetual pavement	P1	75	175	75	270	-	S1	S1-6T6-P-250
	P2	75	200	100	270	-	S1	S1-6T6-P-300
	P3	75	175	75	270	-	S3	S3-6T6-P-250
	P4	75	200	100	270	-	S3	S3-6T6-P-300
Flexible-composite	F1	40	150	-	270	200	S1	S1-6T6-F-Pen
	F2	40	150	-	270	-	S3	S3-6T6-F-Pen
Asphalt concrete (Flexible)	A1	40	250	-	-	200	S1	S1-6T6-A-Pen
	A2	40	250	-	-	100	S3	S3-6T6-A-Pen

3.3.3 Cost of construction and rehabilitation

Average unit prices for construction, milling and overlay operations that were obtained from local road construction companies in the State of Qatar and used in the LCCA analysis are given in Table 22. The prices were supplied per square metre for all layer thicknesses of the eight cases. The rehabilitation cost included both milling of existing layers and overlaying of new layers. It is worth mentioning that the practice in Qatar is to mill the whole surface AC layer of the road and overlay a new layer, even if only small parts of it are rutted. This is very expensive especially if the rutted parts can be simply milled and overlaid or filled.

The cost of construction and overlay for the perpetual pavement was approximately 20% more than that for the conventional pavement due to the use of polymer-modified bitumen

(PMB). In addition, the overlaying cost for the cement-stabilised and crushed stone layers should be ignored in this analysis because they will not be removed or milled.

Table 22. Average unit prices obtained from construction companies in Qatar.

Description		Construction	Milling	Overlay
		$/m^3	$/m^3	$/m^3
AC layer	60-70 Pen	240	58	225
	PG76-10	288	58	270
Cement stabilised		65	-	-
Crushed stone		36	-	-

3.3.4 LCCA analysis and results

Using the analysis results obtained from the M-E PDG, each pavement structure had a different rehabilitation method based on the type of damage and when it occurs and reaches its design limit within the service period of 20 years. Table 23 and Table 24 show the time, in months, when each type of damage occurs.

Table 23. Number of months needed to reach the design limit in longitudinal and alligator cracking.

Pavement structure type	Case #	Number of months to reach the design limit of	
		Longitudinal cracking	Alligator cracking
Perpetual pavement	P1	238	Below limit
	P2	Below limit*	
	P3	96	
	P4	Below limit	
Flexible-composite	F1	165	Below limit
	F2	45	
Asphalt concrete (Flexible)	A1	83	215
	A2	34	Below limit

* "Below limit" means that the damage in the case does not reach the limit within 20 years.

Table 24. Number of months needed to reach the design limit in rutting for each layer.

Pavement structure type	Case #	Number of months to reach maximum rutting on each layer (Design limit = 19 mm (0.75 in))					
		Surface course (AC1)	Upper base (AC2)	Lower base (AC3)	Stabilised base	Sub-base (Crushed stone)	Total rutting (All layers)
Perpetual pavement	P1	200	Below limit	Below limit	Below limit	Below limit	93
	P2	Below limit					164
	P3	201					106
	P4	Below limit					189
Flexible-composite	F1	141	58				11
	F2	141	59				14
Asphalt concrete (Flexible)	A1	Below limit	153				23
	A2		153				33

Examples of the effect of rehabilitation performed on the asphalt concrete layer on other distresses for three examples of the analysis cases are shown in Figure 30 to Figure 32.

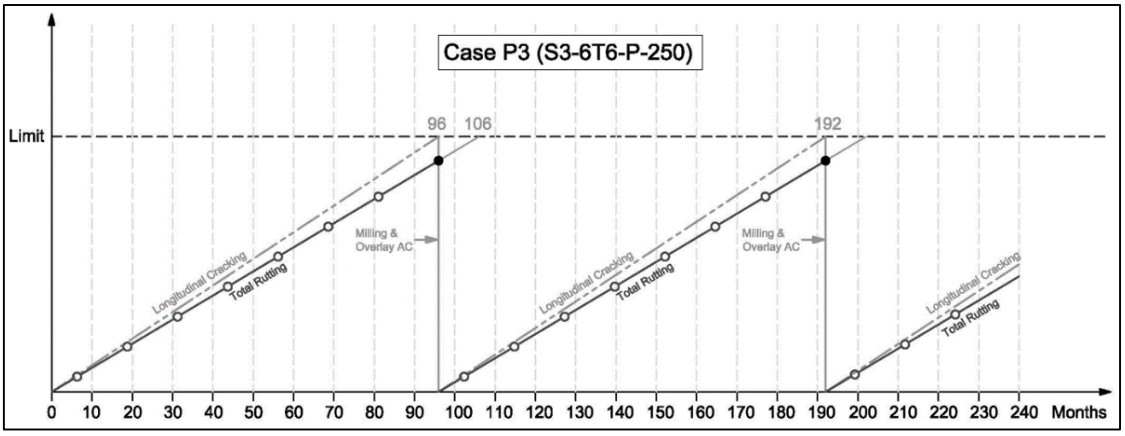

Figure 30. Effect of rehabilitation performed for longitudinal cracking in the AC layer on the total rutting of the layer in case P3.

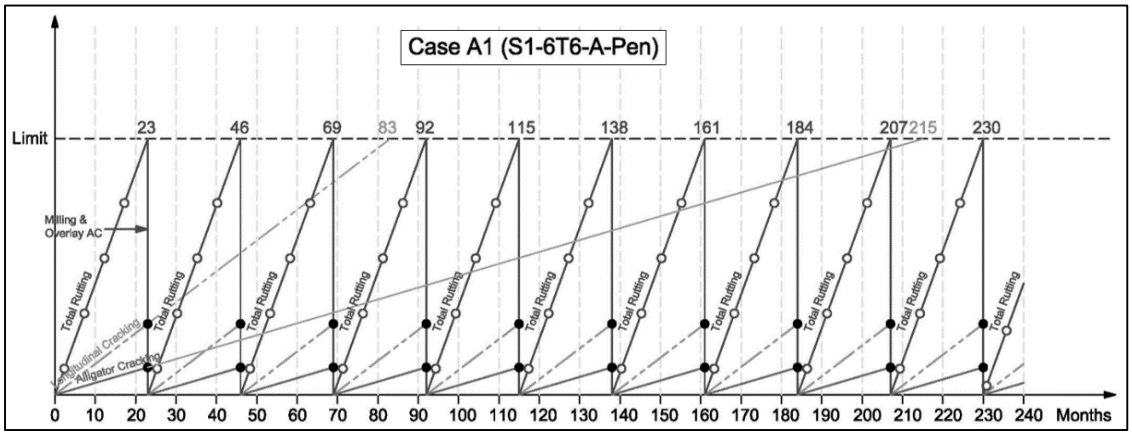

Figure 31. Effect of rehabilitation performed for the total rutting in the AC layer on longitudinal and alligator cracking in case A1.

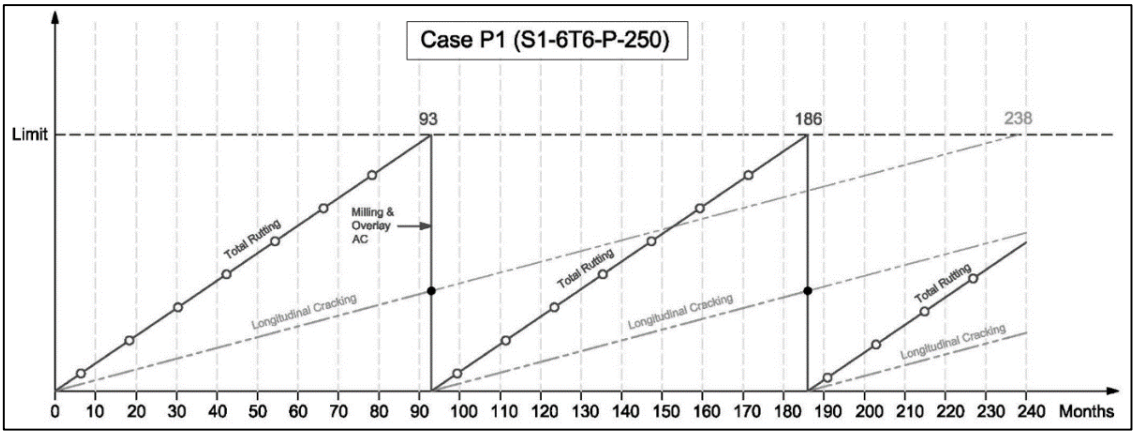

Figure 32. Effect of rehabilitation performed for the total rutting in the AC layer on longitudinal cracking of the same layer in case P1.

According to the results of the M-E PDG and the rehabilitation activities illustrated above, Table 25 presents the number of maintenance cycles needed during the service life of each analysis case in addition to the number of years between each cycle.

Table 25. Number of maintenance activities needed for each case and years between each of them.

Case #	Code	Number of maintenance cycles needed during the service life	Number of years between each maintenance cycle
P1	**S1-6T6-P-250**	2	~ 8
P2	**S1-6T6-P-300**	1	~ 14
P3	**S3-6T6-P-250**	2	8
P4	**S3-6T6-P-300**	1	~ 16
F1	**S1-6T6-F-Pen**	21	~ 1
F2	**S3-6T6-F-Pen**	17	~ 1
A1	**S1-6T6-A-Pen**	10	~ 2
A2	**S3-6T6-A-Pen**	7	~ 3

As presented in Table 25, the conventional pavement structures (F1, F2, A1 and A2) need maintenance every 1-3 years during their service life due to the distresses that occur. Adding to that the work-zone user costs and the consumption of natural resources, it can be concluded how unsustainable and expensive the conventional pavement structures are for the country.

Then, all the previous inputs were used in the LCCA analysis and the results from the LCCAExpress software were displayed as net present value (NPV). Table 26 and Figure 33

present the initial construction NPV and the recurring maintenance NPV added together to obtain the total NPV.

Table 26. Net present value for initial construction, recurring maintenance and the total NPV for each case.

Case #	Code	Initial construction NPV	Recurring maintenance NPV	Total NPV
P1	**S1-6T6-P-250**	$1,438,328	$1,583,247	$3,021,575
P2	**S1-6T6-P-300**	$1,627,775	$834,359	$2,462,134
P3	**S3-6T6-P-250**	$1,438,328	$1,583,247	$3,021,575
P4	**S3-6T6-P-300**	$1,627,775	$771,412	$2,399,187
F1	**S1-6T6-F-Pen**	$954,522	$8,872,691	$9,827,213
F2	**S3-6T6-F-Pen**	$819,044	$7,057,934	$7,876,978
A1	**S1-6T6-A-Pen**	$1,037,100	$6,421,416	$7,458,516
A2	**S3-6T6-A-Pen**	$968,504	$4,366,487	$5,334,991

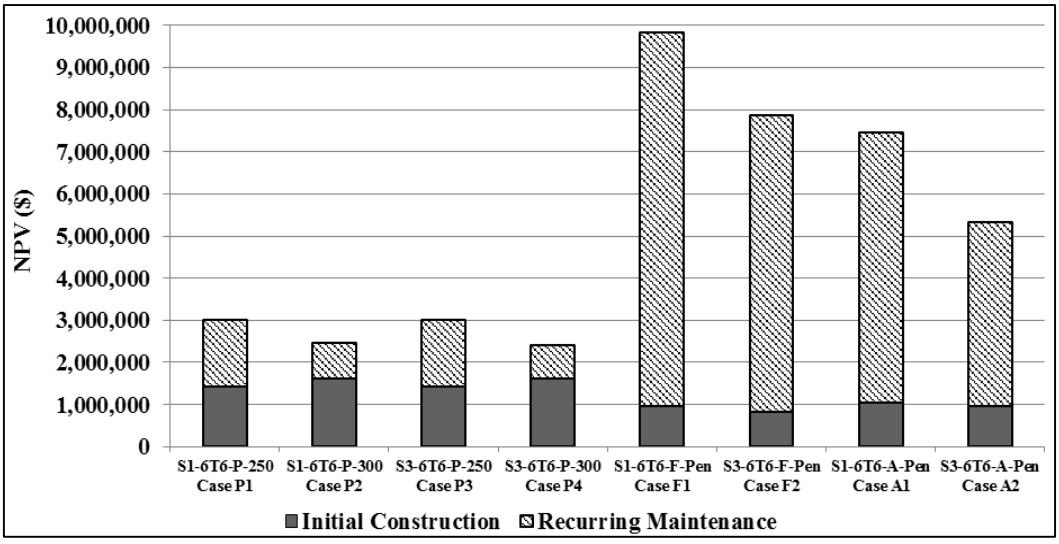

Figure 33. Total NPV for all cases.

As shown in Table 26 and Figure 33, despite the fact that the lowest initial construction cost among cases with S1 subgrade is in the conventional pavement case F1 ($954,522), this case has the highest recurring maintenance cost ($8,872,691) and maintenance should be conducted almost annually during the pavement service life. The lowest recurring maintenance cost is in the perpetual pavement case P2 ($834,359), where maintenance should only be carried out after 14 years. Case P1 has lower initial construction cost ($1,438,328) than case P2 ($1,627,775), but higher recurring maintenance ($1,583,247). Initial construction cost in case A1 ($1,037,100) is almost the same as in case F1, but the former's recurring maintenance cost

($6,421,416) is lower and maintenance should only be carried out biennially during the service life of the asphalt pavement structure (rather than yearly, as for F1).

Table 26 and Figure 33 also show that the lowest initial construction cost is in case F2 ($819,044) for the analysis cases with S3 subgrade. However, the recurring maintenance cost is the highest ($7,057,934) and maintenance should be carried out almost annually during the pavement service life. The lowest recurring maintenance cost is in case P4 ($771,412), where maintenance should be executed every 16 years during its service life, but its initial construction cost is the highest ($1,627,775). Case P3 has lower initial construction cost ($1,438,328) than case P4, but higher recurring maintenance cost ($1,583,247). Case A2 has higher initial construction cost ($968,504) than case F2, but less recurring maintenance cost ($4,366,487), and maintenance should be conducted almost every three years during the service life of the asphalt pavement structure (rather than yearly, as for F2).

In general, by studying all the LCCA analysis results, it can be noticed that the lowest NPV of all cases is in the perpetual pavement case P4 ($2,399,187), as shown in Table 26 and Figure 33. This is in agreement with performance evaluation results obtained using the M-E PDG and presented earlier in this chapter. All perpetual pavement cases have higher average initial construction cost than cases of conventional flexible-composite and asphalt concrete (flexible) structures by almost 30%. However, this increase in initial construction cost is compensated for and can be justified by the significant reduction in the recurring maintenance costs by almost 6.5 times. As shown in Table 26 and Figure 33, case F1 can be considered as the worst case because it had the highest NPV and it needed almost annual recurring maintenance during its 20 years of service. This conclusion supports the significance of using perpetual pavement structures in the State of Qatar in order to have sustainable, economical and high-performing road structures.

3.4 Conclusions

The key objective of this chapter was to identify the main distresses affecting the performance of asphalt concrete pavement structures in Qatar and propose solutions and recommendations to these issues. Therefore, conventional asphalt concrete pavement structures available in the Qatar Highway Design Manual (QHDM) were assessed against major distresses and compared to a proposed perpetual pavement structure using the M-E PDG software. It should be noted that this was the first time that M-E PDG analysis had been performed in the State of Qatar. In addition, a full-scale trial road with six different perpetual pavement structures was constructed in Qatar on a route used by heavy trucks in order to evaluate their performance after a year and a half of service by conducting several field tests.

According to the first stage of M-E PDG analysis, it was concluded that the conventional pavement structures provided in the QHDM, with Marshall mix design and unmodified 60-70 Pen bitumen, are not suitable for the climatic conditions and high traffic loading in the State of Qatar. In addition, the use of polymer-modified bitumen instead of the conventional unmodified bitumen was very useful but insufficient to resist top-down cracking and rutting distresses significantly, especially in the flexible pavement structures which are the common AC pavement structures in Qatar.

Furthermore, increasing the subgrade strength enhanced the performance of the conventional pavement structures against all distress except top-down cracking, which increased significantly. However, it should be noted that this later result should be treated with caution because the top-down cracking model needs to be further examined and calibrated.

The results of M-E PDG analysis on perpetual pavements showed that the use of thick perpetual pavement structures (300 mm base course) with PMB can enhance the resistance to top-down cracking, avoid bottom-up cracking and reduce the total rutting depth and IRI values.

However, if the traffic loading is extremely high (e.g. 3×T6 or 6×T6), permanent deformation (rutting) becomes a problem.

On the other hand, the results of field performance evaluation of the perpetual full-scale trial sections showed a slightly low resistance to rutting, slightly high IRI values and low stiffness during summertime. These distresses and deteriorations are expected consequences of the huge traffic loading on the trial road and the big difference in temperature between spring and summer seasons.

In general, all the results of this chapter indicated that the use of perpetual structures will accommodate the increase in heavy traffic much better than conventional structures. In addition, life-cycle cost analysis of conventional and perpetual structures demonstrated that the initial cost of perpetual pavement structures is about 30% more than conventional pavements. However, perpetual pavement structures are still more economical because they require much less maintenance or rehabilitation work, especially when the asphalt concrete base layer is 300 mm thick. LCCA conclusions matched the performance analysis results from the M-E PDG and supported the importance of implementing perpetual pavement structures in Qatar. This is a paramount finding for the State of Qatar, where there has been a tremendous increase in traffic loading.

It is recommended to conduct more in-depth analysis of the performance of conventional AC mixtures (not structures) in order to specifically identify the major distresses and how to resist them. Thus, the next chapter concentrates on evaluating the performance of different asphalt concrete mixtures (conventional and proposed mixtures) against major distresses (rutting, fracture and fatigue cracking) using several laboratory tests.

4 Performance Evaluation of Alternative Asphalt Concrete Mixtures

According to the performance evaluation results for different asphalt concrete structures presented in the previous chapter, obtained from the M-E PDG software and some field tests, rutting and fatigue (top-down) cracking are the major issues in the conventional pavements in Qatar. The use of perpetual pavement structures with PMB enhanced the performance compared to the conventional structures. This resulted in the conclusion that it was important to evaluate the performance of asphalt concrete mixtures against these major distresses in the laboratory.

In order to better understand these distresses and characterise the mixtures correctly, the following laboratory tests were conducted on some asphalt concrete mixtures:

- Flow number (FN) test to inspect mixtures' resistance to rutting,
- Semi-circular bending (SCB) test to evaluate fracture resistance of mixtures,
- Dynamic modulus ($|E^*|$) test to assess the stiffness and rutting resistance of mixtures,
- Uniaxial tension-compression (T/C) fatigue test to evaluate the fatigue cracking resistance of mixtures.

4.1 Asphalt concrete mixtures evaluated by the laboratory tests

In this part of the study, various types of asphalt concrete mixtures were tested in the laboratory in order to assess their performance against rutting, fracture, temperature susceptibility and, finally, fatigue damage. The evaluated asphalt concrete mixtures include the mixtures of the base layers of the trial road assessed in the previous chapter, as well as field and laboratory mixtures that were compacted and prepared for testing in the laboratory. The following subsections describe each mixture type in detail.

4.1.1 Field cores

The first types of asphalt concrete mixtures tested and assessed in this study are the ones extracted, cut and prepared from the base layers of the trial sections evaluated earlier, in subsection 3.2. Ten full cores (surface, upper and lower base courses) from each section were extracted from one direction only and from the wheel path and centre lane of the trial road, as shown in Figure 34 and Figure 35.

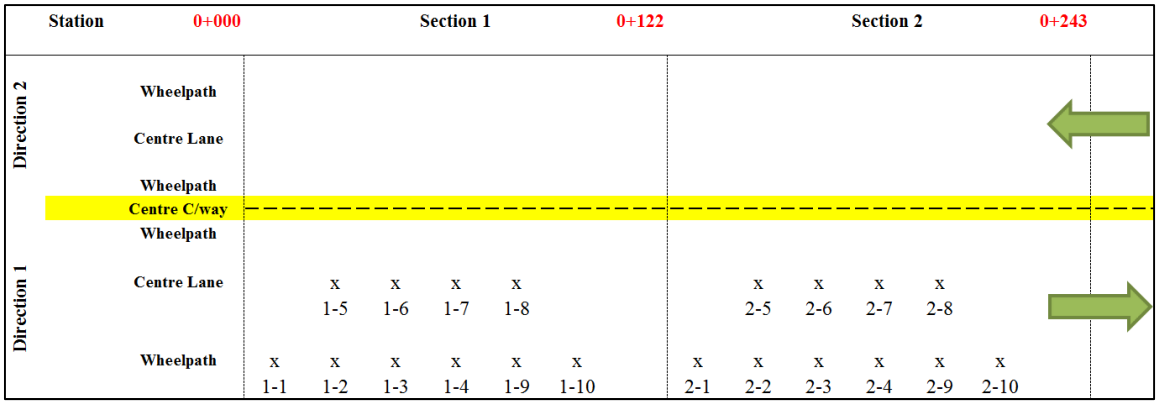

Figure 34. Location and layout of cores extracted from the trial road.

Figure 35. Full field cores extracted from the trial road.

Each field core extracted from the trial road had a diameter of 150 mm and a height of approximately 320 mm including the surface course (70 mm), the upper base course (135 mm) and part of the lower base course (~115 mm). It was noticed that cores extracted from trial section 3, with a lower and upper base course of Limestone aggregate, showed a high degree of segregation, and some cores broke just after extraction (see Figure 36).

Figure 36. Segregation in the extracted field cores from trial section 3.

After removing the surface asphalt concrete layer (~70 mm) from the field core, the upper and lower base layers (~250 mm) of the extracted field cores were then cut and cored from the middle in order to prepare specimens on which to perform the laboratory tests (FN, $|E^*|$ and T/C fatigue) using the Asphalt Mixture Performance Tester (AMPT). The test specimens were prepared to have a diameter of 100 mm and a height of 150 mm (≈ 75 mm from each base layer) according to AASHTO PP 60-14 (2014). This means that the interface between the two base layers was part of the test specimens.

Six field cores, one from each trial section, were used to perform the monotonic semi-circular bending (SCB) test. The base course of each core was cut symmetrically from the middle into two circular slices, each 50 mm in thickness and 152 mm in diameter. Each slice was symmetrically cut into two semi-circular specimens with a notch depth of 12.5 mm (0.5 in).

Table 27 shows the properties of each AC mixture cored from the base course of the trials and tested in the laboratory. The aggregate gradation and other properties of each base course mixture of the field cores were presented earlier, in Table 14 and Table 15, respectively.

Table 27. Properties of asphalt concrete mixtures cored from the base course of the trial road (TRL Client Project Report 282, Phase D, 2010).

Section #	Base course mixture	Bitumen content by weight (%)
1	Marshall/PRD, 40-50 Pen, Gabbro	3.6
2	Marshall/PRD, 60-70 Pen, Gabbro	3.4
3	Marshall/PRD, 60-70 Pen, Limestone	4.4
4*	Marshall/QCS, 60-70 Pen, Gabbro	3.5
5	Marshall/QCS, Shell Thiopave, Gabbro	3.9
6	Marshall/PRD, PG76-22, Gabbro	3.5

* Mixture of trial section 4 is the control mix.

4.1.2 Field mixtures

A local contractor in the State of Qatar used Styrene-butadiene-styrene (SBS) polymers, prepared by Woqod (Qatar Fuel) plant, in two asphalt concrete mixtures for the construction of new pavement structures in Qatar in May 2013. The aggregate used in both field AC mixtures was Gabbro, and the mix design was a Marshall mix following the gradation of a surface course (SC-Type 1) mix in QCS-2010, as shown in Table 28.

Table 28. QCS-2010 aggregate gradation for SC-Type 1 used in the field mixtures (Qatar Construction Specifications (QCS), 2010).

BS sieve size (mm)	SC-Type 1
	Cumulative passing (%)
25.0	100
20.0	98 - 100
14.0	75 - 95
10.0	60 - 81
6.30	47 - 67
2.36	25 - 41
0.60	12 - 23
0.30	8 - 16
0.150	4 - 12
0.075	2 - 6.2

In the first asphalt concrete mixture, the bitumen used was modified by Woqod SBS polymer for "Extreme" traffic loading condition (AASHTO Designation: MP 19-10, 2010) and graded as PG76-10E according to some tests conducted in laboratories in Qatar. This bitumen is also referred to as Highly Modified Bitumen (HiMB). In the other asphalt concrete mixture used on the road, the bitumen used was also modified by Woqod SBS polymer but for

"Standard" traffic loading condition (AASHTO Designation: MP 19-10, 2010) and graded as PG76-22S. In both mixtures, the bitumen content was 4.0% only, which is the practice in Qatar. Thus, both field mixtures are identical except for bitumen grade. A photograph from the construction site of the field mixtures is shown in Figure 37.

Figure 37. Paving of PG76-10E and PG76-22S asphalt concrete mixtures.

During construction, the loose hot mix asphalt of PG76-10E field mixture and PG76-22S field mixture was collected, sent to the laboratory and then compacted at around 150 °C, using the Superpave Gyratory Compactor (SGC), to a diameter of 150 mm and a height of 180 mm. The SGC samples were then cored and cut to the standard diameter of 100 mm and a height of 150 mm, and average air voids of 7%, according to AASHTO PP 60-14 (2014).

Four AMPT tests' specimens of PG76-10E field mixture in addition to three specimens of PG76-22S field mixture were prepared in the asphalt laboratory at Qatar University. The test specimens were subjected to the dynamic modulus ($|E^*|$) and uniaxial (T/C) fatigue tests. The matrix of the specimens fabricated from the field mixtures is shown in Table 29. Figure 38 shows examples of the specimens prepared from the field mixtures.

Table 29. Matrix of the field mixtures.

Mix	Code	Mix design	Aggregate	Bitumen type	Bitumen content by weight (%)	No. of specimens
1	F-Mar-10E	Marshall (SC-Type 1)	Gabbro	PG76-10E	4.0	4
2	F-Mar-22S			PG76-22S		3

Figure 38. Examples of the specimens prepared from the field mixtures for testing.

4.1.3 Laboratory mixtures

Using the facilities available in the asphalt laboratory at Qatar University, three different types of asphalt concrete mixtures were mixed, compacted and prepared for dynamic modulus ($|E^*|$) and uniaxial (T/C) fatigue tests. One mixture was according to SC-Type 1 (Marshall) mix in QCS-2010, and the other two were Superpave mixtures. Gabbro aggregate was used in all laboratory mixtures, and unmodified 60-70 Pen bitumen was used in the Marshall mix and one of the Superpave mixtures. The other Superpave mixture was prepared with Gabbro and polymer-modified PG76-22E bitumen. The specimens were prepared at different bitumen contents and tested to determine the optimum bitumen content for Marshall and Superpave mixtures according to AASHTO T 245 and AASHTO R 35-15 standard procedures, respectively. The matrix of the laboratory mixtures is shown in Table 30.

Table 30. Matrix of the laboratory mixtures.

Mix	Code	Mix design	Aggregate	Bitumen type	Bitumen content (%)
1	L-Mar-Pen	Marshall (SC-Type 1)	Gabbro	60-70 Pen	4.0
2	L-Spav-Pen	Superpave		60-70 Pen	4.3
3	L-Spav-22E	Superpave		PG76-22E	4.5

The aggregate gradation for Marshall-QCS mixture and Superpave mixtures used to prepare the laboratory specimens is shown in Table 31, Figure 39 and Figure 40.

Table 31. Aggregate gradation for laboratory mixtures.

Marshall mixture	
BS sieve size (mm)	Cumulative passing (%)
25.0	100.0
20.0	99.7
14.0	87.1
10.0	76.0
6.30	60.3
2.36	35.2
0.60	16.7
0.30	11.1
0.150	8.1
0.075	4.0
Pan	0.0

Superpave mixtures	
BS sieve size (mm)	Cumulative passing (%)
37.5	100.0
25.0	98.6
19.0	88.2
12.5	76.9
9.5	68.9
4.75	47.1
2.36	26.5
1.18	15.8
0.60	10.5
0.30	7.9
0.150	6.1
0.075	4.2
Pan	0.0

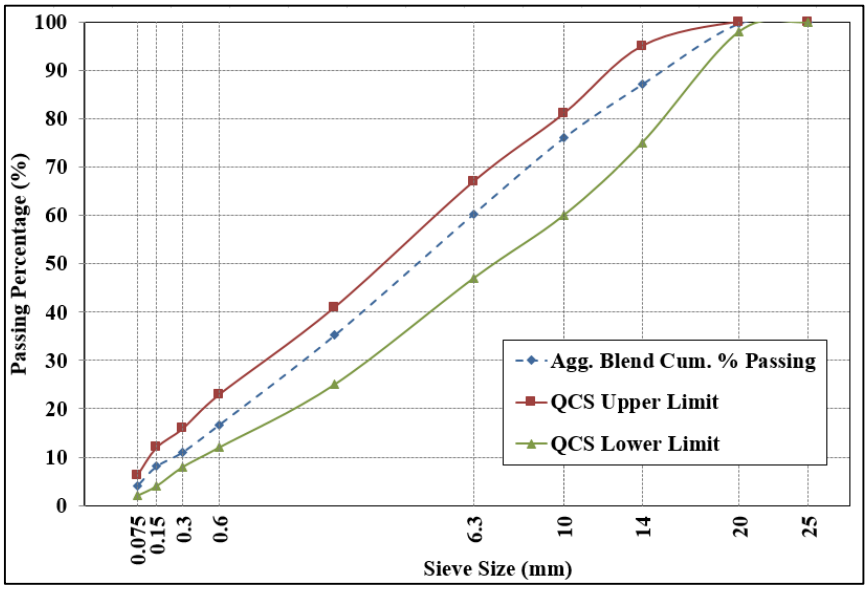

Figure 39. Design gradation of SC-Type 1 Marshall mixture and QCS-2010 limits.

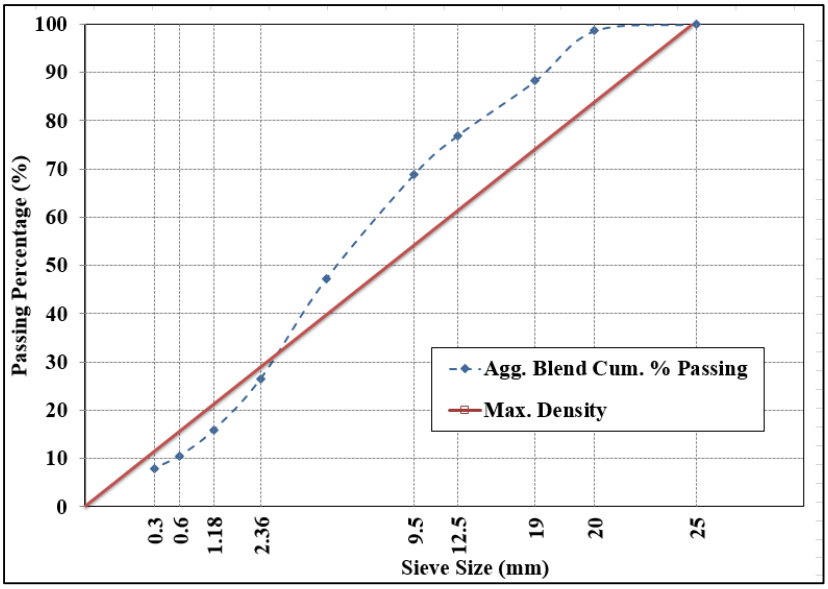

Figure 40. Design gradation of the laboratory Superpave mixtures.

Five replicate specimens of each laboratory mixture were mixed at 163 °C, short-term conditioned in the oven at 135 °C for four hours, and then compacted at around 150 °C using the Superpave Gyratory Compactor (SGC). The SGC samples were then cored and cut to the standard diameter of 100 mm and a height of 150 mm, and average air voids of 7%, according to AASHTO PP 60-14 (2014). The preparation procedure for the laboratory mixture specimens used in the AMPT performance tests is shown in Figure 41.

The flow number (FN) and SCB tests were performed only on the field cores and not on the field and laboratory mixtures. More details will be introduced in the following subsections.

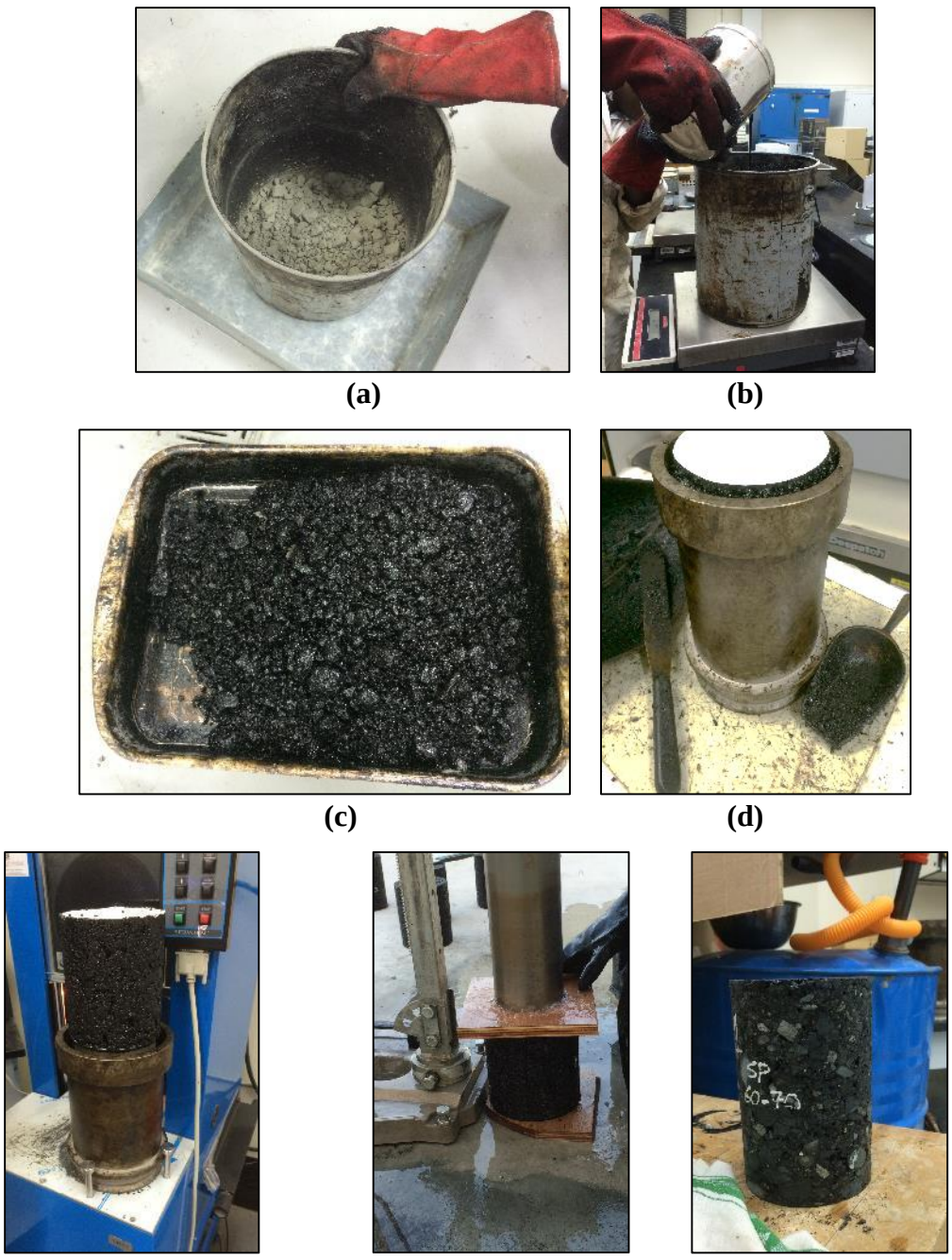

Figure 41. Preparation procedure for laboratory mixtures used in AMPT tests.

4.2 Laboratory testing methodologies

Several laboratory tests were conducted on cylindrical specimens (100 mm diameter and 150 mm high) prepared from the AC mixtures discussed above in order to evaluate their performance against major distresses and identify the suitable mixture for Qatar. The flow number (FN), dynamic modulus ($|E^*|$) and uniaxial tension-compression (T/C) fatigue tests

were all performed using the Asphalt Mixture Performance Tester (AMPT) at Qatar University, as shown in Figure 42.

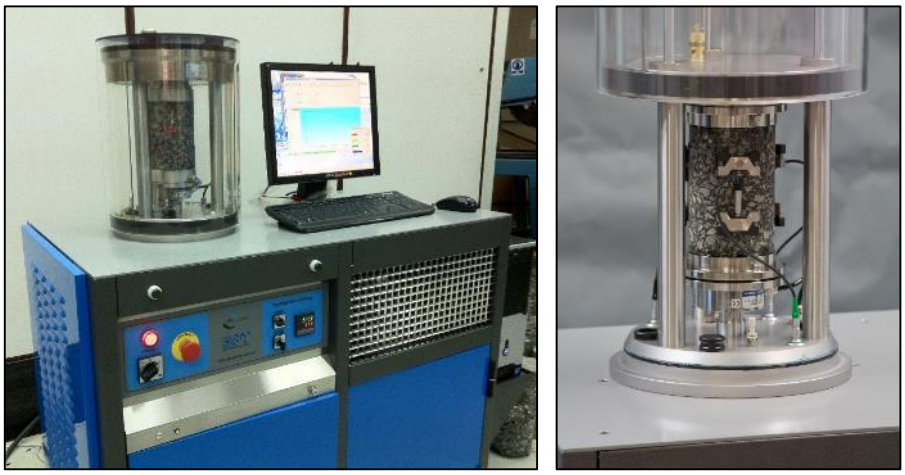

Figure 42. AMPT machine used for flow number, dynamic modulus and uniaxial (T/C) fatigue tests.

The semi-circular bending (SCB) test was conducted using the facility at the University of Liverpool in the UK, as shown in Figure 43. The following subsections describe each laboratory test methodology in detail.

Figure 43. Set-up for monotonic SCB test.

4.2.1 Flow number (FN) test

The flow number (FN) test is a main test within the Simple Performance Test (SPT) suite that shows promise as an HMA rutting performance indicator. The FN test was developed under NCHRP Project 9-19 and applied in the Superpave mix design procedure similar to the

dynamic modulus ($|E^*|$) test (Witczak, et al. (2002), Bonaquist, et al. (2003), Zhu, et al. (2011) and Yan-zhu & Duan-yi (2012)).

The FN test is a destructive test that applies a haversine axial compressive load for 0.1 of a second with a rest period of 0.9 of a second in a single cycle to assess the permanent deformation (rutting) characteristics of asphalt concrete mixtures. Using the AMPT machine, the loading is repeated up to 10,000 cycles or until achieving 50,000 cumulative permanent micro-strain (AASHTO TP 79-11 (2011), AASHTO TP 79-13 (2013) and Kim, et al. (2009)).

The flow number (FN) test using the AMPT is performed following the procedure described in NCHRP 465, 513 and 547 reports (Witczak, et al. (2002), Bonaquist, et al. (2003) and Witczak (2005)). At the time of performing this test, the FN test was not part of the QCS-2010 and no procedure was provided for Qatar conditions. Therefore, and according to some studies by Kim, et al. (2009), Apeagyei, et al. (2011) and Rodezno and Kaloush (2011), the test specimens for the FN test in this study were subjected to 137 kPa deviatoric stress at a high temperature (e.g. 54.4 °C) with zero confinement. The assumed deviatoric stress (i.e. 137 kPa) is considered low if compared to actual stresses applied to pavement structures in Qatar, due to the high traffic volume. However, no specific deviatoric stress value was available in the specifications for Qatar at the time of the test. The data collected from the FN test are presented in terms of cumulative permanent strain (ε_p) versus number of loading cycles (N), as shown in Figure 44.

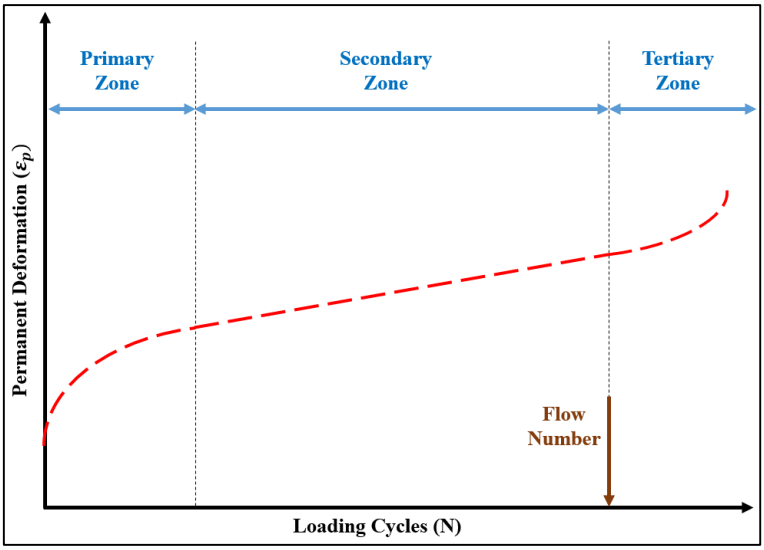

Figure 44. Permanent deformation behaviour against loading cycles.

The cumulative permanent deformation strain (ε_p) curve comprises three distinct zones: primary, secondary and tertiary. The value of ε_p increases rapidly in the primary zone and the incremental deformation decreases in the secondary zone; while, in the tertiary zone, the permanent deformations increase rapidly again. The flow number (FN) value is defined as a number of loading cycles until the beginning of the tertiary zone, as shown in Figure 44 (Witczak (2005) and Kim, et al. (2009)). Accordingly, the higher the flow number value, the better the resistance of the asphalt concrete mixture to permanent deformation (rutting).

4.2.2 Semi-circular bending (SCB) test

The SCB test, first proposed by Chong and Kuruppu (1984), has been widely used by researchers to evaluate the fracture resistance of asphalt mixtures by loading several specimens with different notch depths monotonically or cyclically until failure. Molenaar, et al. (2002), Elseifi, et al. (2012) and Kim, et al. (2012) described this test as a rapid and simple test to be performed on easy-to-prepare specimens, which gives a rigorous characterisation of the mixtures in the laboratory and in quality-assurance testing activities. From the results of this test, the maximum tensile stress (σ_{max}), resilient modulus (M_r), fracture toughness (or stress

intensity factor, K) and fracture energy (G_f) of HMA mixtures can be determined (Molenaar, et al. (2002), Ozer, et al. (2009) and Othman (2011)).

Fracture toughness (K) is a parameter that describes the material's ability to resist the growth of stress concentrations, as shown in Figure 45. Fracture energy (G_f) is the energy released to initiate fracture crack propagation. If the material has a high fracture toughness and energy, this means that it is ductile and has a better resistance to fracture.

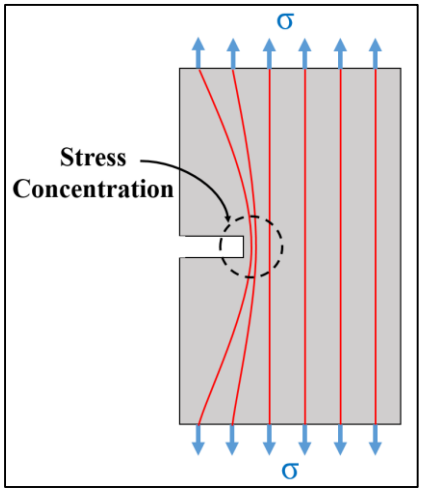

Figure 45. Growth of stress concentration due to cracks.

The configuration of the semi-circular bending (SCB) test consists of a three-point monotonically increasing compressive loading that induces tension in the bottom part of a semi-circular specimen. The set-up of the test involves two supporting rollers at the bottom edge and a loading roller at the mid-point of the semi-circular arch (Liu (2011) and Mull, et al. (2002)). The spacing between the two supports is 0.8 times the diameter of the specimen, as shown in Figure 46.

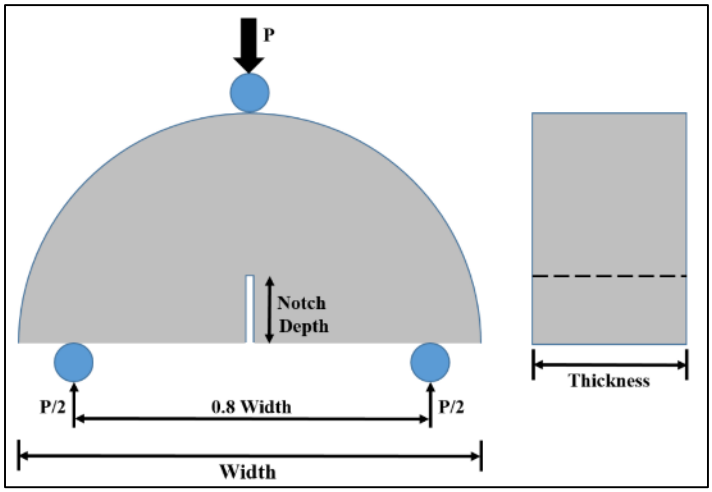

Figure 46. Typical set-up for monotonic SCB test.

The AC mixture cylindrical specimens are cut symmetrically from the middle into two circular slices. Each slice is then symmetrically cut into two semi-circular specimens with a notch depth. Figure 47 shows the preparation steps of the SCB test specimens.

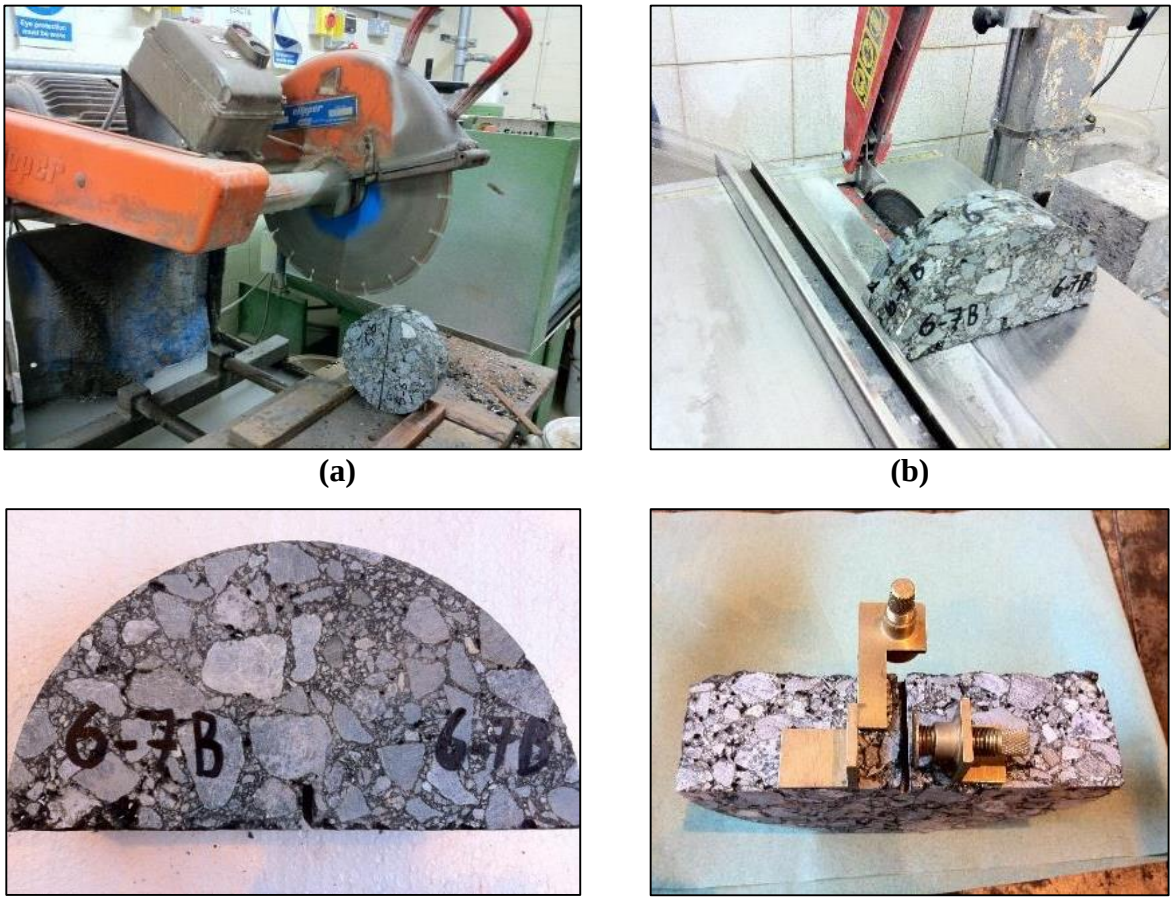

(a) **(b)**

(c) **(d)**

Figure 47. Preparation procedure for SCB test specimens.

Then, the semi-circular specimens are subjected to the monotonic SCB test, and the applied load is displacement-controlled at different loading rates (e.g. 5 mm/min and 10 mm/min) and at a relatively low temperature (e.g. 10 °C) to investigate the effect of loading rate on the performance of the AC mixtures. The applied load, and the horizontal and vertical displacement, in addition to the stress and strain measurements, are monitored and recorded during the test. The collected test data are used to calculate the fracture toughness (K), fracture energy (G_f) and maximum tensile stress (σ_{max}) at the bottom of specimens using the equations shown in Table 32.

Table 32. Equations used to calculate fracture toughness, fracture energy and tensile stress.

Parameter	Equation used	Reference
Max. tensile stress at the bottom of the specimen (σ_{max})	$\sigma = 3.564\frac{P_{ult}}{D.t}$	(Shu, et al., 2010)
Fracture toughness (K)	$K = \left(\frac{\Delta P}{2rt}\right) Y_1\sqrt{\pi a}$	(Lim, et al., 1993)
Fracture energy (G_f)	$G_f = \frac{W}{A_{Lig}}$	(RILEM Technical Committee, 1985)

where,

ΔP = applied load (N),

t = specimen thickness (mm),

r = specimen radius (mm),

Y_1 = normalised stress intensity factor (K) in mode I of crack surface displacement (opening or tensile mode),

a = notch depth (mm),

W = work of fracture (kN.mm),

A_{Lig} = ligament area (mm^2),

P_{ult} = ultimate applied load (N), and

D = specimen diameter (mm).

In a study by Arabani and Ferdowsi (2009), the ability of the SCB test to characterise the tensile strength and fracture toughness of mixtures was compared to a set of common static and dynamic tests. The results showed the SCB test to be reliable and have good correlation with fracture parameters obtained from other fracture tests. In addition, Elseifi, et al. (2012) evaluated the fracture resistance of a number of HMA mixtures using the SCB test, and it was concluded that mixtures with polymer-modified bitumen performed the best. In general, it was noticed that the results of the SCB test are affected by the testing mode (monotonic or cyclic), materials used in the mixture and loading conditions (Li & Marasteanu (2010), Kim, et al. (2012)).

4.2.3 Dynamic modulus ($|E^*|$) test

The dynamic modulus ($|E^*|$) test is a non-destructive key test within the Simple Performance Test (SPT) suite that is used to measure the dynamic modulus (stiffness) and phase angle for asphalt concrete mixtures. This test was developed under NCHRP Project 9-19, similar to the flow number (FN) test, and applied in the Superpave mix design procedure.

In this study, the $|E^*|$ test specimens prepared from the base course of the trial sections are subjected to a repeated dynamic load, with zero confinement, at 4.4, 21.1, 37.8 and 54 °C with loading frequencies of 25, 10, 5, 1, 0.5 and 0.1 Hz (AASHTO TP 79-11, 2011). The 21.1 °C temperature was taken as the reference temperature. On the other hand, the specimens prepared from field and laboratory mixtures are tested at 4, 20 and 40 °C with loading frequencies of 10, 1 and 0.1 Hz for the first two temperatures and 10, 1, 0.1 and 0.01 Hz for the third temperature, according to the latest AASHTO procedure (AASHTO TP 79-13, 2013). The 20 °C temperature was taken as the reference temperature.

The obtained $|E^*|$ values at different test temperatures are then shifted relative to the frequency so that all curves can be aligned to form a single master curve for a mixture (Kim, et al., 2009). Master curves are constructed from the $|E^*|$ test data using a sigmoidal (*S* shape)

fitting function proposed by Pellinen, et al. (2002). The sigmoidal function describes the time (frequency) dependency of the modulus at the reference temperature and can be described as follows:

$$\boldsymbol{Log}(|\boldsymbol{E}^*|) = \boldsymbol{\delta} + \frac{\boldsymbol{\alpha}}{\mathbf{1}+\boldsymbol{e}^{\boldsymbol{\beta}+\boldsymbol{\gamma}(\boldsymbol{log}\boldsymbol{\xi})}} \quad \textbf{Equation 38}$$

where, δ is the minimum dynamic modulus value, and $\delta+\alpha$ is the maximum dynamic value that depends on the bitumen content, air voids and the aggregate gradation of the mixture. Values of β and γ are the regression coefficients for the sigmoidal fitting function that depend on the characteristics of the bitumen and the magnitude of δ and α. The ξ parameter is the reduced frequency (reduced time, t) that is used to calculate the shift factor, $a(T)$, as a function of temperature (T) as follows (ARA, Inc., ERES Consultants Division, 2004):

$$\boldsymbol{\xi} = \frac{\boldsymbol{t}}{\boldsymbol{a}(\boldsymbol{T})} \quad \textbf{Equation 39}$$

$$\boldsymbol{Log}(\boldsymbol{\xi}) = \boldsymbol{Log}(\boldsymbol{t}) - \boldsymbol{Log}[\boldsymbol{a}(\boldsymbol{T})] \quad \textbf{Equation 40}$$

In developing a master curve, the time-temperature correspondence principle is implemented. The dynamic moduli obtained at test temperatures higher than the reference temperature (e.g. 20 or 21.1 °C) are horizontally shifted by the calculated shift factor and merged to lower frequencies, while those obtained at test temperatures lower than the reference temperature are shifted to the higher frequencies, as shown in Figure 48.

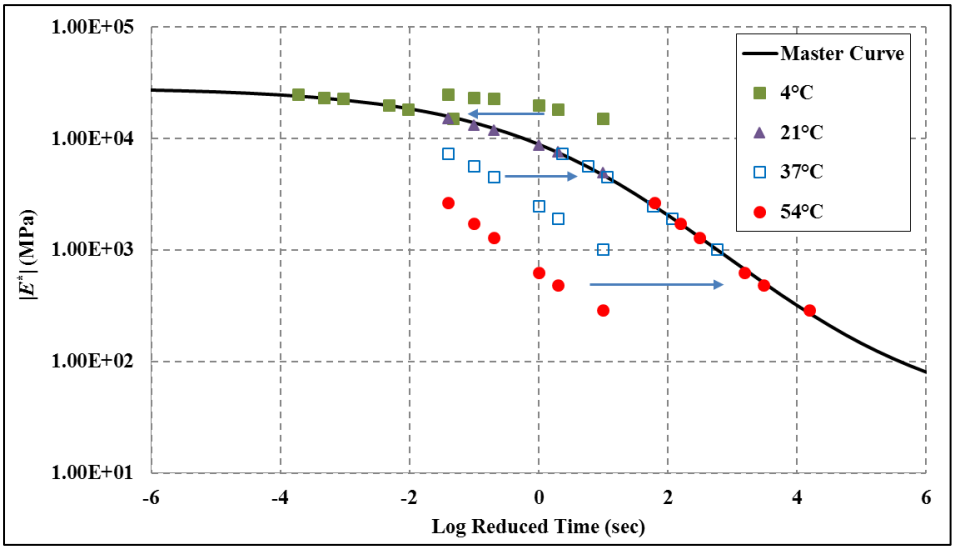

Figure 48. Illustrative example of construction of dynamic modulus master curve.

Mixtures with low difference in stiffness between low reduced time (low temperature) and high reduced time (high temperature) have a low temperature susceptibility.

Mohammad, et al. (2011) conducted dynamic modulus and FN tests on HMA mixtures containing high-reclaimed asphalt pavement (RAP) content with crumb rubber additives. The results showed that the aforementioned tests are useful to characterise the mixtures and discriminate between them. Then, in order to evaluate short- and long-term performance of recycled mixtures, $|E^*|$ and FN tests were performed by Kim, et al. (2009) and Apeagyei, et al. (2011). The results obtained from both tests were affected by the bitumen type and mix design, but were useful enough to evaluate the performance of the mixtures against rutting. Moreover, Clyne, et al. (2003) reported that the $|E^*|$ test was affected mainly by a combined effect of bitumen stiffness and aggregate size distribution.

4.2.4 Uniaxial tension-compression (T/C) fatigue test

The uniaxial (T/C) fatigue test is one of the recently developed tests within the SPT suite. The fatigue test procedure has a dynamic modulus ($|E^*|$) test built into it which is conducted as a fingerprint test for 50 cycles only at fatigue-testing frequency and temperature. The quick $|E^*|$ test is needed to measure the dynamic modulus and phase angle for each

specimen before starting the fatigue test. Then, a cyclic tension-compression (T/C) fatigue test is performed on the asphalt concrete specimen until termination criteria are met or the specimen fails.

In this part of the study, several specimens from different asphalt mixtures were tested under uniaxial cyclic (T/C) fatigue test to characterise their performance against fatigue damage. The same AMPT facility was used but with special plates glued to the top and bottom of the tested specimens, as shown in Figure 49.

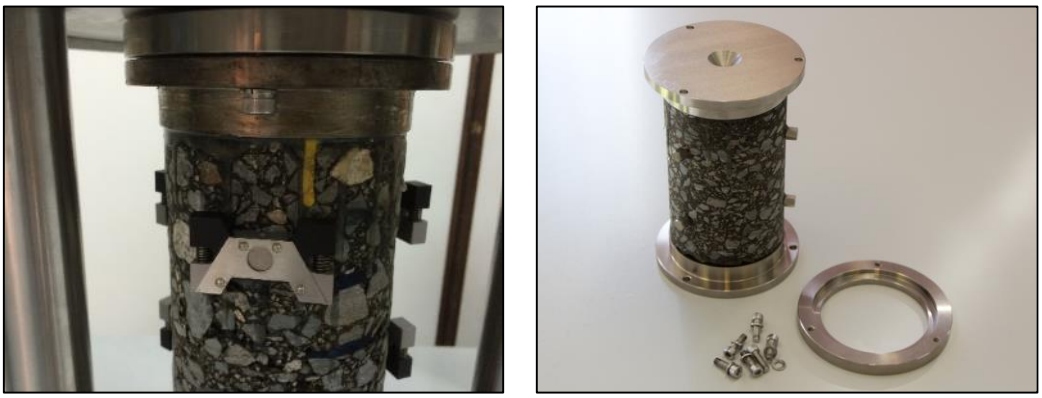

Figure 49. Set-up for uniaxial T/C fatigue test using AMPT.

The cyclic (T/C) fatigue test was conducted with zero confinement at a temperature of 20 °C under controlled-strain condition with loading frequency of 10 Hz. The test was performed under two strain levels for every specimen with maximum of 10 minutes' rest period between them: (i) using low strain amplitude (e.g. 110 με peak-to-peak) to determine mixture properties in the linear viscoelastic range, and (ii) using high strain amplitude (e.g. 260 με peak-to-peak) to obtain the nonlinear viscoelastic properties and prompt fatigue damage. These strain amplitude values were selected based on some previous studies in the literature (Carpenter & Shen (2006) and Haggag, et al. (2011)). The strain amplitude was measured during the test using three 75 mm long linear variable displacement transducers (LVDTs) mounted on the specimens (37.5 mm away from the top and bottom edges of the specimen). The variability of the strain measurements between these LVDTs was confirmed to be quite low because any problem with the measured strain amplitudes will affect the analysis results significantly. Test

data of $|E^*|$, phase angle, stress applied, deformation and other output data were collected every 10 loading cycles, and the termination criterion was to complete 200,000 cycles in both levels unless the specimen fails.

Since each test specimen was subjected to a low strain level and then a high strain level, the results obtained at the high strain level might have suffered from damage that might have developed during the low-strain testing phase.

It is worth mentioning that the AMPT machine is being calibrated from time to time to check if the results are within the acceptable range. A steel-like specimen that was supplied with the AMPT machine and has a specific modulus value is used to perform the calibration. The trial test at different frequencies indicated that the results are within the safe zone (allowable deviation is ±2% of the calibrated value).

4.3 Field cores' results

The test specimens prepared from the base course of the six trial sections were subjected to the four laboratory tests, FN, SCB, $|E^*|$ and T/C fatigue tests. The test data and results obtained from each laboratory test are discussed and summarised in the following subsections.

4.3.1 Flow number (FN) test results

Twelve specimens, two from each field base course, were tested in the flow number (FN) test using AMPT in order to evaluate their performance against rutting (permanent deformation), which is one of the major problems in Qatar. The specimens of the field cores in the FN test were subjected to 137 kPa deviatoric stress at a temperature of 54.4 °C with zero confinement. The flow number result from each mixture was determined by the software incorporated in the AMPT from the cumulative permanent strain (ε_p) versus number of loading cycles (N) curve, as shown in Figure 50.

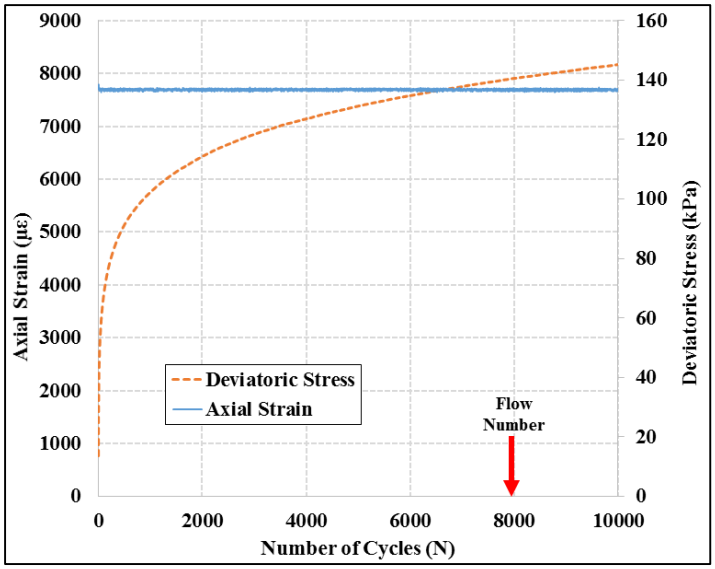

Figure 50. An example of the determination of FN value from the test data of a specimen.

Figure 51 illustrates the average FN results of the flow number test for the specimens of the six trial base course mixtures considered in this study.

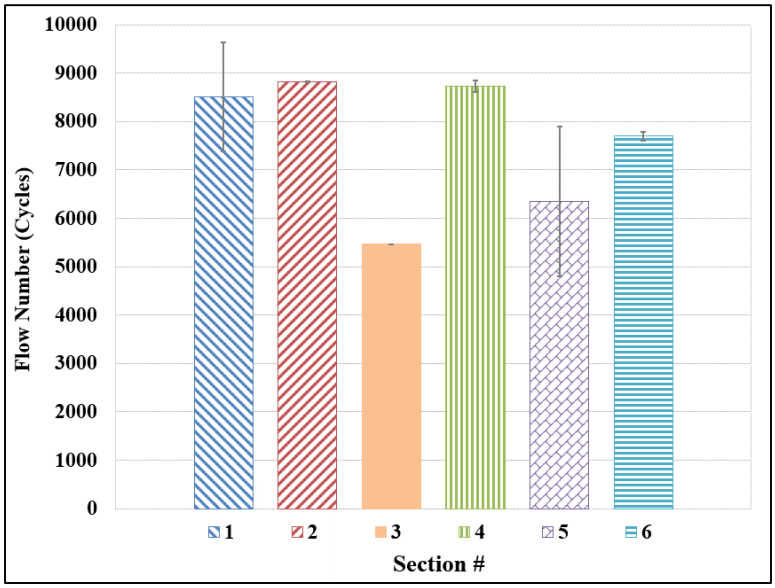

Figure 51. Flow number test results for specimens extracted from each trial section.

All flow number values of the specimens prepared from the field cores are high compared to those published in several previous studies conducted in the United States under similar conditions (Mohammad, et al. (2006), Wang, et al. (2011), Apeagyei, et al. (2011), Kanitpong, et al. (2011), Mohammad, et al. (2011)). The high FN value is indicative that these

field mixtures of the trial sections are expected to have a high resistance to rutting compared to those that were tested in the US studies.

In order to assess the effect of using different bitumen grades on the resistance of mixtures to rutting, FN results for the mixtures of trial sections 1, 2 and 6 and then trial sections 4 and 5 were compared. Figure 51 shows that section 1, with unmodified 40-50 Pen bitumen, and section 2, with unmodified 60-70 Pen bitumen, had very close FN values, while section 6, with PMB, had a slightly lower FN value. On the other hand, Figure 51 also shows that the mixture of section 5, with Shell Thiopave bitumen, had a lower FN value than the control mixture in section 4. In the literature, the flow number (FN) was found to increase with an increase in bitumen high-temperature grade, while the use of modified bitumen in this study did not increase the FN value. Therefore, further investigation is needed to specify the reason behind that. In general, all of the tested mixtures performed well.

The FN results for section 2, with Gabbro, and section 3, with Limestone, were compared to evaluate the influence of using different aggregate types. Section 2 had a significantly higher flow number result than that of trial section 3. This result demonstrated that using Limestone aggregate decreased the ability of the mixtures to resist rutting. This can be attributed to the relatively low angularity of Limestone, which is one of the main factors affecting the reduction of the FN value and shows low rut-resistance.

The effect of using different mix designs was assessed by comparing FN results for trial section 2 (Marshall/PRD) and section 4 (Marshall/QCS). Both trial sections performed similarly in terms of resistance to rutting.

In conclusion, and from the flow number tests conducted on the field cores, it can be stated that the resistance to permanent deformation (rutting) for asphalt concrete mixtures is mainly affected by the bitumen grade, bitumen content, aggregate gradation and aggregate

source. The high rut-resistance of asphalt mixtures can be achieved by a well-designed mixture with the use of polymer-modified bitumen and Gabbro aggregate.

4.3.2 Semi-circular bending (SCB) test results

The SCB test was conducted on the semi-circular specimens prepared from the base course of the trial sections. The SCB test was conducted at loading rates of 5 mm/min and 10 mm/min at a temperature of 10 °C in order to check the influence of loading rate on the fracture resistance of the mixtures of the field cores. These test conditions were deliberately selected to avoid any permanent deformation affecting the results. Figure 52 illustrates the stress-strain curve for each base course's mixture for the trial section obtained from the SCB test data at 5 mm/min.

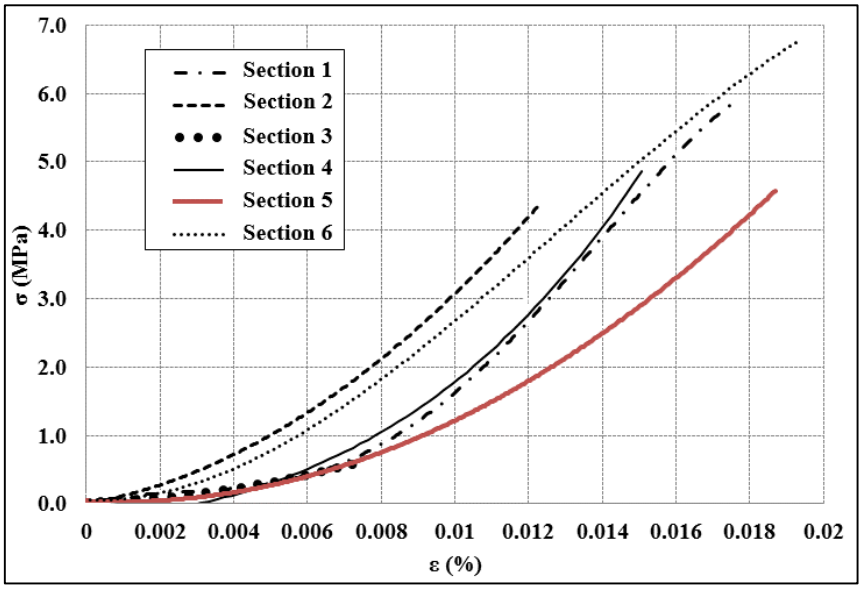

Figure 52. Stress-strain curves obtained from the SCB test for all field cores of the trial sections at 5 mm/min.

Figure 52 shows that some "start-up" effect might have influenced the tests because in the early stage of the test the increase of the strain (ε) with the increase of the stress (σ) is much higher than at the later stage of the test. Quite often a so-called "zero-point correction" is applied in such cases but it was not applied in this case.

It was observed from the test that materials were generally brittle and failed abruptly with little deformation or plastic flow. In addition, Figure 52 shows no well-defined peaks or slow fracture tail, common with softer materials and slower test speeds. It is worth mentioning that no zero point correction was applied to any σ-ε curve in Figure 52 because all curves behaved very similarly.

Then, the collected SCB test data were used to determine the fracture toughness (K), fracture energy (G_f) and maximum tensile stress (σ_{max}) at the bottom of semi-circular specimens of each trial section. Figure 53 to Figure 55 illustrate the results of both SCB tests for each field core of the trial sections in this study.

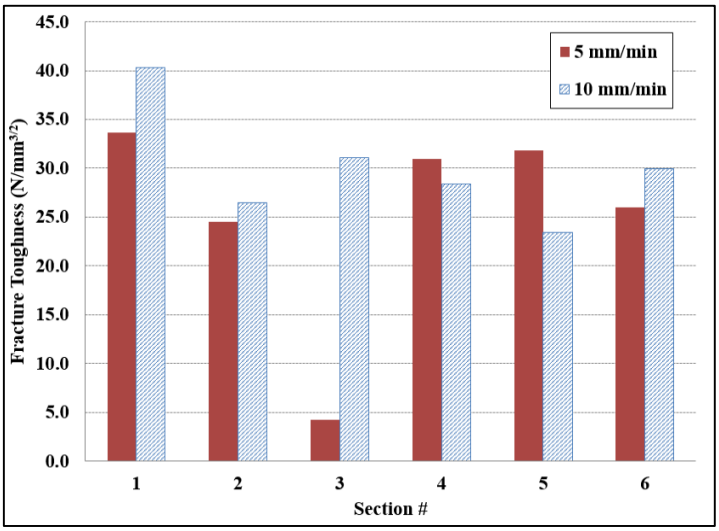

Figure 53. Fracture toughness (K) results for the field cores for both loading rates.

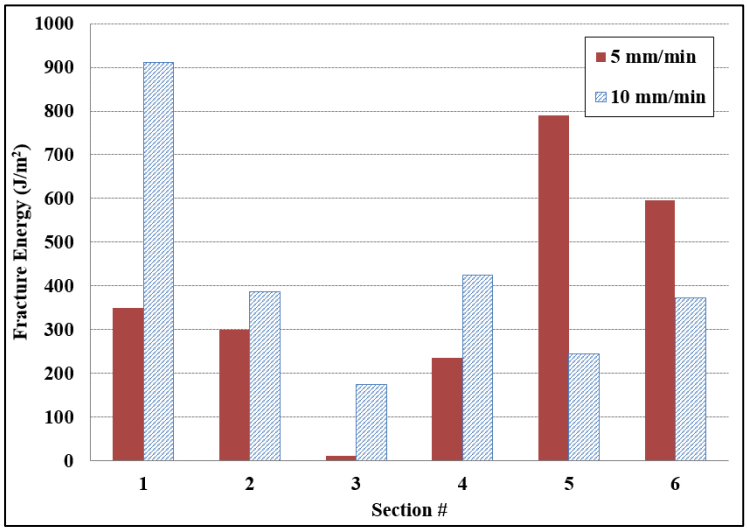

Figure 54. Fracture energy (G_f) results for the field cores for both loading rates.

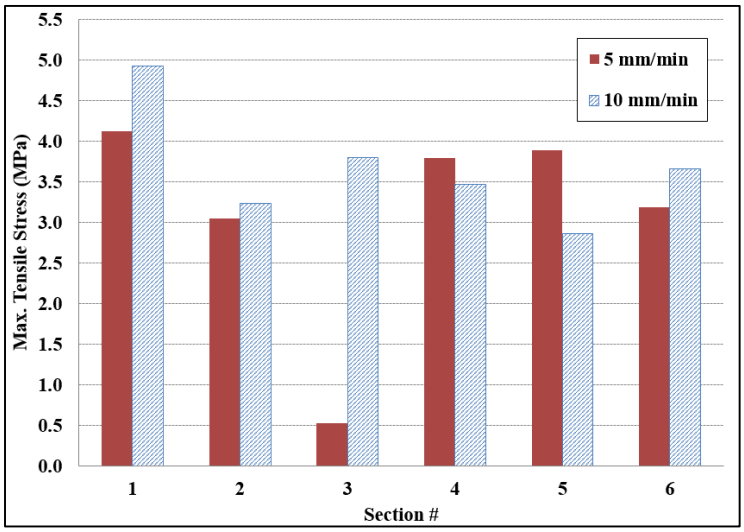

Figure 55. Maximum tensile stress results for the field cores for both loading rates.

Generally, the fracture toughness (K), fracture energy (G_f) and maximum tensile stress (σ_{max}) values of all base courses' mixtures are high, which reflects good performance against fracture. This high resistance to propagation of fracture is primarily caused by the high stiffness of these mixtures. However, the mixture of the base course of section 1, Marshall/PRD with unmodified 40-50 Pen bitumen and Gabbro, had the highest average fracture parameters among the trial mixtures.

To evaluate the significance of bitumen type on resistance to fracture, the results for mixtures of trial sections 1, 2 and 6 were compared. As concluded by Li, et al. (2006), fracture toughness and fracture energy of field specimens are usually affected by bitumen type. In Figure 53, the trial base mixtures were compared based on the fracture toughness (K). The results showed that field cores of trial section 1 with unmodified 40-50 Pen bitumen had the highest fracture toughness in both loading rates. This is the case for maximum tensile stress, but for fracture energy the field cores of section 1 only gave the highest results in the higher loading rate test (10 mm/min). On the other hand, cores from the base course of trial section 2 with unmodified 60-70 Pen bitumen had the lowest fracture toughness, energy and tensile stress

in both loading rates compared to sections 1 and 6. This shows the effect of bitumen grade on fracture resistance.

Field cores of sections 4 and 5 with QCS mix design and Gabbro in the base course were compared to evaluate the significance of using Shell Thiopave bitumen on the resistance to fracture. The results in Figure 53 to Figure 55 show that both field cores had very similar fracture toughness and maximum tensile stress values at both loading rates. However, the case for fracture energy (G_f) is different, as shown in Figure 54. Specimens of the base course of trial section 5, with Thiopave bitumen, dissipated more energy to propagate the crack than that of trial section 4, with unmodified 60-70 Pen bitumen.

The performance of mixtures of trial sections 2 and 3 was assessed to acquire insight into the effect of aggregate type by comparing their results for fracture toughness, fracture energy and tensile stress, as also shown in Figure 53 to Figure 55. The results for the mixture of trial section 3 obtained at the lower loading rate test (5 mm/min) were ignored because the specimen was highly segregated. Generally, the results demonstrated that both mixtures had high fracture resistance but trial section 2, with Gabbro, outperformed with higher fracture energy than section 3, with Limestone, as shown in Figure 54.

The influence of mix design on the fracture resistance was evaluated by comparing the use of Marshall/PRD in section 2 and Marshall/QCS in the control mixture, section 4. From the results shown in Figure 53 to Figure 55, it can be stated that using the conventional mix design Marshall/QCS provided a little more toughness, energy and tensile stress than the PRD mix design. The small difference between the two results emphasised that mix design is not a main factor affecting the fracture resistance compared to bitumen or aggregate type.

4.3.3 Dynamic modulus ($|E^*|$) test results

The specimens prepared from the base course of the trial sections were subjected to the $|E^*|$ test as well in order to evaluate their stiffness and their temperature susceptibility. An

example of the repeated dynamic load/stress applied on the tested specimen, and the resulting axial strain is shown in Figure 56.

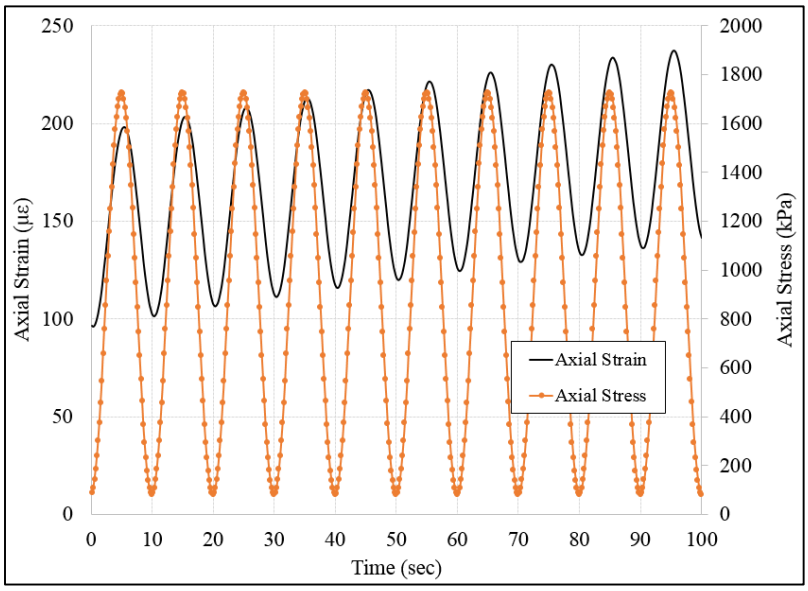

Figure 56. An example of the repeated axial dynamic load applied to a tested specimen and resulting axial strain.

From the $|E^*|$ test data, the dynamic modulus and phase angle of each specimen at every temperature and frequency were determined and used for developing the master curves (Appendix C). The master curves can be developed using a sigmoidal fitting function (i.e. Equation 38) described earlier, in subsection 4.2.3. The shift parameters and the constructed master curves of each trial mixture are shown in Table 33 and Figure 57, respectively.

Table 33. Shift parameters of master curves for the field cores.

Section #	δ	α	β	γ	*A*	*b*	*c*
1	2.867	3.864	-1.634	0.490	0.0009	-0.166	3.062
2	2.708	3.933	-1.807	0.438	0.0010	-0.168	3.086
3	3.168	3.266	-1.663	0.414	0.0009	-0.164	3.028
4	0.109	6.581	-2.324	0.363	0.0011	-0.177	3.208
5	3.613	3.006	-1.594	0.552	0.0008	-0.157	2.939
6	3.277	3.319	-1.534	0.422	0.0009	-0.164	3.044

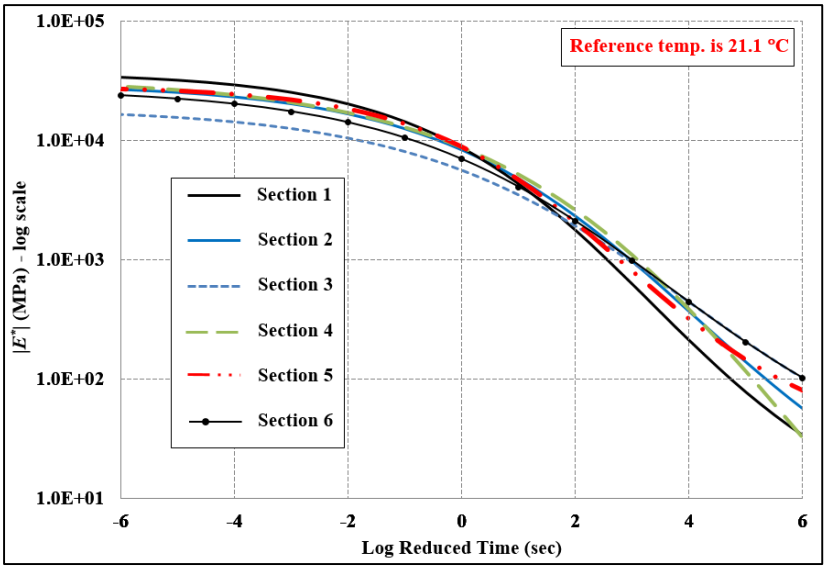

Figure 57. Dynamic modulus master curves for all field cores' mixtures.

Generally, the dynamic modulus values for all mixtures are rather high in the low reduced-time compared to results reported in other studies (Goh, et al. (2011), Kim, et al. (2009), Zhu, et al. (2011) and Bonaquist (2010)). The range of $|E^*|$ values is similar to the values from a previous study by Masad, et al. (2011) conducted on field cores prepared using modified PG76-22 bitumen and extracted from a major freeway in Qatar.

In order to inspect the effect of using different bitumen types/grades on mixture stiffness, master curves of the cores of trial sections 1, 2 and 6 and then trial sections 4 and 5 were compared, as shown in Figure 58 and Figure 59, respectively. Both figures show that all compared mixtures had high dynamic modulus values at low reduced time (high frequency) and low temperature. In contrast, the stiffness of section 1, with unmodified 40-50 Pen bitumen, in Figure 58 became lower than the other trial sections (2 and 6) at high reduced time and temperature. This inferred that polymer-modified bitumen makes asphalt concrete mixtures are stiffer at high temperatures than those made of unmodified bitumen. In addition, the use of polymer-modified bitumen (PMB) flattened the master curve of trial mixture 6 and reduced the effect of temperature and frequency on the stiffness.

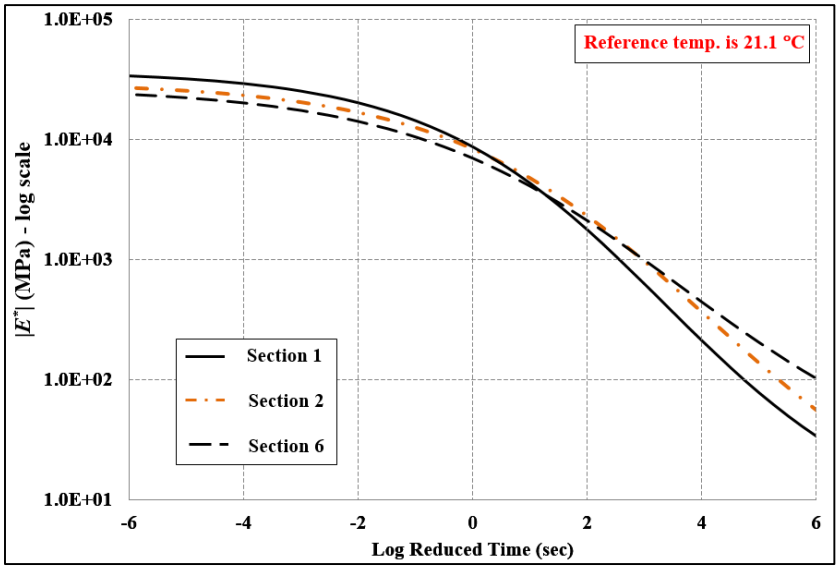

Figure 58. Dynamic modulus master curves for field cores of sections 1, 2 and 6.

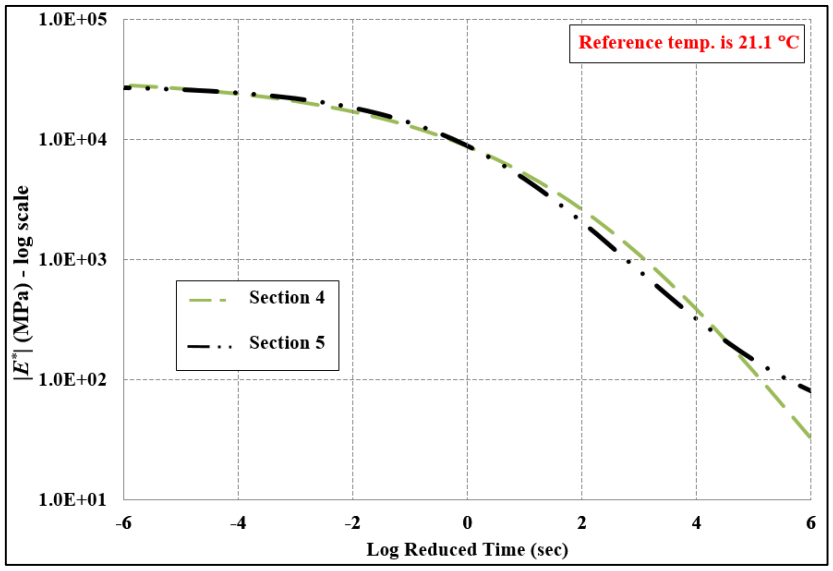

Figure 59. Dynamic modulus master curves for field cores of sections 4 and 5.

Figure 59 shows that there is no difference at low reduced time (high frequency) and temperature between using unmodified 60-70 Pen and Thiopave bitumen when the mix design is QCS and the aggregate used is Gabbro. However, the difference is considerable at a very high reduced time, where section 5 with Thiopave bitumen is stiffer than section 4 with unmodified 60-70 Pen bitumen.

After that, $|E^*|$ master curves of section 2 with Gabbro and section 3 with Limestone were compared to assess the effect of using different aggregate types, as shown in Figure 60.

The mixture of section 3 had higher dynamic modulus than that of section 2 at high reduced times and temperatures.

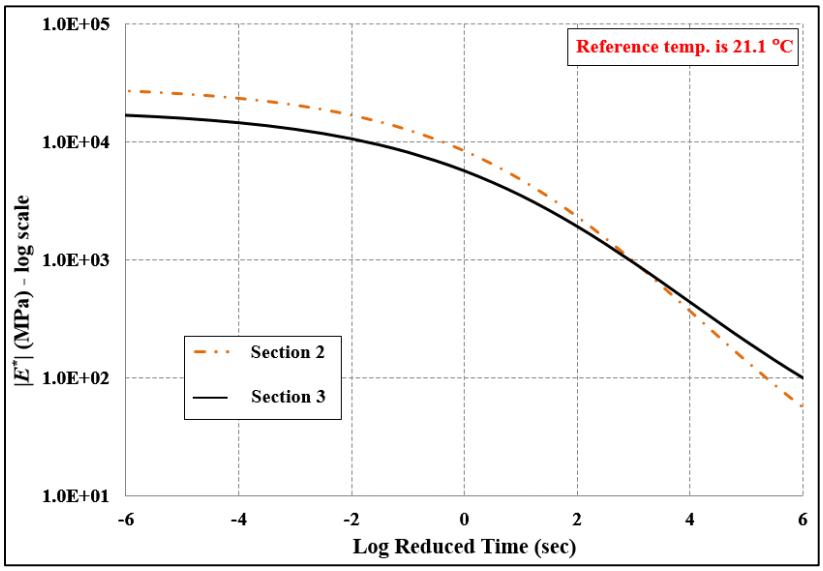

Figure 60. Dynamic modulus master curves for field cores of sections 2 and 3.

In Figure 61, the effect of using different mix designs was evaluated by a comparison between master curves of the base course of section 2 (Marshall/PRD) and 4 (Marshall/QCS). Both mixtures performed the same at low-to-intermediate reduced times, while the base course of section 2 has a slightly higher dynamic modulus value at very high reduced time or temperature. It can be stated that Marshall/PRD and Marshall/QCS design mixes did not have much influence on the stiffness and performance of either section.

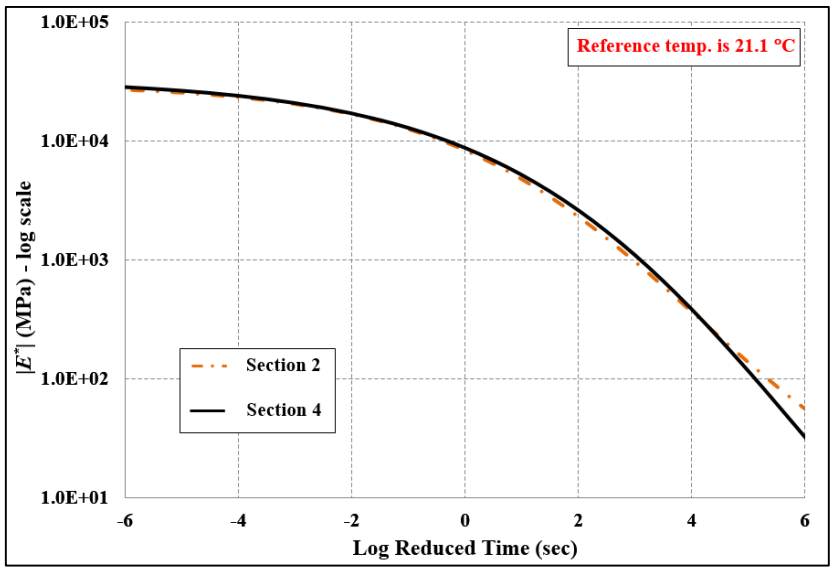

Figure 61. Dynamic modulus master curves for field cores of sections 2 and 4.

From all comparisons above, it was noticed that the dynamic modulus master curves of the tested field cores of the trial road were mainly affected by the bitumen type/grade and aggregate type. In addition, the use of polymer-modified bitumen (PMB) flattened the master curve of the asphalt concrete mixtures and reduced the temperature and frequency susceptibility on the stiffness.

4.3.4 Uniaxial T/C fatigue test results

Another set of specimens prepared from the base course of the trial road were subjected to a uniaxial tension-compression fatigue test with zero confinement, at a temperature of 20 °C in the controlled-strain mode at a loading frequency of 10 Hz. The test was performed twice on every specimen: (i) using a low strain amplitude (ε_0 (L1) = 55 με) to determine mixture properties in the linear viscoelastic range, and (ii) using a high strain amplitude (ε_0 (L2) = 130 με) to obtain the nonlinear viscoelastic properties and prompt fatigue damage. However, both strain levels were, in effect, high enough to surpass the linear viscoelastic (LVE) region and cause damage. Therefore, one of the objectives of the fatigue analysis is to examine if the latest fatigue characterisation approaches can capture the damage that happened in the first fatigue test before starting the second one on the same specimen. Some specimens failed early, before the end of the first fatigue test, and did not complete the 200,000 cycles of the test. Consequently, it was decided to analyse each uniaxial T/C fatigue test independently. The dynamic modulus and phase angle values from the first cycle interval (N = 10) in each uniaxial T/C fatigue test (L1 and L2) were considered as the linear viscoelastic dynamic modulus ($|E^*|_{LVE}$) and the linear viscoelastic phase angle (φ_{LVE}), respectively.

Specimens prepared from the base course of trial section 3 (Limestone aggregate with unmodified 60-70 Pen bitumen) failed very early during the first T/C fatigue test (using strain amplitude of 55 με) and no data were collected. This could indicate that a significant amount

of damage was induced in the specimen during construction and/or the results were affected by segregation, which was earlier observed on samples from section 3.

Before analysing the data from both fatigue tests, the stress and strain amplitudes applied in this controlled-strain fatigue test using AMPT need to be investigated. Figure 62 shows an example of the strain and stress amplitudes applied on the specimens from the base course of field trial section 2 under strain L1 and L2 tests. In some cases of the conducted uniaxial T/C fatigue tests, the raw data after a certain number of loading cycles were discarded and neglected during analysis due to the discrepancy in the data points as shown in Figure 62.

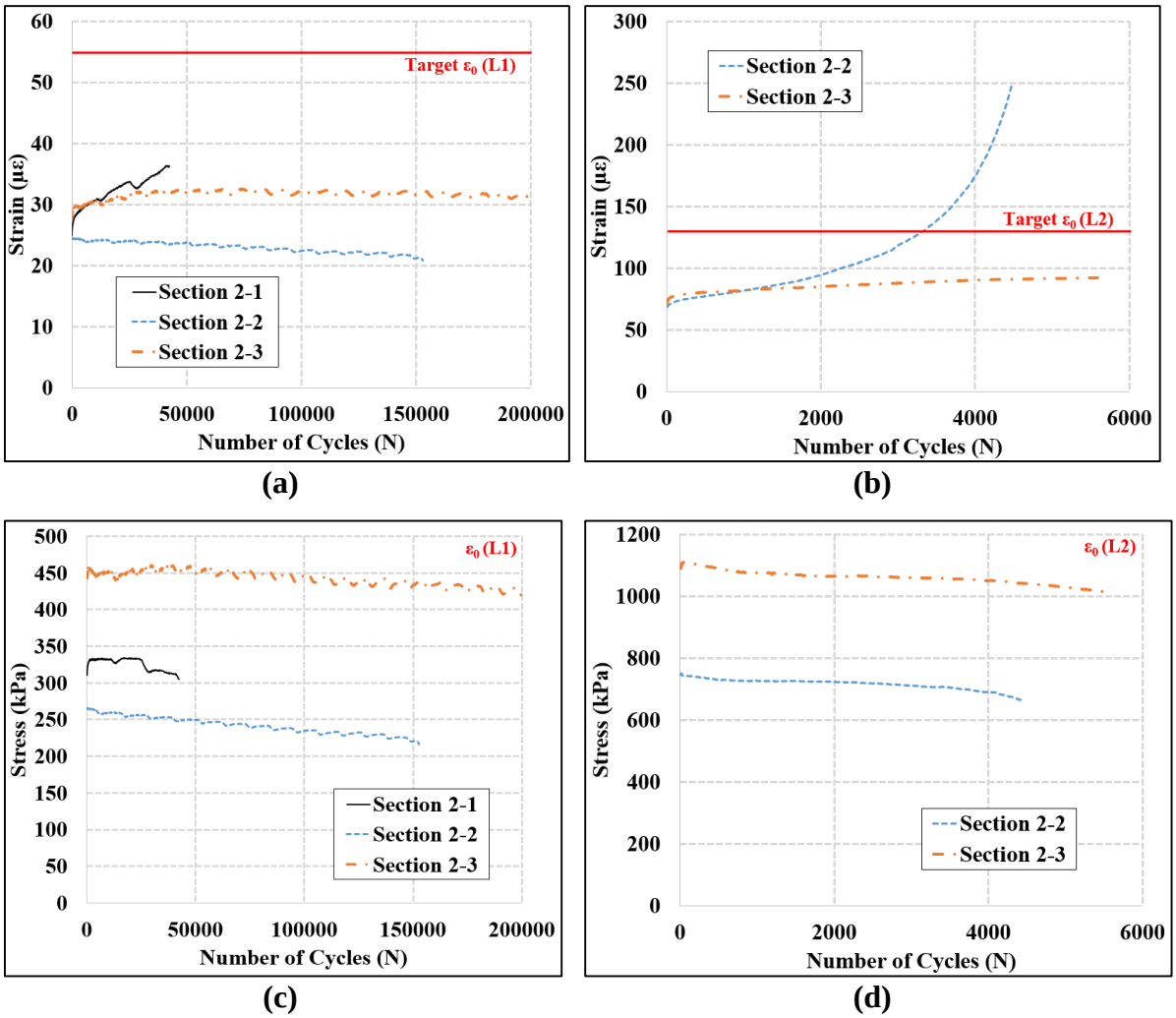

Figure 62. Strain and stress amplitudes applied to the specimens of trial section 2 under both strain levels tests.

According to Figure 62 and the raw data of other trial sections, the strain amplitude was in most cases constant in each test but the target value (i.e. 55 με and 130 με) was not achieved

during both low and high strain amplitude fatigue tests (L1 and L2). This will show a fatigue behaviour for a different strain amplitude, not the target one. In a few cases, the strain increased rapidly and early in the test due to sudden cracking in the specimen. It is important to remember that these mixtures are stiff and this is expected to raise a concern about the durability and fatigue resistance, as mentioned earlier in the results for the $|E^*|$ test. Figure 63 shows the average strain amplitude applied to the tested specimens during the uniaxial T/C fatigue tests (L1 and L2). This will surely affect the reliability of the results, and emphasises the need to use a suitable characterisation approach (e.g. viscoelastic continuum damage approach).

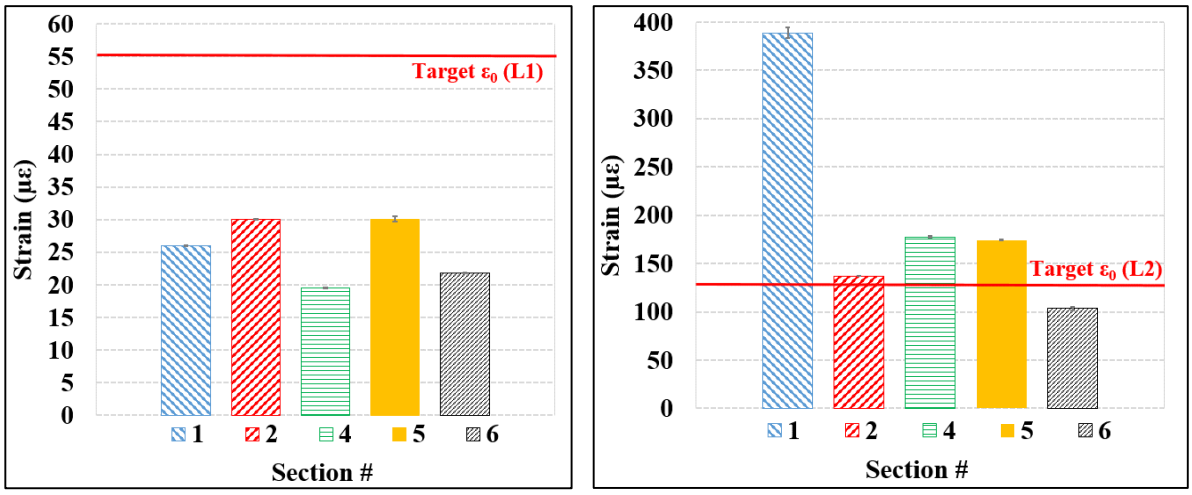

Figure 63. Average strain amplitude applied to the tested field cores.

The main outputs of each fatigue test were dynamic modulus ($|E^*|$) and phase angle (φ) against number of loading cycles (N). The results for each specimen of the field trial sections tested under strain amplitude L1 are presented in Figure 64.

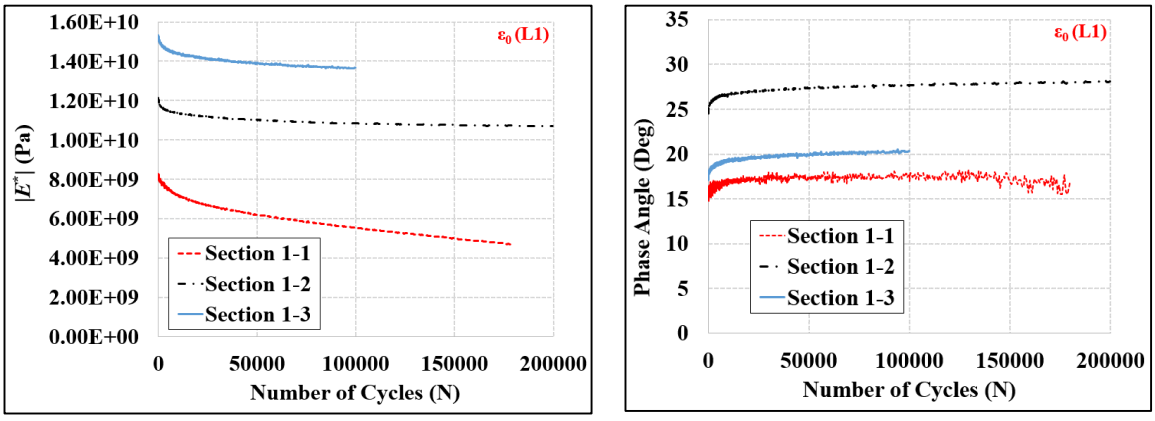

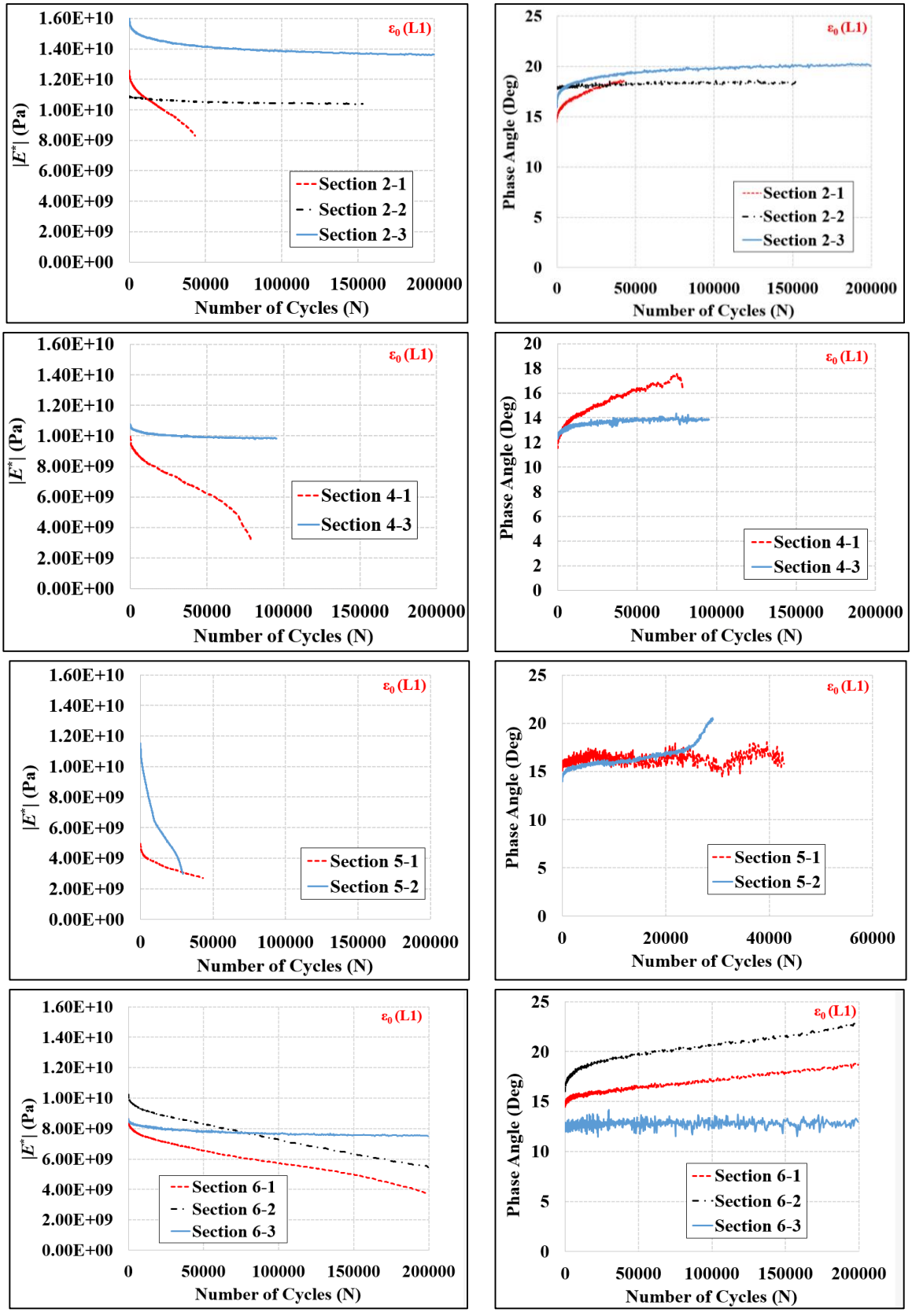

Figure 64. Dynamic modulus and phase angle results for the field cores tested under strain amplitude L1 test.

According to the figures above, the replicate specimens of each mixture of the trial sections showed a different reduction rate of the modulus and increment of the phase angle. These preliminary results cannot be used alone to evaluate the performance against fatigue damage. In addition, damage that happened in the first fatigue test implies that this affected the specimen in the second fatigue test, which implies that the results of the second fatigue test cannot be quantified using the reduction (e.g. 50%) in dynamic modulus value only. A suitable fatigue characterisation approach should be implemented in order to assess each mixture and predict its fatigue life.

The results for each field cores' specimen tested under strain amplitude L2 test (dynamic modulus ($|E^*|$) and phase angle (φ) against the number of loading cycles) are presented in Figure 65.

Similar to the results of the strain level 1 test, the specimens of each trial base course showed a different reduction rate of the dynamic modulus and increment of the phase angle. Many specimens failed early in the second test under strain amplitude of 130 με, as shown in Figure 65. Consequently, the preliminary results and the traditional interpretation (E^* vs. N) of the uniaxial T/C fatigue test cannot be used directly to assess the performance against fatigue cracking.

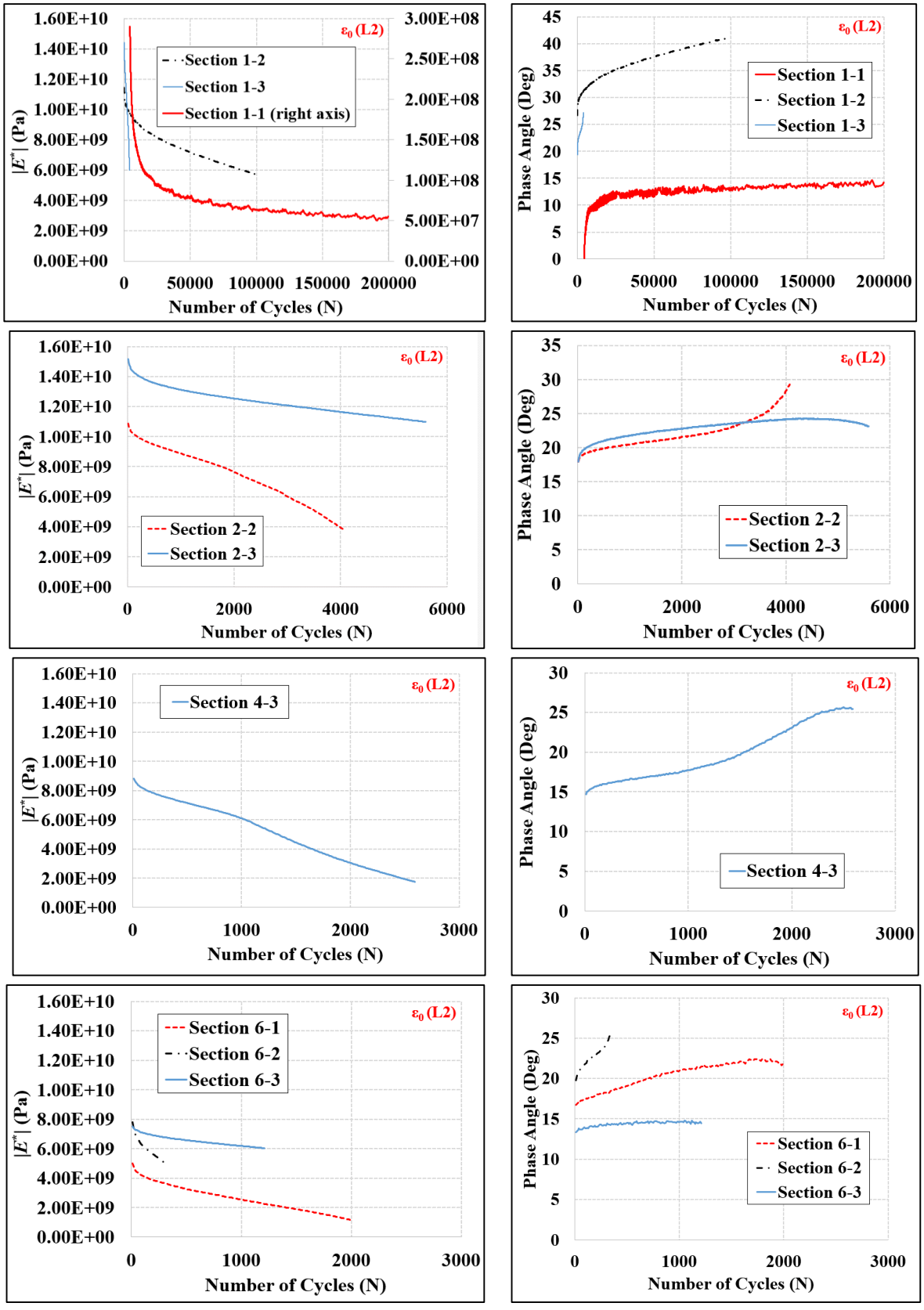

Figure 65. Dynamic modulus and phase angle results for the field cores tested under strain amplitude L2 test.

It is worth mentioning that the interface between the two AC base layers in the specimens prepared from the field cores was checked using X-ray Computed Tomography (CT) at Texas A&M University at Qatar and no major discontinuity was found. Nevertheless, it is most likely that the interface did have an effect on the fatigue results since it is in the weakest plane in the test specimens. In order to avoid this problem in future projects, it is recommended to core the test specimens horizontally from the extracted field cores.

4.4 Field mixtures' results

The test specimens prepared from the field mixtures described earlier in subsection 4.1.2 were subjected to the dynamic modulus ($|E^*|$) and uniaxial T/C fatigue tests only. The FN and SCB tests were not performed here because the results of these tests from the field cores gave clear and consistent conclusions. More concentration is given to the resistance of asphalt concrete mixtures to fatigue cracking.

4.4.1 Dynamic modulus ($|E^*|$) test results

Replicate specimens of the two field mixtures (F-Mar-10E and F-Mar-22S) were subjected to the dynamic modulus ($|E^*|$) test using the AMPT machine at Qatar University. This test was performed in order to evaluate the stiffness and the temperature susceptibility of the field mixtures compacted and prepared in the laboratory. Using the raw data obtained from the $|E^*|$ test, master curves of the field mixtures were developed using a sigmoidal fitting model (equation 38) presented in subsection 4.2.3. The shift parameters and the constructed master curves of each field mixture are shown in Table 34 and Figure 66, respectively.

Table 34. Shift parameters of master curves for the field mixtures.

Mix	Code	δ	α	β	γ	*A*	*b*	*c*
1	**F-Mar-10E**	1.075	3.426	-1.518	0.432	0.0014	-0.2055	3.2388
2	**F-Mar-22S**	1.577	2.788	-1.496	0.530	0.0014	-0.1993	3.1002

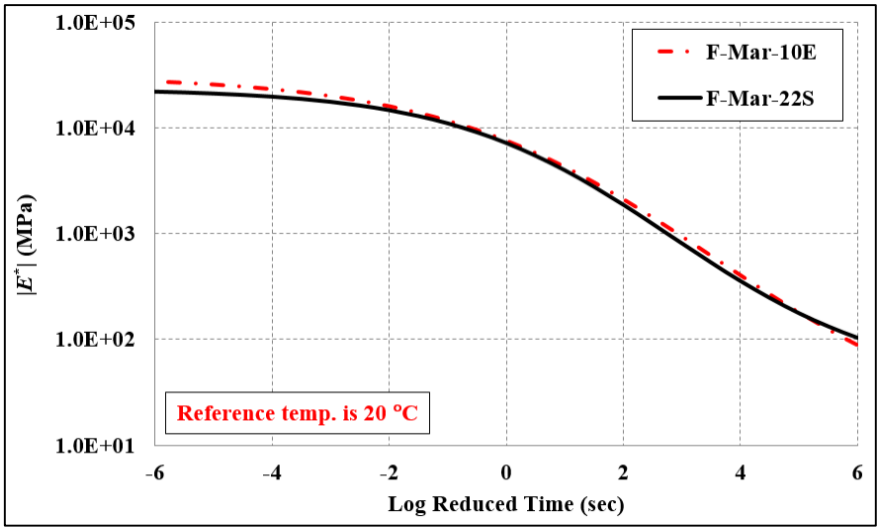

Figure 66. Dynamic modulus master curves for the field mixture specimens.

The master curves indicate that the dynamic modulus ($|E^*|$) values (stiffness) for all field mixtures are high. The range of $|E^*|$ values is similar to those of the mixtures of the trial road discussed in subsection 4.3.3. It can be seen from Figure 66 that both field mixtures are performing similarly, and the polymer-modified bitumen grade did not affect the performance significantly. Both PMB mixtures had a flattened master curve – if compared to unmodified bitumen mixture – which reduces the effect of temperature and frequency on the stiffness.

4.4.2 Uniaxial T/C fatigue test results

Similar to the field cores extracted from the base courses of the trial road, the field mixtures prepared in the laboratory (F-Mar-10E and F-Mar-22S) were also tested in the controlled-strain uniaxial T/C fatigue test. The test was performed with zero confinement, at a temperature of 20 °C with loading frequency of 10 Hz. Each replicate specimen was tested under strain amplitude L1 (55 με) and then strain amplitude L2 (130 με). Both strain amplitudes/levels were high enough to exceed the linear viscoelastic (LVE) region and cause damage. Most of the specimens failed early, before the end of the first fatigue test, and did not complete the 200,000 cycles. Therefore, it was decided to analyse each uniaxial T/C fatigue test independently. Similar to the tests on the field cores' specimens, the dynamic modulus and phase angle values from the first cycle interval (N = 10) in each fatigue test data were

considered as the linear viscoelastic dynamic modulus ($|E^*|_{LVE}$) and the linear viscoelastic phase angle (φ_{LVE}), respectively.

Prior to analysing the fatigue test data, the stress and strain amplitudes applied in this controlled-strain fatigue test using AMPT need to be inspected. Figure 67 shows an example of the strain and stress amplitudes applied on the specimens of F-Mar-10E field mixture under strain L1 and L2.

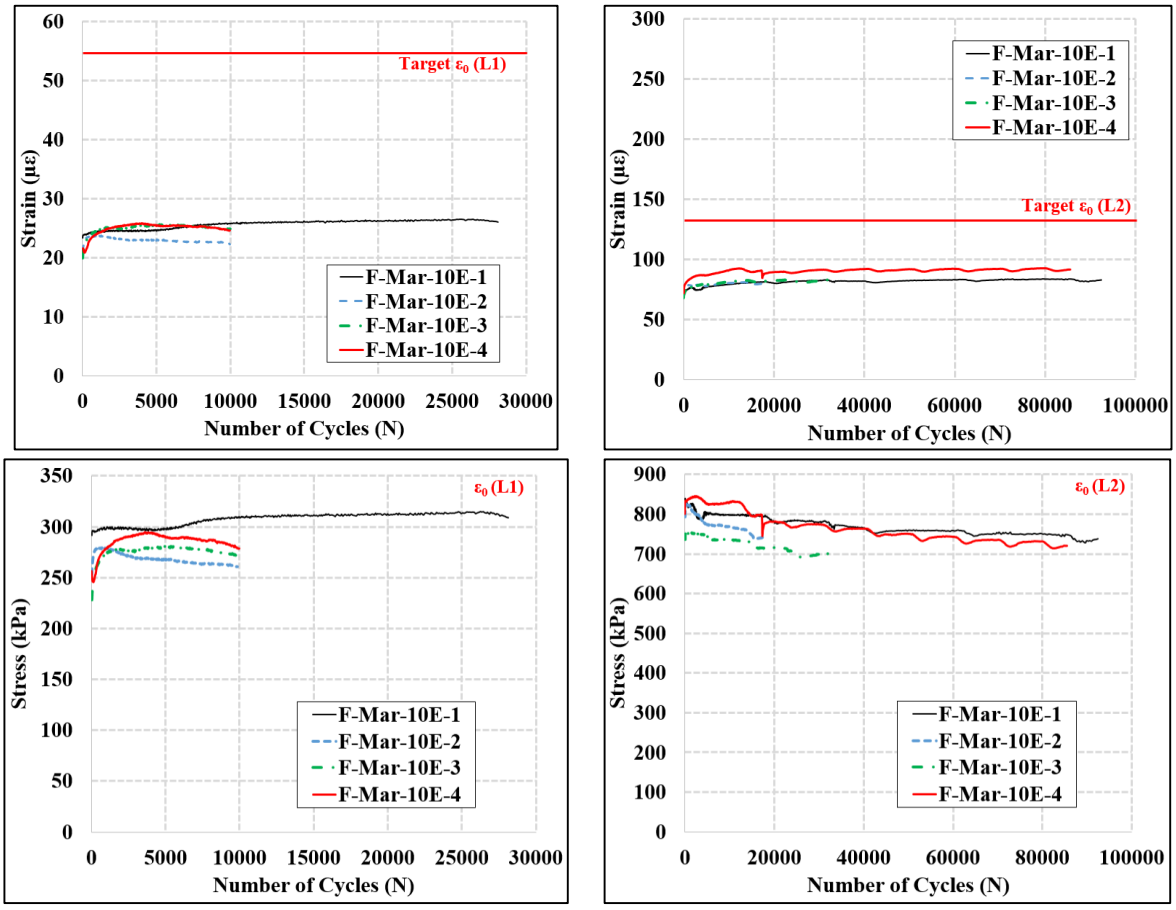

Figure 67. Strain and stress amplitudes applied to the specimens of F-Mar-10E mixture under both strain levels tests.

According to Figure 67 and raw data of the other field mixture (F-Mar-22S), the target strain amplitude was not achieved during either fatigue test (L1 and L2) but it was constant in both tests. This surely affects the prediction of the fatigue life if it is not taken into account by a suitable characterisation approach. Figure 68 shows the average strain amplitude applied on

the tested specimens during fatigue tests (L1 and L2). It is important to remember that these field mixtures are stiff with a low bitumen content (4.0%).

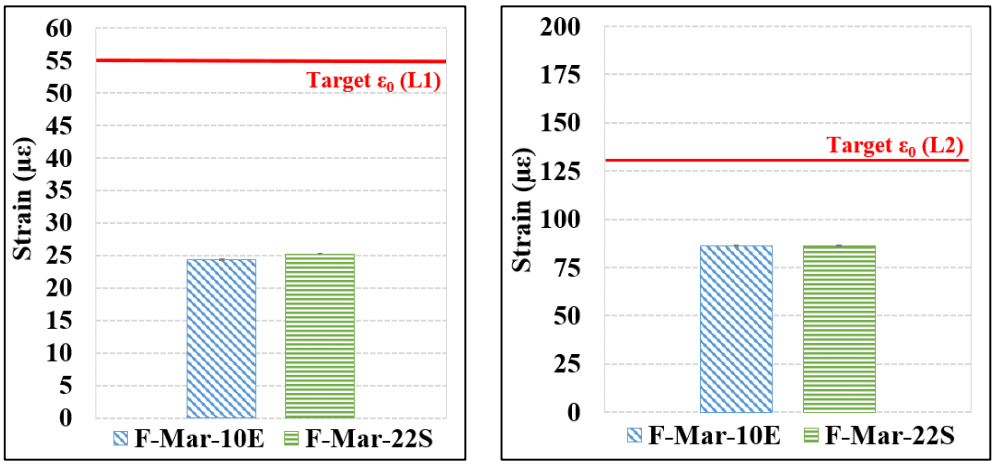

Figure 68. Average strain amplitude applied to the tested field mixtures.

The main outputs of each fatigue test were dynamic modulus ($|E^*|$) and phase angle (φ) against number of cycles. The results for each specimen of the field mixtures tested under strain amplitude level 1 are presented in Figure 69.

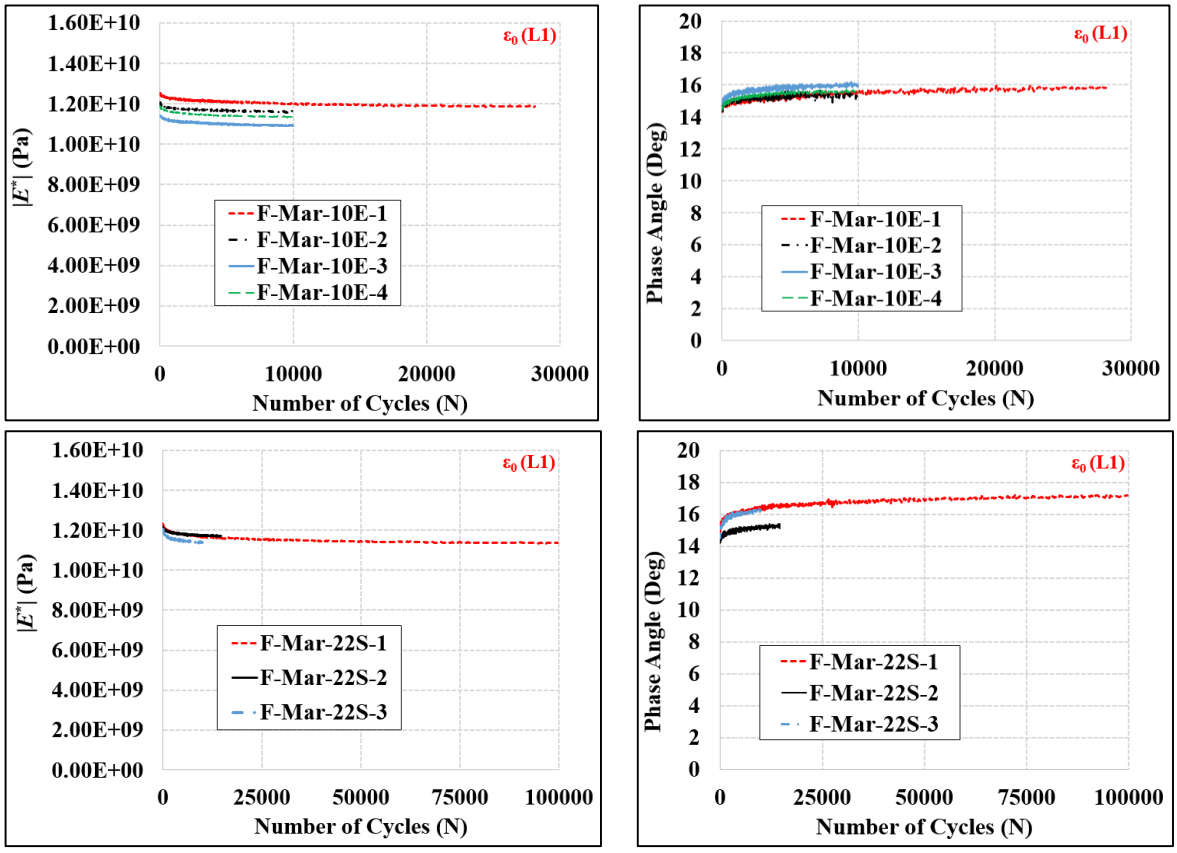

Figure 69. Dynamic modulus and phase angle results for the field mixtures tested under strain amplitude L1 test.

As shown in Figure 69, the specimens of each field mixture showed a similar reduction rate of dynamic modulus and increment rate of phase angle, opposite to the case for the field cores' specimens. However, these results cannot be used alone to evaluate the performance against fatigue cracking or predict fatigue life. In addition, the damage that happened in this first fatigue test and affected the specimen in the second fatigue test is not shown in the dynamic modulus or phase angle curves. Moreover, the figures above show that both field mixtures (F-Mar-10E and F-Mar-22S) are performing very similarly against fatigue damage, yet this is not true and so it is misleading. A fatigue characterisation approach should be employed in order to predict the fatigue life of each mixture and compare them accurately.

The results for each specimen of the field mixtures (F-Mar-10E and F-Mar-22S) tested under strain amplitude level 2 are presented in Figure 70.

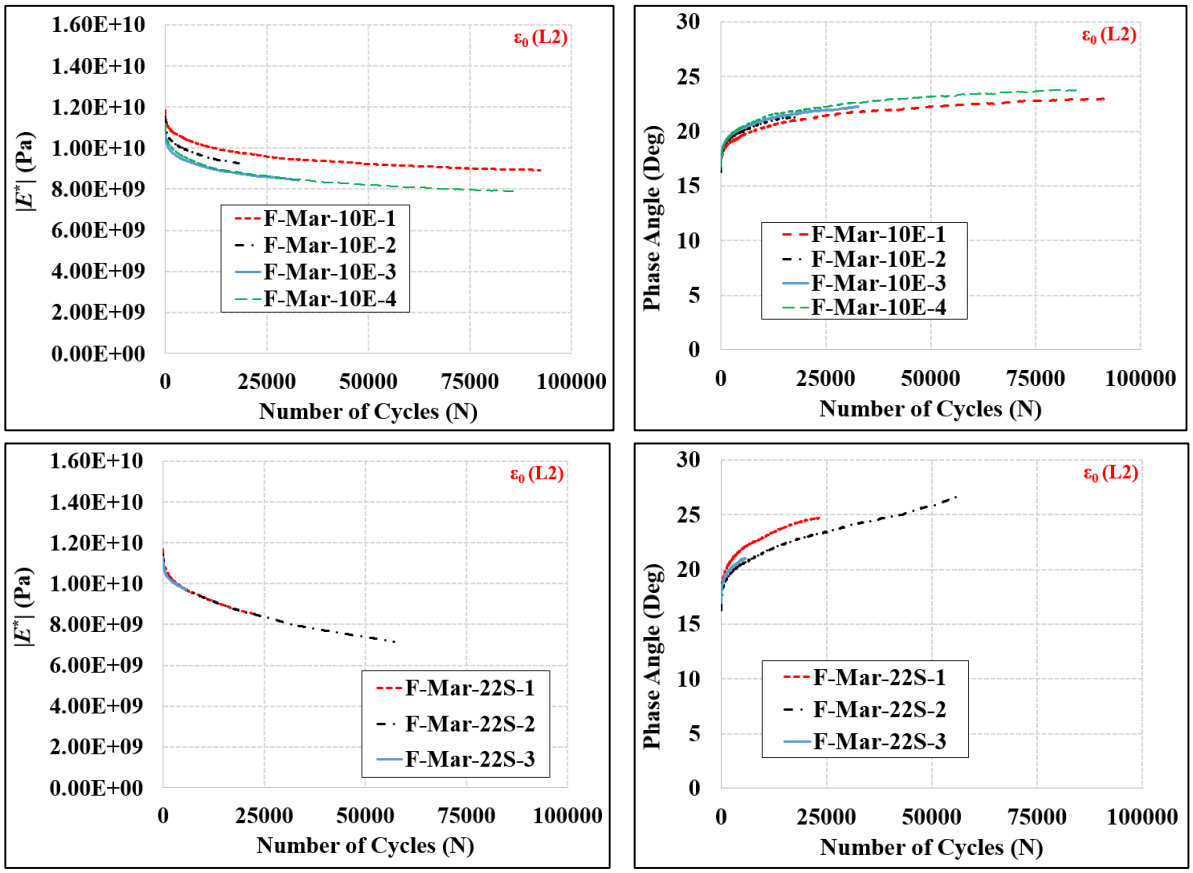

Figure 70. Dynamic modulus and phase angle results for the field mixtures tested under strain amplitude L2 test.

Similar to the results of the strain level 1 fatigue test, the specimens of each field mixture showed a very similar reduction rate of dynamic modulus and increment of phase angle but different fatigue lives. Many specimens failed early in the second test under strain amplitude L2, as shown in Figure 70. Using this traditional interpretation (E^* vs. N) will give unreliable results and conclusions. Thus, in the following chapter, the preliminary fatigue test data are analysed and discussed thoroughly using suitable fatigue characterisation approaches.

4.5 Laboratory mixtures' results

The test specimens prepared from the laboratory mixtures described earlier in subsection 4.1.3 were also subjected to the dynamic modulus ($|E^*|$) and uniaxial T/C fatigue tests only. The flow number (FN) and SCB tests were not conducted here either because the results of these tests from the field cores gave clear and reliable conclusions. Concentration here is given to the resistance of asphalt concrete mixtures to fatigue damage.

4.5.1 Dynamic modulus ($|E^*|$) test results

The raw data collected from the $|E^*|$ test of the laboratory mixtures (L-Mar-Pen, L-Spav-Pen and L-Spav-22E) were used to develop their master curves using the same sigmoidal fitting function used before in this study. The objective of this test was to assess the stiffness and the temperature susceptibility of different AC mixtures mixed, compacted and prepared in the laboratory. Table 35 and Figure 71 show the shift parameters and the constructed master curves of each laboratory mixture, respectively.

Table 35. Shift parameters of master curves for the laboratory mixtures.

Mix	Code	δ	α	β	γ	*A*	*b*	*c*
1	**L-Mar-Pen**	1.006	3.386	-1.151	0.564	0.0004	-0.1396	2.678
2	**L-Spav-Pen**	1.110	3.242	-1.155	0.617	0.0004	-0.1430	2.661
3	**L-Spav-22E**	1.362	2.984	-1.237	0.514	0.0001	-0.1171	2.143

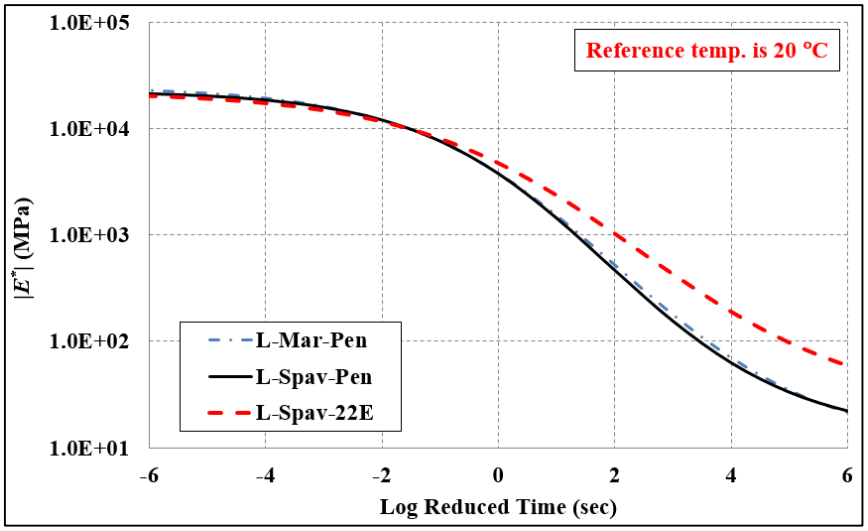

Figure 71. Dynamic modulus master curves for the laboratory mixture specimens.

According to the developed master curves of the laboratory mixtures, the dynamic modulus ($|E^*|$) values for all of them are high at low reduced-time values. In addition, the use of PMB in a Superpave laboratory mixture flattened its master curve and reduced the effect of temperature and frequency on the stiffness significantly.

Figure 71 also shows that the master curves of the laboratory mixtures with unmodified bitumen (L-Mar-Pen and L-Spav-Pen) are very similar.

4.5.2 Uniaxial T/C fatigue test results

After the dynamic modulus ($|E^*|$) test, the laboratory mixtures (L-Mar-Pen, L-Spav-Pen and L-Spav-22E) were tested under controlled-strain uniaxial T/C fatigue test. The test was performed under the same conditions assumed for the field cores and field mixtures (20 °C and 10 Hz). Similarly, each laboratory specimen was tested under strain amplitude L1 (55 με) and then strain amplitude L2 (130 με), and both strain amplitudes were high enough to exceed the LVE region and cause fatigue damage. Most of the tested specimens with 60-70 Pen bitumen failed early, before the end of the first fatigue test, and did not complete the 200,000 cycles. Therefore, it was decided to analyse each uniaxial T/C fatigue test independently. The dynamic modulus and phase angle values from the first cycle interval (N = 10) in each fatigue test data

were considered as the LVE dynamic modulus ($|E^*|_{LVE}$) and the LVE phase angle (φ_{LVE}), respectively.

Based on the raw data obtained from the fatigue test conducted on the laboratory mixtures, the target strain amplitude (55 με or 130 με) was not achieved but remained constant during both tests (L1 and L2). Figure 72 shows the average strain amplitude applied on the tested specimens during fatigue tests (L1 and L2). This will surely affect the reliability of the results if it is not considered using a suitable fatigue characterisation approach.

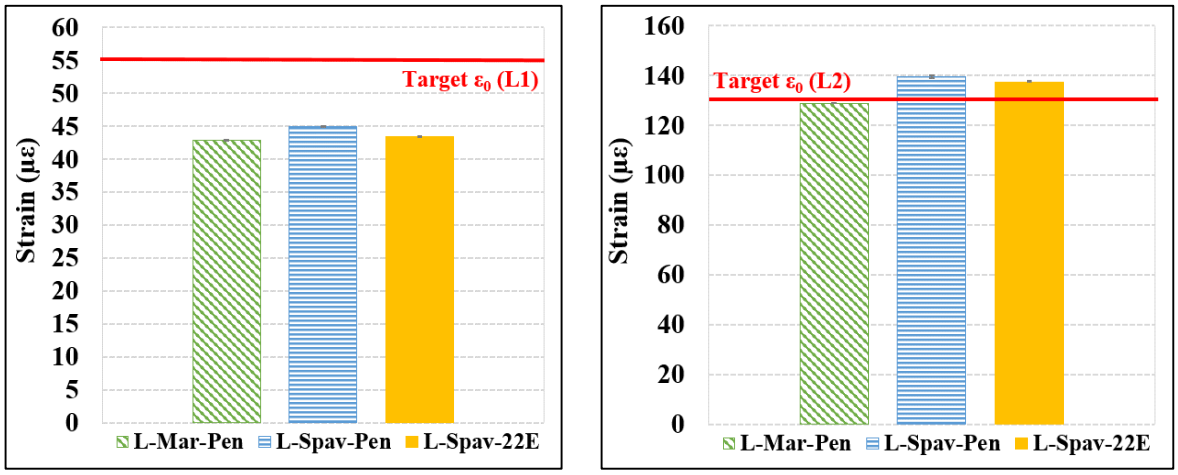

Figure 72. Average strain amplitude applied to the tested laboratory mixtures.

The major outputs of each fatigue test were dynamic modulus ($|E^*|$) and phase angle (φ) against number of cycles. The results for each specimen of the laboratory mixtures tested under strain amplitude L1 are presented in Figure 73.

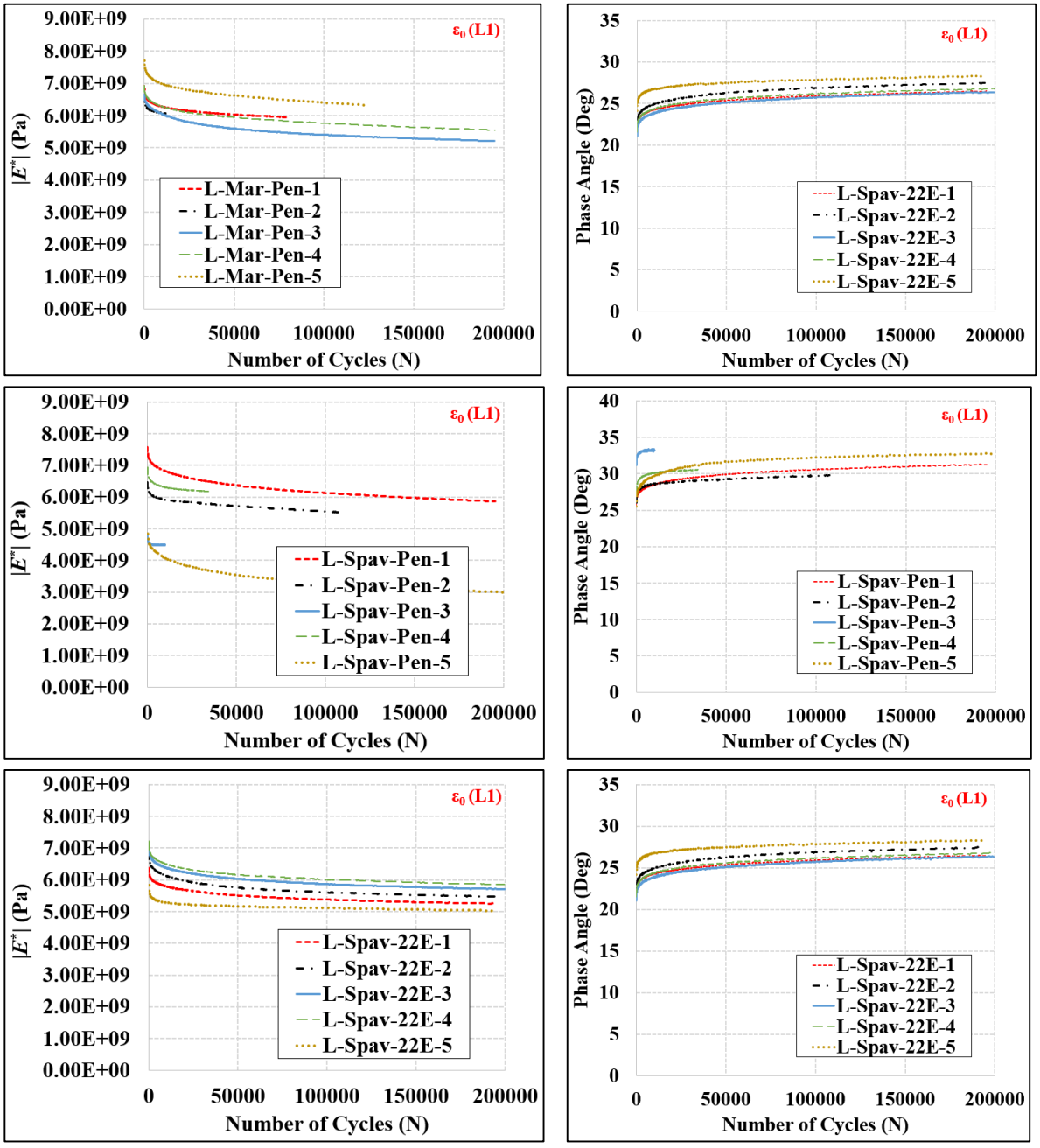

Figure 73. Dynamic modulus and phase angle results for the laboratory mixtures tested under strain amplitude L1 test.

According to Figure 73, the specimens of each laboratory mixture showed a similar reduction rate of modulus and increment of phase angle but different fatigue lives, especially in the mixtures with unmodified bitumen. In addition, damage happened in the laboratory mixtures during this first fatigue test (L1) and affected the specimen in the second fatigue test (L2). However, this is not revealed by the dynamic modulus or phase angle curves. Therefore,

these results alone are not enough to evaluate the performance of these mixtures against fatigue cracking. A fatigue characterisation approach should be implemented in order to identify the fatigue life of each laboratory mixture and compare them.

The results for each specimen of the laboratory mixtures tested under strain amplitude L2 are presented in Figure 74.

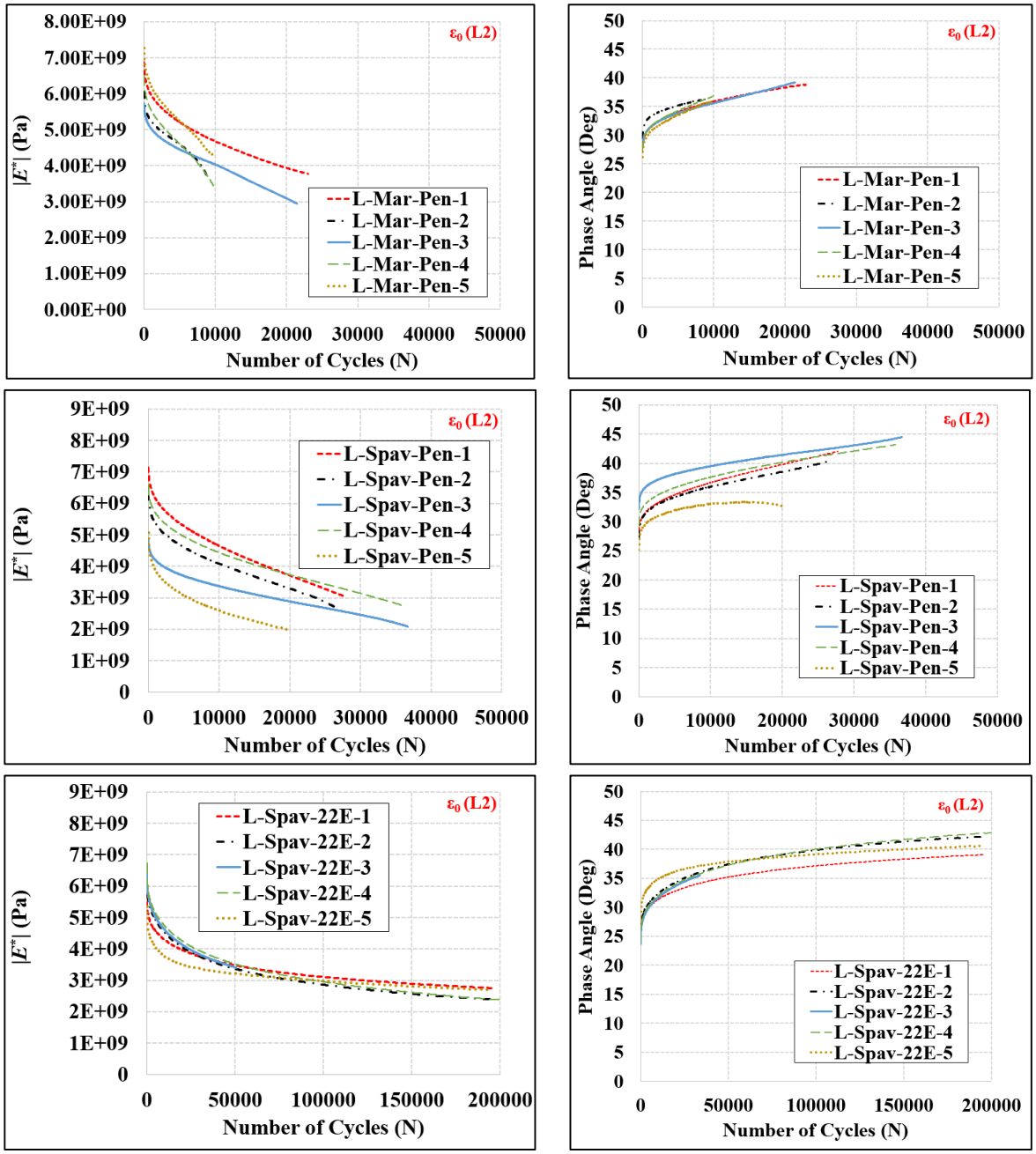

Figure 74. Dynamic modulus and phase angle results for the laboratory mixtures tested under strain amplitude L2 test.

Similar to the results of the fatigue test under strain L1, the specimens of each laboratory mixture showed a close reduction rate of dynamic modulus and increment of phase angle but different fatigue lives. All specimens of L-Mar-Pen and L-Spav-Pen mixtures failed early in the second test under strain amplitude of 130 με, as shown in Figure 74, and this generally shows the superiority of the use of PMB in a Superpave mixture (L-Spav-22E). Since the traditional interpretation (E^* vs. N) was giving undependable results and conclusions, an advanced fatigue characterisation approach was used to analyse the uniaxial T/C fatigue test data. This is described in Chapter 5.

4.6 Conclusions

After the investigation of asphalt pavement structures against different distresses and deteriorations in Chapter 2, it was important to assess the performance on the mixture level. Therefore, and with the aim of assessing the performance of different AC mixtures against rutting, fracture, temperature susceptibility and fatigue damage, several field cores, field mixtures and laboratory mixtures were tested and evaluated in this chapter. The conducted tests were useful to characterise and assess the performance of the mixtures against several major distresses. The following are the main findings based on the results of these laboratory tests:

- All flow number values obtained from the field cores are high, which indicates that these AC mixtures are expected to have high resistance to rutting.
- Resistance to rutting for asphalt concrete mixtures was mainly affected by the bitumen grade, aggregate source and aggregate gradation. The high rut-resistance of asphalt mixtures can be achieved by a well-designed mixture with the use of polymer-modified bitumen and Gabbro aggregate
- The fracture toughness (K) and maximum tensile stress (σ_{max}) values of all field cores' mixtures are high, which reflects good performance against fracture cracking.

- Results of the SCB test revealed that fracture cracking is not a major problem in the field cores' mixtures.
- The dynamic modulus master curves of all tested mixtures were mainly affected by the bitumen type/grade and aggregate type. In addition, the use of polymer-modified bitumen flattened the master curve of the asphalt concrete mixtures and reduced the temperature and frequency susceptibility on the stiffness and rut-resistance.
- According to the fatigue raw data of all tested mixtures, the target strain amplitudes (L1 and L2) were not achieved all the time but remained constant during both fatigue tests. This will surely affect the reliability of the results if it is not considered using suitable characterisation and analysis approaches.
- The replicate specimens of each field and laboratory mixture showed a similar reduction rate of dynamic modulus and increment of phase angle opposite to the field cores' specimens, but different fatigue lives.
- The preliminary results and the traditional interpretation of the data of the uniaxial T/C fatigue test could not be used directly to assess the performance against fatigue cracking. A suitable fatigue characterisation approach is needed.

It is obvious from this part of the study that rutting and fracture cracking are not major distresses for mixtures in Qatar, especially if they are designed following the Superpave mix design with the appropriate modified bitumen content and Gabbro aggregate. However, fatigue damage is a main distress for pavement materials in Qatar, and its characterisation should be investigated in depth. The traditional method (E^* vs. N) to interpret fatigue tests data was not useful to characterise and evaluate mixtures against fatigue damage. Therefore, two advanced fatigue characterisation approaches were selected to be performed on the raw data obtained

from the T/C fatigue test of the tested specimens prepared from different mixtures. These two approaches are presented in detail and their results are discussed thoroughly in the following chapter.

5 Fatigue Damage Characterisation of Asphalt Concrete Mixtures

The uniaxial tension-compression fatigue tests conducted on the field cores, field mixtures and laboratory mixtures were discussed in the previous chapter using the $|E^*|$ and φ results obtained from the fatigue tests. However, these results were not enough to evaluate the performance of the mixtures against fatigue cracking accurately. Therefore, in this chapter, the dissipated energy (DE) approach and the viscoelastic continuum damage (VECD) approach, in their latest form, are introduced in detail and then implemented to analyse the fatigue test data, assess the different AC mixtures and predict their fatigue lives.

5.1 Fatigue characterisation approaches

Before applying the fatigue characterisation approaches, each approach is discussed and presented in detail in the following subsections in order to highlight their advantages and limitations.

5.1.1 Dissipated energy (DE) approach

The theory of the dissipated energy (DE) approach started as a hypothesis by Van Dijk and Visser (1977) that the total dissipated energy (W_{total}) required for complete failure due to fatigue cracking is computed from the total area enclosed by a stress-strain hysteresis loop multiplied by the number of cycles (N). The W_{total} can be calculated using equation 39 for a fatigue test employing sinusoidal loading, as follows:

$$\boldsymbol{W_{total} = \sum_{i=1}^{n} N_i\, \sigma_i\, \varepsilon_i\, \sin \varphi_i} \qquad \textbf{Equation 41}$$

where, N_i is a fixed interval of loading cycles, and σ_i, ε_i and φ_i are mean values for stress amplitude, strain amplitude and phase angle for that interval, respectively.

The total dissipated energy (W_{total}) needed to reach fatigue failure was assumed to be constant irrespective of the loading mode (controlled-strain or controlled-stress), frequency and

temperature. However, laboratory fatigue tests in previous studies showed that the hypothesis that the W_{total} is independent of the mode of loading was not true (Bhasin, et al., 2009).

In addition, the phase angle (φ) in equation 41 is not a true viscoelastic phase angle but an apparent viscoelastic phase angle that quantifies the combined energy dissipated due to viscoelasticity, plastic deformation, and crack growth (i.e. $\varphi_i = \varphi_{VE} + \varphi_p + \varphi_c$). This combined dissipated energy was separated later in a study by Masad, et al. (2008).

Then, Van Dijk and Visser (1977) reported a semi-empirical relationship between the total dissipated energy (W_{total}) and the number of cycles to fatigue failure (N_f):

$$\boldsymbol{W_{total} = A(N_f)^z} \qquad \textbf{Equation 42}$$

where, *A* and *z* are the mixture's constants. Van Dijk and Visser (1977) reported a value of "z" to be around 0.6. Ghuzlan and Carpenter (2000) stated that the constants *A* and *z* depended on the mode of loading (controlled-strain vs. controlled-stress). Therefore, Ghuzlan and Carpenter (2000) proposed the rate of dissipated energy change (RDEC) method in order to overcome the limitations of the W_{total} method presented by Van Djik and co-workers. The RDEC quantifies fatigue damage based on the relative change in dissipated energy (DE) between consecutive cycles rather than the total dissipated energy (W_{total}), as follows:

$$\boldsymbol{RDEC_a = \frac{|DE_a - DE_b|}{DE_a \times (b-a)}} \qquad \textbf{Equation 43}$$

where, DE_a and DE_b are the amount of dissipated energy for the load cycles *a* and *b* where the difference between *a* and *b* is typically 100 cycles. The DE is the area enclosed within the hysteresis loop in a controlled-stress or controlled-strain mode using the strain (ε_0) and stress (σ_0) amplitudes in addition to the phase angle (φ), as follows:

For a controlled-strain test:

$$\boldsymbol{DE_a = \pi \sigma_a \varepsilon_0 \sin(\varphi_a) = \pi E_a^* \varepsilon_0^2 \sin(\varphi_a)} \qquad \textbf{Equation 44}$$

For a controlled-stress test:

$$DE_a = \pi \frac{\sigma_0}{\varepsilon_a} \sin(\varphi_a) = \pi \frac{\sigma_0^2}{E_a^*} \sin(\varphi_a) \quad \textbf{Equation 45}$$

Under controlled-strain or controlled-stress mode, the dynamic modulus (E^*) decreases and the phase angle (φ) increases with each cycle (N). Accordingly, the DE value will definitely increase with number of cycles (N) under controlled-stress mode; however, it might increase or decrease under controlled-strain condition depending on the relative increase in sin(φ) compared to the reduction in the dynamic modulus (E^*) (Bhasin, et al., 2009).

In the RDEC method, the fatigue failure (N_f) is about to happen when there is a significant increase in the magnitude of the DE between sequential cycles, as illustrated in Figure 75.

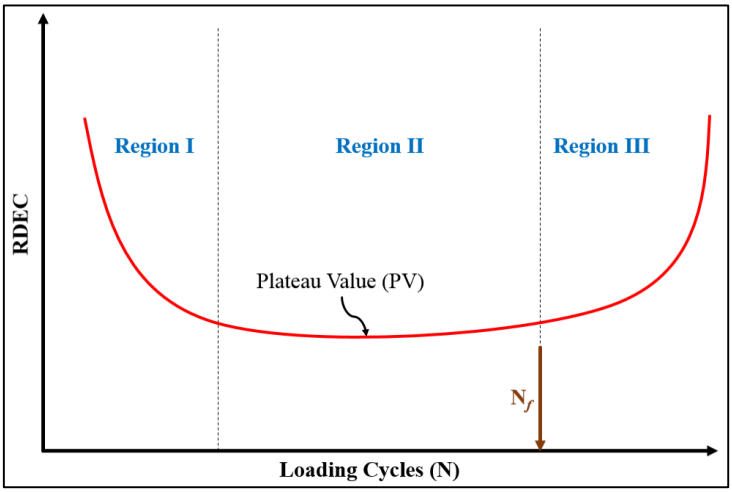

Figure 75. Typical RDEC vs. number of cycles plot.

Ghuzlan and Carpenter (2000) concluded the relationship between rate of dissipated energy change (RDEC) and the number of loading cycles in three regions as follows:

1. Region I: reorientation of the material due to application of the load;
2. Region II: steady-state fatigue crack propagation, i.e., the incremental damage per cycle is almost constant; and
3. Failure or region III: the rate of damage increases rapidly, demonstrating failure.

Region II was defined as the plateau value (PV) and was proposed to be used as a failure criterion that is insensitive to the mode of loading. A relationship was then stated between the PV and the N_f, as follows:

$$\boldsymbol{PV = c\left(N_f\right)^d} \qquad \textbf{Equation 46}$$

And, it can be rewritten as:

$$\boldsymbol{PV \times N_f = \frac{E^{\xi}_{Total}}{E^{\eta}} = c\left(N_f\right)^{d+1}} \qquad \textbf{Equation 47}$$

where, c and d are regression constants, E^{ξ}_{Total} is the total energy dissipated due to damage, and $E^{\eta}$is the viscoelastic energy dissipation value. Ghuzlan and Carpenter (2000) stated that equation 47 was found to be independent of mode of loading.

The advantage of the RDEC method is that it provides a real indication of the damage happening to the AC mixture from one cycle to another by comparing the energy level of a previous cycle and finding how much of it is contributing to the damage (Carpenter & Shen, 2006). In addition, it is insensitive to the loading mode or material type; however, the effect of viscoelasticity has still not been eliminated.

Schapery (1984) stated that by subtracting the true linear viscoelastic phase angle (φ_{LVE}) from the apparent phase angle ($\varphi_{\mathrm{apparent}}$) to find the phase angle corresponding to damage only ($\varphi_{\mathrm{damage}}$), the strain can be changed to an equivalent pseudo-strain (ε^R) or pseudo-stress (σ^R) based on the mode of loading. This might eliminate the influence of viscoelasticity on the calculated dissipated energy, and the dissipated pseudo-strain (-stress) energy (DPSE) resembles only the energy dissipated due to damage, as shown in Figure 76.

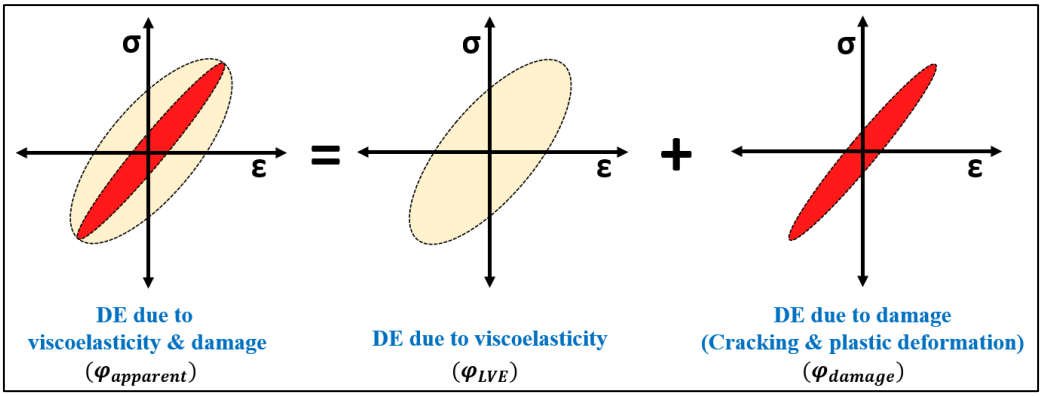

Figure 76. Illustration for the elimination of the influence of viscoelasticity on the calculated dissipated energy.

The DPSE value due to damage at each loading cycle can be calculated for asphalt mixtures as follows:

For a controlled-strain test:

$$DPSE_N = \pi E_N^* \varepsilon_0^2 \sin(\varphi_N - \varphi_{LVE}) \quad \textbf{Equation 48}$$

For a controlled-stress test:

$$DPSE_N = \pi \frac{\sigma_0^2}{E_N^*} \sin(\varphi_N - \varphi_{LVE}) \quad \textbf{Equation 49}$$

where, E_N^* and φ_N are the apparent dynamic modulus and the phase angle values measured at cycle *N*, respectively. The true φ_{LVE} can be measured from a fatigue test conducted at low strain/stress amplitude where no damage is caused to the specimen (Bhasin, et al., 2009). However, this measured true φ_{LVE} is then used in analysing fatigue test data at a high strain/stress amplitude test and, due to the nonlinear viscoelastic (NLVE) behaviour of asphalt mixtures, the calculation of DPSE using the equations above underestimates the viscoelastic DE at a high strain/stress amplitude test and overestimates damage in the material.

To overcome this limitation, Si, et al. (2002) estimated the true φ_{LVE} from the initial cycles of high strain/stress amplitude tests. However, it was overestimated by ignoring any damage that may occur throughout the first few loading cycles of the high strain/stress test. Therefore, studies by Masad, et al. (2008) and Bhasin, et al. (2009) demonstrated that, by a

careful selection of the applied strain/stress amplitude in the fatigue test, the true linear viscoelastic phase angle (φ_{LVE}) can be obtained from the first cycle of the high strain/stress amplitude fatigue test.

The DPSE calculation comprises all factors affecting fatigue cracking. These factors are plastic deformation, heat dissipation, healing and fracture, after eliminating both the nonlinearity of the material and the time-dependent (viscoelasticity) behaviour (Si, et al., 2002).

However, the DPSE magnitude for fatigue test under controlled-strain mode (equation 48) can either increase or decrease with N according to the relative change in the dynamic modulus and phase angle. This is not the case under controlled-stress mode, so the DPSE developed method was still sensitive to loading mode. Therefore, Masad, et al. (2008) separated the DPSE equations into three major components, and all of them are increasing with loading cycles (N) in both modes. The first component (W_{R1}) is the energy dissipated due to the change in phase angle between cycles and calculated by dividing equations 48 and 49 by the ratio of the damage stiffness to the undamaged LVE stiffness (E_N^*/E_{LVE}^*). The second component (W_{R2}) is the energy dissipated due to permanent deformation (rutting) represented by the change in phase angle within each loading cycle. The third component (W_{R3}) is the energy dissipated due to the change in stiffness or dynamic modulus between cycles. The three components can be calculated in both loading modes as follows:

For a controlled-strain test:

$$W_{R1_N} = \pi E_{LVE}^* \varepsilon_0^2 \sin(\varphi_N - \varphi_{LVE}) \qquad \textbf{Equation 50}$$

$$W_{R2_N} = \left(\frac{Area\ of\ stress\ vs.\ pseudostrain\ loop}{\frac{E_N^*}{E_{LVE}^*}} \right) - W_{R1_N} \qquad \textbf{Equation 51}$$

$$W_{R3_N} = \frac{1}{2} \varepsilon_0^2 (E_{LVE}^* - E_N^*) \qquad \textbf{Equation 52}$$

For a controlled-stress test:

$$W_{R1_N} = \pi \frac{\sigma_0^2}{E^*_{LVE}} sin(\varphi_N - \varphi_{LVE}) \quad \textbf{Equation 53}$$

$$W_{R2_N} = \left(Area\ of\ stress\ vs.\ pseudostrain\ loop \times \frac{E^*_N}{E^*_{LVE}}\right) - W_{R1_N} \quad \textbf{Equation 54}$$

$$W_{R3_N} = \frac{1}{2}\sigma_0^2\left(\frac{1}{E^*_N} - \frac{1}{E^*_{LVE}}\right) \quad \textbf{Equation 55}$$

For the total dissipated energy corresponding to fatigue damage (W_R), the first and the third components (W_{R1} and W_{R3}) are summed as follows:

$$W_R = W_{R1} + W_{R3} \quad \textbf{Equation 56}$$

At a particular preselected criterion for number of cycles to failure (N_f), if the total W_R is high for an AC mixture, a better resistance to fatigue damage is expected. This method (W_R), which is the latest form of the DE approach, is implemented in this chapter in order to analyse the controlled-strain fatigue test data and evaluate the performance of each AC mixture against fatigue cracking.

5.1.2 Viscoelastic Continuum Damage (VECD) approach

The viscoelastic continuum damage (VECD) theory was essentially developed based on Schapery's viscoelastic constitutive theory (Schapery, 1987). VECD theory ignores the micro-scale behaviour and attempts to describe the fatigue damage in a material on the macro-scale level as a reduction in the effective stiffness (Lee, et al. (2000) and Underwood, et al. (2012)). In the macro-scale level, the most appropriate approach to evaluate the effective stiffness is to use the stress-pseudo strain modulus (pseudo-stiffness, C) because direct use of the stress-strain modulus in an asphalt concrete mixture is complicated by time dependence, while in the stress-pseudo strain hysteresis loop the time effect is removed, and any reduction in the pseudo-stiffness (C) is a direct consequence of fatigue damage (Baek, 2010).

In addition, the VECD approach shows the ability to unify different temperatures, frequencies and loading modes or levels for analysis of fatigue characteristics of asphalt mixtures (Kutay, et al., 2009). This means that only one uniaxial T/C fatigue test is needed for an asphalt concrete mixture to predict its performance against fatigue under any temperature, frequency, loading mode or level.

Underwood, et al. (2010) stated that the VECD approach was developed based on three main concepts:

1. The elastic-viscoelastic correspondence principle based on pseudo-strain (ε^R) to model the VE behaviour of the material,
2. The continuum damage mechanics-based work potential theory to model the effects of micro-cracks on global constitutive behaviour, and
3. The time-temperature superposition (t-TS) principle with growing damage to include the joint effects of time/rate and temperature.

In the VECD approach, the performance against fatigue damage can be assessed initially by the damage characteristic relationship curve (C-versus-S curve), which is a material property that is independent of loading modes. This relationship relates the pseudo-stiffness (or material integrity), C, to the amount of internal damage in a specimen, S. The pseudo-stiffness is quantified as follows:

$$\boldsymbol{C} = \frac{\boldsymbol{\sigma_0^N}}{\boldsymbol{\varepsilon_N^R}} = \frac{\boldsymbol{\sigma_0^N}}{|\boldsymbol{E^*}|_{\boldsymbol{LVE}} \times \boldsymbol{\varepsilon_0^N}} = \frac{|\boldsymbol{E^*}|_{\boldsymbol{N}}}{|\boldsymbol{E^*}|_{\boldsymbol{LVE}}} \qquad \textbf{Equation 57}$$

where, σ_0^N is the stress amplitude, ε_N^R is the pseudo-strain calculated by multiplying the applied strain amplitude (ε_0^N) by the linear viscoelastic (undamaged) dynamic modulus ($|E^*|_{LVE}$); and $|E^*|_N$ is the dynamic modulus value, all at every loading cycle N.

Then, the amount of internal damage, S, at the peak of each loading cycle can be calculated as follows:

For a controlled-strain test:

$$S_{N+\Delta N} = S_N + \left(\frac{\Delta N}{f}\right)^{\frac{1}{1+\alpha}} \left[-I \frac{\left(\varepsilon_N^R\right)^2}{2} \left(C_{N+\Delta N} - C_N\right)\right]^{\frac{\alpha}{1+\alpha}} \quad \textbf{Equation 58}$$

For a controlled-stress test:

$$S_{N+\Delta N} = S_N + \left(\frac{\Delta N}{f}\right)^{\frac{1}{1+\alpha}} \left[\frac{\left(\sigma_N^R\right)^2}{2\,I} \left(\frac{1}{C_{N+\Delta N}} - \frac{1}{C_N}\right)\right]^{\frac{\alpha}{1+\alpha}} \quad \textbf{Equation 59}$$

where, ΔN is the loading cycle increment, *f* is the constant frequency in hertz and *I* is the ratio between the initial dynamic modulus $|E^*|_{N=1}$ of the tested mixture and its linear viscoelastic (undamaged) dynamic modulus $|E^*|_{LVE}$ used to eliminate specimen-to-specimen modulus variability. In this study, the value of *I* equals to 1 because the linear viscoelastic properties ($|E^*|_{LVE}$ and φ_{LVE}) for each tested specimen were taken as the initial values in the test raw data ($|E^*|_1$ and φ_1), as suggested by Bhasin, et al. (2009).

The σ_N^R in the controlled-stress test is the pseudo-stress calculated by dividing the stress amplitude (σ_0^N) by the $|E^*|_{LVE}$. Then, α is a material parameter that represents the rate of damage growth calculated using the exponent of time, *m*, in the relaxation modulus-time power equation [$E(t) = E_\infty + E_c t^{-m}$] derived by Schapery (1981). The value of *m* represents the material's tendency to release energy while cracking (Kutay, et al., 2008). To obtain the value of *m*, the dynamic modulus $|E^*|$ test results of a mixture at the reference temperature (e.g. 20 °C) are plotted against time (or loading frequencies) and then fitted by the relaxation modulus-time power equation, as shown in Figure 77.

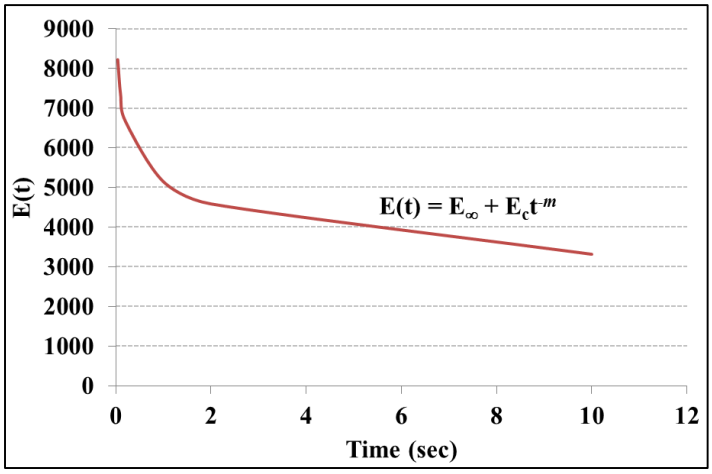

Figure 77. Plot of relaxation modulus-time power equation used to obtain the exponent of time (*m*).

Based on Kutay, et al. (2008) and Masad, et al. (2008), if the surface energy of the material and the fracture process zone are constants, then the value of α =1/*m*. However, if the tensile strength of the material and its surface energy are constants during fracture, then α =1+1/*m*. The analysis of the experimental measurements presented later in this thesis assumes the first case. Therefore, the relationship α =1/*m* is adopted.

Once the damage characteristic curve (C-S curve) is obtained and plotted, one of the following equations can be used to fit it:

$$C(S) = e^{aS^b} \qquad \textbf{Equation 60}$$

$$C(S) = 1 - c_{11}S^{c_{12}} \qquad \textbf{Equation 61}$$

where, *a*, *b*, c_{11} and c_{12} are the fitting constant parameters in the fitting equations and should be universal for each AC mixture. In this study, the exponential equation 60 was used to fit the damage C-S curve. However, if the controlled-strain uniaxial T/C fatigue test conducted on the AMPT was not "truly" a controlled-strain test and the target strain amplitude during the test was not attained, a simulation approach needs to be performed. This was also noticed in the fatigue tests conducted in this study, as shown earlier, in Chapter 4. Such a

simulation procedure was suggested by Kutay, et al. (2008) in order to calculate the fatigue responses of any mixture at any specified strain amplitude.

The simulation is initialised by calculating the true pseudo-strain (ε_T^R) value for controlled-strain test or true pseudo-stress (σ_T^R) value for controlled-stress test. The ε_T^R is computed by multiplying the required (or target) strain amplitude (ε_0) by the linear viscoelastic (undamaged) dynamic modulus ($|E^*|_{LVE}$) of the tested specimen, while the σ_T^R is calculated by dividing the target stress amplitude (σ_0) by the $|E^*|_{LVE}$ value.

Then, at the first loading cycle interval (e.g. N = 10), an initial internal damage parameter (S_0) should be assumed to be as minimum as possible, assuming that there is minimal damage in the specimen before or after the low strain amplitude fatigue test (Underwood, et al., 2012). Therefore, the dynamic modulus at the first interval (e.g. $|E^*|_{N=10}$) equals the linear viscoelastic dynamic modules ($|E^*|_{LVE}$). After that, the simulated internal damage value of the next cycle ($S_{N+\Delta N}$) is calculated as:

For a controlled-strain test:

$$\boldsymbol{S_{N+\Delta N} = S_N + \left(\frac{\Delta N}{f}\right)^{\frac{1}{\alpha}} \left[-I \frac{(\varepsilon_T^R)^2}{2} \frac{dC}{dS_N}\right]^{\alpha}} \qquad \textbf{Equation 62}$$

where, $\frac{dC}{dS_N}$ is a partial derivative of the fitting equation 60 under controlled-strain mode and can be calculated as:

$$\boldsymbol{\frac{dC}{dS_N} = a\, b\, S_N^{b-1}\, e^{a\, S_N^b}} \qquad \textbf{Equation 63}$$

For a controlled-stress test:

$$\boldsymbol{S_{N+\Delta N} = S_N + \left(\frac{\Delta N}{f}\right)^{\frac{1}{\alpha}} \left[\frac{(\sigma_T^R)^2}{2\, I} \frac{dC^{-1}}{dS_N}\right]^{\alpha}} \qquad \textbf{Equation 64}$$

where, $\frac{dC^{-1}}{dS_N}$ is also a partial derivative of the fitting equation 60 under controlled-stress mode and can be calculated as:

$$\frac{dC^{-1}}{dS_N} = -a\ b\ S_N^{b-1}\ e^{-a\ S_N^b}$$ **Equation 65**

Then, the simulated pseudo-stiffness for each cycle ($C_{N+\Delta N}$) can be computed as:

$$C_{N+\Delta N} = e^{a\ S_{N+\Delta N}^b}$$ **Equation 66**

As a result, the simulated damage characteristic curve (C-S simulated) is plotted to represent the fatigue behaviour of an asphalt mixture specimen under a specific and constant strain/stress amplitude.

To be able to compare between different asphalt concrete mixtures against fatigue damage, the fatigue life (N_f) is estimated by a generalised VECD-based formulation derived in a study by Kutay, et al. (2009). The N_f integration formulation is:

For a controlled-strain test:

$$N_f = \int_{S_0}^{S_f} \left[-\frac{(\varepsilon_T^R)^2}{2\ I} \frac{dC}{dS_N} \right]^{-\alpha} f\ dS$$ **Equation 67**

For a controlled-stress test:

$$N_f = \int_{S_0}^{S_f} \left[\frac{(\sigma_T^R)^2}{2\ I} \frac{dC^{-1}}{dS_N} \right]^{-\alpha} f\ dS$$ **Equation 68**

where, S_f is the internal damage parameter value when the pseudo-stiffness (C) is equal to a preselected failure criterion (e.g. $C_f = 0.5$). The S_f value can be calculated using the original fitting equation 60, as follows:

$$S_f = \left(\frac{\ln C_f}{a} \right)^{1/b}$$ **Equation 69**

So, the mixture with high N_f value is expected to have a longer life, resisting fatigue cracking or damage. The VECD approach was selected to be implemented on the fatigue test data discussed in the previous chapter due to some advantages. *The main advantage is that the VECD approach accounts for the initial condition of the specimen before testing (or re-testing at a higher strain amplitude) by selecting a suitable initial internal damage (S_0).* In addition,

after obtaining the fitting parameters (*a* and *b*) for any asphalt concrete mixture, they can be used to predict its fatigue life (N_f) under any temperature, frequency, loading mode or level.

In this chapter, the VECD approach in addition to the W_R method is used to analyse the controlled-strain uniaxial T/C fatigue test data and assess the performance of each AC mixture against fatigue cracking. The objective is to better characterise and evaluate the performance of these mixtures and compare their fatigue lives. In addition, it was important to examine both methods (i.e. W_R and VECD) in order to identify their limitations.

5.2 Uniaxial fatigue test results

Following the dynamic modulus test, all specimens of field cores, field and laboratory mixtures were tested twice under the uniaxial T/C fatigue test. Both tests were performed under a controlled-strain condition with strain amplitude (ε_0) of 55 με (L1) and then 130 με (L2). The data were collected and analysed separately, as in the previous chapter, using the W_R method and then the VECD approach.

5.2.1 Field cores' results

5.2.1.1 Total dissipated energy (W_R) method

Using the raw data from the controlled-strain T/C fatigue tests, the total dissipated energy (W_R) values were computed as the sum of dissipated energies ($W_R = W_{R1} + W_{R3}$) shown earlier, in equations 50 and 52. The W_R result of each mixture was not taken as an average for replicate specimens and plotted in a bar chart as per the practice in the literature. In this study, the W_R result is shown as a curve against number of cycles (N) in order to show the rate of change in the cumulative dissipated energy of each specimen.

The dynamic modulus ($|E^*|_{LVE}$) and phase angle (φ_{LVE}) values used in equations 50 and 52 are those at the first loading cycle interval (i.e. N = 10) of the fatigue test data. Figure 78 to Figure 82 compare the curves of the W_R against the number of cycles (N) for all replicate specimens of each tested trial section under strain L1 test.

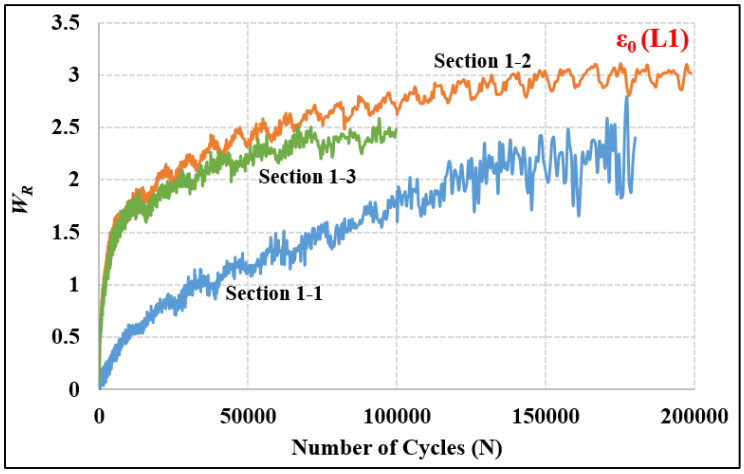

Figure 78. W_R curves for specimens of trial section 1 under strain amplitude L1 test.

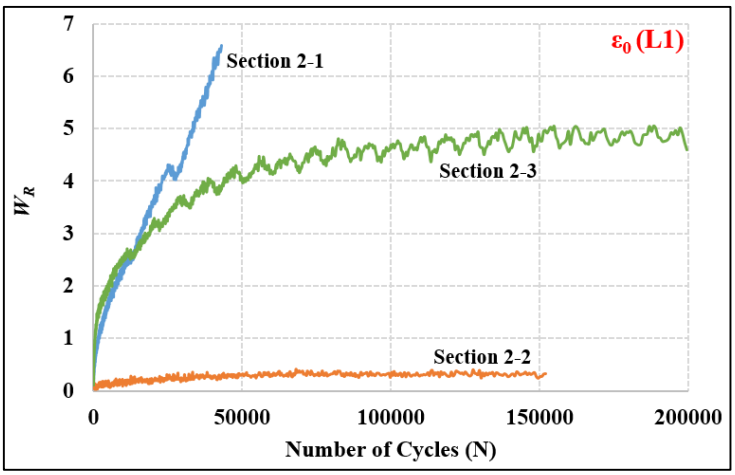

Figure 79. W_R curves for specimens of trial section 2 under strain amplitude L1 test.

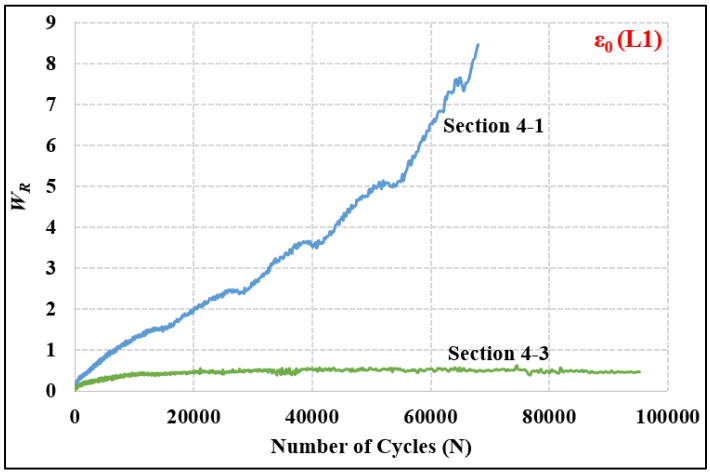

Figure 80. W_R curves for specimens of trial section 4 under strain amplitude L1 test.

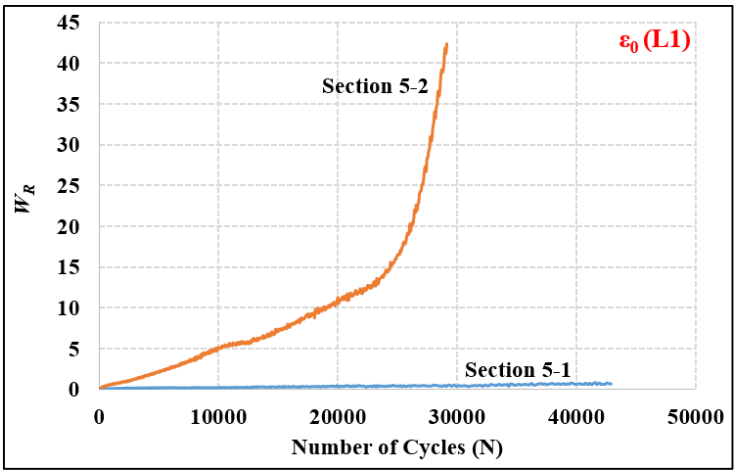

Figure 81. W_R curves for specimens of trial section 5 under strain amplitude L1 test.

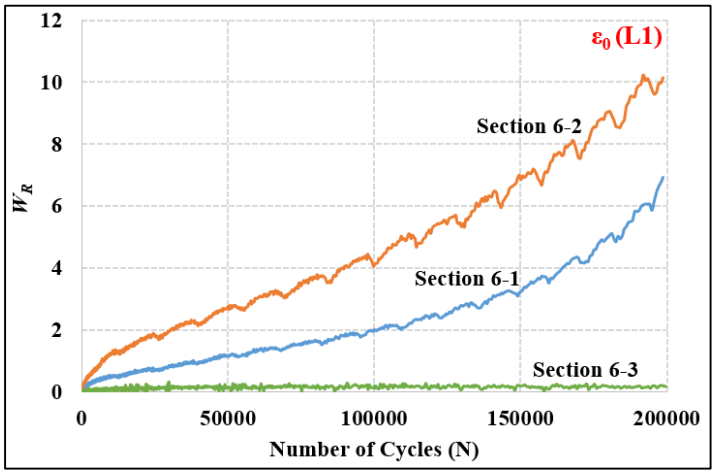

Figure 82. W_R curves for specimens of trial section 6 under strain amplitude L1 test.

According to the results and the dissipated energy (W_R) curves shown in the figures, the W_R curves are divergent, show scatter and no firm conclusions can be drawn from them. It is difficult to specify a failure criterion (N_f) in order to characterise and evaluate the performance of the field cores of each trial section against fatigue cracking. Some specimens suffered quick and considerable damage that makes the W_R curve increases rapidly, as shown in some samples of trial sections 2, 4 and 5.

As discussed by Masad, et al. (2008), the developed total dissipated energy method (W_R) alone does not give an accurate indication regarding the resistance to fatigue cracking because this resistance is also a function of the ability of the material to sustain such changes in dissipated energy.

Figure 83 to Figure 86 illustrate the W_R curves against the number of cycles (N) for all specimens of each trial section under strain L2 test. Two specimens of trial section 5 base (Marshall/QCS with Gabbro and Shell Thiopave bitumen) completed the first fatigue test (L1) and failed very early in the second fatigue test; therefore, no data were collected for section 5.

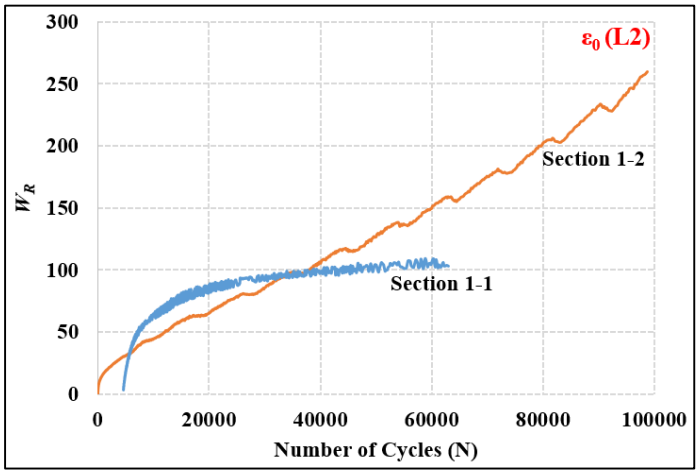

Figure 83. W_R curves for specimens of trial section 1 under strain amplitude L2 test.

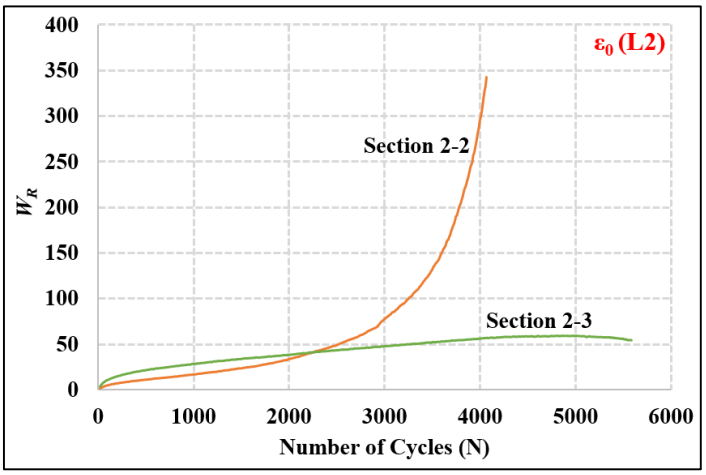

Figure 84. W_R curves for specimens of trial section 2 under strain amplitude L2 test.

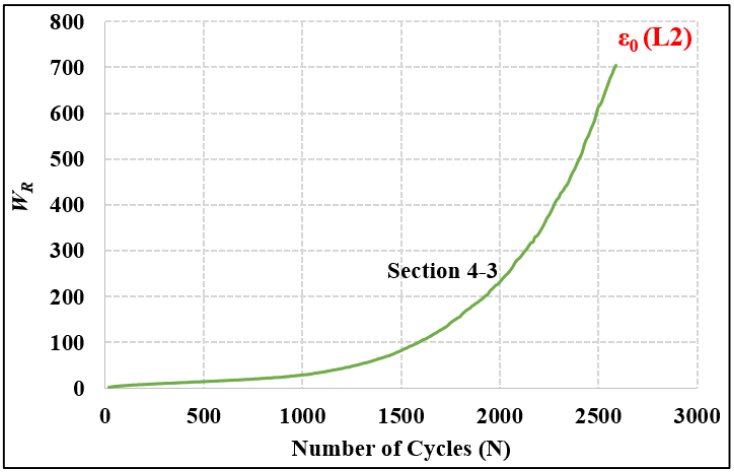

Figure 85. W_R curves for specimens of trial section 4 under strain amplitude L2 test.

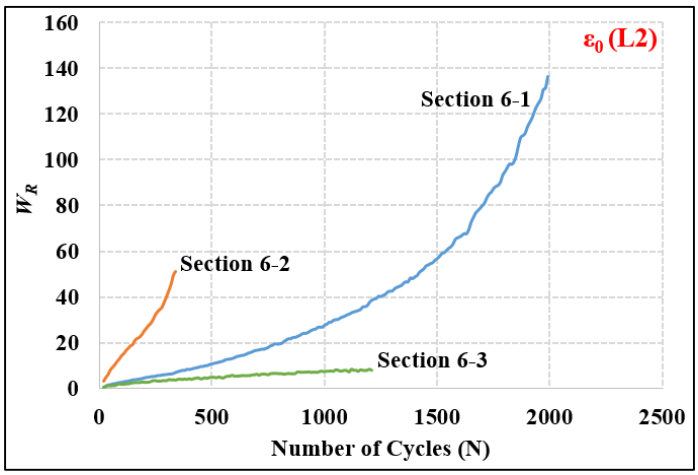

Figure 86. W_R curves for specimens of trial section 6 under strain amplitude L2 test.

It can be noticed from the figures that W_R curves of some samples in trial sections 1 and 4 were excluded from the plots. This is because their total W_R values were very high after a few loading cycles, indicating very early and rapid failure.

Based on the W_R curves, all tested specimens failed very early in the second uniaxial T/C fatigue test and dissipated a lot of energy. This can be attributed to the damage that happened in the specimens at the end of the first fatigue test, and the high crack growth due to the true stress applied on the intact area of the specimens.

Similar to the results of the strain amplitude L1 test, it is hard to state a failure criterion (N_f) in order to evaluate the performance of the field cores of each trial section against fatigue cracking. The total W_R curves were not useful enough to assess the performance of each base

mixture of the trial road against fatigue damage. For example, W_R curves of the specimens of trial section 6 in Figure 86 had different slopes (rate of energy change with cycles), indicating a high discrepancy in the results. As mentioned before, it might very well be that the presence of the interface between the two layers comprising the test specimen could have affected the test results and is the reason for the high discrepancy.

In general, the dissipated energy (W_R) method does not consider the condition of the mixture before testing, and it calculates the dissipated energy based on the applied/actual strain amplitude not the target/true one. Accordingly, and to overcome these limitations, it was important to implement the viscoelastic continuum damage (VECD) fatigue characterisation approach in order to evaluate the mixtures of the trial road accurately.

5.2.1.2 Viscoelastic continuum damage (VECD) approach

The VECD approach is implemented using the original raw data obtained from the uniaxial T/C fatigue tests regardless of the analysis results of the W_R method. The VECD characterisation approach was applied to characterise the fatigue resistance of the base mixtures of trial field cores and estimate their fatigue lives. In this approach, the fatigue performance can be assessed by the damage characteristic curve (C-S curve) and the VECD-N_f integration formulation explained earlier.

Two main inputs are required in the VECD: the linear viscoelastic dynamic (undamaged) modulus ($|E^*|_{LVE}$) and the material damage parameter (α). The $|E^*|_{LVE}$ values of the specimens of the base courses of the trial road were obtained from the first cycle interval (N = 10) of the raw data of each uniaxial fatigue test (L1 & L2) and are presented in Table 36.

Table 36. The $|E^*|_{LVE}$ values for all tested specimens of the field cores.

Section #	Specimen	$\|E^*\|_{LVE}$ (Pa)	
		ε_0-L1 = 55 με	**ε_0-L2 = 130 με**
1	**1**	0.83E+10	0.03E+10
	2	1.21E+10	1.14E+10
	3	1.53E+10	1.44E+10
	COV	**29.6%**	**85.5%**
2	**1**	1.26E+10	Specimen Failed
	2	1.09E+10	1.08E+10
	3	1.61E+10	1.52E+10
	COV	**21.1%**	**85.5%**
4	**1**	1.00E+10	Specimen Failed
	2	Specimen Failed	Specimen Failed
	3	1.07E+10	0.88E+10
	COV	**5.4%**	**-**
5	**1**	0.49E+10	Specimen Failed
	2	1.15E+10	Specimen Failed
	COV	**56.4%**	**-**
6	**1**	0.86E+10	0.50E+10
	2	1.02E+10	0.78E+10
	3	0.86E+10	0.75E+10
	COV	**10.1%**	**22.6%**

According to Table 36, it can be seen clearly that the specimens tested under strain L2 fatigue test were truly damaged (lower $|E^*|_{LVE}$) after the first fatigue (L1) test. However, the damage was not significant to the extent that no data could be collected from the L2 fatigue test, except for some specimens of trial sections 4 and 5. These specimens were prepared from extracted field cores and they were expected to have some initial cracks before testing. Nevertheless, the initial condition of the specimens is always considered in the VECD approach by the initial internal damage value (S_0), as mentioned earlier.

In addition, Table 36 shows that the coefficient of variation (COV) of $|E^*|_{LVE}$ is high among the specimens of most of the field cores in both fatigue tests. Consequently, this will surely affect the inevitability of the evaluation of fatigue damage resistance of the field cores from the trial road.

The effect of material damage parameter α on the damage characteristic curve is significant, and it was concluded in the literature that using α=1/*m* in controlled-strain or controlled-stress tests works out best to represent the fatigue damage resistance of field specimens (Kutay, et al., 2008). Table 37 shows the average material damage parameter (α) for each field core's mixture calculated using the value of *m* of relaxation modulus-time power equation obtained from the dynamic modulus test results at the reference temperature (i.e. 21.1 °C), as discussed earlier in this chapter.

Table 37. Material damage parameter (α) of all specimens of the field cores' mixtures.

Section #	Specimen	*m*	α = 1/*m*
1	**1**	0.244	4.098
	2	0.227	4.405
	3	0.235	4.252
2	**1**	0.202	4.496
	2	0.172	5.814
	3	0.186	5.380
4	**1**	0.175	5.700
	2	0.185	5.403
	3	0.192	5.208
5	**1**	0.192	5.208
	2	0.206	4.773
6	**1**	0.179	5.587
	2	0.198	5.051
	3	0.188	5.319

The mixtures with high damage parameter (α) are expected to have low relaxation and healing capacity but high resistance to rutting (Molenaar, 2007). From Table 37, mixtures of trial sections 2, 4 and 6 have the highest α values, and they were the best to resist rutting according to the results of the FN test shown earlier. In addition, the variability of the damage parameter (α) is reasonably low according to the COV results of the replicates.

The VECD analysis started with the calculation of the pseudo-stiffness modulus (C) and the internal damage (S) of all tested specimens of the trial sections using equations 57 and 58, shown in subsection 5.1.2, respectively. All VECD calculations in this study were conducted using MATLAB R2013a software package. Figure 87 and Figure 88 show the

plotted C-S damage curves for the specimens of each trial section at both strain amplitude fatigue tests, L1 and L2, respectively.

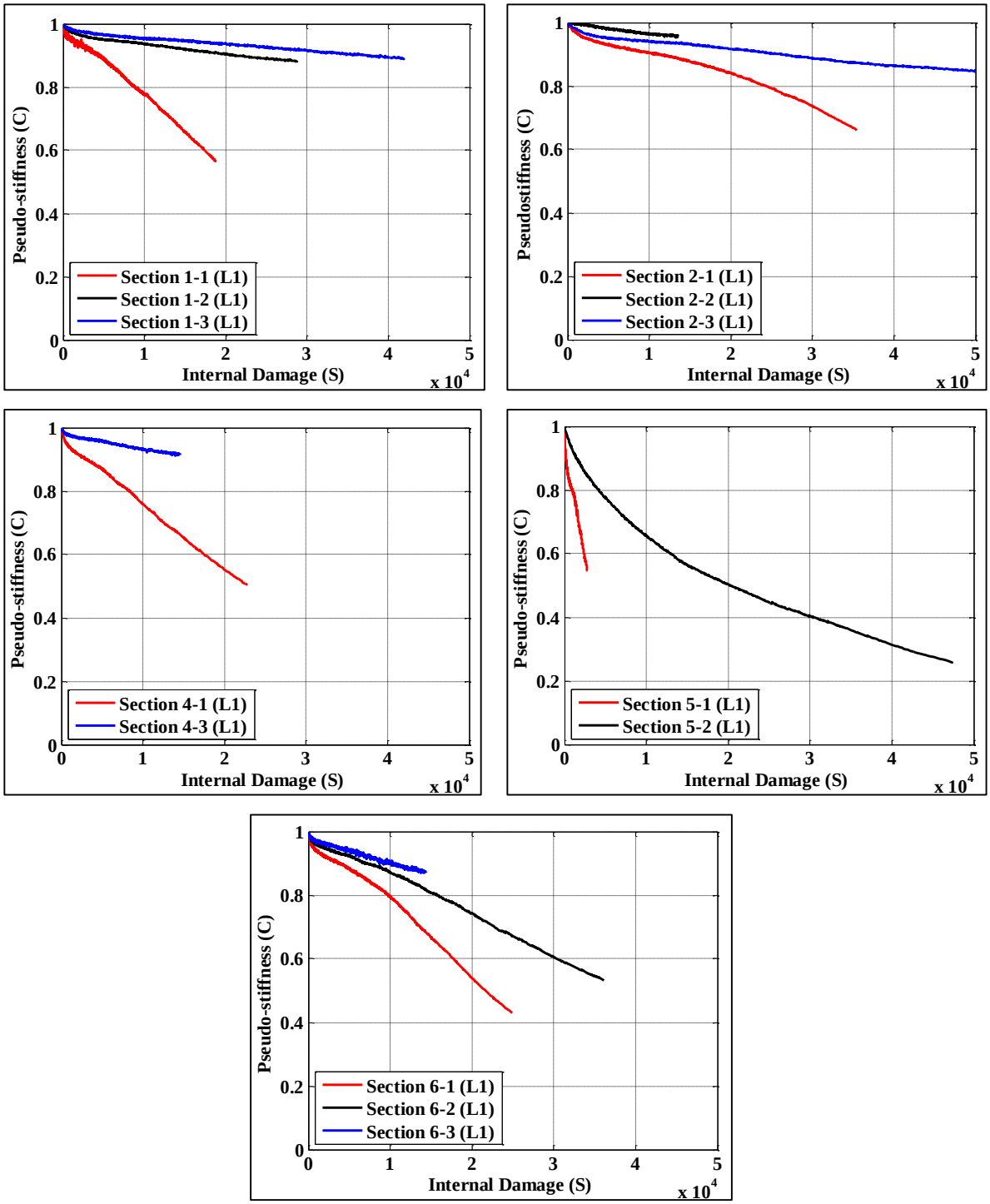

Figure 87. Damage characteristic (C-S) curves for specimens of the field cores under strain amplitude L1 test.

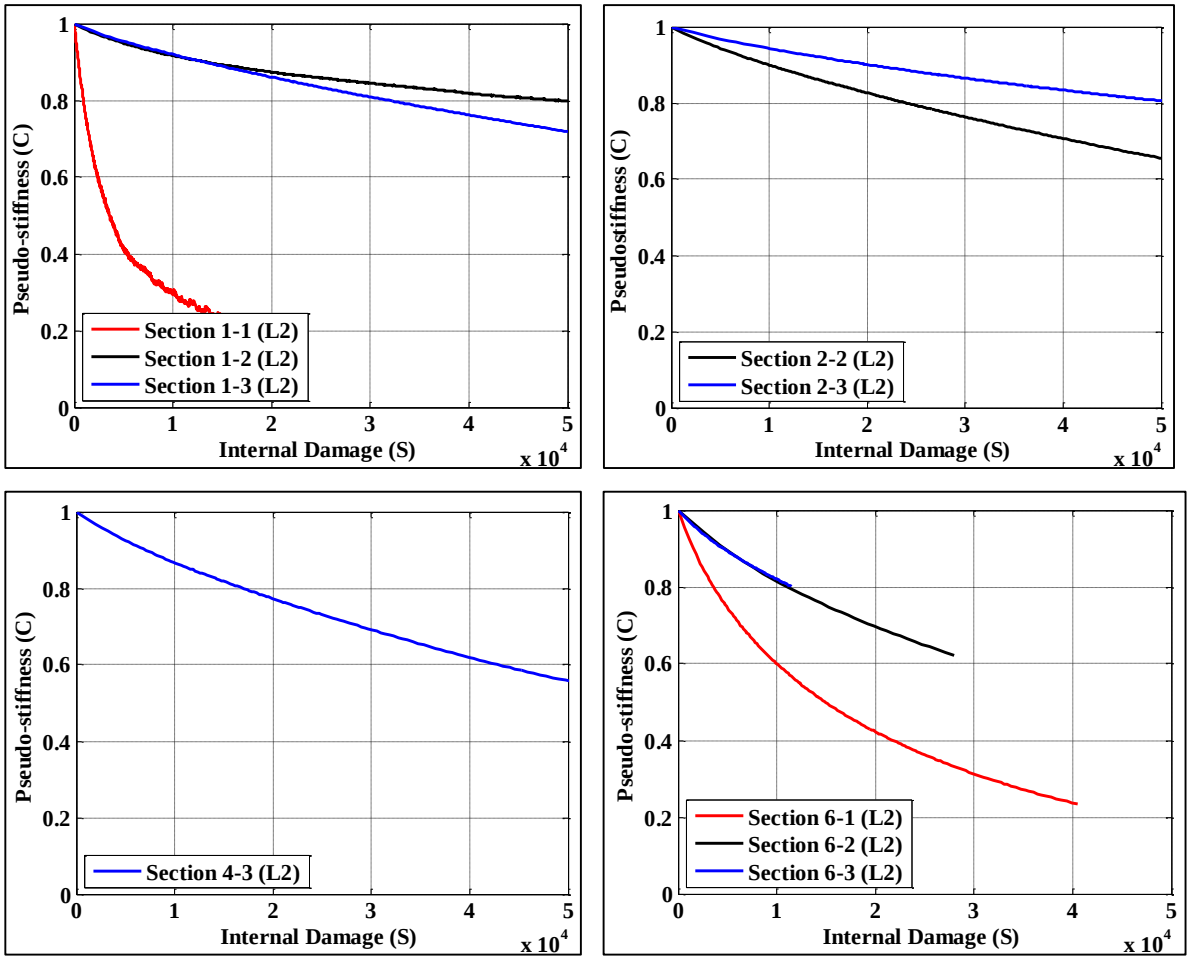

Figure 88. Damage characteristic (C-S) curves for specimens of the field cores under strain amplitude L2 test.

It was noticed that there is no convergence of C-S curves at low or high strain level tests for the same asphalt concrete mixture. This can be attributed to the high variability in the properties among the field cores' specimens of the trial sections. Each one of the damage characteristic curves of the field core specimens was fitted using the exponential equation 60 and the fitting constants, *a* and *b*, are summarised in Table 38. The average and standard error for these fitting parameters are shown in Figure 89.

Table 38. Fitting parameters (*a* and *b*) for all specimens of the field cores.

Section #	Specimen	ε_0-L1 = 55 με		ε_0-L2 = 130 με	
		a	***b***	***a***	***b***
1	**1**	-6.71E-05	0.9000	-9.90E-04	0.7746
	2	-6.05E-04	0.5159	-6.56E-05	0.7583
	3	-2.03E-04	0.5901	-2.87E-05	0.8642
2	**1**	-1.48E-05	0.9568	Specimen Failed	
	2	-1.00E-05	0.8852	-3.95E-05	0.8569
	3	-2.19E-04	0.6110	-4.88E-05	0.7751
4	**1**	-5.03E-05	0.9390	Specimen Failed	
	2	Specimen Failed		Specimen Failed	
	3	-4.37E-04	0.5510	-6.72E-05	0.8360
5	**1**	-1.00E-03	0.7961	Specimen Failed	
	2	-5.66E-04	0.7177	Specimen Failed	
6	**1**	-1.01E-05	1.1027	-4.42E-04	0.7645
	2	-9.74E-06	1.0469	-9.38E-05	0.8336
	3	-2.73E-04	0.6456	-1.03E-04	0.8216

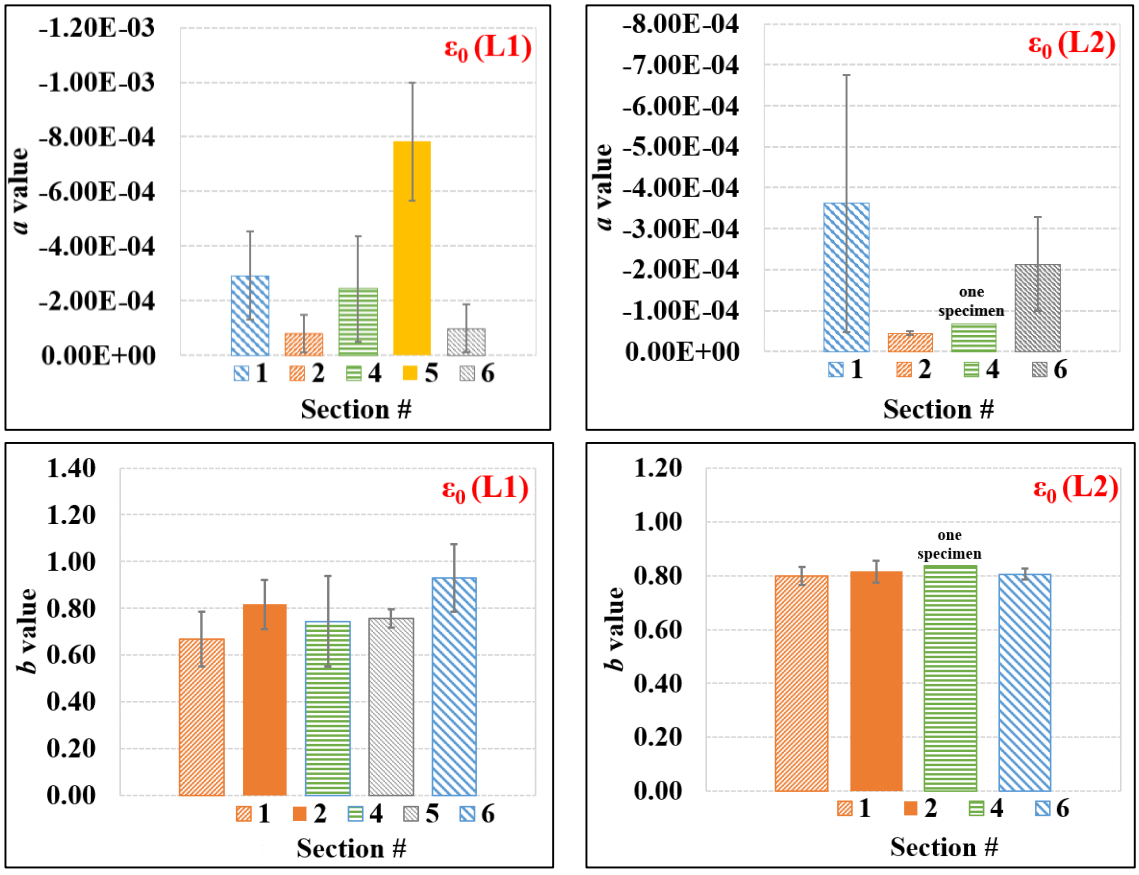

Figure 89. Average "*a*" and "*b*" values of all specimens of the field cores under strain amplitude L1 and L2 tests.

According to Table 38 and Figure 89, it is clear how scattered and variable are the values of the fitting parameters (*a* and *b*) among the specimens of each field core's mixture in

both strain level tests. It is worth mentioning that "*b*" is a parameter that quantifies the rate of reduction in stiffness of the mixture due to the internal damage growth (equation 60), and its level of certainty is important for an accurate evaluation of fatigue life.

As stated earlier, in subsection 4.3.4, the fatigue test conducted on the specimens of the field cores was not actually a controlled-strain test and the applied strain amplitude was constant but not the target value. Therefore, a simulation using the required strain amplitude (ε_0-L1 = 55 με and ε_0-L2 = 130 με) was implemented. The simulation starts by calculating the true pseudo-strain (ε_T^R) value for each specimen of the field cores. Then, equations 62, 63 and 66 were used to plot the simulated damage characteristic (C-S) curves for all field cores, as shown in Figure 90 and Figure 91.

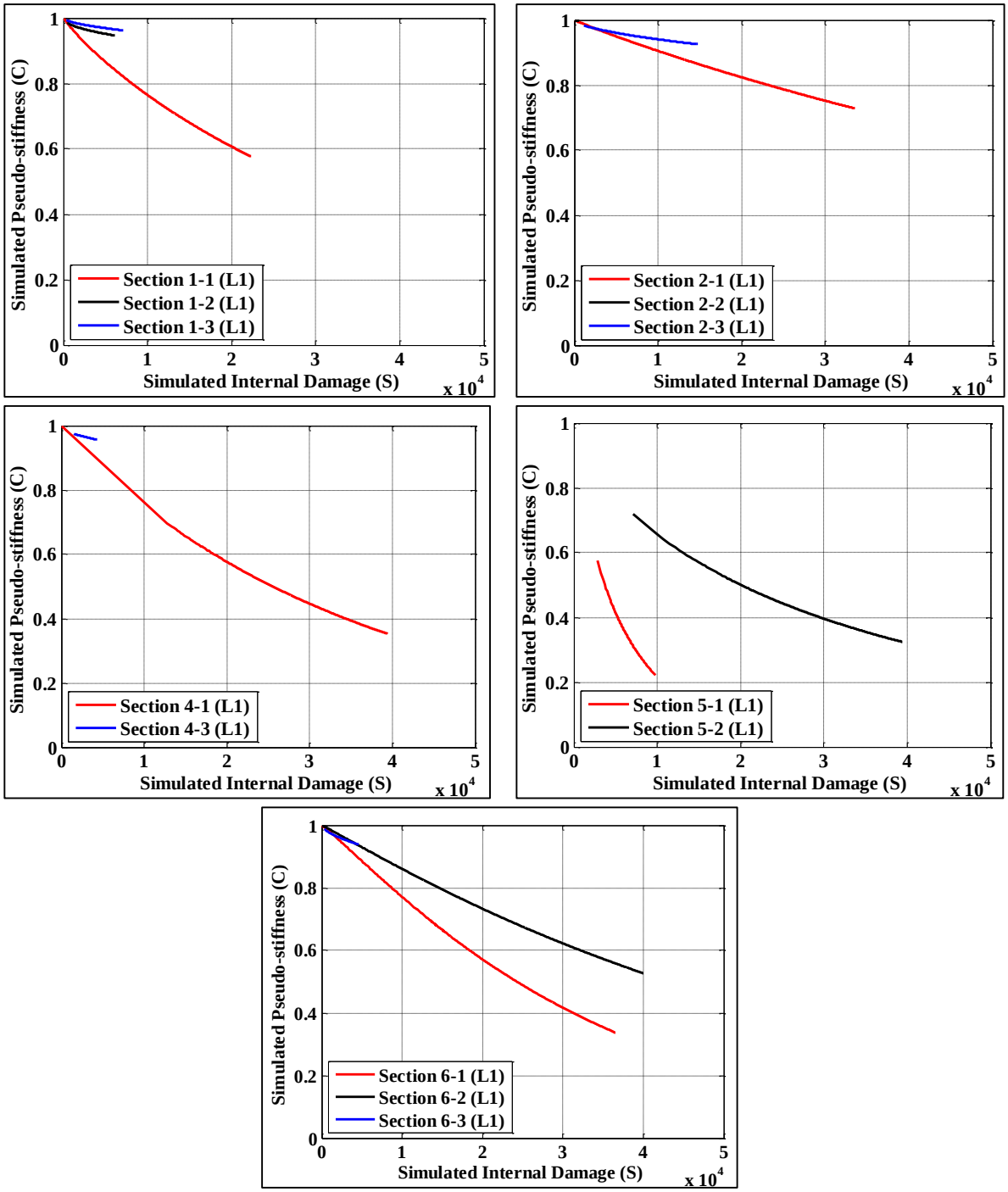

Figure 90. Simulated damage characteristic curves for field core specimens under strain amplitude L1 test.

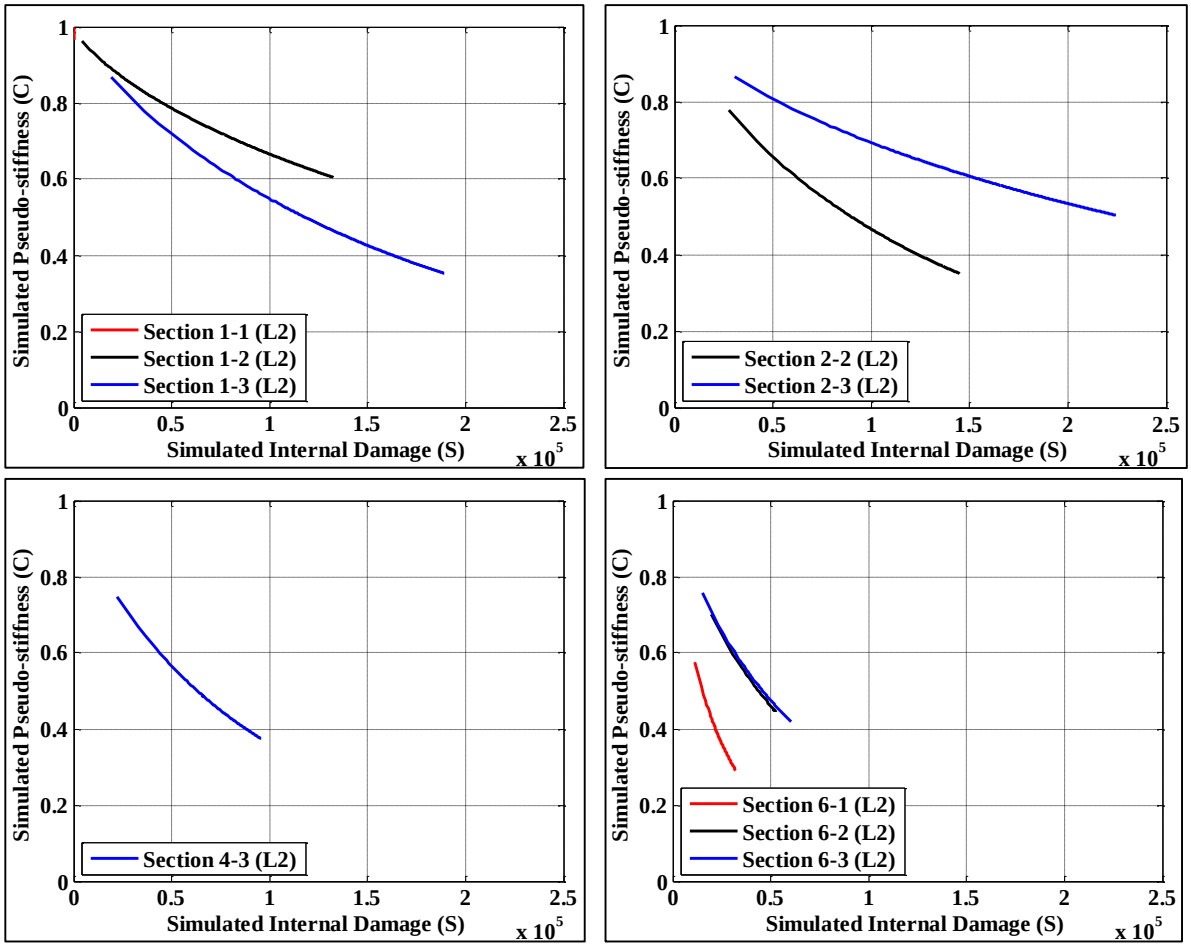

Figure 91. Simulated damage characteristic curves for field core specimens under strain amplitude L2 test.

The value of S_0, in both fatigue tests, for each specimen was selected carefully to represent the initial status of the tested specimen and to minimise the initial stiffness reduction calculated in the simulated pseudo-stiffness (C) values. It was noticed that the S_0 values were not the same, or even similar, for all specimens of each field core, as shown clearly in the figures and Table 39. This can be attributed to the differences of the original status/condition of the specimens after extraction from the field or after the first fatigue test. This surely did affect the reliability of the prediction of the fatigue life (N_f) later because each specimen started the fatigue test from a different damage condition.

Table 39. Initial damage (S_0) for each mixture of the field cores under strain L1 and L2 tests.

Section #	Specimen	Initial internal damage (S_0)	
		ε_0-L1 = 55 με	**ε_0-L2 = 130 με**
1	**1**	31	100
	2	450	4410
	3	330	18990
	COV	**79.8%**	**126.4%**
2	**1**	50	Specimen Failed
	2	3.5	27500
	3	1180	30350
	COV	**162.0%**	**57.9%**
4	**1**	54	Specimen Failed
	2	Specimen Failed	Specimen Failed
	3	1500	22280
	COV	**109.5%**	**57.7%**
5	**1**	2790	Specimen Failed
	2	7080	Specimen Failed
	COV	**61.5%**	**-**
6	**1**	102	11190
	2	20	19500
	3	300	15040
	COV	**102.3%**	**27.3%**

The simulated C-S curves show the actual behaviour of each specimen if it was subjected to the target constant strain amplitude during the fatigue test and the initial condition is considered. That is why they are different in slope from those of the experimental C-S curves. An example of the fatigue test analysis using the VECD approach (simplified in a spreadsheet for demonstration) is shown in Appendix D.

Then, the fatigue resistance of each specimen was assessed by comparing the number of cycles to failure (N_f) calculated using equation 67. The failure criterion was selected to be 50% reduction in the pseudo-stiffness of the specimen (C_f = 0.5). The calculated average N_f values for the field cores of all trial sections are presented in Figure 92 for both fatigue tests.

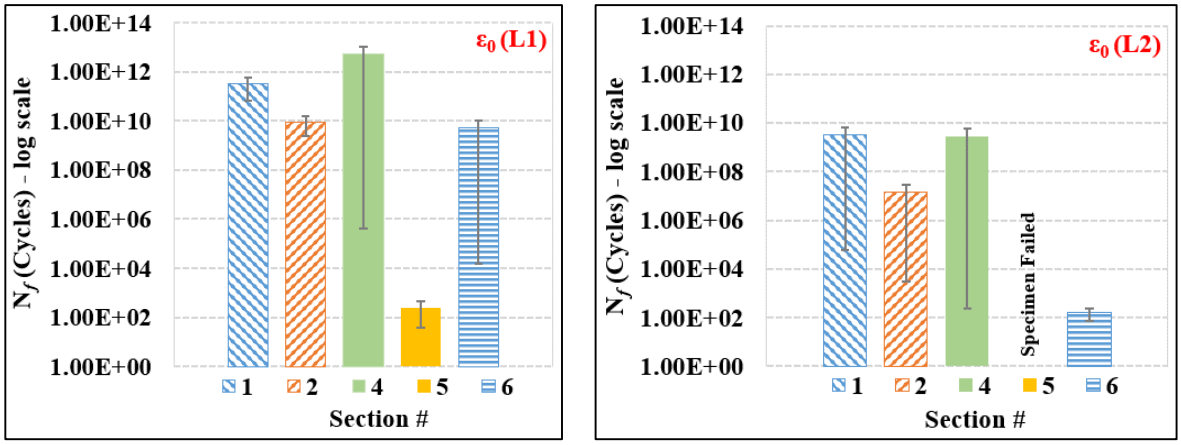

Figure 92. Comparison of average N_f results at C_f = 0.5 for all field cores under strain amplitude L1 and L2 tests.

According to the figures, the fatigue life (N_f) of each field section decreased under the high strain amplitude value and is significantly affected by the initial condition (S_0) of the mixture. Also, opposite to the results of this study, a stiff mixture with unmodified bitumen should have lower fatigue life than that with modified bitumen.

In order to evaluate the effect of using different bitumen types/grades, the average N_f value of trial sections 1, 2 and 6 and then trial sections 4 and 5 were compared. The results presented in Figure 92 manifest clearly that using different bitumen types has a significant effect on fatigue life and resistance. Based on the N_f results of the strain L1 test shown in Figure 92, it is clear that trial sections 2, with unmodified 60-70 Pen bitumen, and 6, with PMB, are performing almost the same against the fatigue cracking. However, trial section 1, with a stiff unmodified 40-50 Pen bitumen, has a higher N_f value (i.e., better performance). On the other hand, trial section 4, the control trial with unmodified 60-70 Pen bitumen, failed at a much higher loading cycle than trial section 5, with Shell Thiopave bitumen. Figure 92 shows again that, under strain L2 test, trial section 1 is performing much better than sections 2 and 6. However, trial section 4 had high variability in its results, while trial section 5 failed early under strain L2 test and no data were collected.

The effect of using different asphalt mix designs on the fatigue cracking resistance is assessed by comparing the average fatigue life (N_f) value of trial sections 2 (Marshall/PRD)

and 4 (Marshall/QCS). Generally, the results displayed in Figure 92 reveal that the effect of using different mix designs on fatigue life is also significant, and the use of the Marshall/QCS mix design improved the performance.

It is understood that the big difference in the initial damage (S_0) between replicate specimens of the field cores affected the certainty of the N_f prediction results. Therefore, more replicate specimens – without an interface – are needed to better evaluate the fatigue life of the mixtures of each field core. The standard error in the N_f results of each trial section in both fatigue tests (L1 and L2) is significantly high and clearly shows their variability and uncertainty. This might lead to contradictory results, and emphasises the importance of looking deeper into the fatigue life (N_f) model used and its parameters.

5.2.2 Field mixtures' results

5.2.2.1 Total dissipated energy (W_R) method

Similar to the analysis of the field cores, the sum of dissipated energies ($W_R = W_{R1} + W_{R3}$) was calculated using the T/C fatigue tests' data for the specimens prepared from field mixtures. The dynamic modulus ($|E^*|_{LVE}$) and the phase angle (φ_{LVE}) values used to find W_R are those at the first loading cycle interval (i.e. N = 10). Figure 93 and Figure 94 compare the curves of the W_R against the number of loading cycles (N) for all specimens of each tested field mixture under strain amplitude L1.

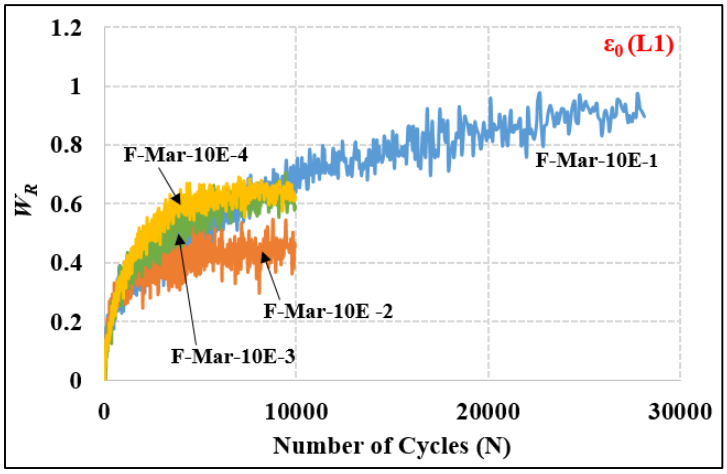

Figure 93. W_R curves for specimens of F-Mar-10E mixture under strain amplitude L1 test.

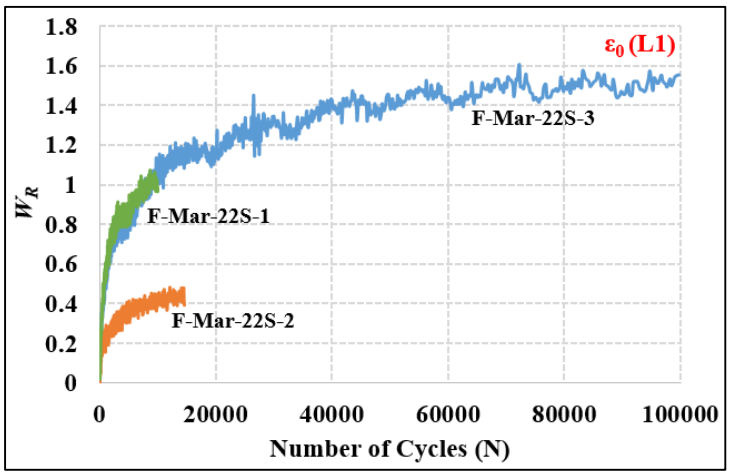

Figure 94. W_R curves for specimens of F-Mar-22S mixture under strain amplitude L1 test.

As shown in the figures for the W_R curves, the replicates of each field mixture did not perform similarly, and no specimen completed the test to the 200,000 cycles. Consequently, the failure criterion (N_f) cannot be easily specified in order to characterise and evaluate field mixtures against fatigue damage by the W_R curves under strain L1 test.

Figure 95 and Figure 96 illustrate the W_R curves against the loading cycles (N) for all specimens of the field mixtures under strain level 2 test.

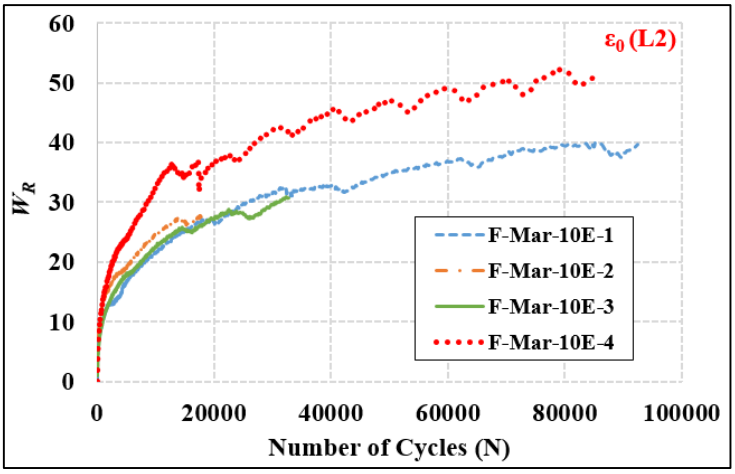

Figure 95. W_R curves for specimens of F-Mar-10E mixture under strain amplitude L2 test.

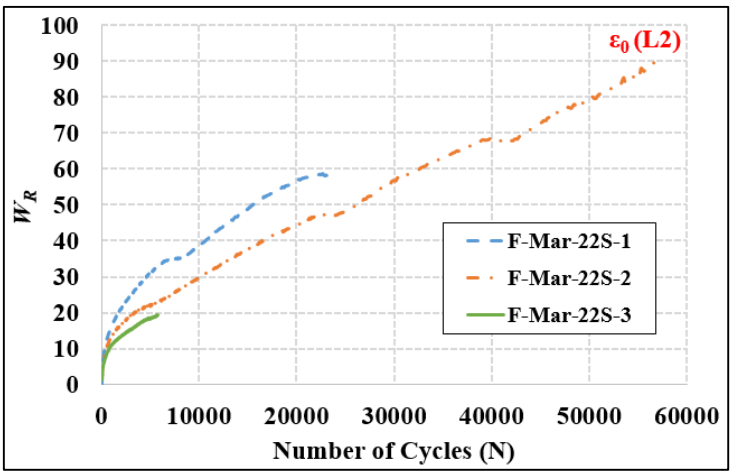

Figure 96. W_R curves for specimens of F-Mar-22S mixture under strain amplitude L2 test.

The W_R curves of the field mixtures under strain L2 test are also misleading and do not consider the condition of the specimens before the second fatigue test. As shown in the figures, specimens of F-Mar-10E and F-Mar-22S mixtures dissipated more energy under strain L2, but still the slopes of the curves are different from specimen to specimen, and no failure criteria can be stated to compare between mixtures. In addition, no replicate specimens of either field mixtures completed the fatigue test to the end, and this generally indicates lower performance.

It can be stated that the W_R method is not useful enough to characterise field mixtures against fatigue cracking under strain L1 and L2 tests. Accordingly, the viscoelastic continuum damage (VECD) fatigue characterisation approach is implemented in the following subsection in order to evaluate the field mixtures accurately.

5.2.2.2 Viscoelastic continuum damage (VECD) approach

The VECD approach is applied using the raw data obtained from the uniaxial T/C fatigue tests regardless of the analysis results of the W_R method. The VECD characterisation approach was used to characterise fatigue cracking resistance of the field mixtures and estimate their fatigue lives (N_f). The fatigue performance can be evaluated by the damage characteristic curve (C-S curve) and the VECD-N_f integration formulation explained earlier in this chapter.

As a first VECD analysis input, the linear viscoelastic dynamic (undamaged) modulus ($|E^*|_{LVE}$) value of each specimen of the field mixtures is obtained from the first cycle interval (N = 10) in both uniaxial fatigue tests (L1 and L2) and is presented in Table 40.

Table 40. The $|E^*|_{LVE}$ for all field mixture specimens.

Mix	Specimen	$\|E^*\|_{LVE}$ (Pa)	
		ε_0-L1 = 55 με	**ε_0-L2 = 130 με**
F-Mar-10E	**1**	1.25E+10	1.18E+10
	2	1.21E+10	1.15E+10
	3	1.14E+10	1.09E+10
	4	1.19E+10	1.12E+10
	COV	**3.8%**	**1.1%**
F-Mar-22S	**1**	1.23E+10	1.17E+10
	2	1.22E+10	1.15E+10
	3	1.20E+10	1.13E+10
	COV	**3.7%**	**1.7%**

According to Table 40, the coefficient of variation (COV) of $|E^*|_{LVE}$ is relatively low among the field mixture specimens in each fatigue test. Therefore, if this small variation is taken into consideration, the accuracy of the evaluation of fatigue damage resistance of the field mixtures will be significantly improved. In addition, the $|E^*|_{LVE}$ values under the high strain amplitude (L2) are a little lower than those under the low strain amplitude (L1). This shows the small amount of damage that occurred in the first fatigue test, and indicates the effect of good laboratory compaction and preparation of the specimens. However, the initial condition of the specimens in both tests is always considered in the VECD approach by the initial internal damage value (S_0) as mentioned earlier.

In addition to the $|E^*|_{LVE}$, the material damage parameter (α) value for each specimen of the tested field mixtures was calculated using the exponent of time (*m*) of relaxation modulus-time power equation attained from the $|E^*|$ test results shown earlier, in subsection 4.4.1, at the reference temperature (i.e. 20 °C) and as summarised in Table 41.

Table 41. Material damage parameter (α) for all field mixture specimens.

Mix	Specimen	*m*	α = 1/*m*
F-Mar-10E	**1**	0.197	5.076
	2	0.215	4.651
	3	0.206	4.854
	4	0.210	4.762
F-Mar-22S	**1**	0.212	4.717
	2	0.204	4.902
	3	0.212	4.717

From Table 41, it is clear that specimens of both field mixtures have similar and high α values. Using these input parameters (i.e. α and $|E^*|_{LVE}$), the VECD analysis started by calculating the pseudo-stiffness modulus (C) and the internal damage (S) of all tested specimens using equations 57 and 58. Figure 97 and Figure 98 show the plotted experimental damage characteristic (C-S) curves for the specimens of F-Mar-10E and F-Mar-22S mixtures at both strain amplitude tests (L1 and L2), respectively.

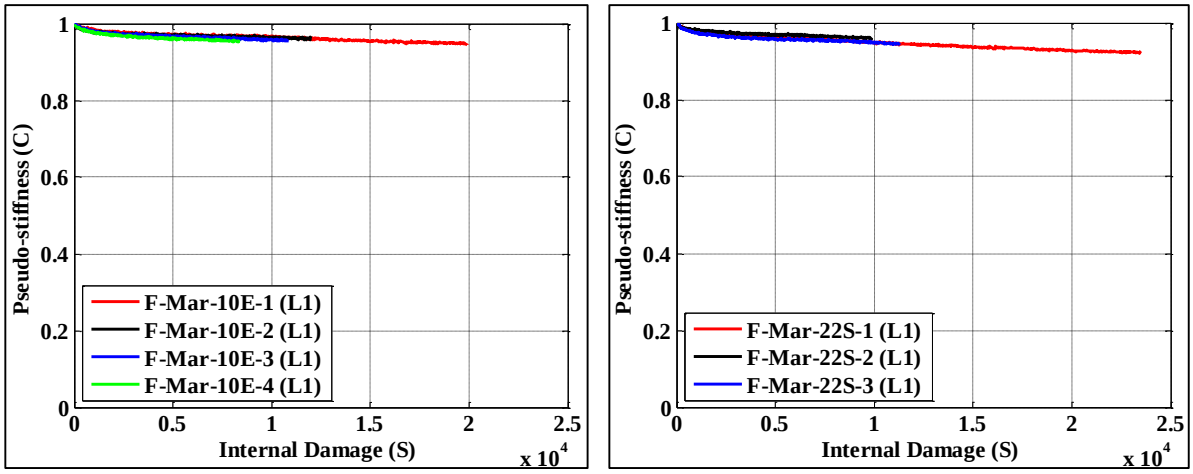

Figure 97. Damage characteristic curves for field mixture specimens under strain amplitude L1 test.

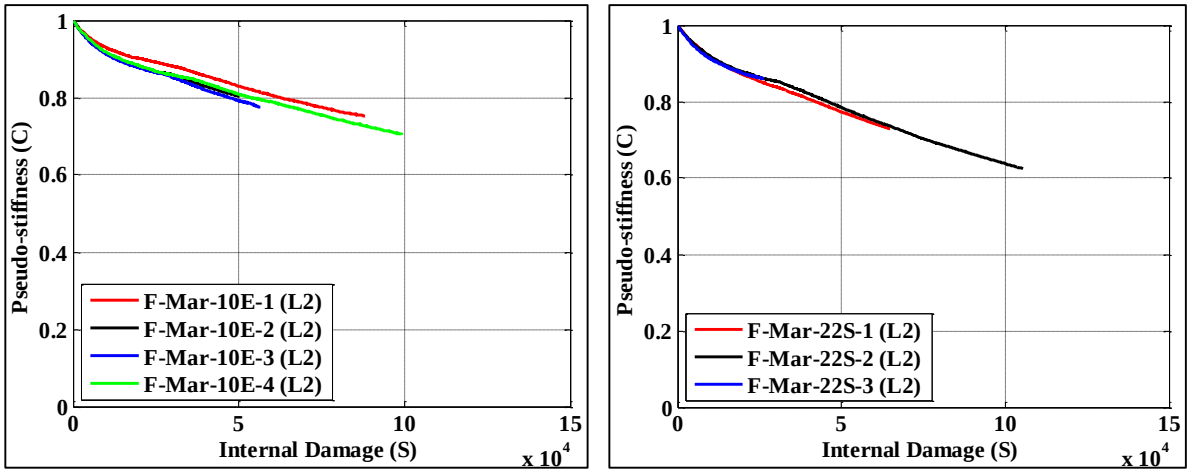

Figure 98. Damage characteristic curves for field mixture specimens under strain amplitude L2 test.

As a result of the low variability in the input parameters of the C-S curves among the field mixture specimens in addition to the small difference between the actual applied strain amplitudes on each of them (Figure 67), it was noticed that there is a clear convergence of the C-S curves at low and high strain level tests for the same field mixture.

After that, each one of the C-S curves of the tested specimens was fitted by the exponential equation 60 using a MATLAB routine. The fitting constants of the exponential model, *a* and *b*, for each specimen of the field mixtures are summarised in Table 42. The average and standard error for these fitting parameters are shown in Figure 99.

Table 42. Fitting parameters *a* and *b* for all field mixture specimens.

Mix	Specimen	ε_0-L1 = 55 με		ε_0-L2 = 130 με	
		a	***b***	***a***	***b***
F-Mar-10E	**1**	-9.03E-04	0.4070	-1.06E-04	0.6919
	2	-1.00E-03	0.3996	-5.27E-04	0.5538
	3	-1.00E-03	0.4115	-3.23E-04	0.6058
	4	-1.00E-03	0.4328	-1.91E-04	0.6497
F-Mar-22S	**1**	-8.38E-04	0.4516	-1.34E-04	0.6985
	2	-1.00E-03	0.4034	-4.93E-05	0.7888
	3	-1.00E-03	0.4358	-4.71E-04	0.5704

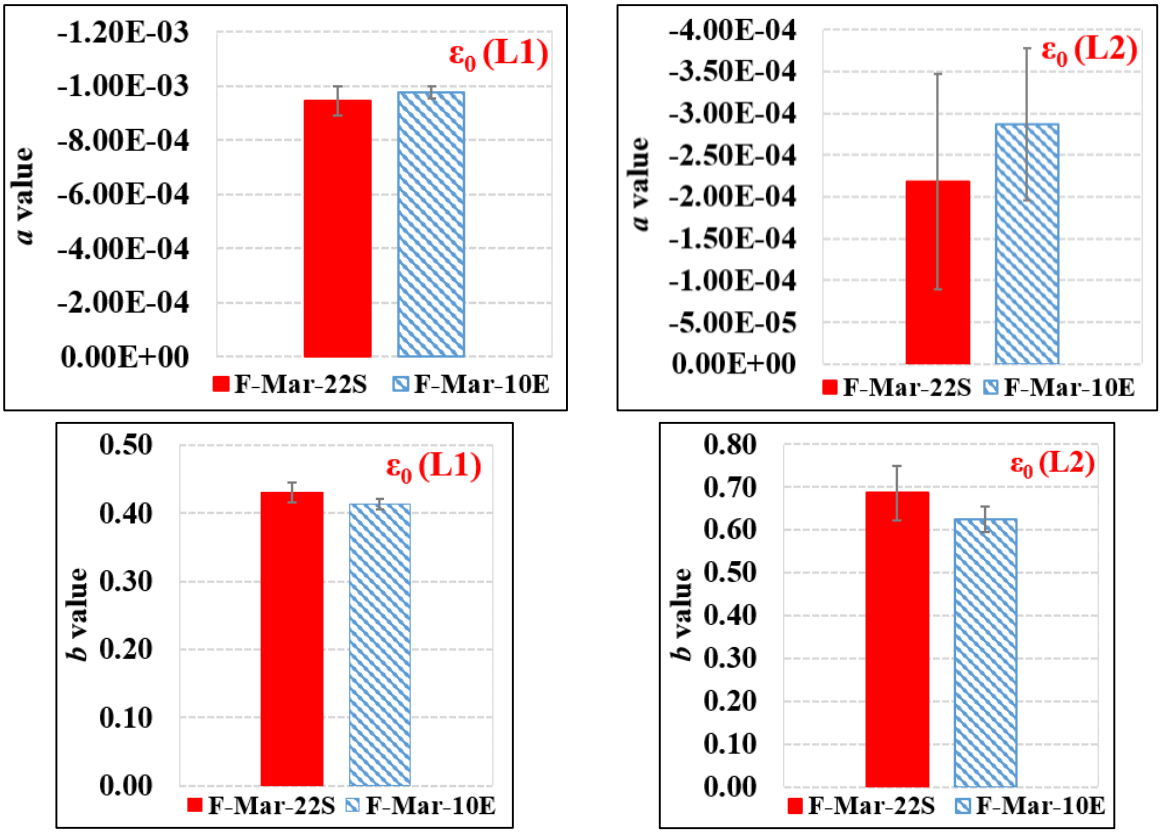

Figure 99. Average "*a*" and "*b*" values of all field mixture specimens under strain amplitude L1 and L2 tests.

According to Table 42 and Figure 99, the scatter in the values of the fitting parameters (*a* and *b*) is relatively low among the specimens of each field mixture in the strain L1 test but high for the *a* values in the strain L2 test. This variation in the fitting constants affects the predicted fatigue life (N_f) significantly, as will be shown later.

Similar to the analysis of the trial sections' base cores, the target strain amplitude of the T/C fatigue test was not achieved, as shown earlier in Figure 68. Therefore, a simulation using the true and required strain amplitude (ε_0-L1 = 55 με and ε_0-L2 = 130 με) was implemented. Equations 62, 63 and 66 were used to plot the simulated damage characteristic (C-S) curves for all field mixture specimens, as shown in Figure 100 and Figure 101.

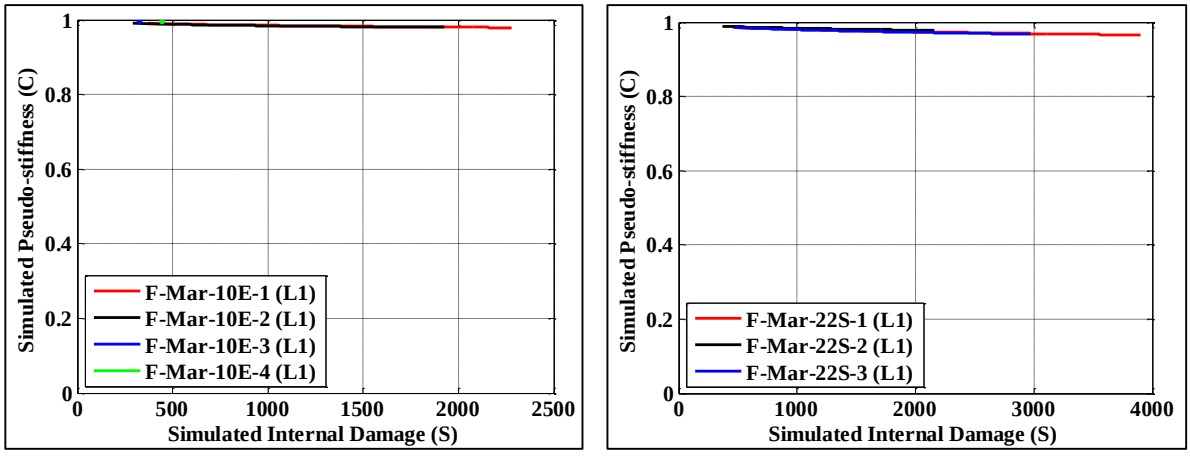

Figure 100. Simulated C-S curves for field mixture specimens under strain amplitude L1 test.

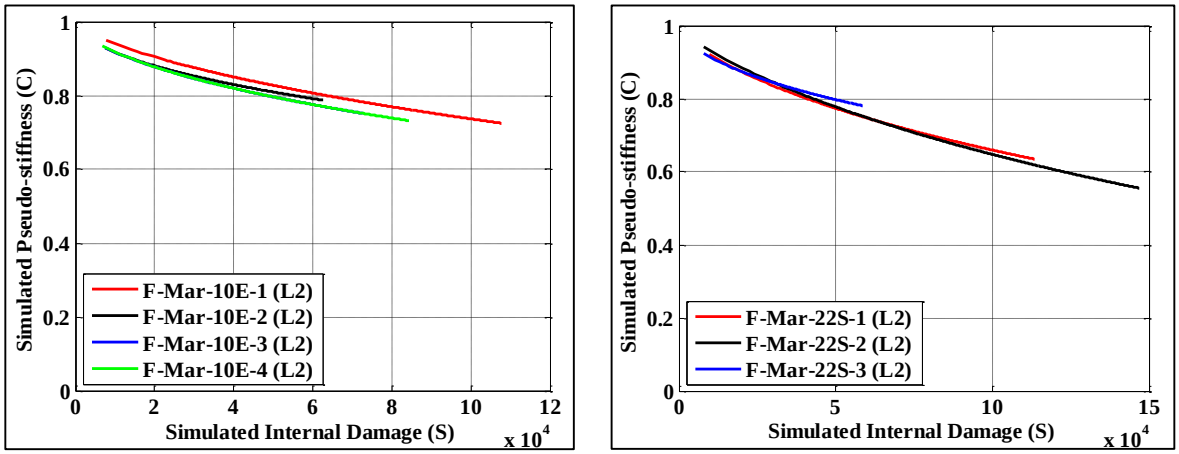

Figure 101. Simulated C-S curves for field mixture specimens under strain amplitude L2 test.

The value of initial internal damage (S_0) for each specimen was selected carefully to represent the initial status of the specimen and to minimise the initial stiffness reduction calculated in the simulated pseudo-stiffness values. As shown in Table 43, and opposite to the case of the field cores, the S_0 values were very similar for all specimens and mixtures, which confirms that this parameter depends on the initial status of the specimen when extracted from the field or prepared in the laboratory.

Table 43. Initial damage (S_0) for each field mixture specimen under strain L1 and L2 tests.

Mix	Specimen	Initial internal damage (S_0)	
		ε_0-L1 = 55 με	ε_0-L2 = 130 με
F-Mar-10E	1	371	7635
	2	293	7414
	3	319	7555
	4	441	6730
	COV	18.3%	5.6%
F-Mar-22S	1	453	9590
	2	370	7990
	3	473	7890
	COV	12.6%	11.2%

The simulated C-S curves of the field mixtures show the actual behaviour of each specimen if it was subjected to the target strain amplitude in the fatigue test and the initial condition is considered. That is why they are a little different in slope than those of the experimental C-S curves.

Resistance to fatigue damage of each specimen was estimated by comparing the number of cycles to failure (N_f) calculated using equation 67. The failure criterion was selected to be 50% reduction in the pseudo-stiffness of the specimen (C_f = 0.5). The average N_f values are presented in Figure 102 for both fatigue tests.

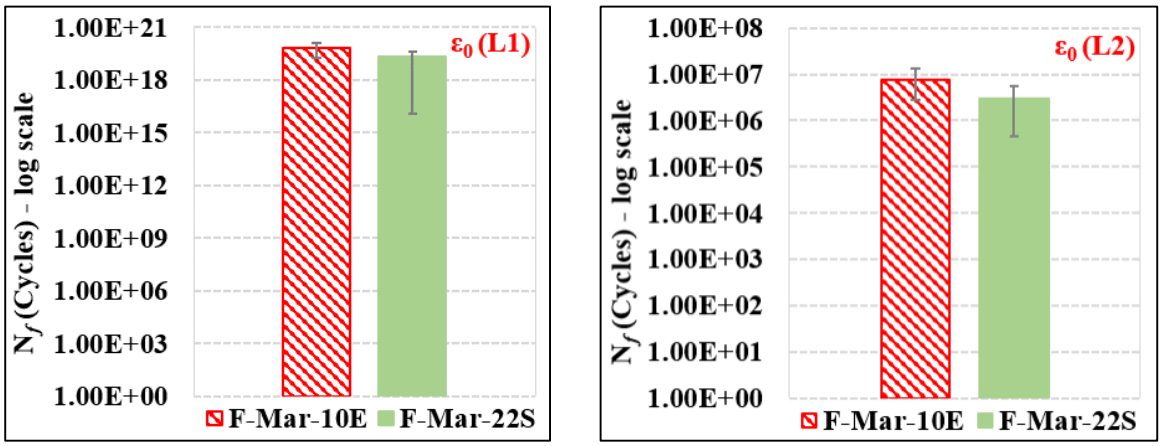

Figure 102. Comparison of average N_f results at C_f = 0.5 for all field mixtures under strain amplitude L1 and L2 tests.

According to the average N_f values of the fatigue test under strain amplitude L1 (55 με), field mixtures with the "Extreme" modified bitumen (PG76-10E) performed better and the

number of cycles to fatigue failure was a little higher than that for mixtures with the "Standard" modified bitumen.

5.2.3 Laboratory mixtures' results

5.2.3.1 Total dissipated energy (W_R) method

The sum of dissipated energies (W_R = W_{R1} + W_{R3}) was computed for the specimens prepared from three different laboratory mixtures using the T/C fatigue tests' data. The dynamic modulus ($|E^*|_{LVE}$) and the phase angle (φ_{LVE}) values used to calculate W_R are those at the first loading cycle interval (i.e. N = 10). Figure 103 to Figure 105 plot the curves of the W_R against the number of cycles (N) for all specimens of each tested laboratory mixture under strain amplitude L1 test.

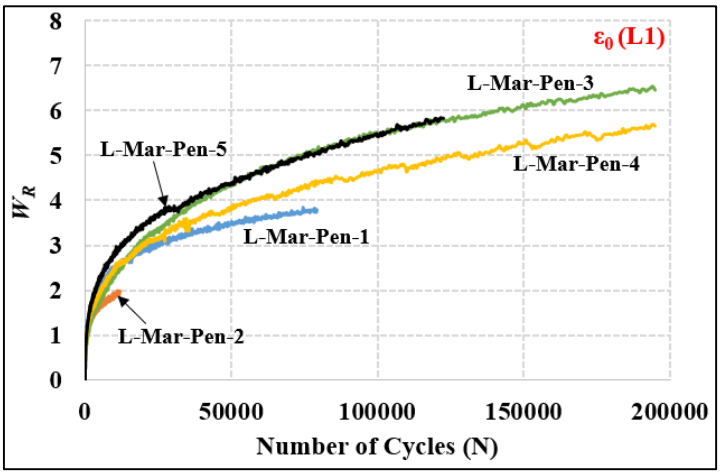

Figure 103. W_R curves for L-Mar-Pen mixture specimens under strain amplitude L1 test.

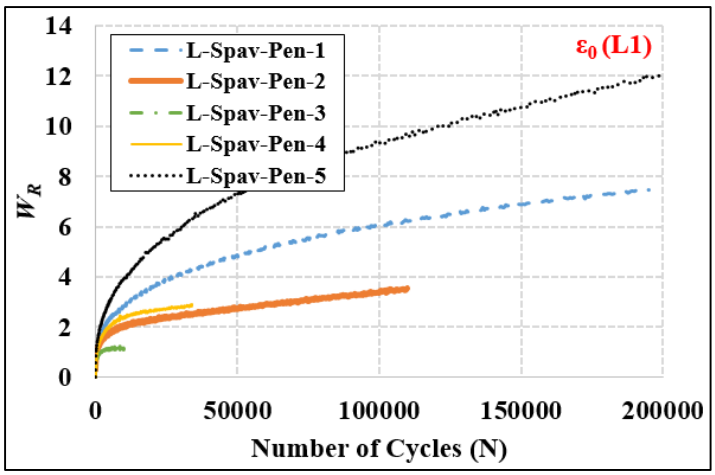

Figure 104. W_R curves for L-Spav-Pen mixture specimens under strain amplitude L1 test.

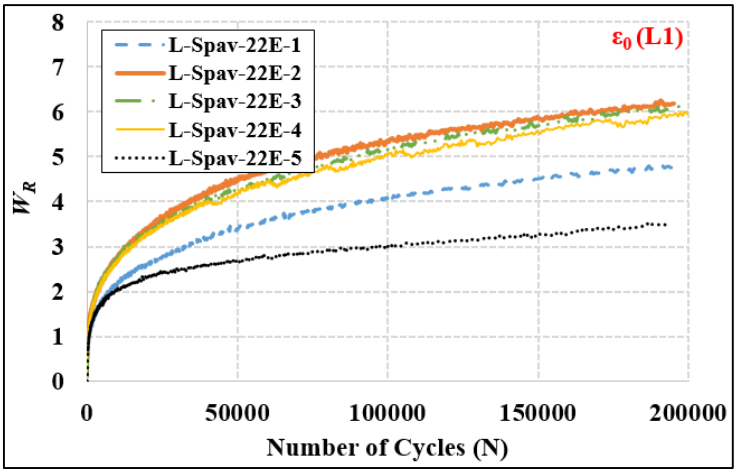

Figure 105. W_R curves for L-Spav-22E mixture specimens under strain amplitude L1 test.

As shown clearly in the figures, there is scatter in the curves of the specimens of each mixture, and not all of them completed the fatigue test. In general, the failure criterion (N_f) cannot be easily stated using the W_R plots in order to evaluate the laboratory mixtures against fatigue cracking under strain L1 test.

Figure 106 to Figure 108 show the W_R curves against the number of cycles (N) for all specimens of the laboratory mixtures under strain L2 test.

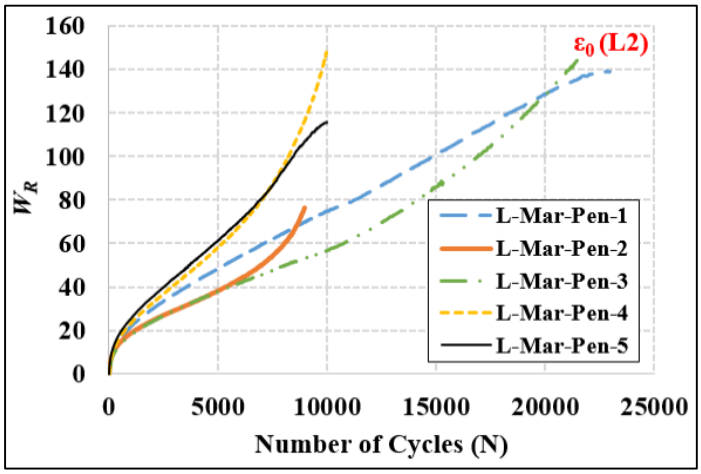

Figure 106. W_R curves for L-Mar-Pen mixture specimens under strain amplitude L2 test.

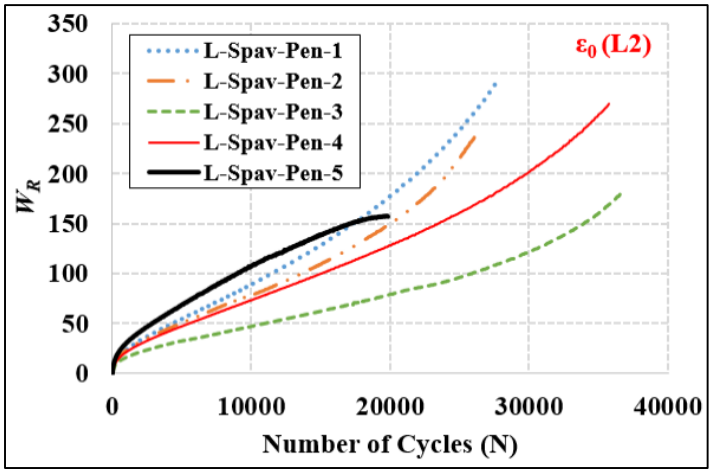

Figure 107. W_R curves for L-Spav-Pen mixture specimens under strain amplitude L2 test.

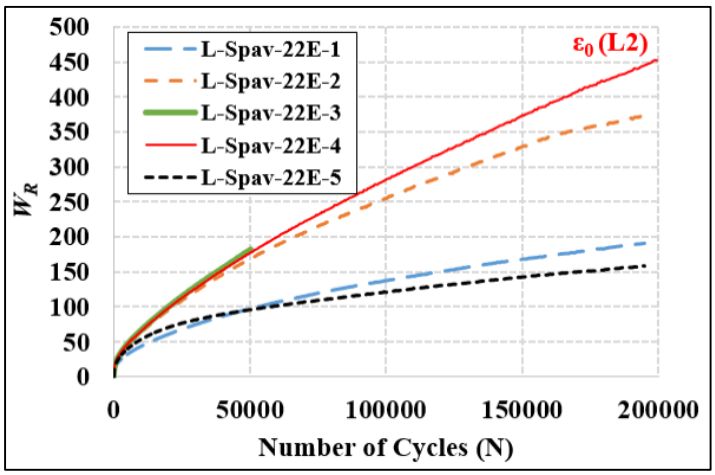

Figure 108. W_R curves for L-Spav-22E mixture specimens under strain amplitude L2 test.

Similarly, the W_R curves of the laboratory mixtures shown in the figures are also deceptive, and not all of them completed the fatigue test. The rate of dissipating energy (slope of W_R curves) is different from specimen to specimen, which makes the performance prediction against fatigue damage more difficult.

In addition, no replicate specimen of L-Mar-Pen and L-Spav-Pen but most of L-Spav-22E mixtures had completed the fatigue strain L2 test. This indirectly indicates the advantage of using a polymer-modified bitumen (PMB) in resisting fatigue damage. Again, laboratory mixtures cannot be assessed and compared against fatigue cracking, only by the W_R curves under strain L2 test. Therefore, and to overcome this limitation, it was vital to implement the

VECD fatigue characterisation approach to assess the laboratory mixtures against fatigue cracking accurately.

5.2.3.2 Viscoelastic continuum damage (VECD) approach

The VECD characterisation approach was applied using the fatigue tests' raw data to obtain the fatigue life (N_f) of the laboratory mixtures tested in this study. The linear viscoelastic dynamic modulus ($|E^*|_{LVE}$) value for each laboratory mixture specimen obtained from the first cycle interval (N = 10) in both uniaxial fatigue tests is presented in Table 44.

Table 44. The $|E^*|_{LVE}$ of all laboratory mixture specimens.

Mix	Specimen	$\|E^*\|_{LVE}$ (Pa)	
		ε_0-L1 = 55 με	**ε_0-L2 = 130 με**
L-Mar-Pen	**1**	6.91E+09	6.88E+09
	2	6.60E+09	6.05E+09
	3	6.65E+09	5.74E+09
	4	6.93E+09	6.50E+09
	5	7.70E+09	7.26E+09
	COV	**6.3%**	**9.4%**
L-Spav-Pen	**1**	7.56E+09	7.14E+09
	2	6.46E+09	6.32E+09
	3	4.78E+09	4.74E+09
	4	6.93E+09	6.59E+09
	5	5.05E+09	4.86E+09
	COV	**20.5%**	**16.5%**
L-Spav-22E	**1**	6.39E+09	5.76E+09
	2	6.87E+09	6.45E+09
	3	7.12E+09	6.58E+09
	4	7.22E+09	6.74E+09
	5	5.83E+09	5.35E+09
	COV	**8.6%**	**9.7%**

According to Table 44, the coefficient of variation (COV) of $|E^*|_{LVE}$ is relatively low among the laboratory mixture specimens in both fatigue tests except L-Spav-Pen mixture, which has higher variation. In general, if this variation is taken into consideration, the accuracy of the evaluation of fatigue damage resistance of the laboratory mixtures will be enhanced. In addition, the $|E^*|_{LVE}$ values under strain L2 test are somewhat lower than those of L1 test, and this shows the amount of damage that occurred in the first fatigue test, although the condition

of the specimens before testing is always considered in the VECD approach by the initial internal damage value (S_0).

Additionally, the average value of the material damage parameter (α) for all specimens of each laboratory mixture was determined using the exponent of time (*m*) determined from the $|E^*|$ results at the reference temperature (i.e. 20 °C) and as summarised in Table 45.

Table 45. Material damage parameter (α) for all laboratory mixture specimens.

Mix	Specimen	*m*	α = 1/*m*
L-Mar-Pen	**1**	0.332	3.012
	2	0.322	3.103
	3	0.335	2.989
	4	0.322	3.107
	5	0.318	3.145
L-Spav-Pen	**1**	0.343	2.915
	2	0.338	2.959
	3	0.333	3.008
	4	0.350	2.855
	5	0.329	3.040
L-Spav-22E	**1**	0.274	3.648
	2	0.268	3.733
	3	0.261	3.827
	4	0.269	3.712
	5	0.277	3.614

From Table 45, it is noticed that the laboratory mixture specimens have very similar α values but they are relatively lower than those of field mixtures or field cores, which is expected as the laboratory mixtures have higher bitumen content.

The VECD analysis started by calculating the pseudo-stiffness modulus (C) and the internal damage (S) of all tested specimens of the laboratory mixtures using equations 57 and 58 discussed in subsection 5.1.2. Figure 109 and Figure 110 show the plotted damage characteristic (C-S) curves for the specimens of L-Mar-Pen, L-Spav-Pen and L-Spav-22E mixtures under both strain amplitude tests, L1 and L2.

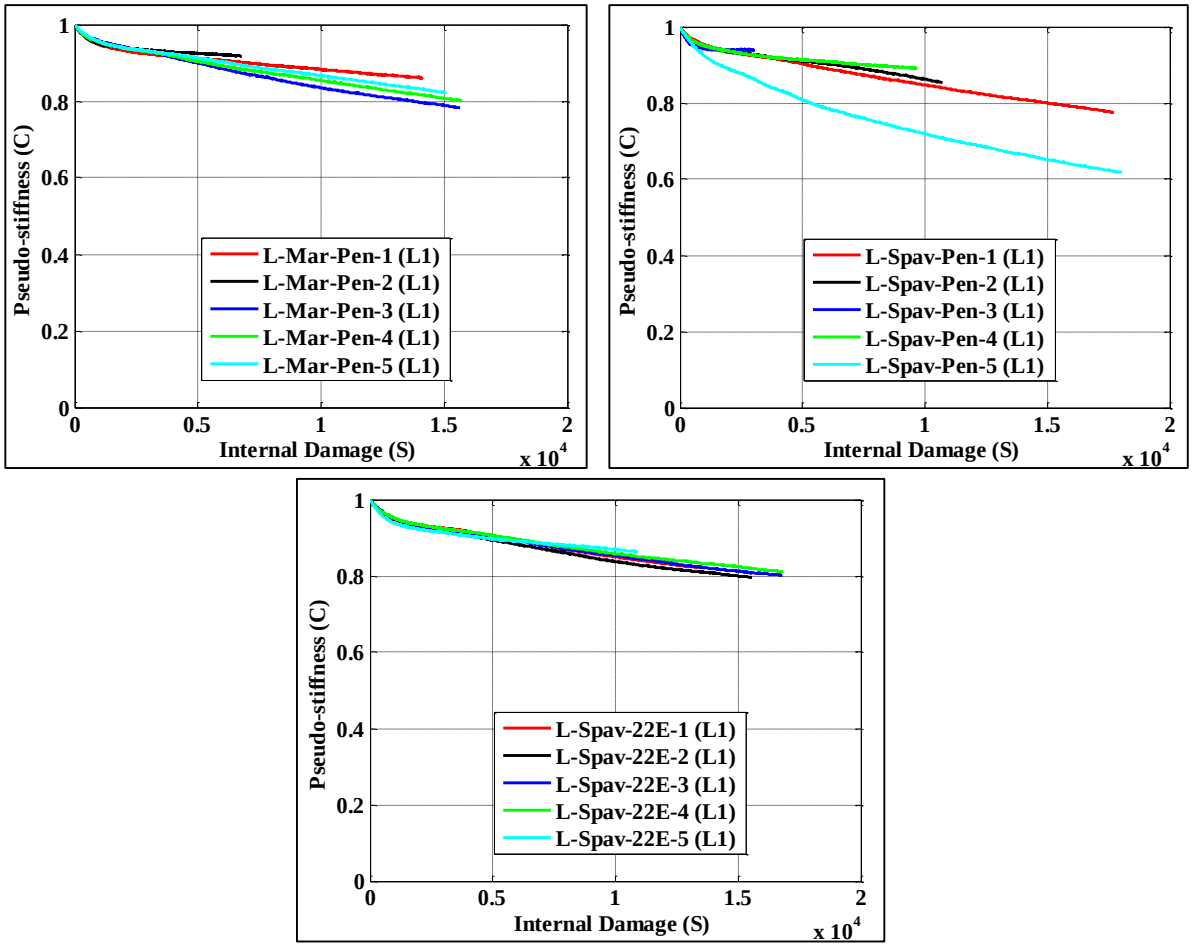

Figure 109. Damage characteristic curves for laboratory mixture specimens under strain amplitude L1 test.

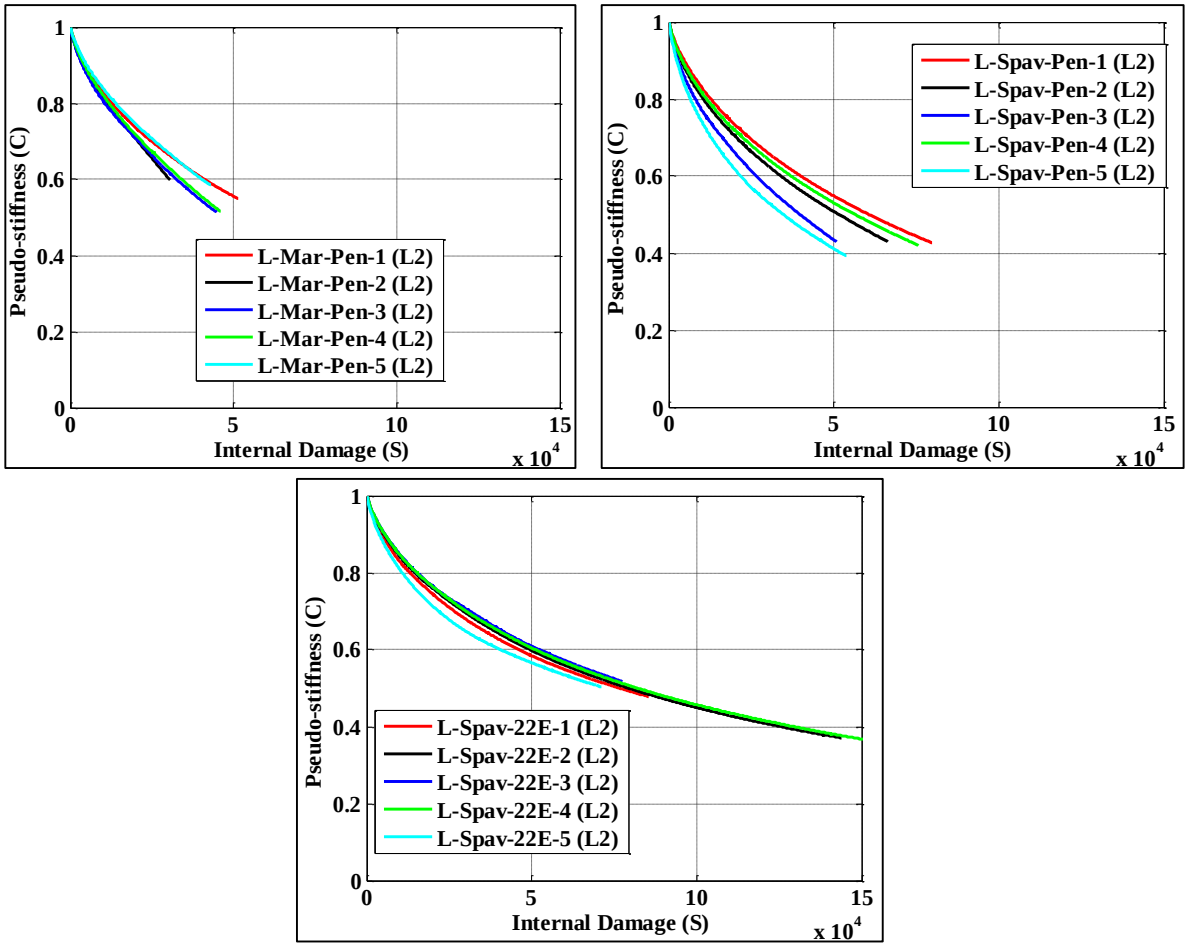

Figure 110. Damage characteristic curves for laboratory mixture specimens under strain amplitude L2 test.

From both sets of figures, the similarity between the C-S curves of the L-Spav-22E specimens is obvious, while the other laboratory mixtures have some scatter.

Each C-S curve of the tested laboratory specimens is then fitted by the exponential equation 60 shown in subsection 5.1.2 using a MATLAB routine. The fitting constants of the exponential model, *a* and *b*, for each specimen are summarised in Table 46. The values of fitting parameter "*b*" are relatively close to each other but values of "*a*" are not similar within the same mixture, and this will surely affect the accuracy of fatigue life prediction.

Table 46. Fitting parameters *a* and *b* for all field mixture specimens.

Mix	Specimen	ε_0-L1 = 55 με		ε_0-L2 = 130 με	
		a	***b***	***a***	***b***
L-Mar-Pen	**1**	-1.00E-03	0.5287	-2.65E-04	0.7117
	2	-1.00E-03	0.5180	-1.51E-04	0.7824
	3	-2.95E-04	0.6952	-2.24E-04	0.7429
	4	-5.08E-04	0.6243	-1.34E-04	0.7894
	5	-6.86E-04	0.5811	-1.42E-04	0.7705
L-Spav-Pen	**1**	-4.70E-04	0.6387	-2.22E-04	0.7305
	2	-1.00E-03	0.5386	-2.94E-04	0.7152
	3	-1.00E-03	0.5505	-3.61E-04	0.7125
	4	-1.00E-03	0.5278	-2.73E-04	0.7161
	5	-8.69E-04	0.6448	-6.04E-04	0.6741
L-Spav-22E	**1**	-7.73E-04	0.5790	-4.62E-04	0.6514
	2	-8.12E-04	0.5832	-3.87E-04	0.6632
	3	-8.52E-04	0.5687	-3.25E-04	0.6769
	4	-9.20E-04	0.5548	-3.79E-04	0.6630
	5	-1.00E-03	0.5473	-8.29E-04	0.6044

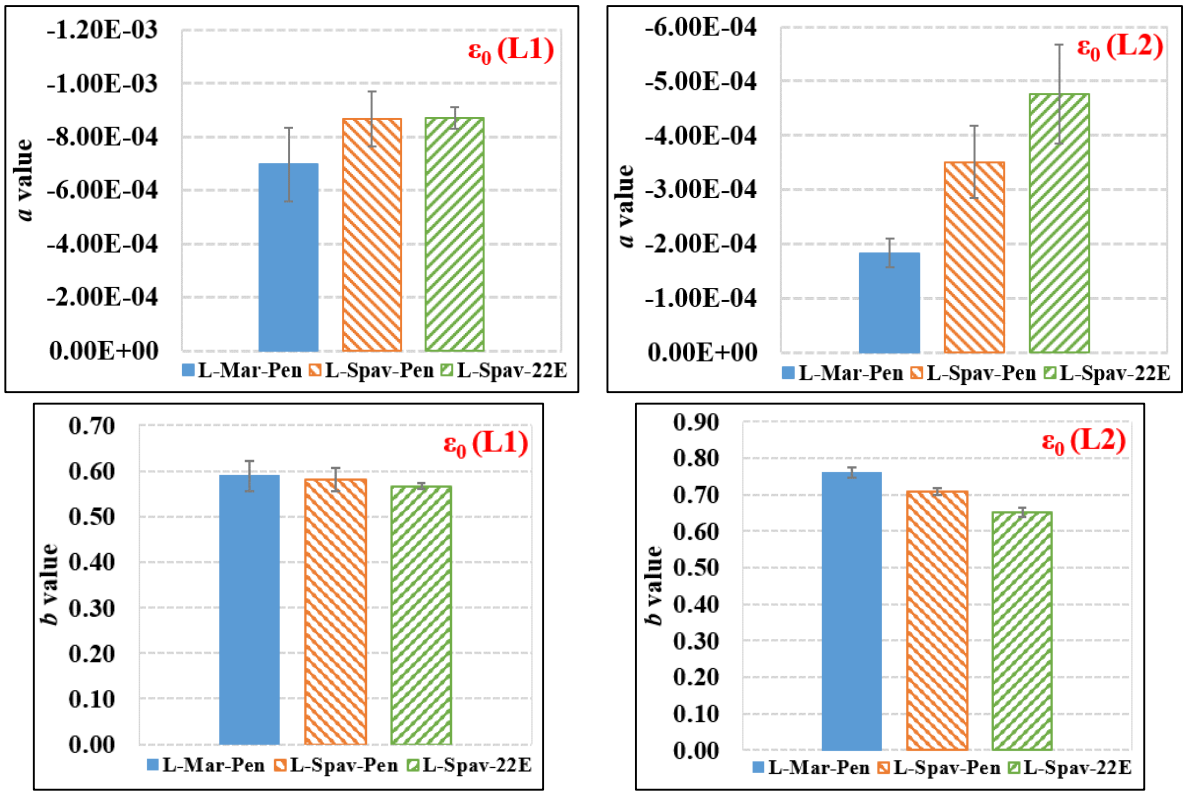

Figure 111. Average "*a*" and "*b*" values of all the laboratory mixture specimens under strain amplitude L1 and L2 tests.

Similar to the VECD analysis of the previous mixtures, the uniaxial T/C fatigue test was not performed under the target strain level. Therefore, a simulation using the true strain

amplitude (ε_0-L1 = 55 με and ε_0-L2 = 130 με) was executed. Equations 62, 63 and 66 mentioned in subsection 5.1.2 were used to plot the simulated damage characteristic (C-S) curves for all laboratory specimens, as shown in Figure 112 and Figure 113.

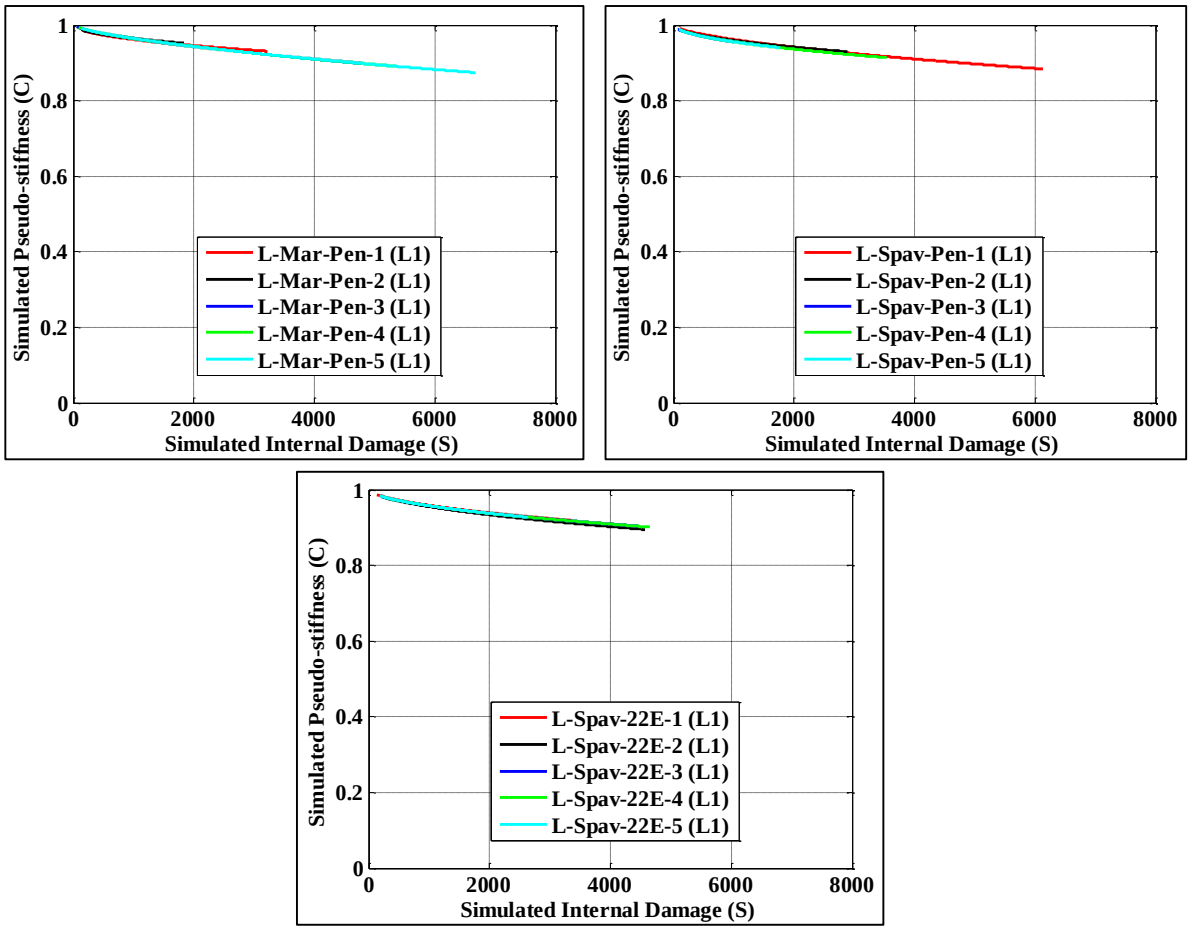

Figure 112. Simulated C-S curves for laboratory mixture specimens under strain amplitude L1 test.

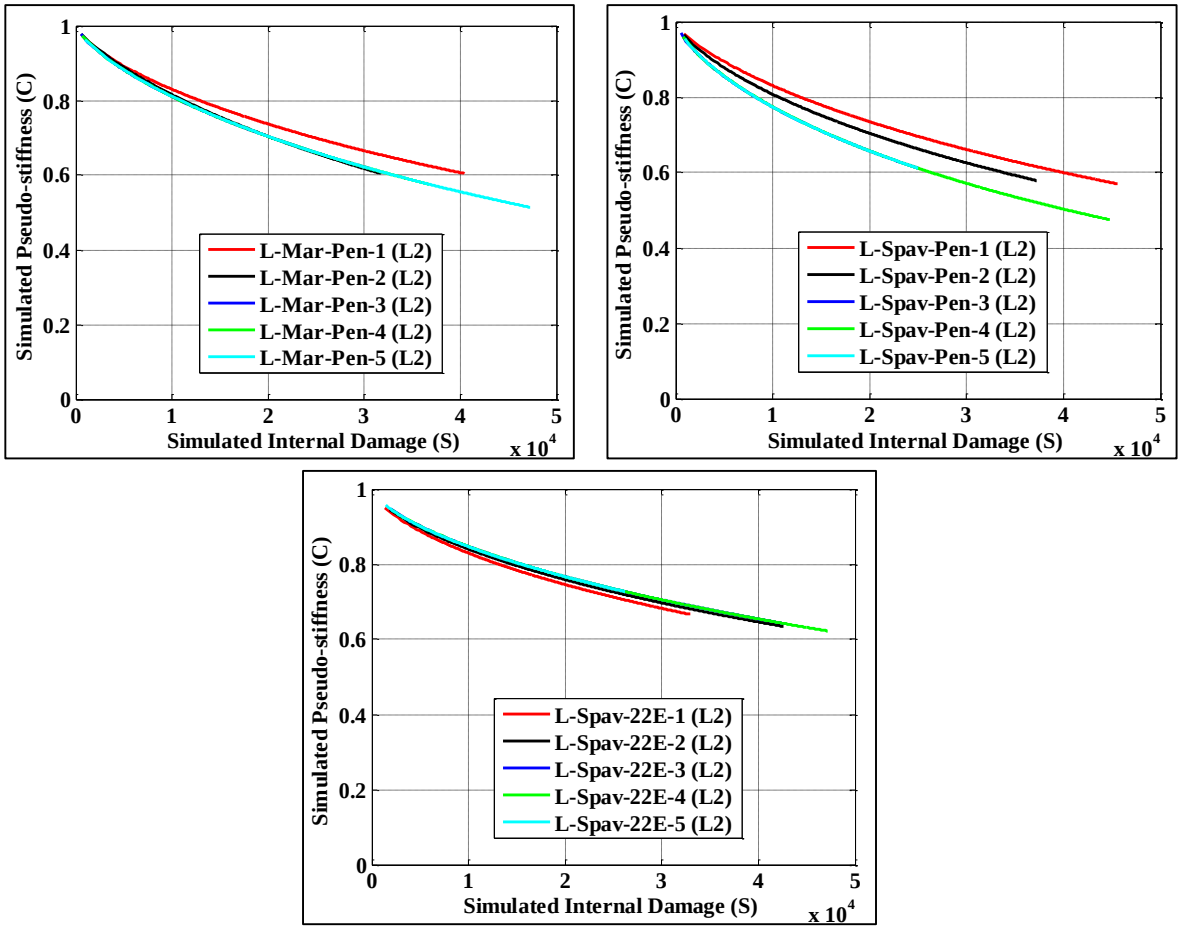

Figure 113. Simulated C-S curves for laboratory mixture specimens under strain amplitude L2 test.

The initial internal damage (S_0) value for each laboratory specimen was selected carefully to represent the initial condition of the specimen before testing and to minimise the initial stiffness reduction calculated in the simulated pseudo-stiffness values. Compared to the case of the field cores and field mixtures, the S_0 values were quite similar to each other and much lower, as shown in Table 47, which confirms again that this parameter depends completely on the initial status of the specimen when extracted from the field or prepared in the laboratory.

Table 47. Initial damage (S_0) for each laboratory mixture specimen under strain L1 and L2 tests.

Mix	Specimen	Initial internal damage (S_0)	
		ε_0-L1 = 55 με	ε_0-L2 = 130 με
L-Mar-Pen	1	155	1448.5
	2	137	575
	3	55.5	520
	4	93	675
	5	139	980
	COV	37.6%	29.9%
L-Spav-Pen	1	99	841
	2	116	799
	3	63	473
	4	141	595
	5	81	908
	COV	34.9%	28.3%
L-Spav-22E	1	134	1344
	2	197	1860
	3	215	1930
	4	205	2030
	5	177	1405
	COV	8.1%	15.3%

The simulated C-S curves and results are then used to calculate the fatigue life (N_f) of each the laboratory mixture specimen using equation 67 shown in subsection 5.1.2. The failure fatigue criterion was selected to be 50% reduction in the pseudo-stiffness of the specimen (i.e. C_f = 0.5). The average N_f values are presented in Figure 114 for both fatigue tests.

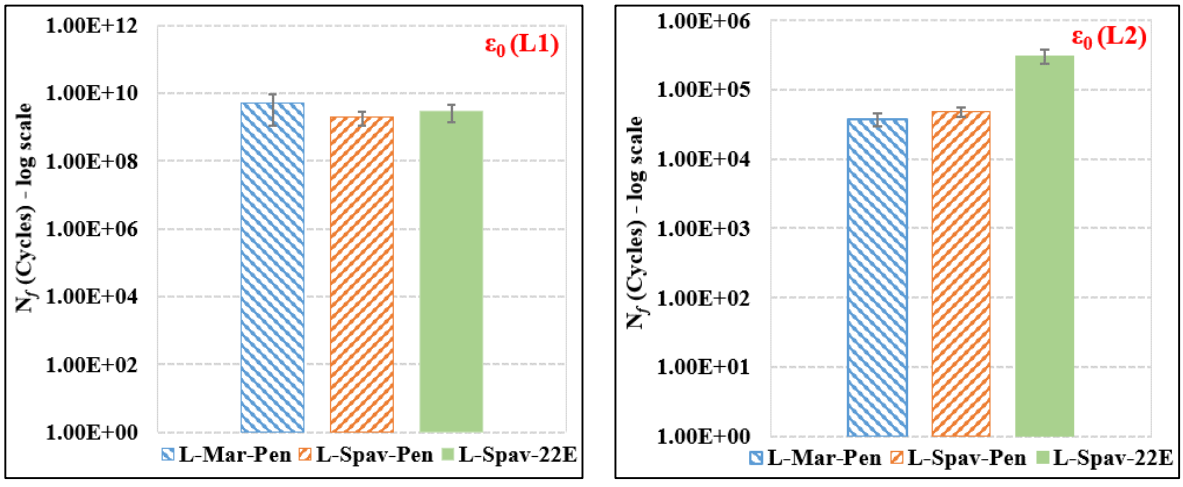

Figure 114. Comparison of average N_f results at C_f = 0.5 for all laboratory mixtures under strain amplitude L1 and L2 tests.

According to the results in Figure 114, the three laboratory mixtures performed almost the same against fatigue damage (very close average N_f values) under strain amplitude L1 (55 με) test. However, the Superpave laboratory mixture with PG76-22E had a higher number of cycles to failure than the other two tested mixtures under strain amplitude L2 (130 με) test.

The variability and uncertainty in fatigue life of the laboratory mixtures are relatively low under strain amplitude L1 and L2 fatigue tests. However, the conclusions of N_f results for L1 differ from those of L2, which shows again that the prediction of N_f is sensitive to the accuracy of its parameters. Therefore, it can be stated that the average N_f results shown in both figures are not enough to decide on which mixture is the best to resist fatigue damage.

5.3 Conclusions

In this chapter, the raw data of the uniaxial T/C fatigue test conducted on specimens prepared from field cores from the base course of the six trial sections, two altered field mixtures and three different laboratory mixtures were all characterised and analysed using the W_R method and VECD approach. The main objective was to implement the advanced methodologies to analyse the fatigue test data, assess the different asphalt mixtures and specify their fatigue lives (N_f) in order to compare them.

The analysis results of the uniaxial T/C fatigue tests for field cores, field and laboratory mixtures generally indicated that using the VECD approach has major advantages over using the W_R method. In the W_R method, it is hard to select a failure criterion (N_f) to evaluate the performance of the tested specimens against fatigue cracking. The total W_R curves had different slopes (rate of energy change with cycles), indicating a high discrepancy in the results, and were not sufficient to assess the performance of all mixtures used in this study. In addition, this dissipated energy (W_R) method does not consider the condition of the mixture (i.e. level of damage) before testing. On the other hand, the VECD approach can unify different temperatures, frequencies and loading modes or levels for analysis of fatigue characteristics of

asphalt mixtures. Furthermore, it accounts for the initial status/condition of the tested specimens before testing.

However, the predicted fatigue life (N_f) for the tested asphalt concrete mixtures – field and laboratory – was highly affected by the uncertainty associated with the fatigue tests as well as the models and their parameters, in addition to the high variability between specimens. Consequently, a more in-depth analysis that accounts for the uncertainty and high variability in predicting the fatigue life (N_f) is needed. In the following chapter, the characterisation of fatigue damage resistance and life prediction are enhanced significantly by incorporating a probabilistic analysis approach.

6 Probabilistic Analysis of Fatigue Life for Asphalt Concrete Mixtures Using the VECD Approach

In the previous chapter, the raw data of the uniaxial T/C fatigue test conducted on different asphalt concrete mixtures were analysed using the total dissipated energy (W_R) method and the VECD approach. However, the results of the W_R analysis showed that the fatigue life criterion (N_f) cannot even be specified due to the high scatter in the results and the difference in the slope of the W_R curves among the replicates of each mixture. In addition, the W_R does not consider the initial status of the specimen before testing. Therefore, and to overcome all previous limitations, the use of the viscoelastic continuum damage (VECD) approach was preferred. In addition, the VECD approach has the ability to unify different temperatures, frequencies and loading modes or levels for analysis of fatigue characteristics of asphalt concrete mixtures. So, only one uniaxial T/C fatigue test is needed for an asphalt concrete mixture (several replicate specimens) to predict its performance against fatigue under any temperature, frequency, loading mode or level.

However, the preferred VECD approach showed a single problem: that the results had relatively high variation, especially for field mixtures, which makes it difficult to predict the fatigue life (N_f) of the tested mixtures accurately. The conclusions of N_f results for L1 fatigue test in some cases differ from those of the L2 test, which indicates that the prediction of N_f is sensitive to the parameters of its model (equation 67). Therefore, it was clear that the average N_f results are not enough or sufficient to decide on which mixture is the best to resist fatigue damage.

In order to overcome this issue, it was decided to develop a probabilistic analysis approach that accounts for the uncertainty associated with fatigue tests, models and their parameters, in addition to the variability of the inputs in the fatigue analysis among specimens of a certain AC mixture. Given the increasing cost of designing and constructing new asphalt

pavements, the probabilistic approach will be helpful for engineers to design pavements with asphalt concrete mixtures that resist fatigue cracking based on an acceptable reliability level or its equivalent probability of failure (p_f).

The VECD approach was selected to be used in this newly developed probabilistic analysis approach because of the aforementioned advantages. The VECD fatigue life model (VECD-N_f) shown in equation 67 and implemented in the previous chapter was deterministic and considered all input parameters as fixed inputs and did not account for their variability.

In this chapter, the development of the probabilistic analysis approach using the VECD-N_f model is introduced and discussed in detail. The objective of this developed probabilistic approach is to predict the performance of mixtures against fatigue damage to a highly reliable level (e.g. 75%). In addition, sensitivity analysis is conducted in order to specify the most significant input parameter affecting the prediction of fatigue life (N_f) for asphalt concrete mixtures.

6.1 Proposed probabilistic analysis framework

In this section, the framework of the proposed probabilistic analysis approach using VECD-N_f equation is presented and discussed.

6.1.1 Parameters and assumptions of the fatigue life model

The first step in the proposed probabilistic analysis approach is to define the fatigue life (N_f) model that will be used in addition to its input parameters. In this study, the VECD-N_f model is implemented, and its input parameters are considered for the developed probabilistic analysis approach. Based on the viscoelastic continuum damage (VECD) approach described earlier, in Chapter 5, the prediction of fatigue life (N_f) of asphalt mixture can be calculated using the following equations:

For a controlled-strain test:

$$N_f = \int_{S_0}^{S_f} \left[-\frac{\varepsilon_0^2 |E^*|_{LVE}^2}{2} \, a \, b \, S_N^{b-1} \, e^{a S_N^b} \right]^{-\alpha} f \, dS \qquad \textbf{Equation 70}$$

For a controlled-stress test:

$$N_f = \int_{S_0}^{S_f} \left[-\frac{\sigma_0^2}{2|E^*|_{LVE}^2} \, a \, b \, S_N^{b-1} \, e^{a S_N^b} \right]^{-\alpha} f \, dS \qquad \textbf{Equation 71}$$

The definition of each parameter in these equations can be found in detail in subsection 5.1.2. Some parameters of these VECD-N_f equations are constants, and the others can be considered as random variables (RVs). By using random inputs, the deterministic N_f model is essentially turned into a stochastic model. In the VECD-N_f model, the strain (ε_0) in the controlled-strain test, and the stress (σ_0) amplitudes in the controlled-stress test in addition to the frequency (*f*) values are constants and fixed during the uniaxial T/C fatigue test. However, the linear viscoelastic dynamic modulus ($|E^*|_{LVE}$), fitting parameters (*a* and *b*) and the material damage parameter (α) are all variables in the VECD-N_f model from specimen to specimen of the same mixture.

Regarding the integration limits of the VECD-N_f equation, the initial internal damage (S_0) is also fixed for any mixture, assuming that there will be no (or negligible) damage in the specimen before testing. However, the internal damage at failure (S_f) is a random quantity defined in terms of variables (*a* and *b*) and the constant preselected fatigue failure criterion (e.g. $C_f = 0.5$), as shown earlier in equation 69.

Then, an appropriate distribution function for each random variable (RV) needs to be identified accurately as a second step of this probabilistic approach. The distribution of an input of the VECD-N_f model ($|E^*|_{LVE}$, *a*, *b* or α) can be determined using a large number of experimental observations for that input and by fitting them to one of the probabilistic distribution types. The larger the number of observations, the more accurate the distribution is. In addition, the interdependency of variables should be taken into account and its distribution

should be specified. The selection of the distribution function is very important and significant in order to perform an accurate probabilistic analysis.

In the next step, a suitable probabilistic analysis method should be selected and implemented using the random variables generated according to their distributions. In this study, it was decided to employ the VECD-N_f model in a probabilistic analysis approach by performing the Monte Carlo Simulation (MCS) method after treating the four input parameters ($|E^*|_{LVE}$, a, b and α) as random variables (RVs).

6.1.2 Probabilistic analysis methodology

Monte Carlo Simulation (MCS) is a problem-solving technique which has been used for a long time to estimate the probability of certain outputs by running a large number of simulations using the entire distributions of the random variables (Maji & Das, 2008). This probabilistic simulation approach (i.e. MCS) is applied to a wide variety of complex problems involving random behaviour.

MCS is the most accurate approximation technique for probabilistic analysis; however, the trade-off is that extensive computational time is required (Luo (2014) and Retherford & McDonald (2010)). It was found that the MCS method could handle several failure modes in pavement materials and structures (e.g. fatigue cracking and rutting) and any limit-state functions. In addition, it was stated in the literature that MCS is suitable and useful for quantifying the variability of the input parameters and in flexible pavement design and analysis (Dilip & Sivakumar Babu, 2013). For all these reasons, the MCS method was selected to be used in this proposed probabilistic analysis approach.

After defining the stochastic model (e.g. VECD-N_f) and specifying the probabilistic distributions for its random variables (e.g. normal, uniform, etc.), a large number of random samples (e.g. 1 million) are generated for each random variable. Then, the output of this stochastic model (e.g. 1 million N_f) is evaluated for each generated set of random samples.

After that, the probability density function (pdf) or the cumulative distribution function (cdf) of the evaluated outputs can be constructed. The pdf is a function that describes the relative probability for a continuous random variable or an output to take on a given or evaluated value, respectively. The cdf is a function that describes the area under a probability density function (pdf) from minus infinity to a specific value of the outputs. Figure 115 illustrates an example of the pdf and the cdf for a normal distribution function.

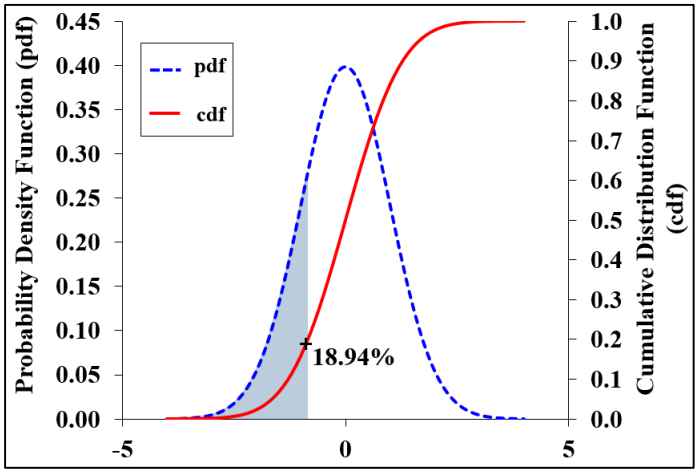

Figure 115. An illustrative example of a pdf and its cdf for a normal distribution function.

Then, by selecting an acceptable reliability level (e.g. 75%) or its equivalent probability of failure (p_f) (e.g. 25%), the output of the model (e.g. N_f) at that reliability level can be determined from the cdf.

It is worth mentioning that MCS is not a new method to use; however, using it with an advanced fatigue characterisation approach (i.e. VECD) and performing it in order to predict the fatigue life (N_f) of an asphalt concrete mixture is a novel contribution.

6.1.3 Sensitivity analysis

The uncertainty associated with the fatigue life (N_f) model is indeed a consequence of the uncertainty of its parameters. The greater the variance of the inputs of the predicted fatigue life is, the less accurate the output of the mathematical model is. Fundamentally, it is important to differentiate between sensitivity analysis and uncertainty analysis. Sensitivity analysis

measures the effect of the variability of the input parameters on the variability of the model output. However, uncertainty analysis quantifies the uncertainty of the model output in terms of its statistical parameters (i.e. mean and standard deviation) and confidence intervals (Cannavó (2012), Saltelli, et al., (2010) and Patelli, et al., (2010)). Figure 116 illustrates the relationship between the uncertainty of the input parameter and the uncertainty of the output due to model sensitivity.

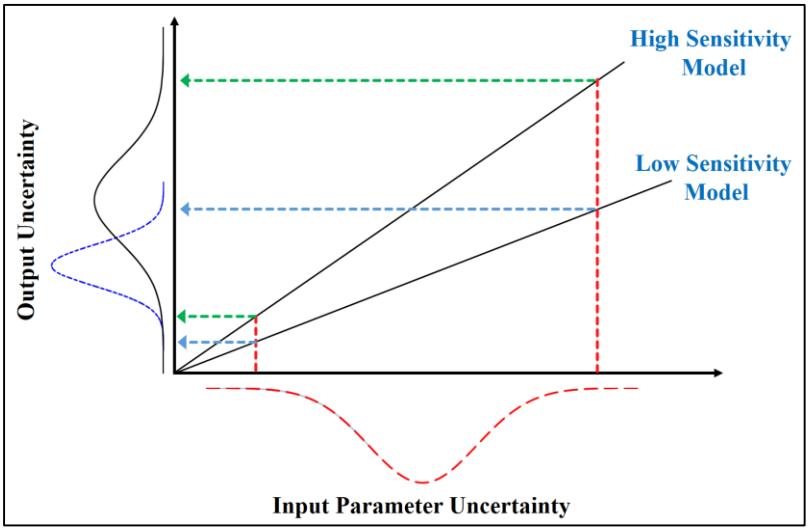

Figure 116. Relationship between input and output uncertainties due to model sensitivity.

Figure 116 shows that the high sensitivity of a model with the uncertainty of its input parameters causes high uncertainty in the output of this model.

According to the literature, Patelli, et al. (2010) concluded that sensitivity analysis is called global sensitivity analysis (GSA) when it deals with the whole range of variation of the input parameters of the model. GSA distributes the entire output uncertainty to the different sources of uncertainty in the inputs and helps in simplifying complex models (Saltelli & Bolado (1998) and Saltelli, et al., (2010)). However, Chen (2005) mentioned that the intensive computational demand for assessing the impact of probabilistic variations is one of the main challenges in GSA.

In order to identify the significance of each input parameter of the VECD-N_f model ($|E^*|_{LVE}$, a, b and α), the global sensitivity analysis (GSA) is implemented using two approaches

developed based on analysis of variance (ANOVA) decomposition. These variance-based approaches are specifically Fourier Amplitude Sensitivity Test (FAST) approach and Sobol' sensitivity approach. The following subsections briefly describe both approaches.

6.1.3.1 FAST approach

The Fourier Amplitude Sensitivity Test (FAST) approach is a variance-based GSA method that has successfully been applied since the 1970s to several modelling problems (Cannavó (2012) and Saltelli & Bolado (1998)). In the FAST approach, the Fourier series expansion is used to approximately represent the output model (e.g. VECD-N_f). As the true value of the input parameter (x_i) is unknown, only the variance of the conditional expectation ($E[Y|x_i]$) for all possible values of this input can be computed. The main concept of the FAST approach is to convert the multi-dimensional integral (I^n) of the expected value of the model's output ($E[Y|x_i] = \int_{In} f(x)dx$) into a one-dimensional integral by expressing every input parameter as a function of a new independent variable using ergodic theorem as recommended by Saltelli et al. (2010) (Cannavó, 2012).

The global sensitivity index or first-order sensitivity index (S_i) is defined based on conditional variances, approximated by performing a Fourier analysis, which indicates the individual effect of the uncertain input parameters on the output of the model as follows:

$$\boldsymbol{Var[E(Y|x_i)] = E\left[\left(Y - E(Y|x_i)\right)^2|x_i\right]} \qquad \textbf{Equation 72}$$

$$\boldsymbol{S_i = \frac{Var\,[E(Y|x_i)]}{Var(Y)}} \qquad \textbf{Equation 73}$$

The value of S_i ranges between 0 and 1 and increases with the increasing of the input factor importance. The FAST approach is suitable for models with no significant interactions among input parameters. In addition, it is computationally cheaper and relatively independent

of the sample size compared to the Sobol' GSA approach. However, the results of this approach were used in this study to verify the results obtained from the Sobol' sensitivity approach.

6.1.3.2 Sobol' sensitivity approach

The GSA Sobol' approach is another variance-based method that has successfully been applied since the 1990s. The Sobol' approach is considered a natural extension of the FAST approach because it calculates the sensitivity indices of joined in addition to individual input parameters. However, Sobol' is computationally intensive and depends on the sample size, which gives more accurate results than the FAST approach (Saltelli & Bolado, 1998).

The Sobol' approach estimates the sensitivity indices (S_i) of the main and total effects for each input parameter (x_i) by a straightforward Monte Carlo integration of the multi-dimensional integral of variances of the model's inputs (D_i). According to a study by Sobol' (2001), the global sensitivity index (S_i) in the Sobol' approach is the ratio of the variance of the input parameter (D_i) and the total variance of all inputs (D), as follows:

$$\boldsymbol{S_i = \frac{D_i}{D}} \qquad \textbf{Equation 74}$$

where,

$$\boldsymbol{D_i = \int_0^1 f_i^2 \, dx_i} \qquad \textbf{Equation 75}$$

$$\boldsymbol{D = \int_0^1 f^2(X) dX - f_0^2} \qquad \textbf{Equation 76}$$

The S_i in the Sobol' approach is also called the first-order sensitivity index and it estimates the expected fraction of the output variance that could be removed if the true value of the parameter is known (Patelli, et al., 2010). Therefore, ranking the input parameters according to their significance can be carried out using the S_i value. The higher the S_i, the greater the influence of the input parameter on the estimated output result. It is worth mentioning that the summation of all S_i values of the input parameters of a model should be equal to one.

It is also worth mentioning that in both GSA approaches (i.e. FAST and Sobol') the quasi-random numbers have been used instead of random numbers for the computation of the Monte Carlo integrals to be quasi-Monte Carlo computation. The generation of quasi-random (or systematic) numbers ensures low discrepancy points and enhances convergence rate compared to the crude (or simple) random sampling, which suffers from clustering (Cannavó (2012) and Saltelli & Bolado (1998)).

6.2 Implementation of the probabilistic analysis approach

In this part of the study, the proposed probabilistic analysis approach discussed above is used to analyse and evaluate the performance of the field cores', field and laboratory mixtures' specimens tested under T/C fatigue test in Chapter 4.

The VECD-N_f model used in this probabilistic approach was described earlier in detail and its parameters were categorised as constants (ε_0 and f) and random variables ($|E^*|_{LVE}$, a, b and α). Unfortunately, the experimental data of the uniaxial T/C fatigue tests of all tested mixtures were very limited and not enough to identify the correct distribution function for each random variable or an interdependency distribution between variables. However, in some previous studies by Luo (2014), Liu (2014), Dilip and Sivakumar Babu (2013), Retherford (2010) and Maji (2008), the input parameters of the classical fatigue characterisation models (i.e. equation 1) were assumed to follow normal distribution function. Consequently, it was decided to assume a normal distribution for each random variable of the VECD-N_f model ($|E^*|_{LVE}$, a, b and α) in this study.

In the following subsections, the results of the probabilistic analysis of each tested mixture are presented and discussed.

6.2.1 Field cores' results

First, the parameters of the normal distribution function for the random variables of the VECD-N_f model for field core specimens are shown in Table 48 to Table 51.

Table 48. Normal distribution function parameters of $|E^*|_{LVE}$ used in the MCS for field cores' mixtures under strain L1 and L2 tests.

N_f's parameter	Dynamic modulus ($\|E^*\|_{LVE}$)					
Distribution parameters	L1			L2		
	μ	σ	COV	μ	σ	COV
Section 1	1.19E+10	3.53E+09	29.6%	8.71E+09	7.44E+09	85.5%
Section 2	1.32E+10	2.65E+09	20.1%	1.30E+10	3.05E+09	23.5%
Section 4	1.03E+10	5.58E+08	5.4%	8.83E+09	0.0*	-
Section 5	0.82E+10	4.64E+09	56.4%	No Data		-
Section 6	0.92E+10	9.28E+08	10.1%	6.79E+09	1.54E+09	22.6%

* Only one specimen of trial section 4 completed the strain amplitude L2 test.

Table 49. Normal distribution function parameters of the fitting parameter "*a*" used in the MCS for field cores' mixtures under strain L1 and L2 tests.

N_f's parameter	Fitting parameter "*a*"					
Distribution parameters	L1			L2		
	μ	σ	COV	μ	σ	COV
Section 1	-2.92E-04	2.80E-04	95.8%	-3.61E-04	5.45E-04	150.7%
Section 2	-8.12E-05	1.19E-04	146.7%	-4.42E-05	6.60E-06	14.9%
Section 4	-2.44E-04	2.74E-04	112.3%	-6.72E-05	0.0	-
Section 5	-7.83E-04	3.07E-04	39.2%	No Data		-
Section 6	-9.76E-05	1.52E-04	155.6%	-2.13E-04	1.98E-04	93.2%

Table 50. Normal distribution function parameters of the fitting parameter "*b*" used in the MCS for field cores' mixtures under strain L1 and L2 tests.

N_f's parameter	Fitting parameter "*b*"					
Distribution parameters	L1			L2		
	μ	σ	COV	μ	σ	COV
Section 1	0.6687	0.2037	30.5%	0.7990	0.0571	7.1%
Section 2	0.8177	0.1825	22.3%	0.8160	0.0578	7.1%
Section 4	0.7450	0.2744	36.8%	0.8360	0.0	-
Section 5	0.7569	0.0554	7.3%	No Data		-
Section 6	0.9317	0.2494	26.8%	0.8066	0.0369	4.6%

Table 51. Normal distribution function parameters of the material damage parameter "α" used in the MCS for field cores' mixtures under both strain levels tests.

N_f's parameter	Material damage parameter "α"		
Distribution parameters	μ	σ	COV
Section 1	4.252	0.1535	3.6%
Section 2	5.230	0.6717	12.8%
Section 4	5.437	0.2478	4.6%
Section 5	4.846	0.3316	6.8%
Section 6	5.319	0.2680	5.0%

Given the relation between the fitting parameters, *a* and *b*, the generation of the random variable "*a*" was obtained/estimated from the generated "*b*" values using the following equation derived from the original exponential C-S model:

$$\boldsymbol{a = \frac{ln(C_0)}{S_0^b}} \qquad \textbf{Equation 77}$$

The value of the initial internal damage (S_0), which is also a lower limit for the N_f integration equation, was assumed to be the average of the S_0 values selected for each specimen of the field cores' trials, as shown in Table 52. The value of the initial pseudo-stiffness (C_0) was chosen to be around 0.9.

Table 52. Average initial damage (S_0) for each field cores' mixture under strain L1 and L2 tests.

Section #	Average S_0	
	ε_0-L1 = 55 με	**ε_0-L2 = 130 με**
1	270	7833
2	411	28925
4	777	22280
5	4935	-
6	141	15243

In order to perform the probabilistic analysis, a set of MATLAB routines was developed in this study to generate one million realisations of the four random variables ($|E^*|_{LVE}$, *a*, *b* and α) and to conduct the MCS analysis and estimate one million N_f values.

The output of the probabilistic analysis using MCS is a cumulative distribution function (cdf) curve of the fatigue life (N_f), as shown in Figure 117. Then, based on the target reliability (e.g. 75%), the number of cycles to failure (N_f) is determined to compare between the tested mixtures.

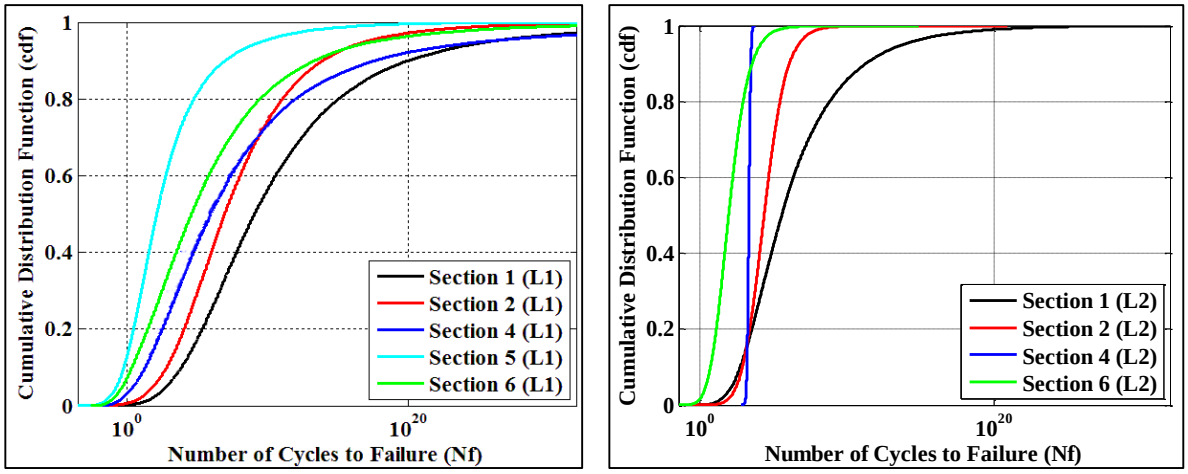

Figure 117. The cdf curves of the MCS using normally distributed RVs for field cores' mixtures under strain L1 and L2 tests.

Based on the cdf curves, the fatigue lives of the field cores' mixtures under strain L1 test are much longer than those of strain L2. This can be accredited to the internal damage that occurred in the specimen due to the first test under strain amplitude 1 (55 με) before being tested again under strain amplitude 2 (130 με). In addition, and as a substantial advantage, the cdf curves of the trial sections in both strain levels are in the same order, which shows a consistent behaviour and conclusion opposite to the deterministic results shown earlier, in subsection 5.2.1.2.

In order to compare fatigue damage between field cores' mixtures, the N_f value at a probability of failure of 25% (first quartile) was determined from the cumulative distribution function (cdf) curve of each trial section's mixture, as shown in Table 53.

Table 53. N_f results for the first quartile of field cores' mixtures under strain L1 and L2 tests.

Section #	ε_0-L1 = 55 με	ε_0-L2 = 130 με
1	1.01×10^{6}	7.6×10^{3}
2	3.76×10^{4}	3.8×10^{3}
4	1.61×10^{3}	1.8×10^{3}
5	5.73	-
6	107.1	18.9

The N_f results showed clearly that the low bitumen content in the mixture with PMB (trial section 6) affected the fatigue resistance and decreased its fatigue life significantly. In addition, the use of unmodified 40-50 Pen bitumen gave more fatigue life to the mixture

compared to the use of unmodified 60-70 Pen bitumen, and this might be due to the very low bitumen content (3.4%) in the base course of section 2. Moreover, the use of the Marshall/PRD mix method in the field cores of section 2 increased the fatigue life (N_f) compared to the use of the Marshall/QCS method in the base course of section 4 under low and high strain amplitude tests. Finally, the use of Thiopave bitumen in section 5 did not improve the performance of the mixture against fatigue.

In general, it can be easily stated that the specimens prepared from the base course of section 1 are performing the best against fatigue damage among the trial sections, with 75% reliability. This is the case under both fatigue tests and no contradiction in the results was found.

6.2.2 Field mixtures' results

The parameters of the normal distribution function for the random variables of the VECD-N_f model for field mixture specimens (F-Mar-10E and F-Mar-22S) are shown in Table 54 to Table 57.

Table 54. Normal distribution function parameters of $|E^*|_{LVE}$ used in the MCS for field mixtures under strain L1 and L2 tests.

N_f's parameter	Dynamic modulus ($\|E^*\|_{LVE}$)					
Distribution parameters	L1			L2		
	μ	σ	COV	μ	σ	COV
F-Mar-10E	1.20E+10	4.55E+08	3.8%	1.14E+10	4.17E+08	3.7%
F-Mar-22S	1.22E+10	1.37E+08	1.1%	1.15E+10	1.89E+08	1.7%

Table 55. Normal distribution function parameters of the fitting parameter "*a*" used in the MCS for field mixtures under strain L1 and L2 tests.

N_f's parameter	Fitting parameter "*a*"					
Distribution parameters	L1			L2		
	μ	σ	COV	μ	σ	COV
F-Mar-10E	-9.17E-04	1.67E-04	18.2%	-8.44E-05	1.37E-05	16.3%
F-Mar-22S	-6.54E-04	4.29E-04	65.6%	-1.53E-04	1.17E-04	76.9%

Table 56. Normal distribution function parameters of the fitting parameter "*b*" used in the MCS for field mixtures under strain L1 and L2 tests.

N_f's parameter	Fitting parameter "*b*"					
Distribution parameters	L1			L2		
	μ	σ	COV	μ	σ	COV
F-Mar-10E	0.4184	0.0222	5.3%	0.7277	0.0185	2.5%
F-Mar-22S	0.5032	0.1004	20.0%	0.7060	0.0859	12.2%

Table 57. Normal distribution function parameters of the material damage parameter "α" used in the MCS for field mixtures under both strain levels tests.

N_f's parameter	Material damage parameter "α"		
Distribution parameters	μ	σ	COV
F-Mar-10E	4.8359	0.1804	3.7%
F-Mar-22S	4.7786	0.1068	2.2%

Similar to the field cores, the generation of the random variable "*a*" was obtained from the generated "*b*" values using equation 77 derived from the original exponential C-S model. In addition, the value of the initial internal damage (S_0) was assumed to be the average of the S_0 values selected for each field mixture specimen, as shown in Table 58. The value of the initial pseudo-stiffness (C_0) was chosen to be around 0.9.

Table 58. Average initial damage (S_0) for each field mixture under strain L1 and L2 tests.

Mix	Average S_0	
	ε_0-L1 = 55 με	ε_0-L2 = 130 με
F-Mar-10E	356	7334
F-Mar-22S	432	8490

To implement the probabilistic analysis on the field mixtures, the same set of MATLAB routines was used to generate one million realisations of the four random variables ($|E^*|_{LVE}$, *a*, *b* and α) and to conduct the MCS analysis, and estimate one million N_f values.

The output of the probabilistic analysis using MCS is a cumulative distribution function (cdf) curve of the fatigue life (N_f), as shown in Figure 118. Then, based on the target reliability (e.g. 75%), the number of cycles to failure (N_f) is determined to compare between tested mixtures.

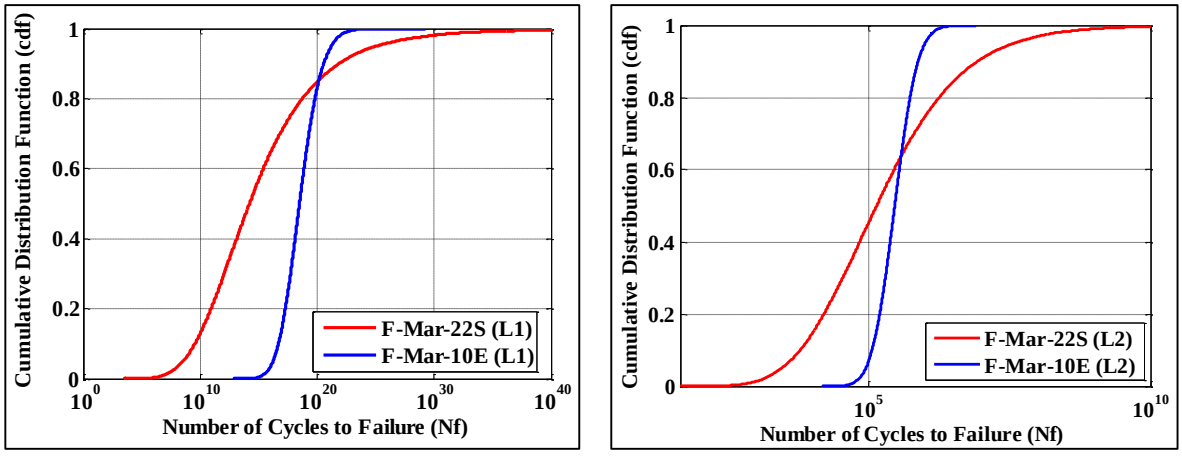

Figure 118. The cdf curves of the MCS using normally distributed RVs for field mixtures under strain L1 and L2 tests.

Based on the cdf curves, the fatigue lives of the field mixtures under strain L1 are much longer than those of strain L2. This can be attributed to the internal damage that occurred in the specimens due to the first test under strain amplitude L1 (55 με) before being tested again under strain amplitude L2 (130 με).

In order to compare fatigue cracking between field mixtures, the N_f value at a probability of failure of 25% (first quartile) was determined from the cumulative distribution function (cdf) curve of each mixture, as shown in Table 59.

Table 59. N_f results for the first quartile of field mixtures under strain L1 and L2 tests.

Mix	ε_0-L1 = 55 με	ε_0-L2 = 130 με
F-Mar-10E	3.3×10^{17}	1.7×10^{5}
F-Mar-22S	3.3×10^{11}	2.3×10^{4}

As clearly shown in Table 59, it can be easily stated that the mixture prepared with PG76-10E is performing much better against fatigue cracking under both loading levels than the mixture prepared with PG76-22S, with 75% reliability.

6.2.3 Laboratory mixtures' results

The parameters of the normal distribution function for the random variables of the VECD-N_f model for specimens of the laboratory mixtures (L-Mar-Pen, L-Spav-Pen and L-Spav-22E) are shown in Table 60 to Table 63.

Table 60. Normal distribution function parameters of $|E^*|_{LVE}$ used in the MCS for laboratory mixtures under strain L1 and L2 tests.

N_f's parameter	Dynamic modulus ($\|E^*\|_{LVE}$)					
Distribution parameters	L1			L2		
	μ	σ	COV	μ	σ	COV
L-Mar-Pen	6.96E+09	4.41E+08	6.3%	6.49E+09	6.11E+08	9.4%
L-Spav-Pen	6.12E+09	1.25E+09	20.5%	5.99E+09	9.89E+08	16.5%
L-Spav-22E	6.68E+09	5.75E+08	8.6%	6.17E+09	5.96E+08	9.7%

Table 61. Normal distribution function parameters of the fitting parameter "*a*" used in the MCS for laboratory mixtures under strain L1 and L2 tests.

N_f's parameter	Fitting parameter "*a*"					
Distribution parameters	L1			L2		
	μ	σ	COV	μ	σ	COV
L-Mar-Pen	-6.98E-04	3.09E-04	44.2%	-1.37E-04	7.75E-05	56.7%
L-Spav-Pen	-8.68E-04	2.30E-04	26.5%	-3.37E-04	1.55E-04	46.2%
L-Spav-22E	-8.71E-04	9.01E-05	10.3%	-4.76E-04	2.03E-04	42.6%

Table 62. Normal distribution function parameters of the fitting parameter "*b*" used in the MCS for laboratory mixtures under strain L1 and L2 tests.

N_f's parameter	Fitting parameter "*b*"					
Distribution parameters	L1			L2		
	μ	σ	COV	μ	σ	COV
L-Mar-Pen	0.5895	0.0729	12.4%	0.7976	0.0600	7.5%
L-Spav-Pen	0.5693	0.0677	11.9%	0.7147	0.0235	3.3%
L-Spav-22E	0.5666	0.0154	2.7%	0.6518	0.0280	4.3%

Table 63. Normal distribution function parameters of the material damage parameter "α" used in the MCS for laboratory mixtures under both strain levels tests.

N_f's parameter	Material damage parameter "α"		
Distribution parameters	μ	σ	COV
L-Mar-Pen	3.0709	0.0670	2.2%
L-Spav-Pen	2.9555	0.0737	2.5%
L-Spav-22E	3.7068	0.0824	2.2%

Similar to the previous mixtures, the generation of the random variable of fitting parameter "*a*" was obtained from the generated "*b*" values using equation 77 derived from the original exponential C-S model. In addition, the value of the initial internal damage (S_0) was assumed to be the average of the S_0 values selected for each laboratory mixture specimen, as shown in Table 64. The value of the initial pseudo-stiffness (C_0) was chosen to be around 0.9.

Table 64. Average initial damage (S_0) for each laboratory mixture under strain L1 and L2 tests.

Mix	Average S_0	
	ε_0-L1 = 55 με	ε_0-L2 = 130 με
L-Mar-Pen	116	840
L-Spav-Pen	100	723
L-Spav-22E	186	1714

To implement the probabilistic analysis on the laboratory mixtures, the same set of MATLAB routines was used to generate one million realisations of the four random variables ($|E^*|_{LVE}$, a, b and α) and to conduct the MCS analysis, and estimate one million N_f values.

The output of the probabilistic analysis using MCS is a cumulative distribution function (cdf) curve of the fatigue life (N_f), as shown in Figure 119. Then, based on the target reliability (e.g. 75%), the number of cycles to failure (N_f) is determined to compare between the tested mixtures.

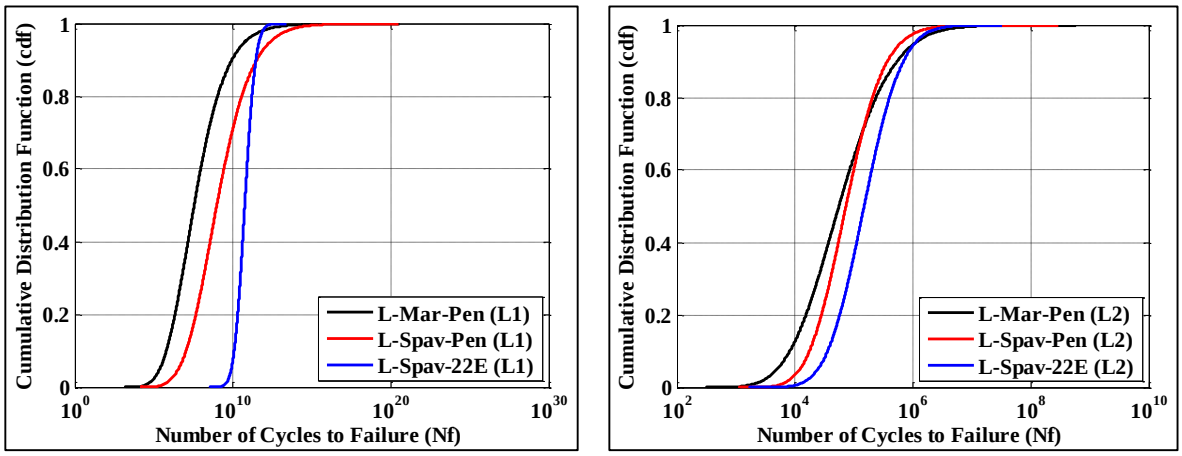

Figure 119. The cdf curves of the MCS using normally distributed RVs for laboratory mixtures under strain L1 and L2 tests.

Based on the cdf curves, the fatigue lives of the laboratory mixtures under strain L1 test are much longer than those of strain L2 test. This can be attributed to the internal damage that occurred in the specimens due to the first fatigue test under strain amplitude 1 (55 με) before being tested again under strain amplitude 2 (130 με).

In order to compare fatigue cracking between laboratory mixtures, the N_f value at a probability of failure of 25% (first quartile) was determined from the cumulative distribution function (cdf) curve of each mixture, as shown in Table 65.

Table 65. N_f results for the first quartile of laboratory mixtures under strain L1 and L2 tests.

Mix	ε_0-L1 = 55 με	ε_0-L2 = 130 με
L-Mar-Pen	3.6×10^6	2.0×10^4
L-Spav-Pen	8.2×10^7	3.4×10^4
L-Spav-22E	2.5×10^{10}	6.9×10^4

The results clearly revealed the advantage of using polymer-modified bitumen (PMB) in a Superpave mixture and showed that the fatigue damage resistance of the mixture with PG76-22E (L-Spav-22E) is better and has longer service life than that of the other laboratory mixtures, with 75% reliability.

Based on the probabilistic analysis results for all mixtures in this chapter, it can be concluded that the proposed approach is better at evaluating the performance of asphalt concrete mixtures against fatigue cracking. In addition, the comparison between different mixtures is much easier and more consistent in both loading levels' (L1 and L2) tests, even with the field core specimens.

6.2.4 Sensitivity analysis results

A well-developed set of MATLAB routines was used in the implementation of the global sensitivity analysis (GSA) on the input parameters of the fatigue life (VECD-N_f) model in this study. This set of MATLAB routines was originally developed by Cannavó (2012) to calculate the sensitivity indices of any user-defined model and was combined in a toolbox named GSAT (Global Sensitivity Analysis Toolbox) in MATLAB.

GSAT starts by generating two sets of 20,000 quasi-random specimens to be used in the quasi-random Monte Carlo Simulation. Then, the GSAT subroutines use the user-defined

model (e.g. VECD-N_f) to calculate the results of the FAST and Sobol' sensitivity analysis approaches, as described in detail in Cannavó (2012).

In this study, the fatigue life (VECD-N_f) model was defined in the GSAT routines in MATLAB and its input parameters ($|E^*|_{LVE}$, b and α) were analysed to identify their significance individually. The importance and significance of fitting parameter "a" is investigated indirectly from the investigation of fitting parameter "b". The joined sensitivity indices of the input parameters were ignored because, in the probabilistic analysis discussed earlier, the interdependency distribution between them were also ignored due to limited experimental data.

Based on the literature, generating 20,000 quasi-random specimens is more than enough for accurate results in GSAT analysis (Patelli, et al., 2010). However, different numbers of generated quasi-random specimens were used in the sensitivity analysis, and the results are shown in Table 66.

Table 66. Global sensitivity index (S_i) for VECD-N_f input parameters.

GSA approach	Number of quasi-random specimens	Global sensitivity index (S_i)		
		$\|E^*\|_{LVE}$	b	α
Sobol'	**20,000**	2.69E-04	1.0	2.69E-04
	100,000	-1.50E-04	1.0	-1.50E-04
	500,000	2.76E-06	1.0	2.76E-06
FAST	**20,000**	0.2663	0.9317	9.29E-02

According to the GSAT results, the sensitivity index (S_i) for parameter "b" in all cases is the highest. This indicates that the fitting parameter "b" and, indirectly, the fitting parameter "a" play a decisive role in the output of the fatigue life (N_f) model. However, the other two input parameters ($|E^*|_{LVE}$ and α) have negligible influence on the output of the VECD-N_f model.

This conclusion was expected because the value of the internal damage at failure (S_f), which is the upper limit for the N_f integration model, is highly affected by the value of "b" and "a", as shown in equation 69 in subsection 5.1.2.

6.3 Probabilistic analysis protocol

The developed probabilistic analysis approach for prediction of fatigue life (VECD-N_f) is summarised in some clear protocol steps that can be used in the future by pavement engineers. The procedure is as follows:

1. A loose asphalt concrete mixture is collected from a construction site or prepared in a laboratory for fatigue life prediction and characterisation.
2. At least five replicate specimens (100 mm diameter and 150 mm high) are prepared at a target air void content ±0.5 percent and short-term aged in accordance with AASHTO Standard PP 60.
3. The dynamic modulus ($|E^*|$) test is conducted on the specimens according to AASHTO Standard TP 79-11.
4. The results of $|E^*|$ test are then used to calculate the material damage parameter (α) using the exponent of time, *m*, in the relaxation modulus-time power equation [$E(t) = E_\infty + E_c t^{-m}$].
5. The uniaxial (tension-compression) fatigue test (controlled-strain or controlled-stress) is conducted on the same specimens under low and high strain amplitudes (e.g. 55 με and 130 με) at room temperature (20 °C) and 10 Hz frequency.
6. The fatigue test data are analysed using the VECD approach to obtain the fitting parameters (*a* and *b*) of the exponential equation 60 mentioned in subsection 5.1.2, in addition to the linear viscoelastic dynamic modulus ($|E^*|_{LVE}$) for each tested specimen of the mixture.
7. The developed probabilistic analysis approach with Monte Carlo Simulation (MCS) is then performed using the input parameters of the

fatigue life (VECD-N_f) model ($|E^*|_{LVE}$, a, b and α) to obtain the cumulative distribution function (cdf) curve for the tested mixture.

8. The predicted fatigue life (N_f) for the mixture can be determined from the cdf curve at a probability of failure of 25% or a preselected reliability level (e.g. 75%).
9. If the results of the predicted fatigue life (N_f) fail to satisfy the requirements, the design of the asphalt mixture should be modified.

6.4 Conclusions

From the results of fatigue analysis for asphalt concrete mixtures using the total dissipated energy (W_R) method and the VECD approach, it was concluded that neither method was sufficient to characterise fatigue resistance because of the high variability in the results, especially the field cores. The use of the viscoelastic continuum damage (VECD) approach was preferred and its results gave better conclusions compared to W_R. However, neglecting the uncertainty in the VECD-N_f model and its parameters induces a limitation in the analysis of fatigue damage and makes it difficult to predict the fatigue life (N_f) of the tested mixtures accurately.

In this chapter, a probabilistic analysis approach was developed using the VECD-N_f model in order to predict the performance of asphalt mixtures against fatigue cracking. The proposed probabilistic approach accounts for the uncertainty associated with fatigue tests, models and their parameters, in addition to the variability of the inputs in the fatigue analysis among specimens of a certain AC mixture. Given the increasing cost of designing and constructing new asphalt pavements, the probabilistic approach will be helpful for engineers to design pavements with asphalt concrete mixtures that resist fatigue cracking based on an acceptable reliability level or its equivalent probability of failure (p_f).

The random variables (RVs) of the VECD-N_f model ($|E^*|_{LVE}$, a, b and α) were generated following a normal distribution function due to the limited experimental data. However, it is recommended to test more specimens in the future to specify the correct distribution function for these variables.

The fatigue life (VECD-N_f) results of the newly developed probabilistic analysis approach were much more consistent and reliable than those of deterministic analysis shown in Chapter 5. In addition, the results showed no contradiction between the results of low and high strain amplitude fatigue tests.

Sensitivity analysis was then performed on the VECD-N_f model, and the results indicated how significant the fitting parameters (a and b) are to the prediction of fatigue life (N_f). More accurate values of these parameters will enhance the prediction of fatigue life (N_f), especially with the use of the developed probabilistic approach.

This established probabilistic analysis approach is very practical and useful for engineers, and will be beneficial to foresee the fatigue cracking resistance of asphalt mixtures in the field.

7 Conclusions and Recommendations

The significant increase in the population and growth of the economy in the State of Qatar has led to a substantial increase in traffic loading. This is affecting the performance of the existing roads and highways, especially against rutting and fatigue (top-down) cracking. In addition, the implementation of Marshall mix design with unmodified 60-70 Pen bitumen in the conventional pavement designs in the region has led to poor performance against major distresses. Therefore, this study intended to investigate mechanistic-based characterisation and modelling of the performance of the conventional asphalt concrete mixtures and compare them with alternative proposed mixtures with a focus on fatigue characterisation in the State of Qatar.

The study started with performance evaluation of the conventional pavement structures in Qatar compared to a proposed perpetual pavement structure using the M-E PDG software. Then, full-scale trial pavement structures were assessed against permanent deformation and ride quality or smoothness using some field tests. After that, the study focused on the mixture level and conducted several laboratory tests on altered asphalt mixtures in order to examine their performance against rutting, fracture cracking, temperature susceptibility and fatigue damage. However, the deterministic approaches of fatigue characterisation were not sufficient to compare mixtures and predict their fatigue lives precisely. Therefore, the study concluded by developing a new probabilistic analysis approach for fatigue life integrating the viscoelastic continuum damage (VECD) approach.

In brief, the main contribution of this research study was to examine the limitations of conventional fatigue characterisation approaches and to enhance the ability of the viscoelastic continuum damage (VECD) approach to predict fatigue resistance for asphalt mixtures by incorporating probabilistic analysis into this approach.

7.1 Conclusions

The general conclusions from the results discussed in the preceding chapters can be summarised as follows:

- The regional studies concentrated on the permanent deformation as a main distress in the region. However, the observations in the region and specifically in Qatar indicated that fatigue (top-down) cracking is also a distress of concern.
- The results of performance analysis on M-E PDG software evidenced how effective it is to replace the conventional unmodified bitumen with polymer-modified bitumen for pavements in Qatar and countries in the region with similar climatic conditions.
- The M-E PDG analysis results also indicated that the use of perpetual designs makes pavements much more accommodating of the increase in traffic loading than conventional designs, without causing excessive damage.
- Bitumen grade and aggregate type/angularity significantly affect the stiffness and the resistance of asphalt mixtures to rutting, fatigue cracking and fracture.
- Life-cycle cost analysis of conventional and perpetual structures demonstrated that the initial cost of perpetual pavement structures is about 30% more than conventional pavements. However, perpetual pavement structures are still more economical because they require much less maintenance or rehabilitation work.
- Asphalt mixtures with polymer-modified bitumen had the least temperature susceptibility, while mixtures with unmodified bitumen had the highest temperature susceptibility.
- The fracture toughness (K), fracture energy (G_f) and maximum tensile stress (σ_{max}) values of mixtures prepared from field cores of the trial road were high, which reflects good performance against fracture cracking.

- The dynamic modulus master curves of all tested mixtures were mainly affected by the bitumen type/grade and aggregate type. In addition, the use of polymer-modified bitumen flattened the master curve of the asphalt concrete mixtures and reduced the temperature and frequency susceptibility on the stiffness and rut-resistance.
- The replicate specimens of each field and laboratory mixtures tested under cyclic T/C fatigue test showed a similar reduction rate of dynamic modulus and increment of phase angle opposite to the field cores' specimens but different fatigue lives.
- The preliminary results and the traditional interpretation of the data of the uniaxial T/C fatigue test are insufficient to directly assess the performance against fatigue cracking.
- Asphalt mixtures with polymer-modified bitumen might not show improvement in resistance to fatigue damage if the design of these mixtures has relatively low bitumen content.
- The use of the VECD approach has major advantages over simply calculating the total DE. However, even for the laboratory mixtures, the predicted fatigue life (N_f) using the VECD approach was highly affected by the variability in the input parameters of the fatigue life model.
- In order to overcome the limitation of the deterministic VECD approach, a probabilistic VECD analysis approach was developed in this study to predict the fatigue resistance of asphalt mixtures.
- The fatigue life (N_f) results of the probabilistic analysis approach were much more consistent and reliable than those of deterministic analysis.

- Results of sensitivity analysis on the VECD-N_f model showed how significant the fitting parameters (*a* and *b*) are to the prediction of fatigue life.

7.2 Recommendations

This study has focused on improving the ability of the viscoelastic continuum damage (VECD) approach to predict fatigue life for asphalt mixture by integrating probabilistic analysis into this approach. The results in this thesis showed that the probabilistic approach is promising but requires further developments.

First, the distributions of the random variables of the VECD-N_f model were assumed to follow a normal distribution function based on the limited experimental data. Consequently, it is recommended in the future to test a large number of specimens to have enough data in order to identify the distribution function of each random variable accurately. Second, although the effect of bitumen type/grade and aggregate type/angularity on the performance of asphalt pavements was studied and investigated in this thesis, it is recommended in the future to look deeper into the effect of aggregate gradation, bitumen content and air voids on the performance of any asphalt concrete mixture, especially against fatigue cracking.

Publications

Journal papers

Sadek, H., Masad, E., Sirin, O., Al-Khalid, H., Sadeq, M., and Little, D., 2013, "Implementation of Mechanistic-Empirical Pavement Analysis in the State of Qatar". *International Journal of Pavement Engineering*. 15(6), 495–511.

Sadek, H., Masad, E., Sirin, O., Al-Khalid, H., and Hassan, K., 2014b, "Performance Evaluation of Full-Scale Sections of Asphalt Pavements in the State of Qatar". *Journal of Performance of Constructed Facilities. ASCE Journal of Performance of Constructed Facilities* DOI: 10.1061/(ASCE)CF.1943-5509.0000627.

Sadek, H., Masad, E., Al-Khalid, H., Mehrez, L., and Sirin, O. 2016, "Probabilistic Analysis of Fatigue Life for Asphalt Pavements Using VECD Approach". (Under preparation).

Conference papers

Sadek, H., Masad, E., Sirin, O., Al-Khalid, H., and Little, D., 2012, "The Implementation of Mechanistic-Empirical Pavement Design Method to Evaluate Asphalt Pavement Design in Qatar". 5th Eurasphalt & Eurobitume Congress, 13-15th, June 2012. Istanbul, Turkey.

Sadek, H., Masad, E., Sirin, O., Hassan, K., and Al-Khalid, H., 2013, "Evaluation of Mechanical Properties of Alternative Pavement Designs for the State of Qatar". 2nd MESAT Conference, 5-7th, February 2013. Sharjah, UAE.

Sadek, H., Masad, E., Sirin, O., Al-Khalid, H., and Hassan, K., 2014, "Characterization of Fatigue Resistance of Alternative Pavement Designs for the State of Qatar". Proceeding of the 3rd International Conference on Transportation Infrastructure, 22-25th April 2014. Pisa, Italy.

Sadek, H., Masad, E., Al-Khalid, H., and Sirin, O., 2015, "Fatigue characterisation of full-scale pavements using viscoelastic continuum damage approach for Qatar". Proceeding of

the 6th International Conference Bituminous Mixtures and Pavements, 10-12 June 2015. Thessaloniki, Greece.

References

AASHO Committee on Design, 1961. *AASHO Interim Guide for the Design of Flexible Pavement Structures,* Washington, D.C.: American Association of State Highway Officials.

AASHTO Designation: MP 19-10, 2010. *Standard Specification for Performance-Grade Asphalt Binder using Multiple Stress Creep Recovery (MSCR) Test,* Washington, D.C.: American Association of State Highway and Transportation Officials.

AASHTO PP 60-14, 2014. *Standard Practice for Preparation of Cylindrical Performance Test Specimens Using the Superpave Gyratory Compactor (SGC),* Washington, D.C.: American Association of State Highway and Transportation Officials.

AASHTO T193, 2010. *Standard Method of Test for the California Bearing Ratio,* Washington, D.C.: American Association of State Highway and Transportation Officials.

AASHTO TP 79-11, 2011. *Determining the Dynamic Modulus and Flow Number for Hot Mix Asphalt (HMA) Using the Asphalt Mixture Performance Tester (AMPT).,* Washington, D.C.: American Association of State Highway and Transportation Officials.

AASHTO TP 79-13, 2013. *Standard Method of Test for Determining the Dynamic Modulus and Flow Number for Hot Mix Asphalt (HMA) Using the Asphalt Mixture Performance Tester (AMPT),* Washington, D.C.: American Association of State Highway and Transportation Officials.

AASHTO TP 8-64, 2002. *Method for Determining the Fatigue Life of Compacted Hot-Mix Asphalt (HMA) Subjected to Repeated Flexural Bending,* Washington, D.C.: AASHTO Provisional Standards.

AASHTO TP T 321-03, 2007. *Standard Method of Test for Determining the Fatigue Life of Compacted Hot-Mix Asphalt (HMA) Subjected to Repeated Flexural Bending,* Washington, D.C.: American Association of State Highway and Transportation Officials.

Al-Abdul Wahhab, H. I., Asi, I. M. & Ramadhan, R. H., 2001. Modeling Resilient Modulus and Temperature Correction for Saudi Roads. *Journal of Materials in Civil Engineering,* 13(4), pp. 298-305.

Al-Abdul Wahhab, H. I. & Balghunaim, F. A., 1994. Asphalt Pavement Temperature Related to Arid Saudi Environment. *Journal of Materials in Civil Engineering,* 6(1), pp. 1-14.

Al-Abdul Wahhab, H. I. et al., 1999. Design and Maintenance Criteria for Saudi Bituminous Concrete Mixes. *Building and Environment,* Volume 13, pp. 623-631.

Al-Hadidy, A. I. & Yi-qiu, T., 2010. Comparative Performance of the SMAC Made with the SBS- and ST-Modified Binders. *Journal of Materials in Civil Engineering,* 22(6), pp. 580-587.

Al-Khateeb, G., 2011. A Simple Quantitative Method for Identification of Failure due to Fatigue Damage. *International Journal of Damage Mechanics,* 20(1), pp. 3-21.

Al-Khateeb, G., Shenoy, A., Gibson, N. & Harman, T., 2006. A New Simplistic Model for Dynamic Modulus Predictions of Asphalt Paving Mixtures. *Journal of the Association of Asphalt Paving Technologists,* Volume 75, pp. 1254-1293.

Apeagyei, A. K., Diefenderfer, B. K. & Diefenderfer, S. D., 2011. Rutting Resistance of Asphalt Concrete Mixtures That Contain Recycled Asphalt Pavement. *Journal of Transportation Research Board,* Volume 2208, pp. 9-16.

ARA, Inc., ERES Consultants Division, 2004. *Guide for Mechanistic-Empirical Design of New and Rehabilated Pavement Structures - NCHRP 1-37A Final Report: Appendix C,* Washington, D.C.: ERES Consultants Division, Transportation research Board, National Research Council.

Arabani, M. & Ferdowsi, B., 2009. Evaluating The Semi-Circular Bending Test for HMA Mixtures. *International Journal of Engineering Transaction A: Basics,* 22(1), pp. 47-58.

Artamendi, I. & Khalid, H., 2005. Characterization of Fatigue Damage for Paving Asphaltic Materials. *Fatigue & Fracture of Engineering Materials & Structures,* Volume 28, pp. 1113-1118.

Asi, I. M., 2006. Laboratory Comparison Study for the Use of Stone Matrix Asphalt in Hot Weather Climates. *Construction and Building Materials,* Volume 20, pp. 982-989.

Baek, C. M., 2010. *Investigation of Top-Down Cracking Mechanisms Using the Viscoelastic Continuum Damage Damage Finite Element Program,* Raleigh, North Carolina: North Carolina State University.

Baus, R. L. & Fogg, J. A., 1989. AASHTO Flexible Pavement Design Equation Study. *Journal of Transportation Engineering,* 115(5), pp. 559-564.

Bhasin, A., Castelo Branco, V. T. F., Masad, E. & Little, D., 2009. Quantitative Comparison of Energy Methods to Characterize Fatigue in Asphalt Materials. *Journal of Materials in Civil Engineering,* 21(2), pp. 83-92.

Bonaquist, R., 2010. *Wisconsin Mixture Characterization Using the Asphalt Mixture Performance Tester (AMPT) on Histirical Aggregate Structures,* Wisconsin: Wisconsin Department of Transportation.

Bonaquist, R. F., Christensen, D. W. & Stump, W., 2003. *NCHRP Report No. 513: Simple Performance Tester for Superpave Mix Design: First-Article Development and Evaluation,* Washington, D.C.: National Cooperative Highway Research Program.

BS EN 12697-32:2003, 2003. *Bituminous Mixtures. Test Methods for Hot Mix Asphalt. Laboratory Compaction of Bituminous Mixtures by Vibratory Compactor,* London, UK: BSI.

Bubshait, A. A., 2001. Quality of Pavement Construction in Saudi Arabia. *Practice Periodical on Structural Design and Construction,* 6(3), pp. 129-136.

Cannavó, F., 2012. Sensitivity Analysis for Volcanic Source Modeling Quality Assessment and Model Selection. *Computers & Geosciences,* Volume 44, pp. 52-59.

Carpenter, S. H. & Shen, S., 2006. Dissipated Energy Approach to Study Hot-Mix Asphalt Healing in Fatigue. *Journal of the Transportation Research Board,* Volume 1970, pp. 178-185.

Castelo Branco, V. T. F., Masad, E., Bhasin, A. & Little, D., 2008. Fatigue Analysis of Asphalt Mixtures Independent of Mode of Loading. *Journal of the Transportation Research Board,* Volume 2057, pp. 149-156.

Ceylan, H., Coree, B. & Gopalakrishnan, K., 2008. Design of Rigid Pavements in Iowa Using the Mechanistic-Empirical Pavement Design Guide. *Baltic Journal of Road & Bridge Engineering,* 3(4), pp. 219-225.

Ceylan, H., Coree, B. & Gopalakrishnan, K., 2009. Evaluation of the Mechanistic-Empirical Pavement Design Guide for Implementation in Iowa. *Baltic Journal of Road & Bridge Engineering,* 4(1), pp. 5-12.

Chen, W., Jin, R. & Sudjianto, A., 2005. Analytical Variance-Based Global Sensitivity Analysis in Simulation-Based Design Under Uncertainty. *Journal of Mechanical Design,* 127(5), pp. 875-886.

Chong, K. P. & Kuruppu, M. D., 1984. New Specimen for Fracture Toughness Determination for Rock and Other Materials. *International Journal of Fracture,* Volume 137, pp. 59-62.

Christian, J. & Baecher, G., 1999. Point-Estimate Method as Numerical Quadrature. *Journal of Geotechnical and Geoenvironmental Engineering,* 125(9), pp. 779-786.

Clyne, T. R., Li, X., Marasteanu, M. O. & Skok, E. L., 2003. *Dynamic and Resilient Modulus of Mn/DOT Asphalt Mixtures,* Minnesota: Minnesota Department of Transportation.

Daniel, J. S., Bisirri, W. & Kim, Y. R., 2004. Fatigue Evaluation of Asphalt Mixtures Using Dissipated Energy and Viscoelastic Continuum Damage Approaches. *Journal of the Association of Asphalt Paving Technologists,* Volume 73, pp. 557-583.

Darter, M., McCullough, B. & Brown, J., 1972. Reliability Concepts Applied to the Texas Flexible Pavement System. *Highway Research Record,* Issue 407, pp. 146-161.

Demos, G. P., 2006. *Life Cycle Cost Analysis and Discount Rate on Pavements for the Colorado Department of Transportation,* Colorado: National Technical Information.

Dilip, D. M. & Sivakumar Babu, G. L., 2013. Methodology for Pavement Design Reliability and Back Analysis Using Markov Chain Monte Carlo Simulation. *Journal of Transportation Engineering,* Volume 139, pp. 65-74.

Dongre, R. et al., 2005. Field Evaluation of Witczak and Hirsch Models for Predicting Dynamic Modulus of Hot-Mix Asphalt. *Journal of the Association of Asphalt Paving Technologists,* Volume 74, pp. 381-442.

Dynatest Elmod6 Version 6.1.44., 2010. Copenhagen: Dynatest International.

Elseifi, M. A., Mohammad, L. N., Ying, H. & Cooper III, S., 2012. Modeling and Evaluation of the Cracking Resistance of Asphalt Mixtures Using the Semi-Circular Bending Test at Intermediate Temperatures. *Road Materials and Pavement Design,* 13(S1), pp. 124-139.

Fatani, M. et al., 1992. *National Research Project: Evaluation of Permanent Deformation of Asphalt Concrete Pavement in Saudi Arabia,* Riyadh: King Abdulaziz City for Science and Technology.

Ferne, B., 2006. Long-life pavements—a European study by ELLPAG. *International Journal of Pavement Engineering,* 7(2), pp. 91-100.

Gdoutos, E. E., 2005. *Fracture Mechanics: An Introduction.* 1 ed. Dordrecht: Springer Netherlands.

Ghuzlan, K. A. & Carpenter, S. H., 2000. Energy-derived, Damage-based Failure Criterion for Fatigue Testing. *Journal of the Transportation Research Board,* Volume 1723, pp. 141-149.

Goh, S., You, Z., Williams, C. & Li, X., 2011. Preliminary Dynamic Modulus Criteria of HMA for Field Rutting of Asphalt Pavements: Michigan's Experience. *Journal of Transportation Engineering,* 137(1), pp. 37-45.

Graeff, A. G., Pilakoutas, K., Neocleous, K. & Peres, M. V., 2012. Fatigue Resistance and Cracking Mechanism of Concrete Pavements Reinforced with Recycled Steel Fibres Recovered from Post-Consumer Tyres. *Engineering Structures,* Volume 45, pp. 385-395.

Haggag, M. M., Mogawer, W. S. & Bonaquist, R., 2011. Fatigue Evaluation of Warm-Mix Asphalt Mixtures: Use of Uniaxial, Cyclic, Direct Tension Compression Test. *Journal of Transportation Research Board,* Volume 2208, pp. 26-32.

Harr, M. E., 1987. *Reliability Based Design in Civil Engineering.* New York: McGraw-Hill.

Jie, S., Yu, J. & Zhao, H., 2011. Two-Parameter Weibull Distribution Theory Testing Analysis in Fatigue Life of Asphalt Mixture. *Applied Mechanics and Materials,* Volume 97-98, pp. 45-48.

Kanitpong, K., Charoentham, N. & Likitlersuang, S., 2011. Investigation on the Effects of Gradation and Aggregate Type to Moisture Damage of Warm Mix Asphalt Modified with Sasobit. *International Journal of Pavement Engineering,* 13(5), pp. 451-458.

Kim, Y., Lee, H. & Heitzman, M., 2009. Dynamic Modulus and Repeated Load Tests of Cold In-Place Recycling Mixtures Using Foamed Asphalt. *The Journal of Materials in Civil Engineering,* 21(6), pp. 279-285.

Kim, Y. -R., Zhang, J. & Ban, H., 2012. Moisture Damage Characterization of Warm-Mix Asphalt Mixtures Based on Laboratory-Field Evaluation. *Construction and Building Materials,* Volume 31, pp. 204-211.

Kuruppu, M. D. & Chong, K. P., 2012. Fracture toughness testing of brittle materials using semi-circular bend (SCB) specimen. *Engineering Fracture Mechanics,* Volume 91, pp. 133-150.

Kutay, M. E., Gibson, N. & Youtcheff, J., 2008. Conventional and Viscoelastic Continuum Damage (VECD) Based Fatigue Analysis of Polymer Modified Asphalt Pavements. *Journal of Association of Asphalt Paving Technologists,* Volume 77, pp. 395-434.

Kutay, M. E., Gibson, N., Youtcheff, J. & Dongré, R., 2009. Use of Small Samples to Predict Fatigue Lives of Field Cores: Newly Developed Formulation on Viscoelastic Continuum Damage Theory. *Transportation Research Record: Journal of the Transportation Research Board,* pp. 90-97.

LCCAExpress, 2011. Version 2.0. Developed by Timm D. H., 2011. USA: Asphalt Pavement Alliance.

Lee, H. J., Daniel, J. S. & Kim, Y. R., 2000. Continuum Damage Mechanics-Based Fatigue Model of Asphalt Concrete. *Journal of Materials in Civil Engineering,* 12(2), pp. 105-112.

Lim, I. L., Johnson, I. W. & Choi, S. K., 1993. Stress Intensity Factors for Semi-Circular Specimens Under Three-Point Bending. *Engineering Fracture Mechanics,* 44(3), pp. 363-382.

Li, N., Molenaar, A., van de Ven, M. & Wu, S., 2013. Characterization of fatigue performance of asphalt mixture using a new fatigue analysis approach. *Construction and Building Materials,* Volume 45, pp. 45-52.

Liu, F. & Wang, D., 2012. Performance of Asphalt Mixture Used for Asphalt Treated Base of Perpetual Pavements. *Advanced Materials Research,* Volume 415-417, pp. 1531-1536.

Liu, H. & Xu, X., 2014. *Reliability Analysis of Asphalt Pavement Considering Two Failure Modes.* Wuhan, Taylor & Francis Group, pp. 291-295.

Liu, J., 2011. Fatigue Life Evaluation of Asphalt Rubber Mixtures Using Semi-Circular Bending Test. *Advanced Materials Research,* Volume 255-260, pp. 3444-3449.

Li, X. -J. & Marasteanu, M. O., 2010. Using Semi Circular Bending Test to Evaluate Low Temperature Fracture Resistance for Asphalt Concrete. *Experimental Mechanics,* Volume 50, pp. 867-876.

Li, X. et al., 2006. *Investigation of the Low-Temperature Fracture Properties of Three MnROAD Asphalt Mixtures,* Minnesota: Minnesota Department of Transportation; Office of Research Services, MN/RC-2006-15.

Luo, Z., Xiao, F., Hu, S. & Yang, Y., 2013. Probabilistic Analysis on Fatigue Life of Rubberized Asphalt Concrete Mixtures Containing Reclaimed Asphalt Pavement. *Construction and Building Materials,* Volume 41, pp. 401-410.

Luo, Z., Xiao, F. & Sharma, R., 2014. Efficient Reliability-Based Approach for Mechanistic-Empirical Asphalt Pavement Design. *Construction and Building Materials,* Volume 64, pp. 157-165.

Maji, A. & Das, A., 2008. Reliability Considerations of Bituminous Pavement Design by Mechanistic–Empirical Approach. *International Journal of Pavement Engineering,* 9(1), pp. 19-31.

Masad, E., Castelo Branco, V. T. F., Little, D. & Lytton, R., 2008. A Unified Method for the Analysis of Controlled-Strain and Controlled-Stress Fatigue Testing. *International Journal of Pavement Engineering,* 9(4), pp. 233-246.

Masad, E., Kassem, E. & Little, D., 2011. Characterization of Asphalt Pavement Materials in the State of Qatar. *Road Materials and Pavement Design,* 12(4), pp. 739-765.

Mathew, T. V. & Krishna Rao, K. V., 2007. Flexible Pavement Design. In: *Introduction to Transportation Engineering.* Madras: National Programme on Technology Enhanced Learning.

Mbarki, R., Kutay, M. E., Gibsonb, N. & Abbas, A. R., 2012. Comparison Between Fatigue Performance of Horizontal Cores from Different Asphalt Pavement Depths and Laboratory Specimens. *Road Materials and Pavement Design,* 13(3), pp. 422-432.

McCall, J., 1958. Probability of Fatigue Failure of Plain Concrete. *American Concrete Institute,* 55(8), pp. 233-244.

McCall, J. T., 1958. Probability of Fatigue Failure of Plain Concrete. *Journal of American Concrete Institute,* 55(8), pp. 233-244.

M-E PDG, Version 1.1, 2009. Arizona State: Arizona State University.

Mehrez, L., Kassem, E., Masad, E. & Little, D., 2015. Stochastic Identification of Linear-Viscoelastic Models of Aged and Unaged Asphalt Mixtures. *Journal of Materials in Civil Engineering,* 27(4).

Merrill, D., Van Dommelen, A. & Gáspár, L., 2006. A Review of Practical Experience Throughout Europe on Deterioration in Fully-Flexible and Semi-Rigid Long-Life Pavements. *International Journal of Pavement Engineering,* 7(2), pp. 101-109.

Mohammad, L. N., Cooper Jr., S. B. & Elseifi, M. A., 2011. Characterization of HMA Mixtures Containing High Reclaimed Asphalt Pavement Content with Crumb Rubber Additives. *Journal of Materials in Civil Engineering,* 23(11), pp. 1560-1568.

Mohammad, L. N. et al., 2006. Permanent Deformation Analysis of Hot-Mix Asphalt Mixtures with Simple Performance Tests and 2002 Mechanistic-Emperical Pavement Design Software. *Journal of Transportation Research Board,* Volume 1970, pp. 133-142.

Molenaar, A. A. A., 1983. *Structural Performance and Design of Flexible Road Construction and Asphalt Concrete Overlays,* Delft: Ph.D Thesis, Delft University of Technology.

Molenaar, A. A. A., 2007. Prediction of Fatigue Cracking in Asphalt Pavements: Do We Follow the Right Approach?. *Journal of Transportation Research Board,* Volume 2001, pp. 155-162.

Molenaar, A. A. A., Scarpas, A., Liu, X. & Erkens, S. M. J. G., 2002. Semi-Circular Bending Test: Simple but Useful?. *Journal of the Association of Asphalt Paving Technologists,* Volume 71, pp. 794-815.

Monismith, C. L., Epps, J. A. & Finn, F. N., 1985. *Improved Asphalt Mix Design.* San Antonio, TX, Asphalt Paving Technology, pp. 347-406.

Mull, M. A., Stuart, K. & Yehia, A., 2002. Fracture Resistance Characterization of Chemically Modified Crumb Rubber Asphalt Pavement. *Journal of Materials Science,* Volume 37, pp. 557-566.

Naji, J. A. & Asi, I. M., 2008. Performance Evaluation of Asphalt Concrete Mixes Containing Granular Volcanic Ash. *Journal of Materials in Civil Engineering*, 20(12), pp. 754-761.

NCHRP 1-37A Final Document: Appendix GG-1: Calibration of Permanent Deformation Models for Flexible Pavements, 2004. *Guide for Mechanistic-Empirical Design of New and Rehabilated Pavement Structures,* Washingtion, D.C.: Applied Research Associates, Inc., ERES Consultants Division, Transportation research Board, National Research Council.

NCHRP 1-37A Final Document: Appendix II-1: Calibration of Fatigue Cracking Models for Flexible Pavements, 2004. *Guide for Mechanistic-Empirical Design of New and Rehabilated Pavement Structures,* Washingtion, D.C.: Applied Research Associates, Inc., ERES Consultants Division, Transportation research Board, National Research Council.

NCHRP 1-37A Final Report: Appendix C, 2004. *Guide for Mechanistic-Empirical Design of New and Rehabilated Pavement Structures,* Washingtion, D.C.: Applied Research

Associates, Inc., ERES Consultants Division, Transportation research Board, National Research Council.

Othman, A. M., 2011. Evaluation of Hydrated Lime Effect on the Performance of Rubber-Modified HMA Mixtures. *Journal of Elastomers and Plastics,* Volume 43, pp. 221-237.

Ozer, H. et al., 2009. Evaluation of RAP Impact on Hot-Mix Asphalt Design and Performance. *Journal of the Association of Asphalt Paving Technologists,* Volume 78, pp. 317-351.

Pasetto, M. & Baldo, N., 2015. *Fatigue Characterization of Modified Asphalt Concretes by Means of Dissipated Energy Approaches.* Thessaloniki, Greece, Taylor & Francis Group, pp. 379-384.

Patelli, E., Pradlwarter, H. J. & Schuëller, G. I., 2010. Global Sensitivity of Structural Variability by Random Sampling. *Computer Physics Communications,* Volume 181, pp. 2072-2081.

Pellinen, T. K., Witczak, M. W. & Bonaquist, R. F., 2002. *Asphalt Mix Master Curve Construction Using Sigmoidal Fitting Function with Non-liner Least Squares Optimization.* New York, US, American Society of Civil Engineers, pp. 83-101.

Qatar Construction Specifications (QCS), 2010. Doha: The State of Qatar.

Qatar Highway Design Manual (QHDM) - Section 9, 1997. Doha: The State of Qatar.

Qatar Statistics Authority, 2013. *Qatar Statistics Authority - The State of Qatar [www.qsa.gov.qa/eng/PS-Archive.htm]*. [Online].

Retherford, J. Q. & McDonald, M., 2010. Reliability Methods Applicable to Mechanistic–Empirical Pavement Design Method. *Journal of the Transportation Research Board,* Volume 2154, pp. 130-137.

RILEM Technical Committee, 1985. Determination of Fracture Energy of Mortar and Concrete by Means of Three-Point Bend Tests on Notched Beams. *Materials and Structures,* 18(4), pp. 285-290.

Rodezno, M. & Kaloush, K., 2011. Guide on the Selection of Appropriate Laboratory Stress Levels for the Flow Number Test. *Journal of Testing and Evaluation*, 39(6).

Rosenblueth, E., 1975. *Point Estimates for Probability Moments.* USA, Proceedings of the National Academy of Sciences, pp. 3812-3814.

Saltelli, A. et al., 2010. Variance Based Sensitivity Analysis of Model Output. Design and Estimator for the Total Sensitivity Index. *Computer Physics Communications*, Volume 181, pp. 259-270.

Saltelli, A. & Bolado, R., 1998. An alternative way to compute Fourier amplitude sensitivity test (FAST). *Computational Statistics & Data Analysis*, 26(4), pp. 445-460.

Schapery, R. A., 1981. On Viscoelastic Deformation and Failure Behavior of Composite Materials with Distributed Flaws. *Advances in Aerospace Structures and Materials,* pp. 5-20.

Schapery, R. A., 1984. Correspondence Principles and Generalized J-integral for Large Deformation and Fracture Analysis of Viscoelastic Media. *International Journal of Fracture,* Volume 25, pp. 194-223.

Schapery, R. A., 1987. Deformation and Fracture Characterization of Inelastic Composite Materials using Potentials. *Polymer Engineering and Science*, 27(1), pp. 63-76.

Shu, X., Huang, B. & Vukosavljevic, D., 2010. *Evaluation of Cracking Resistance of Recycled Asphalt Mixture Using Semi-Circular Bending Test.* Shanghai, China, American Society of Civil Engineers, pp. 58-65.

Singh, S., Anmbedkar, B., Mohammadi, Y. & Kaushik, S., 2008. Flexural Fatigue Strength Prediction of Steel Fibre Reinforced Concrete Beams. *Electronic Journal of Structural Engineering*, Volume 8, pp. 46-54.

Singh, S. P., Mohammadib, Y. & Kaushikc, S. K., 2006. Probability of Fatigue Failure of Steel Fibrous Conceret Containing Mixed Fibers. *Asian Journal of Civil Engineering (Building and Housing),* 7(1), pp. 1-12.

Singh, S., Singh, B. & Kaushik, S., 2005. Probability of Fatigue Failure of Steel Fibrous Concrete. *Magazine of Concrete Research,* 57(2), pp. 65-72.

Si, Z., Little, D. N. & Lytton, R. L., 2002. Characterization of Microdamage and Healing of Asphalt Concrete Mixtures. *Journal of Materials in Civil Engineering (ASCE),* 14(6), pp. 461-470.

Sobol', I. M., 2001. Global Sensitivity Indices for Nonlinear Mathematical Models and their Monte Carlo Estimates. *Mathematics and Computers in Simulation,* Volume 55, pp. 271-280.

Tangella, R., Craus, S. C. S., Deacon, J. A. & Monismith, C. L., 1990. *Summary Report on Fatigue Response of Asphalt Mixtures,* Washington, D.C.: Rep. to Strategic Highway Research Program.

Tayebali, A. et al., 1994. *Mixture and Mode-of-Loading Effects on Fatigue Response of Asphalt-Aggregate Mixtures.* St.Louis, MO, US, Association of Asphalt Paving Technologists, pp. 118-151.

The Public Works Authority (Ashghal), 2012. Doha: The State of Qatar.

Thompson, M. S., 1966. Shear strength and elastic properties of lime-soil mixtures. *Highway Research Record,* Issue 139, pp. 1-14.

Tigdemir, M., Karasahin, M. & Sen, Z., 2002. Investigation of Fatigue Behaviour of Asphalt Concrete Pavements with Fuzzy-Logic Approach. *International Journal of Fatigue,* Volume 24, pp. 903-910.

Timm, D. H. & Newcomb, D. E., 2006. Perpetual Pavement Design for Flexible Pavements in the US. *International Journal of Pavement Engineering,* 7(2), pp. 111-119.

Timm, D. H. & Tran, N., 2014. *Structural and Life Cycle Cost Analysis of Two Perpetual Pavements.* Pisa, CRC Press, pp. 357-363.

Timm, D. & Priest, A., 2006. Year of the Pavement. *Roads & Bridges,* 1 January, 44(9), pp. 38-41.

Timm, D., Robbins, M. & Willis, J. R., 2014. *Characteristics of Two Perpetual Pavements at the NCAT Test Track.* Pisa, CRC Press, pp. 349-355.

TRL Client Project Report 282, Phase C, 2010. *Performance of Existing Pavement in Qatar,* Doha: Transport Research Laboratory.

TRL Client Project Report 282, Phase D, 2010. *Design of Site Trials,* Doha: Transport Research Laboratory.

Tsai, B.-W., Bejarano, M., Harvey, J. & Monismith, C., 2005. Prediction and Calibration of Pavement Fatigue Performance Using Two-Stage Weibull Approach. *Journal of the Association of Asphalt Paving Technologists,* Volume 74, pp. 697-732.

Underwood, B. S., Baek, C. & Kim, R., 2012. Simplified Viscoelastic Continuum Damage Model as Platform for Asphalt Concrete Fatigue Analysis. *Journal of the Transportation Research Board,* Volume 2296.

Underwood, B. S., Kim, Y. R. & Guddati, M. N., 2010. Improved Calculation Method of Damage Parameter in Viscoelastic Continuum Damage Model. *International Journal of Pavement Engineering,* 11(6), pp. 459-476.

Van Dijk, W. & Visser, W., 1977. Design, The Energy Approach to Fatigue for Pavement. *Asphalt Paving Technology,* Volume 46, pp. 1-40.

Wang, H. et al., 2011. Effect of Mineral Filler Characteristics on Asphalt Mastic and Mixture Rutting Potential. *Journal of Transportation Research Board,* Volume 2208, pp. 33-39.

Witczak, M. W., 2005. *NCHRP Report No. 547: Simple Performance Tests: Summary of Recommended Methods and Database,* Washington, D.C.: National Cooperative Highway Research Program.

Witczak, M. W. et al., 2002. *NCHRP Report No. 465: Simple Performance Test for Suprpave Mix Design,* Washington, D.C.: National Cooperative Highway Research Program.

Xiao, F., Zhao, W. & Amirkhanian, S. N., 2009. Fatigue Behavior of Rubberized Asphalt Concrete Mixtures Containing Warm Asphalt Additives. *Construction and Building Materials,* 23(10), pp. 3144-3151.

Yan-zhu, P. & Duan-yi, W., 2012. Experimental Study on Dynamic Modulus Master Curve of ATPB Mixture. *Applied Mechanics and Materials,* Volume 117-119, pp. 1556-1560.

Zhu, H. et al., 2011. Developing Master Curves and Predicting Dynamic Modulus of Polymer-Modified Asphalt Mixtures. *Journal of Materials in Civil Engineering,* 23(2), pp. 131-137.

Appendix A

Characteristics of fresh PG76-22

Property	Results
Softening point (ring & ball)	74.5 °C
Penetration at 25 °C	44 dmm
Dynamic viscosity at 120 °C	5500 mPas
Dynamic viscosity at 135 °C	1960 mPas
Dynamic viscosity at 150 °C	940 mPas
Dynamic viscosity at 180 °C	340 mPas
Fraass breaking point	-24 °C
Ductility at 25 °C	87 cm
Elastic recovery at 25 °C	92%
Storage stability 3 days at 180 °C, Delta R&B top-bottom	0 °C

Appendix B

Results for the Trial Pits Extracted from the Trial Sections

The two pits taken from the trial road were analysed and their properties were investigated in the laboratory. Results for the sub-base and subgrade layers are summarised in the following subsections.

Sub-base properties

From the particle size distribution, it was found that the descriptive term of the sub-base for both sections is silty/clayey, sandy, gravel, as shown in the table below, as per BS 5930: 1999.

Gravel	Sand	Silt/Clay
77%	18%	8%

The maximum dry density (MDD) and the optimum moisture content (OMC) of the sub-base layer were evaluated in the laboratory using the BS 1377 4.5 kg rammer method. The results for each section are as follows:

Section #	Maximum dry density (Mg/m^3)	Optimum moisture content (%)
2	2.22	8.3
5	2.19	8.0
Average	2.21	8.2

The California Bearing Ratio (CBR) value for the sub-base layer for both trial pits was determined using BS 1377:Pt.4:1990: Clause 7, AMD 13925-02, as follows:

CBR	Top of specimen	Base of specimen
@ 2.50 mm penetration	> 99%	> 99%
@ 5.00 mm penetration	> 99%	> 99%

Therefore, a CBR value of 100% could be used for the sub-base and the final moisture content was determined to be 9.4% in average. In addition, the liquid limit (LL) was determined using BS 1377:Pt.2:1990: Clause 4.3, AMD 9027-97 for both trial pits and it was 33%. Finally, the plastic limit (PL) and the plasticity index (PI) were determined using BS 1377:Pt.2:1990: T 5.3, AMD 9027-96, for both trial pits, as shown in the table below.

Section #	Plastic limit (PL)	Plasticity index (PI)
2	23%	10
5	24%	9

Subgrade properties

From the particle size distribution, it was found that the descriptive term of the subgrade for the trial pit of section 2 is silty/clayey, very sandy, gravel, while trial pit of section 5 is very silty/clayey, very sandy, gravel, based on the results shown in the table below. This term is based on BS 5930: 1999.

Section #	Gravel	Sand	Silt/Clay
2	43%	37%	20%
5	45%	31%	24%

The maximum dry density (MDD) and the optimum moisture content (OMC) of the subgrade layer were evaluated using the BS 1377 4.5 kg rammer method. The results for each section are as follows:

Section #	Maximum dry density (Mg/m^3)	Optimum moisture content (%)
2	2.140	8.0
5	2.130	7.8
Average	2.135	7.9

The California bearing ratio (CBR) values for the subgrade layer for both trial pits were determined using BS 1377:Pt.4:1990: Clause 7, AMD 13925-02, as shown below. The final moisture content was determined to be 12.5% on average.

Section #	CBR	Top of specimen	Base of specimen
2	**@ 2.50 mm penetration**	26% corrected	26% corrected
5		36% corrected	40% corrected
2	**@ 5.00 mm penetration**	24% corrected	26% corrected
5		32% corrected	33% corrected

In addition, the liquid limit (LL) was determined using BS 1377:Pt.2:1990: Clause 4.3, AMD 9027-97 for the trial pit of section 2 and that of section 5 and it was 33% and 32%, respectively. Finally, the plastic limit (PL) and the plasticity index (PI) were determined using BS 1377:Pt.2:1990: T 5.3, AMD 9027-96 for both trial pits, as follows:

Section #	Plastic limit (PL)	Plasticity index (PI)
2	24%	9
5	24%	8

Appendix C

Example of the Dynamic Modulus ($|E^*|$) Test Data

Conditions		Specimen 1		Specimen 2		Modulus		Phase Angle	
		core 6-5		core 6-6					
Temp., C	Freq, Hz	Modulus, MPa	Phase Angle, degree	Modulus, MPa	Phase Angle, degree	Average, MPa	CV, %	Average, degree	Std Dev, degree
4.4	25	18693	6.69	21494	7.03	20093.5	9.9	6.86	0.2
4.4	10	17464	7.23	20046	7.81	18755	9.7	7.52	0.4
4.4	5	16603	7.53	19019	8.46	17811	9.6	7.995	0.7
4.4	1	14502	9	16449	10.22	15475.5	8.9	9.61	0.9
4.4	0.5	13528	9.79	15378	11.05	14453	9.1	10.42	0.9
4.4	0.1	11357	11.93	12721	13.45	12039	8.0	12.69	1.1
21.1	25	11026	13.58	12884	14.81	11955	11.0	14.195	0.9
21.1	10	9635	15.06	11246	16.39	10440.5	10.9	15.725	0.9
21.1	5	8638	16.26	10063	17.53	9350.5	10.8	16.895	0.9
21.1	1	6524	19.22	7355	20.79	6939.5	8.5	20.005	1.1
21.1	0.5	5717	20.36	6360	21.8	6038.5	7.5	21.08	1.0
21.1	0.1	4086	23.13	4296	24.44	4191	3.5	23.785	0.9
37.8	25	5110	24.02	6245	24.15	5677.5	14.1	24.085	0.1
37.8	10	4104	25.46	4931	25.41	4517.5	12.9	25.435	0.0
37.8	5	3464	26.26	4086	26.09	3775	11.7	26.175	0.1
37.8	1	2210	28.44	2455	28.2	2332.5	7.4	28.32	0.2
37.8	0.5	1849	28.34	2008	27.92	1928.5	5.8	28.13	0.3
37.8	0.1	1141	28.84	1156	28.81	1148.5	0.9	28.825	0.0
54	25	2361	28.76	2530	31.01	2445.5	4.9	29.885	1.6
54	10	1739	28.96	1802	30.99	1770.5	2.5	29.975	1.4
54	5	1404	28.47	1452	29.98	1428	2.4	29.225	1.1
54	1	812.4	27.82	740.4	30.85	776.4	6.6	29.335	2.1
54	0.5	669.5	26.58	579.3	29.96	624.4	10.2	28.27	2.4
54	0.1	428.6	24.31	322.5	29.23	375.55	20.0	26.77	3.5

Appendix D

Example of the Fatigue Test Analysis Using the VECD Approach

	A	B	D	G	H	I	J	K	L	M	N	O	P	Q	R	S	T	U	V
1	Cycles	Dynamic Modulus (Pa)	Stress (Pa)	Strain	Pseudo-Strain (kPa)	Pseudo-Stress	Pseudo-Stiffness (C)	ΔN	ΔC	ΔS	Internal Damage (S)	C_n	Error	SSE	a	b	$C = \exp(aS^b)$		
2	10	6.65E+09	2.73E+05	4.10E-05	2.73E+02	4.10E-05	1.000			0	0	1.0000	0	0.022468	-2.88E-04	0.697941			
3	20	6.64E+09	2.72E+05	4.09E-05	2.72E+02	4.08E-05	0.998	10	-0.0017	2.24E+01	2.24E+01	0.9975	6.52E-07						
4	30	6.61E+09	2.71E+05	4.10E-05	2.73E+02	4.07E-05	0.994	10	-0.0046	4.73E+01	6.97E+01	0.9944	6.08E-07						
5	40	6.61E+09	2.71E+05	4.10E-05	2.73E+02	4.07E-05	0.993	10	-0.0005	8.47E+00	7.82E+01	0.9940	6.16E-07						
6	50	6.59E+09	2.71E+05	4.10E-05	2.73E+02	4.07E-05	0.991	10	-0.0022	2.75E+01	1.06E+02	0.9926	2.64E-06						
7	60	6.59E+09	2.70E+05	4.10E-05	2.73E+02	4.06E-05	0.990	10	-0.0013	1.86E+01	1.24E+02	0.9917	4.29E-06						
8	70	6.57E+09	2.70E+05	4.11E-05	2.73E+02	4.06E-05	0.988	10	-0.0017	2.29E+01	1.47E+02	0.9907	7.78E-06						
9	80	6.57E+09	2.70E+05	4.10E-05	2.73E+02	4.05E-05	0.987	10	-0.0007	1.16E+01	1.59E+02	0.9902	8.96E-06						
10	90	6.57E+09	2.70E+05	4.11E-05	2.73E+02	4.05E-05	0.987	10	-0.0006	1.05E+01	1.69E+02	0.9897	1E-05						
11	100	6.56E+09	2.69E+05	4.10E-05	2.73E+02	4.04E-05	0.985	10	-0.0012	1.69E+01	1.86E+02	0.9890	1.33E-05						
12	110	6.56E+09	2.69E+05	4.10E-05	2.73E+02	4.04E-05	0.985	10	0.0001		1.86E+02	0.9890	1.27E-05						
13	120	6.55E+09	2.69E+05	4.11E-05	2.73E+02	4.05E-05	0.985	10	-0.0009	1.38E+01	2.00E+02	0.9885	1.52E-05						
14	130	6.55E+09	2.68E+05	4.10E-05	2.73E+02	4.03E-05	0.984	10	-0.0006	1.06E+01	2.11E+02	0.9880	1.69E-05						
15	140	6.54E+09	2.68E+05	4.10E-05	2.73E+02	4.03E-05	0.983	10	-0.0009	1.37E+01	2.24E+02	0.9875	2E-05						
16	150	6.54E+09	2.69E+05	4.11E-05	2.73E+02	4.04E-05	0.983	10	0.0001		2.24E+02	0.9875	1.88E-05						
17	160	6.53E+09	2.68E+05	4.11E-05	2.74E+02	4.03E-05	0.981	10	-0.0018	2.36E+01	2.48E+02	0.9866	2.77E-05						
18	170	6.53E+09	2.68E+05	4.10E-05	2.73E+02	4.03E-05	0.982	10	0.0006		2.48E+02	0.9866	2.2E-05						
19	180	6.52E+09	2.68E+05	4.11E-05	2.74E+02	4.03E-05	0.980	10	-0.0017	2.23E+01	2.70E+02	0.9858	3.09E-05						
20	190	6.52E+09	2.68E+05	4.11E-05	2.74E+02	4.03E-05	0.980	10	-0.0001	1.84E+00	2.72E+02	0.9857	3.09E-05						
21	200	6.52E+09	2.68E+05	4.11E-05	2.74E+02	4.03E-05	0.980	10	-0.0006	1.01E+01	2.82E+02	0.9853	3.34E-05						
22	210	6.53E+09	2.68E+05	4.10E-05	2.73E+02	4.02E-05	0.981	10	0.0010		2.82E+02	0.9853	2.28E-05						
23	220	6.52E+09	2.68E+05	4.11E-05	2.73E+02	4.02E-05	0.979	10	-0.0012	1.71E+01	2.99E+02	0.9847	2.88E-05						
24	230	6.51E+09	2.68E+05	4.11E-05	2.73E+02	4.02E-05	0.979	10	-0.0006	1.09E+01	3.10E+02	0.9843	3.17E-05						
25	240	6.51E+09	2.68E+05	4.12E-05	2.74E+02	4.03E-05	0.978	10	-0.0003	6.14E+00	3.16E+02	0.9841	3.27E-05						
26	250	6.51E+09	2.68E+05	4.11E-05	2.74E+02	4.03E-05	0.979	10	0.0002		3.16E+02	0.9841	3E-05						

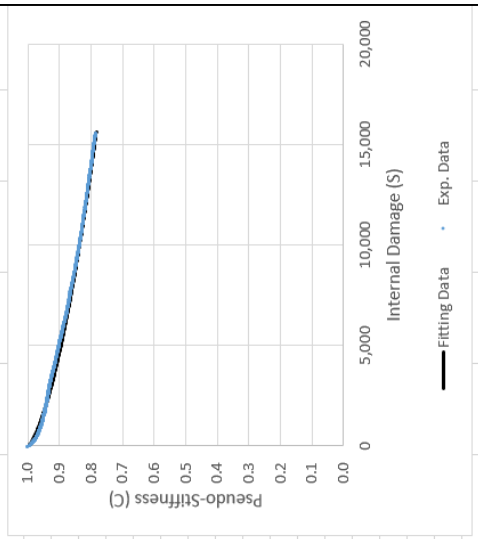

	Y	AA	AB	AC	AD
1	True Pseudo-Strain (kPa)	$\Delta S_{simulated}$	$S_{simulated}$	dC/dS	$C_{simulated}$
2	366.02	0.00E+00	5.55E+01	-5.94E-05	0.9953
3	366.02	6.21E+01	1.18E+02	-4.72E-05	0.992
4	366.02	3.12E+01	1.49E+02	-4.39E-05	0.9906
5	366.02	2.51E+01	1.74E+02	-4.18E-05	0.9895
6	366.02	2.18E+01	1.96E+02	-4.03E-05	0.9886
7	366.02	1.95E+01	2.15E+02	-3.92E-05	0.9878
8	366.02	1.79E+01	2.33E+02	-3.82E-05	0.9872
9	366.02	1.66E+01	2.50E+02	-3.74E-05	0.9865
10	366.02	1.56E+01	2.65E+02	-3.67E-05	0.9859
11	366.02	1.47E+01	2.80E+02	-3.61E-05	0.9854
12	366.02	1.40E+01	2.94E+02	-3.55E-05	0.9849
13	366.02	1.34E+01	3.07E+02	-3.51E-05	0.9844
14	366.02	1.28E+01	3.20E+02	-3.46E-05	0.984
15	366.02	1.23E+01	3.33E+02	-3.42E-05	0.9836
16	366.02	1.19E+01	3.44E+02	-3.38E-05	0.9832
17	366.02	1.15E+01	3.56E+02	-3.35E-05	0.9828
18	366.02	1.12E+01	3.67E+02	-3.32E-05	0.9824
19	366.02	1.09E+01	3.78E+02	-3.29E-05	0.982
20	366.02	1.06E+01	3.89E+02	-3.26E-05	0.9817
21	366.02	1.03E+01	3.99E+02	-3.23E-05	0.9814
22	366.02	1.00E+01	4.09E+02	-3.20E-05	0.981
23	366.02	9.81E+00	4.19E+02	-3.18E-05	0.9807
24	366.02	9.59E+00	4.28E+02	-3.16E-05	0.9804
25	366.02	9.39E+00	4.38E+02	-3.14E-05	0.9801
26	366.02	9.20E+00	4.47E+02	-3.12E-05	0.9798